A Class of Solutions for Extrusion through Converging Dies

A Thesis Submitted for award of the Degree

of

Doctor of Philosophy

by

Akshaya Kumar Rout

Under Supervision of

Prof. K. P. Maity

Department of Mechanical Engineering of

National Institute of Technology

Rourkela-769008

Orissa, India

August- 2010

Dedicated to

My

Father

Late Baishnaba Charana Rout

DECLARATION

I hereby declare that this submission is my own work and that, to the best of my knowledge and belief, it contains no material previously published or written by another person nor material which to a substantial extent has been accepted for the award of any other degree or diploma of the university or other institute of higher learning, except where due acknowledgement has been made in the text.

Akshaya kumar Rout

Date: 31-08-2010

Dr. Kalipada Maity
Professor
Department of Mechanical Engineering
National Institute of Technology
Orissa, India

CERTIFICATE

This is certify that the thesis entitled *"**A Class of Solutions for Extrusion through Converging Dies"*** being submitted by Mr. Akshaya Kumar Rout, Roll No: 50703002, for the award of the degree of DOCTOR OF PHILOSOPHY of the National Institute of Technology, Rourkela, Orissa (India), is a record of bonafide research work carried out by him under my supervision. Mr. Akshaya Kumar Rout has worked three and half years on the above problem and this has reached the standard fulfilling of the requirements and the regulation relating to the degree. The results embodied in this thesis have not been submitted to any other University or Institution for the award of any degree or diploma.

Prof. Kalipada Maity

Date: 31-08-2010

ACKNOWLEDGEMENTS

That author is highly indebted to Dr. K. P. Maity, Professor, Department of Mechanical Engineering, National Institute of Technology, Rourkela for his invaluable encouragement, helpful suggestion and supervision at all stages of this investigation. The author also wishes to express his gratitude to Dr. S. K. Sahoo, Professor in Mechanical Engineering Department, NIT, Rourkela for many fruitful discussions that was held with him especially during the experimental stages of this study.

The author expresses his deep sense of gratitude for his Father-in-Law, Prof. Purnachandra Das, whose constant encouragement and moral support that, has helped him to complete this work

All the faculty member and office staff of Mechanical Engineering Department for their direct and indirect helps in carry out this research work.

Thanks are also due to all the technical staff of the Mechanical Engineering Department and Central workshop of NIT, Rourkela for their assistance during the experimental work. Special thanks to Mr. Rabikumar, Mr. Reddy, Mr. Sethy, for their assistance during the experimental works.

Finally I thank my family members for their continual love, support and untiring endurance.

Akshaya Kumar Rout

ABSTRACT

Extrusion, as a metal forming process, has definite advantages over rolling for production of three- dimensional section shapes. The very large reductions achieved in this process, even at high strain rates, have made it one of the fastest growing metal forming methods. With the increasing demand for sections of different shapes, it has become essential to develop analytical methods for their solution.

The present investigation is a sincere attempt to develop a class of solutions for extrusion of different sections from round and square billet through converging dies by three-dimensional upper bound method as well as Finite element method. Three dimensional upper bound solutions are based on both continuous velocity field and discontinuous velocity field. The continuous velocity fields are based on dual stream function method. The discontinuous velocity fields are based on SERR (spatial elementary rigid region) technique.

Upper bound method based on SERR technique is used for analysis of extrusion of pentagon, octagon, triangular and rhomboidal sections from round billet using linear converging die. The constant friction factor is assumed at the die billet interface. The single point formulation has been used keeping the die orifice in the centroid of billet axis so that product emerges straight. The extrusion pressure and die profile has been determined for different reductions and friction factors.

The results are compared with square or flat faced die. It is observed that there is drastic reduction in extrusion pressure in converging die.

Upper bound analysis has been carried out for extrusion of square section from square billet using Bezier and polynomial shaped curved dies. The optimum die profile is obtained from analysis. The variation of extrusion pressure and optimum die length with respect to reduction and friction factor has been determined. It is observed that the friction factor plays a significant role at high reduction.

FEM modeling has been carried out extrusion of square sections from square billet using DEFORM-3D software. The die profiles of cosine, bezier and polynomial shapes are considered. The rigid-plastic material model has been considered.

A mathematically contoured non-linear converging die has been designed for extrusion of square and triangular section from round billet. CAD models of die profile have also been developed. FEM modeling has also been carried out to determine extrusion pressure, effective stress, effective strain rate and temperature using DEFORM-3D software.

The experiments have been conducted to verify the proposed theory partially. The extrusion test rigs have been fabricated to carry out extrusion through mathematically contoured dies. Experiments have been conducted both for dry and lubricated conditions.

CONTENTS

List of Tables

List of Figures

Nomenclature

English symbols (in alphabetical order)

a_{i1}, $a_{i2,}$ a_{i3}	Coefficients in the equation of the ith face
A_{fj}	Area of the jth face having friction
A_i	Area of the ith face of the rigid region
A_b, A_p	Cross-section areas of the billet and product
A	Half width of the product
a	One side of the triangle
b	Other side of the triangle
c	Major axis of the rhombus
d	Minor axis of the rhombus
D	Diameter of the billet
D_1	Diameter of the equivalent product
e	Distance of the vertices from the center in the exit plane (polygonal section)
F	Die profile function F (z)
F'	First derivative of F (z)
F''	Second derivative of F
H	Height of the triangle
J	Upper-bound power consumption
k	Yield stress in shear
L	Length of the die
L_0	The position of floating point (12)
L_1	Length of each side of the approximating polygon
m	Friction factor on the die surface
M	Number of sides of the approximating polygon
$\hat{n}$	Unit vector normal to a surface
P_{av}	Average extrusion pressure
R	Radius of the billet
S	Surface of the velocity discontinuity
S_f	Friction surface

V	Velocity vector in general
V_b,	Billet velocity
V_p	Product velocity
V_x, V_y, V_z	Components of velocity in Cartesian co-ordinates
ΔV_i	Velocity discontinuity across the ith face
$\lvert\Delta V\rvert_s$	Magnitude of the velocity discontinuity at S
$\lvert\Delta V\rvert_{sf}$	Magnitude of the velocity discontinuity at
W	Half-width of the billet
x, y, z	Axes of general Cartesian co-ordinates
$\frac{P_{avg}}{\sigma_0}$	Non-dimensional extrusion pressure
ε_{ij}	Components of strain rate tensor
θ	Equivalent semi-cone angle
σ_0	Yield stress (Flow stress) in uniaxial tension or compression
φ	Function representing the equation of a planer surface
ψ_1, ψ_2	Dual stream functions
$\acute{\varepsilon}_{xx}, \acute{\varepsilon}_{yy}, \acute{\varepsilon}_{zz}$	Direct strain-rate components
$\acute{\varepsilon}_{xy}, \acute{\varepsilon}_{yz}, \acute{\varepsilon}_{zx}$	Shear strain-rate components
Ψ	Internal angle of the regular polygon
Φ	Rhombus angle

Abbreviations

CAD	Computer aided design
CAM	Computer aided manufacturing
UTM	Universal testing machine
CNC	Computerized numerical control
EDM	Electro discharge machine
SERR	Spatial elementary rigid region
3D	Three dimensional
KAVF	Kinematically-admissible velocity field
DEFORM	Design environment for forming
PR	Percentage reduction
CG	Center of gravity
SEM	Scanning electron microscope
U-B	Upper-bound
S D	Square die
H D	Homogeneous deformation
L C	Linearly converging
R A	Right angled

CHAPTER-1

Introduction

1.1 Background

With the rapid growth of industrialization and technology, the necessity of metal forming operations have increased manifold. In contrast to other manufacturing requirements, the metal forming operation enjoys certain advantages in terms of improved mechanical properties of the product as well as minimization wastage of material in terms of scrap.

Extrusion process plays a major role in massive metal deformation process in which cross-sectional area of billet is reduced by pushing with a ram and squeezing through a die. Very often many empirical rules are followed to determine process parameters, extrusion load and geometries of die profiles. However, empirical relations have limited applications and can not be applied universally under various conditions. A great deal of research have been carried out by different investigators in the recent decades to understand the complex mechanism of metal deformation process in the extrusion process both for two dimensional and three dimensional process. It is evident that geometry of dies plays the most critical role in controlling the extrusion process parameters in case of conventional tapered dies.

During the last decade, considerable attention has been directed towards the use of mathematically contoured curved dies for extrusion. The basic advantage in the use of such dies lies in the fact that there is smooth flow of metal, less redundant work and less deformation load. In the past conical dies are preferred to mathematically contoured dies because of their ease of manufacture. However, now-a-days, the manufacture of mathematically contoured dies has become much easier because of availability of sophisticated computer numerical control machines.

Because of the large forces required in extrusion, most metals are extruded hot where the deformation resistance of metal is low. However, cold extrusion is possible for many metals and has become an important commercial process. The reaction of the extrusion billet with the container and die results in high compressive stresses that effectively reduce cracking of materials during primary breakdown from the ingot. This is an important reason for increased utilization of extrusion on the working of

metals difficult to form, like stainless steel, nickel based alloys and other high temperature materials.

The variables influencing an extrusion process are: (i) the percentage of area reduction, (ii) the die geometry, (iii) the product geometry, (iv) the speed of extrusion, (v) the billet temperature, and (vi) lubrication. In a manufacturing situation the above parameters should be suitably optimized to achieve the best results. The ram speed and temperature have major influence on plastic properties of the billet material and their effect can be studied by choosing a suitable constitutive equation. But the effect of reduction, die and product geometry on stresses and strains is rather difficult and this has remained an active area of research for the past few decades.

1.2 Different Types of Conventional Dies

The different types of conventional dies are; (i) Square dies (ii) Tapper or Linearly converging dies and Curved or mathematically contoured dies.

Table 1 : Comparison between Flat, Tapper and Curve Dies

SR NO.	FLAT	TAPPER	CURVE DIE
1	Dead metal zone	No Dead metal zone	No Dead metal zone
2	Conventional	Conventional	Non-Conventional
3	High Frictional Force	Less Frictional Force compared to flat die	Less Frictional Force compared to both
4	Lubrication not possible	Lubrication possible	Lubrication possible
5	No internal work of deformation and also no frictional work at die billet interface	Internal work of deformation, Shear work at entry and exit plane and also frictional work at die billet interface are present	Internal work of deformation, Shear work at entry and exit plane and also frictional work are present

1.3 Die Materials

Generally die materials are; (i) Various grades of tool steels (ii) Cemented carbides (iii) Steels bonded carbides (iv) Molybdenum high speed steel.

1.4 Application of Dies

Basically those dies are used in Steel, Aluminium, Copper, Zinc, Lead and Tin industry.

1.5 Problems with Conventional Dies

The common problems are; (i) High extrusion pressure (ii) Low production rate (iii) Formation of dead metal zone (iii) Poor surface finish (iv) More frictional force (v) Less dimensional accuracy (vi) More redundant work by using conventional dies.

1.6 Different Types of Curve Dies

The different curved dies are; (i) Cosine (ii) Convex circular (iii) Concave circular (iv) Convex elliptic (v) Concave elliptic (vi) Convex parabolic (vii) Concave parabolic (viii) Convex hyperbolic (ix) Polynomial shaped die (x) Bezier shaped curved die.

1.7 Classification of Extrusion

Classification of Extrusion process are; (i) Forward Extrusion (ii) Backward Extrusion (iii) Combined Backward and Forward Extrusion (iv) Side Extrusion (v) Hydrostatic Extrusion

1.8 Literature Review

Kudo [84] has presented the flow patterns on various sections of lead billets during various plane-strain forging and extrusion operations by using upper-bound approach method. It is found to be satisfactory, simple and reliable for practical purposes. Bachrach and Samanta [10] presented a numerical method for slip-line field analysis of rigid perfectly plastic material, which analyses metal forming operations as constrained optimization problems. They developed the solution for the extrusion through curved dies with zero exit angle and non-zero entrance angle using the proposed method and computed the extrusion pressure with respect to reduction with other parameters. Yamada and Hirakawa [194] investigated large deformation and instability analysis using FEM for smooth and frictional work and tool interface. Tjetta and Heimlund [179] have discussed the various aspects of the finite element simulations of cold forging process in process design of aluminium chesis component using a thermo elasto-viscoplastic constitutive model. Knoerr et al. [89] investigated various 2D metal forming processes using DEFORM software and simulated the results with practical applications. Storen [6] has highlighted the mechanics and

metallurgy of advances in extrusion process. Kim et al. [108] have carried out computer aided simulation 3D modeling of metal deformation processes using DEFORM software for different practical applications. Vickery and Monaghan [184] carried out experimental investigation of a combined forging extrusion process for an axisymmetric component and also developed an analytical model for that. Choi et al. [34] also developed the analytical FEM model for extrusion of semi-solid material using A 356 materials and validated the model with experiments. Clause et al. [10] made an investigation of material properties and geometrical dimensions of Al extrusions. Williams et al. [187] carried out computational modeling of extrusions and forging considering the non-Newtonian fluid flow. Kumar et al. [96] investigated non re-entry cold extrusion using upper-bound model through different die profiles. He concluded that the third order stream lined and cosine die profile is best among the other die profiles. Barisic et al. [17] investigated the backword extrusion. Malayappan et al. [122] investigated the extrusion forging effect for Aluminium with the help of an extrusion die constraint. Ajiboye et al. [5] carried out investigation of extrusion of square, rectangular, I and T section using different die land and die profiles using upper bound analysis. Narayanasamy et al. [132] investigated experimentation of barreling of aluminium alloy billets using extrusion forging operation with different lubricants. Kobayashi and Thomson [86] carried out upper bound and lower bound solution for axisymmetric problems for compression between two parallel blocks and for frictionless extrusion of a bar through tapered dies. An upper-bound solution based on a kinematically admissible velocity field to the axisymmetric extrusion through conical dies has been proposed by Halling and Mitchell [65] by using a digital computer programme to accommodate the work of circumferential straining and the effects of die friction for a full range of cone angles, reductions and frictional conditions. Chen and Ling [22] carried out an upper-bound solution for axisymmetric extrusion through curved dies of different profiles such as cosine, elliptic and hyperbolic type. Frisch and Mata-Pietric [52] investigated upper bound solution of axi-symmetric components through cosine, elliptical and hyperbolic die profiles and validated experiments with good agreements. Kar et al. [58] have reformulated the spatial elementary rigid regions (SERR) technique of Gatto and Giarda to render it suitable for analysis of extrusion through square dies. The non-dimensional extrusion

pressure for various reductions are computed for extruding square bars through square dies by using SERR technique.

Yang et al. [198] carried out upper bound solution of extrusion of arbitrarily shaped sections using generalized velocity approach and validated with experiment. Lee et al. [108] investigated the extrusion of tube using UBET (upper bound elemental technique). Das and Johnson [39] have suggested the new slip-line field solutions for end extrusion through square dies with slipping friction at the work piece-die interfaces. The variation of the mean steady state extrusion pressure with reduction has been computed for these fields. Maccarini et al. [117] carried out finite element simulation with experimental validation. Peng [134] carried out upper bound analysis for extrusion of rod with the assumption of curved exit and entry place. Wifi et al. [189] investigated combined FEM and upper bound analysis for modeling metal flow and die stress analysis. Valberg [183] has investigated the metal flow in the direct axisymmetric extrusion of aluminium by means of a grid-pattern technique, which is made from indicator pins (AlCu2.5), which are inserted into holes drilled into the billet (A1MgSil). The grid pattern is obtained when one half of this plane is rotated about the axis and added on top of the other half of the plane.

Reinikainen et al. [143] analysed extrusion of copper using DEFORM software with the assumption of isothermal process with two different frictional boundary conditions. Bae and Yang [13] carried out an upper-bound analysis of backward extrusion of internally elliptical shaped tubes from round billet. Bae and Yang [14] have determined the extrusion load and the average extruded height for the three-dimensional backward extrusion of internally non-axisymmetric tubes from round billets. Experiments are carried out with fully-annealed commercial aluminum alloy billets at room temperature using various shaped punches. The theoretically predicted values of the extrusion load, average extruded height and those determined experimentally are found to be in good agreement. An analysis of backward extrusion process has been carried out using upper bound method for production of internally circular shaped tubes from arbitrarily shaped billets by Bae and Yang [45]. Guo et al. [57] investigated hot forward and backward extrusion using visco-plastic FEM. Kang et al. [90] carried out simulation of preform design using Finite Element Modeling and validated with experimental confirmation. Reddy et al. [144] investigated the

combined upper-bound /slab method to compare eight different die shapes namely third and fourth order polynomial, cosine, elliptical, hyperbolic, conical and Blazynski's CRHS. It is concluded that third and fourth order polynomial and cosine die are the best amongst all profiles. Reddy et al. [145] applied the combined upper bound method/ FEM to analyse four different shapes namely stream lined, cosine, hyperbolic and conical for axisymmetric components assuming visco-plastic material.

Reddy et al. [146] investigated the process of tube extrusion using FEM and a streamlined die for a strain hardening material.Kuzman et al. [91] investigated material flow in combined backward and forward extrusion using DEFORM software. The analysis of extrusion of circular-shaped bars from polygonal billets based on upper bound method is analysed by Kim et al. [92] with determination of extrusion loads, the velocity distribution and the average length of extruded billets. Sahu et al. [154] investigated extrusion of hexagonal section bars from rectangular billets through the square dies using upper bound analysis. Reddy et al. [147] have presented a finite element model to obtain the temperature distribution in the work piece as well as in the tooling in hot and warm extrusion processes. The comparison of the combined thermo-mechanical finite element method (TMFEM) is made with experimental results. Then it is seen that the temperature distribution and the extrusion power obtained by the combined upper bound/finite element method (UBFEM) are in good agreement with those of TMFEM. Gouveia et al. [43] the new distributions at the fixed mesh positions is determined by using work hardening material and a combined Eulerian-Lagrangian formation, which is based on the utilization of an updated Lagrangian temporary mesh, to calculate the strain and stress fields, coupled with a mathematical scheme to interpolate the strain and stress tensors into the Eulerian mesh.

Sahoo et al. [157] have developed an analytical method based on the upper-bound theory to investigate the extrusion of triangular section bars from square/rectangular billets through the square dies by using SERR (Spatial Elementary Rigid Region) technique. The non-dimensional extrusion pressure at various area reductions is computed for different billet aspect ratios assuming unequal dead metal height at corner points by using SERR technique. The results have been computed with the slip line field solution of the equivalent plane-strain condition. Semiatin and

Delo [161] have analysed the angular extrusion of equal channel of difficult –to-work alloys such as commercial-purity titanium (CP Ti) and AISI 4340 steel. Lee et al. [111] investigated UBET analysis of non axisymmetric forward and backward extrusion. Salim [165] has developed a theoretical model for plane strain deformation based on a slip line field (SLF) solution for a section of product in plane strain drawing. The results are compared to those of the finite element method. It is seen that the shear strain at a position close to the contact area is greater than that of the centre of the product. The simulations are performed for copper-clad aluminum rod to predict the distributions of temperature, effective stress, and effective strain rate and mean stress for various sheath thickness, die exit diameters and die temperatures by Kang et al. [97] using DEFORM software. The results agree fairly with experiments. Byon and Hwang [16] modeled optimal design of die profile for hot and cold extrusion. Yang and Lee [202] predicted strain conditions of the equal channel angular extrusion using finite element analysis. Bourke et al. [18] modeled the plastic deformation zone with finite element technique and predicted the extrusion load with ram displacement. Kumar and Prasad [52] have proposed a combined rigid plastic finite element (RPFE) model for steady state axisymmetric extrusion process using a kinematically admissible velocity field obtained from the upper bound model proposed by Kumar, et al. [100] Optimal power and temperature distribution and effects of various process parameters in cold as well as hot extrusion processes are determined with RPFE method using the deformation field. The result obtained agrees well with the experiment and analysis. Darani et al. [40] have simulated the extrusion of L sections using upper bound method.Azad et al. [2] modeled the cold forward extrusion of aluminium using optimum curved die profile using ABACUS software. It is observed that there is considerable reduction in extrusion load compared to the optimal conical die. Altan et al. [3] investgated extrusion of equal channel angular extrusion (ECAE) using upper bound method and studied the effect of friction, radius of inner corner of the die and the dead metal zone. Yang et al. [203] modeled the equal channel angular extrusion using finite element technique in terms of process parameters including the bent angle and channel width. It is observed that there exits morphological stability of extruded product, when the width of billet channel is larger than the entrance one. Yang et al. [204] have established a model of hydrodynamic

lubrication during cold extrusion based on elastic–plastic theory and metal-forming mechanism. The proposed model has also used the frictional boundary condition during rigid-plastic finite element simulation of cold extrusion. The numerical result is discussed and compared with the experimental results and it is seen to be in good agreement between them. Kim and Kim [101] investigated the analysis of 3D deformation during the angular extrusion of equal channel. Saboori et al. [169] investigated numerical and experimental study of forward and backward extrusion. Jooybari et al. [60] carried out investigations of backward extrusions using ABACUS software. Ajiboye and Adeyemi [4] investigated upper bound analysis for cold extrusion and studied the effect of die length.

Son et al. [170] used FEM modeling for equiangular channel extrusion. Bakhshi et al. [19] used a new combined upper bound and slab method. They have proposed for estimating the deformation load for cold rod extrusion of aluminum and lead in an optimum curved die profile. The experimental results and the comparison of an optimum conical die have also been determined by using the finite element software, ABAQUS. It is observed that the extrusion load in the optimum curved die during the deformation is considerably less than that in the optimum conical die. Eivani and Taheri [46] presented a solution for evaluating total strain in those dies consisting of two or more ECAE sub-dies. A complete agreement is found between calculated and previous results by other authors. Xu et al. [190] carried out optimization for pressing equal-angle channel for producing ultra fine grain materials. Li and Xie [115] have discussed the effect of the binder content on the extrusion behavior of the 316L stainless steel seamless pipe. Good thin-walled pipes have been obtained after sintering at 1100^0 C, and at that temperature, a microstructure with the bottle-necks forming between the round particles has formed that guarantees the thin-walled pipes having the pores with homogeneous size distribution. Mamalis et al. [120] has studied the effect of strain hardening features of borus materials by cold extrusion through a conical die. Malpani and Kumar [121] have analyzed the three dimensional complex geometry tube extrusion processes having generalized die and mandrel profiles by a feature based upper-bound model. The analysis is based on kinematically admissible velocity field to obtain the optimal extrusion pressure by optimizing the die length using variable interval golden section method. The

experimental and the proposed analytical results have been compared with other researchers and it is seen to be in good agreement between them. Yoon et al. [205] have investigated the effects external and internal factors on the deformation in homogeneity during ECAP. The finite element analysis of plastic deformation is employed for this purpose in conjunction with die corner angle and strain harden-ability of metallic work-pieces. Abrinia and Makaremi [6] have presented the three-dimensional solution for the extrusion of sections with larger dimensions than the initial billet with a generalized kinematically admissible velocity field by using the upper bound theorem. In this paper unlike flat-faced dies the material has to flow over two kinds of surfaces, i. e. on converging and diverging surfaces and the extrusion of square and rectangle sections and the optimum die length and the process parameters such as friction, extrusion ratio and aspect ratio also have been computed. Gao and Cheng [63] found that the extrusion temperature must be higher than the eutectoid reaction temperature of the commercial aluminum bronze alloy (Cu–10% Al–4% Fe) alloy during hot rolling. The grain size of alloy gradually reduced with the increase of the pass number of ECAE and the mechanical properties are significantly improved after ECAE. The phase transformation temperature of the alloy can also be reduced by ECAE process. The internal power and the power dissipated on frictional surface, and velocity discontinuity surfaces are developed by using a kinematically admissible velocity field for the tube extrusion process by Ebrahimi et al. [48]. They also determined the optimum die angle, the critical die angle and also the effect of constant friction factor and reduction in area on the optimum die angle. The theoretically predicted values of the load–displacement curves and those determined experimentally are found to be in good agreement. The axi-symmetric bi-metallic tubes through profiled shaped dies and over profile shaped mandrels is extruded by a generalised slab method by Chitkara and Aleem [32]. An experimental investigation into forward extrusion of bi-metallic tubes made of cp aluminium and hc copper is also carried out and the resultant non-dimensionalised extrusion pressures, flow patterns and characteristic deformation modes are observed. The theoretical results of extrusion pressures are compared with the experiment as well as those of other author's results and it is seen to be in good agreement between them. Chitkara and Aleem [33] have investigated the extrusion-piercing of hollow tubes starting from

either solid circular or initially hollow billets by using different shapes of axi-symmetric die-mandrel combinations. The experimental results are studied by characteristic deformation modes during processing of these tubes made of tellurium lead and commercially pure aluminium. The working pressures based on the generalised upper bound analysis are compared with the experimental and with those estimated earlier from the slab method of analysis given by Chitkara and Aleem and it is seen to be in good agreement between theoretical, and those determined experimentally. Balasundar et al. [20] investigated equal channel angular pressing die to extrude a variety of materials using numerical modeling. Three important parameters such as die corner angle, friction and constitutive relationship of materials have been taken into consideration. An upper bound and slab method analysis has been carried out for a single-hole extrusion process for the same sizes of the holes; the ram force in a single-hole extrusion process is more than in a multi-hole extrusion process by Sinha et al. [174]. The stresses in the die are computed using the finite element method. Reihanian et al. [148] analyzed equal channel angular extrusion using linear and rotational velocity fields by upper bound method. It is found that PDZ (plastic deformation zone) becomes larger with increasing the constant friction factor and the inner corner radius. The forces are calculated for the equal channel angular extrusion process and it is seen to be in good agreement between theoretical and those determined experimentally. Paydar et al. [139] investigated equal channel angular pressing-forward extrusion with consolidation of Al particles. This process prevents surface cracking with improvement in microstructure and mechanical properties. There is also increase in self-diffusion co-efficient of Al due o the exerted back pressure. Forhoumand and Ebrahimi [53] has used the finite element method for simulation to the effect of geometrical parameters such as die corner radius and gap height as well as process condition such as friction on the process using ABACUS. The finite element results are compared with experimental data in terms of forming load and material flow in different regions. The comparison between the theoretical and the experimental results are shown in good agreement. The generalized rigid-plastic boundaries with optional variables are used to minimize the power by the upper-bound method by using a theoretical model to analyze arbitrary profiles of extrusion dies by Haung et al. [71]. It is explained only by using the four sets of

profile dies (cosine, elliptic, hyperbolic, and conic) with different slopes at the entrance and exit. Experiments are conducted in order to compare the results with those of the theoretical model. It is found that the predicted load and flow patterns are in good agreement with the experimental observation. The elastic plastic behaviour of material and also non-deformable tools are simulated by using the FEM during the product creation process by Post et al. [140]. The simulations have started by considering the half way of the total process and to decrease the total modeling time and to increase the accuracy by means of this measured values. The results of these measurements are used to verify models, based on the transformation behavior of strain-induced martensite. A stress analysis is performed inside plastic zone and inlet and outlet channels depending on contact friction and the billet geometry by considering the equal channel angular extrusion (ECAE) of sufficiently long rectangular billets with different width-to-thickness ratios by Segal V. M. [172]. Also the tools are designed by optimization of the processing mechanics. It is found that flat billets with $W/T>>1$ provide important technical advantages for processing of massive slab-like billets and technology commercialization on the large metallurgical scale. Segal V. M. [166] observed that variations in boundary conditions have a moderate effect on equivalent strains but the strain distribution depends noticeably on friction uniformity and the channel geometry during Equal Channel Angular Extrusion (ECAE) by the slip line method. The characteristic deformation mode corresponds to single shear or to sequence of shears along slip lines. The monotonic loading is realized only in the cases of zero and maximum friction during single pass. Jin et al. [82] have studied the load/displacement and energy-absorption characteristics of AA6061-T6 round extrusions under a cutting deformation mode. The experimental results showed that the cutting deformation mode exhibited a high average crush force efficiency of 0.95 compared to average values of 0.66 and 0.20 for progressive folding and global bending deformation modes, respectively. The mean steady-state was observed 45.58 kN and validated with experiment.

Li S. et al. [113] formulated a comprehensive finite element (FE) model to analyze the formation of the plastic deformation zone (PDZ) and evolution of the working load with ram displacement during a single pass of equal channel angular extrusion (ECAE) with intersection angle 90^0. The PDZ was affected by the strain

hardening and friction by which the material filled the die and also it was governed by the die geometry, independent of material response and friction.

Shin et al. [151] have developed the non-axisymmetric extrusion processes by using the computer program and a new three-dimensional numerical method. A stream-lined die is used to minimize the total extrusion pressure for the extrusion of square, hexagonal and 'T' sections from round billet. The computed results for the cross-sectional grid distortion have been found to be in good agreement with the experimental results. Kar and Das [93] have formulated the SERR technique which has been used to analyze extrusion of I-section bars from square or rectangular billets through square dies and the computed results have been compared with experimental data. There is fair agreement between theory and experiment. The final-stage extrusion load and average length of the extruded products in the square die extrusion of non-axisymmetric bars from round billets are determined by a simple kinematically-admissible velocity field by Kim et al. [94]. Experiments have been carried out with hard-solder billets at room temperature using various shaped dies. The theoretical predictions of the extrusion load and average length of the extruded products are in good agreement with the experimental results. The extrusion of bars of channel section from square or rectangular billets through rough Square dies has been presented by an upper-bound analysis by Sahoo et al. [158]. A class of kinematically admissible discontinuous velocity fields, based on the reformulated SERR technique, is calculated and the velocity field giving the lowest upper-bound is identified. They also computed the upper-bound extrusion pressure for various area reductions. The defects such as twisting and bending in the non axisymmetric square-die extrusion through a model material test are reduced by a new design by Kim et al.[95] In the model material test, L-shaped and U-shaped plasticine bars are extruded by using a square-die, with uniform bearing-land width and a uniform exit velocity of the products. Chitkara and Celik [28] investigated the three-dimensional off-centric extrusion of arbitrarily shaped sections from arbitrarily shaped billets through linearly converging and smooth curved dies are analyzed by an upper bound theory. The extrusion pressures is obtained by upper-bound method, for a given reduction in area, the material property, friction condition and off-centric positioning of the exit cross-section, predictions of the deforming grid pattern, curvature of the extruded products.

The design of three dimensional off-centric extrusions of arbitrarily shaped dies, for the off-centric extrusion of square sections from round billets are developed by using an upper-bound theory and also verified with experiment by Celik and Chitkara [29]. Computations are carried out both for the converging and smooth curved dies. The theoretical predictions are observed to be in good agreement with the experimental results. A new kinematically admissible velocity fields (KAVFs) are proposed by Hwang et al. [69] to determine the forming load, the extruded length and the velocity distribution according to the stroke in the combined extrusion process of a socket wrench from solid cylindrical billets. Experiments are carried out with antimony–lead billets at room temperature at dry condition. The forming load and the extruded length are compared between the theory and the experimental results; it is found that the theoretical predictions are in good agreement with the experimental results. The experimental extrusion force is determined by using an ECAE die with a circular cross-section having sharp corner by Paydar et al. [137]. The developed model predicts that the size of the plastic deformation zone and the relative extrusion pressure increases with increasing the constant friction factor. It is seen that there is a good agreement between the theoretical and the experimental results.

The internal metal deformation is analyzed with the aid of a special transformation combined with the upper-bound method by using the modified method of die construction by Yang and Lan. [196]. The process is discussed for the hydrofilm extrusion of various sections such as squares, rectangles, ellipses and clover shapes and various factors. Experiments are performed for clover and square sections using the dies which are manufactured by NC machine based on the suggested theoretical design. The experimental results are compared with the theoretical prediction and it is seen that the theory is in reasonable agreement with the experimental results. Assempour and Hassannejasil [7] investigated the minimization of the exit profile curvature in non-symmetric T-shaped section for extrusion. A set of non-uniform velocity equations are obtained by using the equations from Chitkara works. The optimum die is designed, which yields the minimum exit curvature by variation of the Bezier coefficients and off-centricity values. To verify the suggested objective functions, the direct extrusion process was simulated physically by

plasticine. Comparisons of the exit curvatures showed good results concerning the objective functions in minimization of the profile curvature.

An upper bound solution to the problem of the prediction of draw stress ratio for the direct drawing of section is investigated by Basily and Sansome [11] and it is shown that the predicted values are higher than those for the drawing of round rod. It is also compared with lower bound solution. The two state variables, the hardness for strain hardening from slip dominated plastic distortion and the porosity for damage from growth of micro voids are included by Lee and Hahm [98]. Simulations of axisymmetric drawing/extrusion have shown that the accumulated porosity in drawing is much bigger than that in extrusion while the difference between the hardness distributions in these processes are insignificant. The effects of the process conditions; such as conical die angle, friction and drawing/extrusion speed and the mechanical properties are also examined. Boer et al. [12] applied the upper-bound approach to drawing of square rods from round billets, by employing a method of co-ordinate transformation.

The pass schedule optimal design in multi-pass extrusion and drawing have presented by using the finite element analysis by John and Hwang [79]. The procedure to calculate the design sensitivities is given, and a numerical test is conducted to evaluate the accuracy of the predicted design sensitivities. Comparison is made between the optimal and initial design to examine the effect of optimization on the process and product.

Lee et al. [112] designed the optimal die profile for uniform microstructure in hot extruded product. The microstructure evolution, such as dynamic and static recrystallization, and grain growth, is investigated by using the program combined with Yada and Senuma's empirical equations and rigid-thermo viscoplastic FEM. The die profile of hot extrusion is represented by a Bezier–curve to generate all the possible die profiles for a given extrusion ratio and initial radius of the billet. It is seen that the theoretical predicted results of simulation is in good agreement with that of the experiment.

Sheng et al. [171] have modeled and analyzed the shape bulb shield by FEM code DYNAFORM v5.2. Simulation prediction matches well with the measurement from the prototype test. A surface distortion problem is also identified and a solution

is obtained through punch nose radius effect on stress distribution analysis. Morrison used the concept of Richmond and Devenpick [142] to design streamlined wired drawing dies of minimum length. The velocity field is proposed by utilizing the principle of volume constancy by means of upper bound theorem and also a thermal-finite element analysis is utilized to determine temperature distribution within the metal as well as to calculate the flow stress of deforming material by Serajzadeh and Mahmoodkhani [173]. The calculated time–temperature curves as well as roll forces have been compared with the measured ones and a good agreement has been observed among them. In this case, relatively lower computational effort is required in comparison with the standard finite element codes. The decrease in apparent density in strip drawing of aluminum for several die angles are computed and compared with that from experiments by Lee and Hahm [109]. Simulations of axisymmetric drawing/extrusion have shown that the accumulated porosity in drawing is much bigger than that in extrusion while the difference between the hardness distributions in these processes are insignificant. The effects of the process conditions, such as conical die angle, friction and drawing/extrusion speed and the mechanical property are also determined. Srinivasan and Venugopal [155] deal with an experimental investigation concerning the open die extrusion (ODE) of three materials of varying physical properties and mechanical properties. Two geometrical configurations (solid and tube) and two methods (by direct and indirect techniques) are considered to examine the influence of these variables in the generation and retention of heat in the deformation zone with the objective of ensuring a greater achievable strain. Jooybari [80] modelled for cold extrusion of aluminium in dry condition. The relationship among radial tip distance, maximum forming load and shear friction factor is characterized by the FEA by Kang et al. [98]. It is observed that the linear relationships among these three are maintained for the various tested materials. It is observed that the linear relationships among these three are maintained for the various tested materials. It is also found that the friction condition at the punch is always higher than that at the lower die interface. Das and Maity [41] computed the mean extrusion and die pressures for a number of die geometries and for different frictional condition at the interface at different reductions by using the slip line field for wedge shaped die. It is found that the mean extrusion pressure increases with increases corresponding to die

angle ‘α’ and friction factor for the transition field. The optimum die angle increases with increase in reduction and friction factor. The Statistical methods applied to the results of the experimental tests indicated that some processes by Caminaga et al. [35] and lubricants could be used as substitutes for common lubricants used in industry, since they presented results of extrusion load and product quality similar to those obtained in the industry with the conventional lubrication. It is found that for just one deformation stage, wheat flour is the best lubricant, and that for two deformation stages, the mineral oil is the best. The efficiency and effectiveness of design of bulk metal forming processes are increased by using finite element simulations by Im et al. [73]. The global average shear friction factor, a linear relationship between the non dimensionalized radial tip distance and shear friction factor is numerically determined for AL6061-O for various lubrication conditions. The global average friction condition at the bottom die interface is determined to be about 60 percent of the one at the punch in the backward extrusion under the present conditions. Yih C. S. [192] suggested the two stream functions for ideal fluid in three dimensions in place of one as in the case of a two-dimensional flow. Each stream function represents a class of surfaces called stream surfaces. The intersection line of two stream surfaces, one taken from each class, is a three-dimensional stream line. Petzov et al. [135] have described a theoretical model of the generalized kinematic velocity field for the axisymmetrical flow of a bi-component system, which can be applied to dies with either straight or curved profiles. A program has been developed for the numerical solution of the theoretical model. It might find application in the computer-aided design of dies having optimal geometrical parameters after improving and optimizing the model. Mihelic and Stok [119] have considered the finite element discretization and non- linear mathematical programming techniques based on the tool design optimization in steady extrusion processes. The minimization energy consumption and the maximization of area reduction are obtained numerically by assuming the Lagrange incremental elastic- plastic finite element formulation in modelling the material flow. The considered optimization approach, are compared to the known theoretical solutions, it is found that the discussed approach is quite effective. Ulysse [181] has considered the design of a plane strain two-hole extrusion dies for uniform exit flow by using the finite-element method combined with techniques of

mathematical programming. The experimental data for a two-out extrusion die with bearings have been used to validate the numerical results. Tryland et al. [180] have carried out uniaxial tensile tests to obtain the variation of the material properties from one aluminium extrusion to another as well as over the cross-section and along the extrusion. The effect of loading and the anisotropy is determined through uniaxial tensile tests in three different directions: 0^0, 45^0 and 90^0 by performing the tension and compression test. Ulysee [182] suggested a numerical model using the finite-element method combined with techniques of mathematical programming for extruding aluminium using the flat-faced die with the traditional die flow correctors. Analytical sensitivities have been developed from the discretized finite-element equations in order to compute the necessary derivatives during optimization. Heiburg et al. [68] have applied material selection methods to the selection of extruded aluminium alloys components. They also investigated the competition between materials cost and processing cost in relation to materials extrudability and shape complexity. Kumar and Prasad [99] developed part drawing of given shape to be extruded by using line, arc, circle, polyline and ellipse entities of AutoCAD Rel-12 and also created the corresponding DXF file. It is combined with a rigid plastic finite element (RPFE) model for steady state axisymmetric hot extrusion using the kinematically admissible velocity field. The temperature distribution in cold as well as hot extrusion process from the upper-bound method has been determined to study the effect of process parameters. There is a good agreement between theory and experiment. Giuliano [59] used commercial finite element software to determine the flow defect in the combined forward–backward cold extrusion of a billet. The final results of numerical simulations and photograph of cross-sectioned part will be used for illustration of manufacturing part. Flat and conical dies of H, T, L, elliptical and two-hole sections have been designed on the basis of upper bound technique for cold and hot extrusion by Kumar and Vijay [102]. Experimental investigation has been conducted for average extrusion pressure in cold case for lead alloy billets and in hot case for commercial grade aluminum billets respectively. Extrusion pressure obtained from both the alloy has been compared with a finite element based commercial package Hyper Xtrude. Theoretical results obtained by the upper bound technique and the Hyper Xtrude are compared well with the experimental results. The diameter ratios

and interferences are determined by using the maximum inner pressure without yielding of rings after shrink fitting and during cold forging by using the maximum inner pressure without yielding of rings after shrink fitting and during cold forging by using Lame's equation by Har et al. [70]. The rigid-plastic FE analysis of backward extrusion process using DEFORM has been performed and the analysis of elastic deformation of the dies has been done by using ANSYS with non-linear contact. In the simulation results, it has been found that the use of high stiffness materials to the first stress ring of forging dies can reduce the elastic deformation of die insert without failure. Zheng et al. [206] carried out numerical analysis using FEM for sheet metal extrusion process.The mesh distortion, the field of material flow, the distributions of the stress and strain can be predicted by using finite element method. By simulating, it is proposed that the extruded material can be divided into five areas according to their different features of deformation, and also the material in the areas of deformation can further be divided into three parts according to their different features of compression and elongation. The experimental results are compared with the simulated results and it is seen that the theory is in reasonable agreement with the experimental results. Johnson et al. [77] have analyzed the extrusion process with plane strain deformation using slip-line field technique by neglecting the elastic strains, work-hardening, temperature, and strain-rate effects. This method is highly successful in clearly defining the rigid and the plastic zones and explained the strain history as observed in a grid deformation test besides predicting the extrusion pressure with reasonable accuracy. Hughes et al. [66] have extruded the mild steel and type 316 stainless-steel billets to bar through flat dies using glass lubrication, reheating temperatures of 1070 degree , 1170 degree , and 1280 degree C, and ram speeds of 25-240 mm/s. under the low effective coefficient of friction (0. 002-0. 011) that leads to extrusion without formation of a dead-metal zone, and hence to a low redundant work factor.

Nagpal et al. [126] carried out analysis of the three-dimenional metal flow in extrusion of different shapes with the help of dual stream function method Tomita and Sowerby [178] carried out an approximate analysis of plane strain deformation of rate sensitive material using numerical technique. The theoretically predicted forming pressure, taking $\alpha = 0.3$, and compared with the available data, showed reasonably

good agreement with the experimental values. The effects of friction, die semi angle, height reduction ratio and material strain hardening on the extrusion load of aluminum are investigated using a finite element procedure based on a dual stream formulation to analyze the plane strain forward extrusion through wedge shaped dies by Hwan [67]. The computed results are compared with the existing analytical solutions and it is seen that the solutions are in reasonable agreement among those results. Leung et al. [114] have presented the development of an effective process of strain measurement for severe and localized plastic deformation. It is found that, only a 10% difference in effective strains between the experimental findings with and without remeshing. Meanwhile, the developed process is further applied to the fine-blanking operation and the strain measurement for fine-blanking is found absolutely accurate. Eivani and Taheri [47] proposed a new method for estimating strain in equal channel angular extrusion (ECAE). A solution is presented for evaluating total strain in those dies consisting of two or more ECAE sub-dies. Narayanasamy et al. [133] have carried out an experimental investigation of aluminium alloy billets during extrusion-forging using different lubricants. It is observed that the protrusion height increases with the increase in the approaching angle for a given extrusion load. The relationship among the various bulge parameters namely the hoop stress, the hydrostatic stress and the stress ratio parameters are also established. Gunasekera and Hoshino [55] have described a new method for obtaining optimal die shape which produces minimum stress in the extrusion or the drawing of non axisymmetric polygonal sections from round bar through straightly converging dies. The forming stress for different regular polygonal sections for a given reduction of area, material property, and frictional condition are determined by using an upper bound technique based on the kinematically admissible velocity field. There is a good agreement between theory and experiment. The extrusion of polygonal sections through streamlined dies by using an upper-bound solution has been investigated by Gunasekera and Hoshino [56]. It is obvious that the streamlined die is superior to the straightly converging dies from the aspect of reducing the extrusion load. This methodology can also be applied for extrusion of other curved dies such as concave and convex parabolic. Narayanasamy et al. [130] have designed the streamlined extrusion die based on the principle of constant area reduction over the length of the die. An attempt is also made

to identify an analytical solution for designing a streamlined extrusion die for a square cross-section. Six kinematically admissible velocity fields are developed for use in upper bound models for axisymmetric extrusion through various dies, including extrusion through adaptable dies and three base velocity fields are also presented by assuming proportional angles, areas and distances from the centerline in the deformation zone by Gordon et al. [60]. Gordon et al. 61] have also presented the six velocity fields for extrusion through a spherical die. The number and distribution of pseudo-independent parameters in the flexible functions, and the form of the angular flexible function are compared for all velocity fields. A spherical extrusion shape is used to evaluate and compare the three velocity fields. From the results it is found that the sine-based velocity field is the best. Further Gordon et al. [62] have modeled the streamlined dies without the surface of velocity discontinuity power terms. Ketabchi and Seyedrezai [103] have analyzed the extrusion of L-section with two different streamlined dies, one with Limason-shaped intermediate section and the other without intermediate section. From the experimental results, it is found that, the extrusion with the second die needs much more energy than that requires for the first die having intermediate section. These important results are in good agreement with macro examination and theoretical analysis of metal flow pattern of L-section extrusion in flat face die. Ponalagusamy et al. [138] have designed the streamlined extrusion dies, based on the fifth order polynomial equation and determined velocity components and strain rates along x, y, and z directions in the deformation zone. It is observed that the velocity components Vx, Vy, and Vz increase with an increase in the extrusion ratio for extruding square and hexagonal sections from the circular billet. However, the rate of increase is less for hexagonal section as compared to the square cross section for the same extrusion ratio. Chitkara and Adeyemi [25] have obtained the experimental results by upper bound solution by using SERR technique for extrusion of I and T shaped sections from square billets through the curved die at different fraction area reduction. Yang et al. [140] have derived a generalised kinematically admissible velocity field for axisymmetric extrusion through curved dies by considering rigid-plastic boundaries expressed in terms of arbitrarily chosen continuous functions. A third-order and fourth-order polynomial is chosen for the die boundary and the bounding function for the plastic region respectively. The work hardening effect is

considered in the formulation. The plastic boundaries as well as stream lines are affected by various process parameters. Hoshino and Gunasekara [72] have proposed the extrusion of square sections from round billet by an upper bound solution.The major advantage of the method is that it only requires the establishment of the streamline of a particle in a three-dimensional coordinate system. Kar and Sahoo [104] have analyzed the extrusion of square bars from round billets. The circular cross section of the round billet is approximated by a regular polygon of equal area and the number of sides of the polygon is progressively increased until convergence of the extrusion pressure is achieved. Sahoo et al. [159] have analyzed the extrusion of hexagon-section bars from round billets through linearly converging dies. It is found that, the optimal die-geometry (the equivalent semi-cone angle) can be obtained for different reductions of area and friction conditions for reasonable upper-bound extrusion pressures. This can be extended to obtain the solution of generalized problems of non-axisymmetric extrusion or drawing through converging dies. Sahoo [162] has carried out experimental work to compare some of the theoretical results predicted using SERR analysis. Experiments are performed for hexagon, channel, triangle and cross-type sections from rectangular billets using square dies. The upper-bound analysis of extrusion of different sections through square dies can be carried out by using proposed discontinuous velocity field. The theoretical results are compared with experimental non-dimensional mean extrusion pressure and it is found to within 14% for the range of reductions studied. Sahoo and Kar [163] have investigated the drawing of hexagon section bars from round billets through the straightly converging dies. The SERR technique is eminently suitable for analyzing drawing/extrusion of sections having re-entrant corners. The approximation of the curved surface to planer surfaces and the three dimensional nature of the problem gives higher value which can be minimized by increasing the number of sides of the polygon and the number of floating points. It can be concluded that for the limited purposes the present technique can be extended to obtain solution for generalized non-axisymmetric drawing or extrusion through converging dies. The computations are carried out by Celik and Chitkara [30] to predict the upper-bound to the extrusion pressures, the deforming grid patterns and curvature of the extruded product for a given reduction in area, material property, friction condition and off-centric circular

sections with varying die lengths and reduction in areas. The theoretical predictions are observed to be in good agreement with the experimental results. Sahoo and kar [164] have attempted to find an upper bound solution for the extrusion of square section from round billet through the taper die. The SERR (Spatial Elementary Rigid Region) technique is modified and approximated to get a class of KAVF, which is used to obtain the lowest upper bound. This velocity field is utilized to optimize the non-dimensional average extrusion pressure and the equivalent die angle for every relevant combination of the coefficient of friction and reduction of area. Sahoo [167] has extruded the T-section bars from round billet through straight taper die. Computation for the upper bound pressure is carried out for various process variables such as area reduction, die angle and interface friction. The theoretical predictions are compared with that of known experimental results and found to be well within engineering accuracy. Sahoo et al. [175] have applied an upper bound solution for the extrusion of channel section from round billet through the taper die. The rigid-perfectly plastic model of the material is assumed, and the spatial elementary rigid region (SERR) technique is presented for which the kinematically admissible velocity field is found out by minimizing the plastic dissipation of power. The present analysis allows for specification of process control parameters and their relation to extrusion load, equivalent die angle, reduction ratios and friction factor. Nagpal and Altan [125] used the dual stream function method to formulate kinematically admissible velocity fields in case of three-dimensional metal deformation processes.

Chang and Choi [23] have proposed an upper bound solution for extrusion through axisymmetric curved dies. Chang and Choi [24] have presented the velocity fields of tube extrusion problems through curved dies for an incompressible material. These velocity fields are also applicable to conical and square- cornered dies. The graphical presentation is also shown for the tube extrusion processes through conical dies of small cone angle and also the effect of die geometry and friction. Nagpal et al. [125] have considered an axisymmetric extrusion of a rigid-perfectly plastic material through curved dies under steady state conditions. A computer program is written to obtain the boundaries which yield the lowest upper-bound for a given reduction, length of the die and frictional conditions at die surface. Comparison of theoretical flow fields with experimental visioplasticity data for conical dies, are observed to be

in good agreement with the experimental results. Yang and Lee [193] have proposed a new method of analysis for the extrusion of arbitrarily shaped sections through curved die profiles by an upper-bound method to compute pressure for extrusion through curved die profiles for a complex section with a curved boundary.

Cho and Yang [26] have investigated the hydro film extrusion process which includes strain-hardening effects and viscosity variation in the fluid due to pressure by applying an upper-bound method and hydrodynamic lubrication theory for the analysis of metal forming and fluid flow respectively. Experiments are carried out at room temperature, for several reductions of area, using axisymmetric curved dies and it is seen that the extrusion pressure shows good agreement with experimental verifications for mild steel using castor oil as the lubricant. Cho and Yang [27] have used the upper-bound method and hydrodynamic lubrication theory for considering the work-hardening effect of metal and the variation of fluid viscosity. Experiments are carried out at room temperature for various diameter ratios of the tube, using the axisymmetric curved die. The theoretical prediction of extrusion pressure shows good agreement with experimental measurements for mild steel specimens, using castor oil as the lubricant. Yang et al. [197] have derived a generalised kinematically admissible velocity field for axisymmetric extrusion through curved dies by employing rigid-plastic boundaries expressed in terms of arbitrarily chosen continuous functions. A third-order and fourth-order polynomial is chosen for the die boundary and the bounding function for the plastic region respectively. The extrusion pressure, the final effective strain of the extruded billet, and the grid distortion patterns in axisymmetric forward extrusion through arbitrarily curved dies has been analysed by Yang [199]. The process parameters are optimized by using an upper-bound extrusion pressure and also a biquadratic polynomial is chosen for the die profile. Experiments are carried out for AISI 4140 steel billets at room temperature and it is seen that the extrusion pressure shows good agreement with experimental results. Maity [117] investigated the extrusion of square section from square billet through mathematically contoured die with profiles such as cosine, circular, parabolic, elliptic and hyperbolic using upper-bound method. It is concluded that cosine die profile yields the minimum extrusion pressure. Yang et al. [200] have analyzed the noncircular sections such as elliptic and clover-leaf sections through curved dies by finite element analysis for

steady-state three-dimensional extrusion. The work-hardening effect is considered by integrating the effective strain rate along each stream line through interpolation by the least squares method. Experiments are carried out at room temperature and the experimental results are compared with numerical results in flow pattern and strain distribution. Yang et al [201] have concerned with an analysis of forward extrusion of composite rods through curved dies. The upper-bound method is employed to determine the extrusion pressure for various process variables. The experiments are carried out with commercially pure aluminum and copper billets for various reductions of area and cone angles at room temperature. The comparison shows that the second-order flow function is in better agreement with the experimental observation both in extrusion loads and in deforming regions. Maity et al. [118] have proposed an upper-bound analysis for the extrusion of square sections from square billets through curved dies having prescribed profiles. Kinematically-admissible velocity fields are derived using the dual-stream-function technique. It is shown that a cosine-shaped die with zero entry and exit angles yields the lowest extrusion pressure in the absence of friction, whilst the best upper-bound is provided by a straight tapered die under sticking-friction conditions. The non-dimensional extrusion pressure for varying reductions are computed for extruding square bars from square billets through the curve die by Sahoo et al. [156]. The results are compared with slip-line field solution as well as experiments. Wifi et al. [186] have determined the extrusion pressure of the hot forward rod extrusion process for arbitrarily curved dies is obtained by implementing an incremental slab method. The material used is carbon steel, the shape of the optimum curved die profile is found to depend on the extrusion ratio, coulomb-friction coefficient and not to be affected by the extrusion velocity. It is found that the optimum curved die profile produces lower stress levels than those produced using the optimum conical die profile found in the earlier literature by using FEM analysis. Ponalagusamy et al. [136] have investigated the extrusion process through bezier die profile and compared the results with polynomial die profile. It is observed that the Bezier curve based dies yields lower extrusion pressure compared to other dies for constant friction factor and area of reduction. Narayanasamy et al. [132] have investigated the upper bound method for extrusion of circular cross-section from circular billet through cosine profile. It has been found

that the die designed based on cosine profile is superior to the conventional shear dies and the straightly converging dies. It is also proposed to validate the results by the experiments. Frisch and Mata-Pietric [51] have investigated the upper bound solutions with experimental flow studies through different axisymmetric curved dies with analytic geometry but failed to investigate for three dimensional extrusions through mathematically contoured dies. Gatto and Giarda [54] have analyzed the SERR (Spatial Elementary Rigid Regions), a three-dimensional kinematic model by limit analysis for plastic deformation. The characteristics of some spatial figures, the limit analysis of the three dimensional cases are considered as particularly useful in partitioning the plastic volume together with some simple applications of the methods to practical cases of extrusion. Sahoo et al. [168] have analyzed the spatial elementary rigid region (SERR) technique for extrusion of section having re-entrant corners and the extrusion of triangular section bars from round billets through linearly converging dies. The circular cross-section of the round billet is approximated by a regular polygon of equal area and the number of sides of the approximating polygon is progressively increased until convergence of the extrusion pressure is achieved. Sahoo et al. [160] investigated the steady-state non-dimensional extrusion of asymmetric polygonal section bars through rough square dies by an upper bound solution with the SERR technique for the single point formulation and the non-dimensional average extrusion pressure is minimum when billet aspect ratio is one for the both sections. Wang et al. [188] observed that the compressive tests of Zr–Cu–Ni–Al metallic glass are performed with different strain rates at a temperature of 683 K. According to the experimental results, the forming evolution of a metallic glass micro-gear is simulated using a finite element simulation software DEFORM 3D, and the forming load is predicted at different processing parameters. The predicted work piece geometry shows good agreement with experimental result. It is found that the finite element simulation results are in reasonable agreement with the experimental observation. Jufu et al. [83] investigated the extrusion on room temperature mechanical properties of cast Mg–9Al–Zn alloy, such as yield strength, ultimate tensile strength and elongation can be enhanced heavily by equal channel angular extrusion. Park et al. [141] evaluated the effects of surface morphology and voids formed in the metal sheet–prepreg interface of GLARE laminates. The experiments

were carried out with aluminum sheets on which the surface morphology was systematically varied by different roughness levels of surface textures (sanding and nylon-pad abrasion) and chemical etches. An exponential relationship was obtained between ILSS, roughness and autoclave pressure for GLARE laminates. Through experimental studies, appropriate processing parameters should be optimized to achieve acceptable GLARE laminate construction. Segal [176] discussed the possible approaches for realization of continuous equal-channel angular extrusion (ECAE) and also investigated Slip line field solutions for different cases of active and passive frictions. It is found that CECAE provides lower extrusion pressure, higher effective strains and better approximation to simple shear deformation mode than ordinary ECAE. Optimization of the main characteristics is performed for the concept of CECAE with an additional coining roll. Masoudpanah and Mahmudi [123] employed the shear punch testing (SPT) technique and the uniaxial tension tests to evaluate the mechanical properties of the equal channel angularly pressed (ECAPed) AZ31 magnesium alloy. They also studied the microstructural, textural evolutions and deformation behavior of the extruded and ECAPed AZ31 magnesium alloy. It is found that the ECAPed alloy showed lower yield strength and higher tensile ductility, as compared to the extruded materials. It was concluded that shear punch testing technique could be used in the study of directional mechanical behavior of the ECAPed magnesium alloys.

Song and Yue-hui [177] studied the effects of die-pressing pressure and extrusion on the microstructures and mechanical properties of powder metallurgy fabricated SiC particle reinforced pure aluminum composites by optical microscopy, SEM microscope and mechanical testing machine. Kucukomeroglu [105] investigated the mechanical and wear properties of severely deformed Al–12Si alloy by equal-channel angular extrusion/pressing (ECAE/P) and also applied the equal-channel angular extrusion technique to the as-cast eutectic Al–12Si alloy to improve their tensile properties and wear resistance. Nagpal [126] has done some theoretical and experimental investigation of three-dimensional metal-forming problems by using the converging dies.

It is evident from the literature review that extrusion process seems to be an emerging technology with economical process for production of product of different

shapes with improved mechanical property and better surface integrity. But it is also highly essential to reduce the extrusion load with smooth flow of material in the deformation zone to reduce the power consumption and the rejection of the product due to poor quality. In order to achieve the above requirements, the geometry of die profile plays a significant role. The converging dies play critical role in reducing the extrusion load with improvement of smooth flow of material in the deformation zone compared to flat or square die. Till date, a lot of investigations on extrusion through square dies have been reported. But work reported for three dimensional extrusions through converging die is not adequate despite its advantages over square dies. In the present investigations a class of solutions has been presented for three dimensional extrusions through linear or non-linear converging die for extrusions of different sections from round as well as square billets under different frictional boundary conditions using both upper bound method and finite element modeling. The theory is verified by partial validation of experiments.

1.9 Objective of the Present Investigation

(i) Upper bound analysis of extrusion of triangular, rhomboidal, pentagonal and octagonal sections from round billet using SERR technique through linear converging dies.

(ii) An upper bound analysis of extrusion of square section from square billet through polynomial shaped die using dual stream function method.

(iii) An upper bound analysis of three-dimensional extrusion through mathematically contoured Bezier shaped die for extrusion of square section from square billet using dual stream function method.

(iv) FEM modeling of extrusion of square section from square billet through Bezier, polynomial and cosine shaped die.

(v) Design of non-linear converging die profiles for extrusion from round billet to triangular and square sections

(vi) FEM modeling of triangular and square section from round billet through curved dies.

(vii) Partial validation of experiment.

1.10 Outline of the Thesis

Chapter I is devoted to introduction and the review of literature on two and three dimensional process analysis of extrusion.

Chapter II deals with the theoretical analysis of upper bound technique for three-dimensional metal deformation problems

Chapter III deals with the upper bound solution for the extrusion of triangular and rhomboidal sections through linear converging dies using discontinuous velocity fields through SERR technique. The upper bound loads are calculated using the corresponding optimum discretization scheme.

Chapter IV deals with the upper bound solution for the extrusion of pentagonal and octagonal sections through linear converging dies using discontinuous velocity fields through SERR technique. Also the upper bound loads are calculated using the corresponding optimum discretization scheme. The effect of product and billet geometry on mean extrusion pressure is also examined.

Chapter V deals with upper bound techniques employed for the analysis of three dimensional metal deformation problems based on dual stream function method. Attention is especially focused on the continuous velocity field method where a general procedure is suggested for the determination of the velocity field when the deformation occurred during the extrusion of square sections from square billet through polynomial and bezier shaped curved dies. 3D FEM modeling has been carried out for extrusion of square sections through cosine, bezier, and polynomial die profile using DEFORM software.

Chapter VI deals with the development of geometry of a mathematically contoured non-linear converging die profile from round to triangular and square section. Further FEM modeling has been carried out for extrusion of triangular and square section from round billet using 3D-DEFORM software.

Chapter VII deals with experimental investigation of extrusion of different sections through linear and non-linear converging die for extrusion of different sections from round and square billet. Experimental set-up has been fabricated for extrusion of different sections with different die profiles.

Chapter VII deals with the conclusions and the future scope of the present investigation.

Upper Bound Technique for Three-Dimensional Metal Deformation Problems

2.1 Introduction

For problems relating to many metal working operations, exact solution for the load to cause unconstrained plastic deformation is either non-existent or is too difficult to compute. In such cases, approximate analysis is available to establish the deformation load. Two such approximate methods have found extensive application in the analysis of quasi-static metal forming process, viz., the upper bound and the lower bound techniques.

The upper-bound theorem predicts the power necessary to perform the desired metal forming at the prescribed velocities. However, since the velocity field for a given problem is generally not known, the power for any velocity field as calculated by the upper-bound theorem is greater than or equal to the actual power.

The development also applies to any velocity field which satisfies the boundary and plasticity requirements. Thus for any possible velocity field there also exists an associated total power. The actual velocity field is that which minimizes the associated total power and the actual total power is the minimum associated total power. The formal statement of the upper-bound theorem is that amongst all kinematically admissible velocity fields, the actual field minimizes the work-function *J*, where:

$$J = J_1 + J_2 + J_3 \tag{2.1}$$

In which J_1 is the work dissipated for internal deformation.

For a material obeying Levy-Misses flow rule, the internal power J_1, is given by

$$J_1 = \frac{2\sigma_0}{\sqrt{3}} \int_v \sqrt{\tfrac{1}{2}\dot{\varepsilon}_{ij}\dot{\varepsilon}_{ij}}\; dv \tag{2.2}$$

Where, σ_0 = yield stress in uniaxial tension, and

ε_{ij} = strain rate tensor which is defined as

$$\varepsilon_{ij} = \frac{1}{2}\left[\frac{\partial V_i}{\partial X_j} + \frac{\partial V_j}{\partial X_i}\right] \tag{2.3}$$

Here, V_i and V_j represents the velocity components in Carteian coordinates.

J_2 is the work dissipated at surfaces of velocity discontinuity.

$$J_2 = \frac{\sigma_0}{\sqrt{3}} \int_{S_i} |\Delta V|_{S_i} dS_i \tag{2.4}$$

and J_3 is the work dissipated due to friction at the die-work piece interface (Jth face):

$$J_3 = \frac{m\sigma_0}{\sqrt{3}} \int_{SD_i} |\Delta V|_{SD_i} dS_{D_i} \tag{2.5}$$

where m is the friction factor and $|\Delta V|_{Si}$ and $|\Delta V|_{SDi}$ are the magnitude of velocity discontinuities at the surfaces S_i and S_{Di} respectively.

The power J, calculated from equation (2.1), will be exact when the kinematically admissible velocity field postulated for the forming process under consideration is actual one, but, if it is different from the actual, equation (2.1) yields an upper bound to the power necessary for the forming operation in question. This is precisely the upper bound method as suggested by Hill [64] for a rigid and perfectly plastic material.

This chapter is devoted to a brief discussion of the various technique normally employed to derive kinematically admissible velocity fields in case of three-dimensional metal deformation problems. While such techniques for plane strain problems are well established, their application to three-dmensional problems is relatively recent. The following section presents a brief review of the methods normally employed to construct admissible velocity fields for three-dimensional problems. A generalized procedure is presented to construct the velocity field when the deformation zone is subdivided into rigid tetrahedral blocks.

2.2 Theory and analysis of the extrusion

Extrusion is one of the best amongst all metal forming processes; advantages of metal forming process: (i) Saving in material due to less wastage (ii) Strength is increased due to cold work and better grain flow. (iii) Corrosion and wear resistance are improved (iv) Fatigue properties are improved (v) Better tolerances in geometry and size of the product (vi) Production rates are increased.

2.3 Metal forming analysis

The analysis of the stresses in the metal working process has been an important area of plasticity for the past few years. Since the forces and the deformations generally are quite complex, it is usually useful to use simplifying assumptions to obtain a traceable solution. As the strain involved in plastic deformation process is very large, it is usually possible to neglect elastic strain and consider only the plastic strain (rigid-plastic region). The strain hardening is also neglected. The principal use of analytical study of metalworking process is for determining the forces required to produce a given deformation for a certain geometry prescribed by the process and is the ability to make an accurate prediction of the stress, strain, and velocity at every point in the deformed region of the work piece, since the calculations are useful for selecting or designing the equipment to do a particular job. In this area an existing theory is generally adequate for the task. In general, any theory consists of three sets of equations: (i) Static equilibrium of force equation; (ii) Levy Mises equation expressing a relation between stress and strain rate; (iii) Yield criterion

In general case, these are nine independent equations containing nine unknown's six stress components and three strain rate components. While an analytical method is only possible if a sufficient number of boundary conditions are specified, the mathematical difficulties in general solutions are formidable. The most analysis of actual metal working process is limited to two dimensional, symmetrical problems.

The methods of analysis in increasing order of complexity and ability to predict final details are;

(i) The slab method of analysis; (ii) Slip line field theory; (iii) Upper bound solution; (iv) Lower bound solution; (v) Finite element analysis

(i) The slab method of analysis

This method assumes that the metal deforms uniformly in the deformation zone. A square grid placed in the deformation zone would be distorted into rectangular elements. It is the easiest method and widely used in strength of material. It calculates the average forming stress from the work of plastic deformation.

(ii) Slip line field theory

This method assumes the no homogeneous deformation and is based on the fact that any general state of stress in plain strain consists of pure shear plus a hydrostatic pressure. Slip line is in fact a two dimensional vector diagram, which shows the deviation of maximum shear stress identified with the direction of slip at any point. Slip line is always a network of lines possessing crossing each other at right angle .It is built up by trial and error method.

(iii) Upper bound solution

An upper bound analysis provides an overestimation of the required deformation force. It is more accurate because it will always result in an overestimation of the load that the press or the machine will be called upon to deliver. In this case factor of safety will be automatically built in. In this analysis, the deformation is assumed to take place by rigid body movement of triangular blocks in which all particles in a given element moves with the some velocity. A kinematically admissible velocity should satisfy the continuity equation, velocity boundary condition and volume constancy condition. The power of deformation calculated from this is higher than the actual one, called upper bound. When applying upper bound, the first step is to conceive of a velocity field for the deforming body. There exists an infinite no stress field that satisfy the prescribed condition for a lower bound solution and an infinite number of velocity that satisfy the upper bound condition.

(iv) Lower bound solution

The power of deformation calculated from statistically admissible stress field which satisfies the stress equilibrium and yield criterion is always lower than the

actual one, it is called lower bound solutions. Lower bound solutions are those, which provide values for the total power, which are lower than the actual one. Here the first step is the formulation of a stress tensor, which is far more difficult to conceive. It is more complex to analyze, so less work has been performed. Thus, only equation of equilibrium, yield criterion and statistical boundary condition are the only requirements. The assumed stress field i.e. velocity field is never of such general form as to include all admissible fields due to our limited capability in handling the mathematics in the most general form.

(v) Finite element analysis

Finite element method involves extensive computations mostly repetitive in nature. Hence, this method is suitable for computer programming and solutions. Of these problems can be obtained easily using programming on electronic digital computers. Finite element computer programs have become widely available, easier to use and can display results with attractive graphics. It is hard to disbelieve finite element results because of the effort needed to get them and the polish of this presentation. It is possible that most finite element analyses are so flawed that they cannot be trusted. Even a poor mesh, improper element type, incorrect loads or improper supports may produce results that appear reasonable in casual inspection.

The finite element method, developed originally as a concept of structural analysis, is being extensively applied now-a-days to wider regions of non-structural problems. Metal forming is one of such regions. With the advent of high speed personal computer the finite element analysis, which was previously the exclusive domain of larger systems, now can be performed on one's desktop in a cost-efficient and convenient way. The analysis of FEM has been carried out in the present investigation by using commercial package, DEFORM-3D.

2.4 Different Techniques for deriving the Kinematically Admissible Velocity in three -dimensional metal deformation problems.

Five techniques have been reported to find out the kinematically admissible velocity fields for Three -Dimensional metal deformation problems.

(i) Dual stream function method

(ii) Conformal Transformation Technique

(iii) Generalized velocity field technique, and

(iv) SERR technique

The first three techniques lead to continuous velocity fields in the deformation region where the velocity at any point is described by a continuous function of the space coordinates whereas the fourth method leads to discontinuous velocity fields.

2.4.1 Dual stream function method

For ideal fluid in three dimensions, Yih [192] suggested the use of two stream functions in place of one as in the case of a two-dimensional flow. Each stream function represents a class of surfaces called stream surfaces. The intersection line of two stream surfaces, one taken from each class, constitutes the three-dimensional stream line. Nagpal [125] used these dual stream functions to determine kinematically admissible velocity fields for different three-dimensional plastic flow problems.

Let φ_1 (x, y, z) and φ_2 (x, y, z) be two continuous functions satisfying the boundary conditions on velocity. These two functions, therefore, can be treated as a pair of dual stream functions. The three velocity components are then given as:

$$V_x = \left(\frac{\partial \varphi_2}{\partial y}\right)\left(\frac{\partial \varphi_1}{\partial z}\right) - \left(\frac{\partial \varphi_1}{\partial y}\right)\left(\frac{\partial \varphi_2}{\partial z}\right) \tag{2.6a}$$

$$V_y = \left(\frac{\partial \varphi_2}{\partial z}\right)\left(\frac{\partial \varphi_1}{\partial x}\right) - \left(\frac{\partial \varphi_1}{\partial z}\right)\left(\frac{\partial \varphi_2}{\partial x}\right) \tag{2.6b}$$

$$Vz = \left(\frac{\partial \varphi_2}{\partial x}\right)\left(\frac{\partial \varphi_1}{\partial y}\right) - \left(\frac{\partial \varphi_1}{\partial x}\right)\left(\frac{\partial \varphi_2}{\partial y}\right) \tag{2.6c}$$

The velocity field generated through equations ((2.6a) to 2.6c)), become kinematically admissible since the continuity condition is implicitly satisfied. The only limitations of this procedure are that it may be extremely difficult to find dual stream functions when the shape of the section is complex or when it involves re-entrant corners.

2.4.2 Conformal transformation technique

In ideal fluid flow problem in three dimensions, the equation of a stream line is given by

$$\frac{dx}{V_x} = \frac{dy}{V_y} = \frac{dz}{V_z} \tag{2.7}$$

By finding a transformation function that transforms an intermediate section in the deformation zone along the axis into a unit square (or circle), it can be stated as

$$\frac{dx}{F(x, y, z)} = \frac{dy}{G(x, y, z)} = \frac{dz}{1} \tag{2.8}$$

Functions F and G depend upon the parameters of the section geometry which are the functions of x, y and z. Comparing equations (2.7) and (2.8)

$$\frac{V_x}{F(x, y, z)} = \frac{V_y}{G(x, y, z)} = \frac{V_z}{1} \tag{2.9}$$

The axial velocity components V_z is found by applying the continuity condition (or volume constancy condition) to the deformation zone. Thus

$$V_z = \frac{A_b V_b}{A(Z)} \tag{2.10}$$

where, A_b, V_b = billet cross-section area and billet velocity respectively, and A(z) = cross-sectional area of the die cavity at any point on z-axis. Hence the velocity components V_x and Vy can be calculated using equation (2.9)

This method is similar to the dual stream function method in the sense that in either case the velocity at any point in the deformation zone is calculated from the corresponding equation for the stream line through that point. But this method is more versatile and can deal with problems involving relatively complex geometries for which dual stream functions may be difficult to guess. With all these advantages, however, its application is limited to only such sections where the shape of the product is similar to that of billet. Hence it is more suitable for polygonal sections with axial symmetry (sections that can be inscribed in a circle) but may lead to considerably difficulties when dealing with sections with re-entrant corners.

2.4.3 Generalized velocity field technique

The conformal Mapping Technique discussed in the preceding section suffers from three basic limitations. These are : i) for a mapping function to exist, the sectional symmetry must be maintained throughout the deforming region, ii) surfaces of velocity discontinuity at entry and exit must be assumed planner, and iii) velocity across any intermediate section in the deforming zone must be assumed constant so that it can be calculated from the continuity condition. Hence the conformal mapping technique can be applied only to limited problems.

When the billet and the product shapes are dissimilar, section symmetry does not exist the deforming region, such a situation is encountered when a polygonal shape is extruded from a round billet. Yang and his associates [193,195] have proposed a method in which the velocity at any point in the deformation zone is expressed as a general function of the space coordinates. The proposed method has none of the limitations of the conformal mapping technique and has been used to analyze extrusion of clover and regular polygonal sections from round billets. This method is also suitable for predicting intermediate shapes of the die profile when extrusion is carried out with the help of converging dies. However, this method is tedious and involves considerable amount of computation for prediction of upper bound load.

2.4.4 The SERR Technique

The SEER (spatial elementary rigid region) technique for analysis of three dimensional metal deformation problems was first proposed by Gatto and Giarda [54]. The distinguishing feature of this technique is that the deformation zone is discretized into rigid regions thus providing a discontinuous velocity field in the deformation zone.

In plane strain solution, the velocity in a rigid region is determined when its components along two mutually perpendicular directions are known. Thus, the problem involves only two unknown and two equations necessary to determine them are obtained by considering the mass continuity condition on two faces bordering this rigid region. Hence the planner rigid region is

always a triangle and this has formed the basis for the construction of the well known velocity fields by Johnson

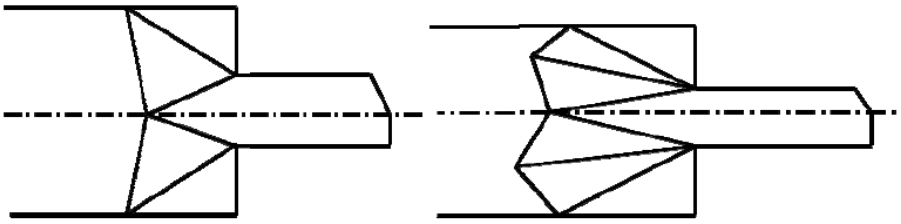

Fig. 2.1 Johnson's Velocity Fig. 2.2 Kudo's Velocity field

and kudo shown in Fig 2.1 and Fig 2.2 for plane strain extrusion. In a three dimensional deformation problem, however, the spatial velocity in a rigid zone has three unknown components and their determination necessitates the setting up of three equations from the mass continuity condition. Thus the spatial elementary rigid region for a three dimensional deformation problem must be tetrahedral in shape. This is the basic of the SERR technique as proposed by Gatto and Giarda [54]. The above authors analyzed the extrusion of square section through wedge shaped dies with the help of the SEER technique. They also suggested method by which complex geometrical shapes like prism and pyramid can be discretized into elementary tetrahedrons. The limitation of this technique appears to be applied only when the deformation zone is bounded by planner faces.

In the SERR technique, the deformation zone is envisaged to consist of tetrahedral rigid blocks, each block separated from others by planes of velocity discontinuity. Each rigid region has its own internal velocity vector consistent with the boundary conditions. Thus, if there are N rigid blocks, then the number of unknown internal velocity vectors is also N (thus, 3N spatial velocity components). The velocity at entry to the deformation zone (the billet velocity) is considered to be prescribed and the velocity at the exit has a single component since its direction is known from the physical description of the problem. Therefore the total number of unknown velocity components in the global level becomes 3N+1. All these unknown

velocity components can be uniquely determined if an equal number of equations are generated. This is done by applying the mass continuity condition to the bounding faces of all the tetrahedral rigid blocks taken together. It may be noted that the set of velocity equations so generated becomes consistent and determinate if and only if the SERR (spatial elementary rigid region) blocks are tetrahedral in shape, so that, the number of triangular bounding faces automatically becomes 3N+1.

To illustrate the application of the above principles, let the ith bounding face in the assembly of tetrahedrons be in the plane

$$\phi(x, y, z) \equiv a_{i1}x + a_{i2}y + a_{i3}z + 1 = 0 \tag{2.11}$$

The coefficients a_{i1}, a_{i2} and a_{i3} in Eq. (2.11) above can be determined by specifying the co-ordinates of the three vertices of this triangular face. Then the unit normal vector to this face is

$$\hat{n} = \frac{\nabla \phi}{\left| \nabla \phi \right|} \tag{2.12}$$

If V_1 and V_2 are the velocity vectors on both sides of the ith face, the condition for continuity is

$$\hat{n}_i \, . V_1 = \hat{n}_i \, . V_2 \tag{2.13}$$

A determinate set of velocity equations is generated by applying equation (2.13) to all the bounding faces in the assembly of tetrahedrons. The boundary conditions on the velocity field are also enforced through this equation. For example, if a face lies on a plane of symmetry then the right-hand side of equation (2.13) is made zero to admit the condition that no mass flow occurs normal to these faces.

2.5 Discretisation of the deformation zone in Extrusion

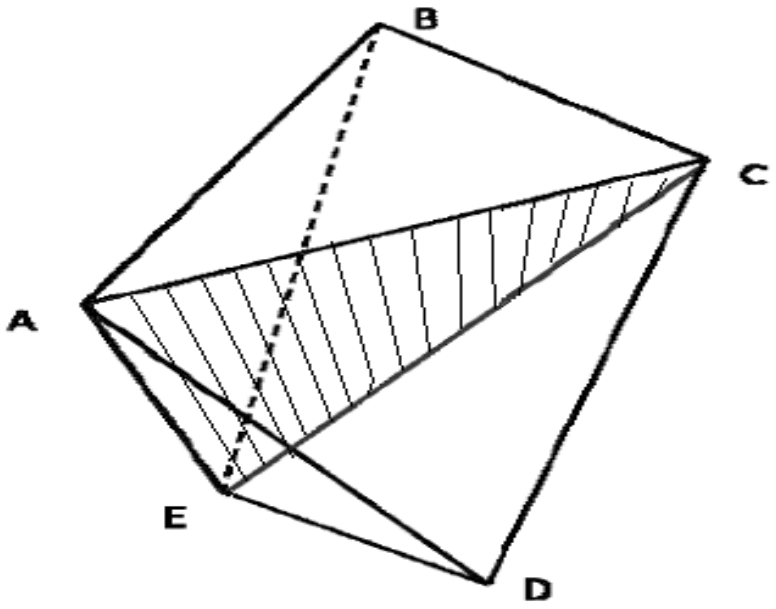

Fig. 2.3 Discretization of pyramid into two tetrahedrons

Pyramid: ABCDE; Tetrahedrons: 1. ABCE 2. ACDE; Common face: ACE

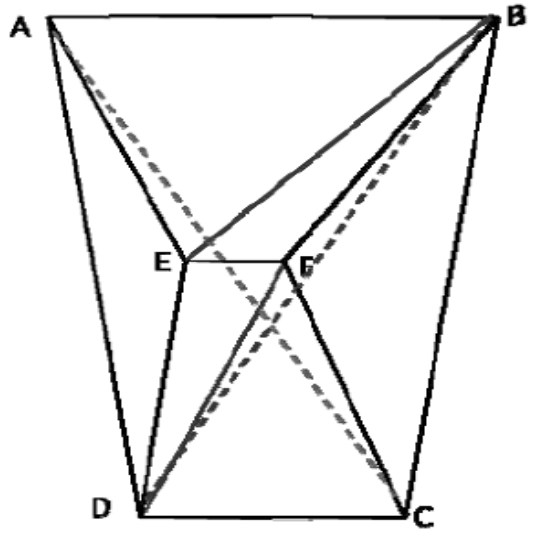

Fig. 2.4 Discretization of prism into three tetrahedrons

Prism: ABCDEF; Tetrahedrons are: 1. ABED, 2. BEDF, 3. BFDC; Common faces are: 1. BED for tetrahedrons 1 and 3, 2. BFD for tetrahedrons 2 and 3.

The deformation zone in extrusion may consist of simply a pyramid as in case of extrusion of triangular section during taking one floating point or combination of pyramids and prisms as in case of triangular section extrusion during taking double floating point. A pyramid can be discretized into two tetrahedrons as demonstrated in Fig 2.3. These two tetrahedral regions have two internal velocity vectors one for each region having six component by choosing a coordinate frame. When the inlet velocity for this pyramidal zone is prescribed, these are seven unknown velocity components to be determined to establish the velocity field. Thus seven equations are necessary and sufficient to determine the velocity field. The two tetrahedrons of pyramidal region have a common face. Thus there are seven independent bounding faces which on applying the continuity condition, generate a set of seven equations which contain the unknown velocity components on solving this set of seven velocity equations, the velocity field is uniquely determined.

In similar fashion, a prism can be discretized into three tetrahedrons with ten independent bounding faces that can generate a set of ten velocity equation for establishing the corresponding velocity field. The discretization of a prism into tetrahedrons is shown in Fig 2.4. When a deformation zone consists of a combination of pyramid and prisms the discretization of the combined region into tetrahedrons and subsequently application of continuity condition to all the independent bounding faces, generate a system of determinate velocity components. The prism and pyramid can be discretized into 3 tetrahedrons in 6 and 2 different ways respectively shown in table 2.1.

The deformation zone in case of metal forming that occurs in a closed channel (such as extrusion or drawing), can be sub-divided into sub-zones that are prismatic, pyramidal or tetrahedral in shape or a combination of these shapes. Since the elementary blocks are to be tetrahedral in nature, the prismatic or pyramidal sub-zones are discretised ultimately into tetrahedrons.

Table 2.1 Conversions of Prism and Pyramid into Tetrahedron

Structure	Total No. of Tetrahedrons	No. of ways
Pyramid	2	2
Prism	3	6

2.6 The Continuity of a Discontinuous Velocity Field

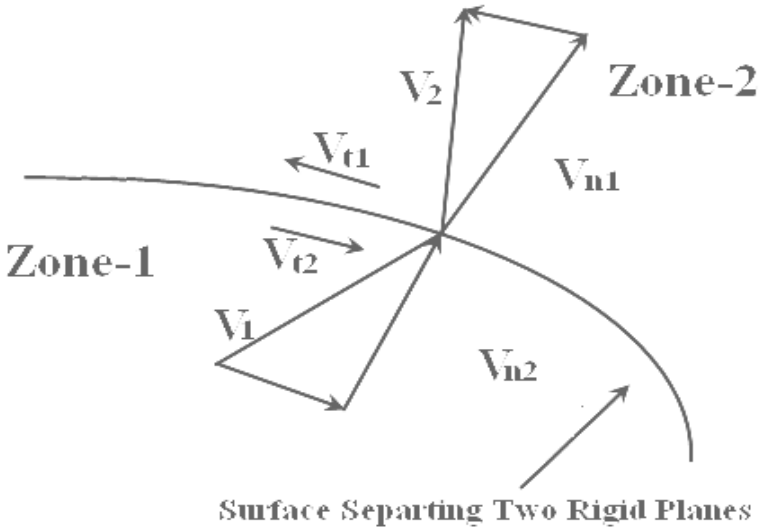

Fig 2.5 A general surface separating two rigid region

The Fig.2.5 shows a surface separating two spatial regions with V_1 and V_2 as the velocity vector on both sides. The components of these two vectors normal to the separating surface Φ are given by the equation (2.14) and (2.15)

$$\vec{V}_{1n} = \hat{n}.\vec{V}_1 = \left(\nabla\phi/|\nabla\phi|\right).\vec{V}_1 \tag{2.14}$$

$$\vec{V}_{2n} = \hat{n}.\vec{V}_2 = \left(\nabla\phi/|\nabla\phi|\right).\vec{V}_2 \tag{2.15}$$

If A and ρ denotes the surface area of the segment and the material density respectively, then the mass flow rate across the surface segment taken from both sides. Thus the mass continuity condition (also known as volume constancy condition, since the material is incompressible) i. e.

$$(\rho A)_1.V_{1n} = (\rho A)_2.V_{2n} \tag{2.16}$$

From the equation 2.14 and 2.15, cancelling $|\nabla\varphi|$ which is scalar quantity so that V_{1n} and V_{2n} must equal, so?

$$\nabla\phi.\vec{V}_1 = \nabla\phi.\vec{V}_2 \tag{2.17}$$

It is to be pointed out that the regions on both sides of the surface Φ in Fig (2.5) are rigid if $\vec{V}_1$ and $\vec{V}_2$ are constant velocity vectors with equation (2.15) being linear. The linearity of equation (2.16) is assured when surface Φ is a plane. Thus the bounding face may lie on the die surfaces or planes of symmetry. Since no material flow occurs across faces, equation (2.17) takes the following form;

$$\nabla\phi.\vec{V}_1 = 0 \qquad (2.18)$$

The equation of each of the triangular faces can be determined when the co-ordinates of three vertices are specified. Then the velocity equation can be formed by applying the mass continuity condition either in the form of equation (2.16) or (2.17) as appropriate. The velocities of material in the zones are V1 and V2 respectively are not identical. The components of velocity in the normal and tangential direction of the surface are Vn1 , Vn2 and Vt1, Vt2. The normal velocity Vn1 should be equal to Vn2 for the continuity of the material. The tangential velocity Vt1 and Vt2 need not be equal. The difference is called the velocity discontinuity ΔV and is given as follows

$$\Delta V = V_{t1} - V_{t2} \qquad (2.19)$$

The method of solution elucidated in the previous section is illustrated here taking the example of a plane strain extrusion process. The geometry of the process is shown in Fig. 2.6 for a through square die. Dead metal Zones ABC and DEF are formed on both side of the extrusion axis. Only one half of the deformation zone, consisting of the triangle ABO, is considered for this analysis. Thus, this triangle planner elementary rigid region is bounded by lines AB, BO and AO which are also lines of velocity discontinuity. The co-ordinate frame shown Fig 2.6 is taken such that the x- axis coincides with the extrusion axis.

2.7 Solution of a Plain Strain Problem

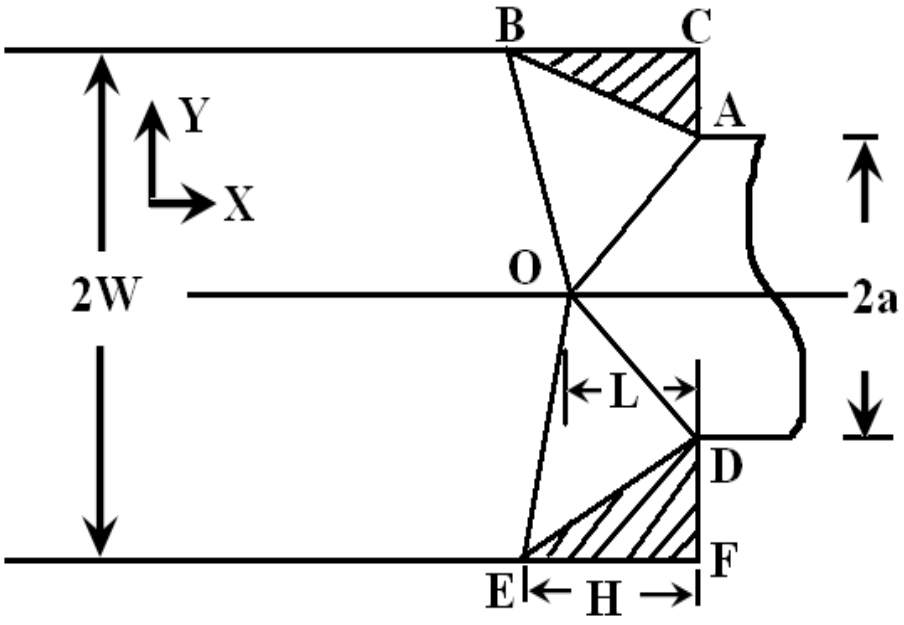

Fig. 2.6 Solution of a Plain Strain Extrusion

Therefore the billet and product velocity vectors have only one component each. The co-ordinates of the vertices A, B and O are (0, a), (-H, W) and (-L, 0) respectively. It is to be noted here that while a and W are known parameters , being the half widths of the product and the billet respectively, L and H are two parameters of the deformation zone which are not a prior known. H is the overall length of the deformation zone along the extrusion axis and L is the distance of the flow of the floating-O from the midpoint of the die orifice. These two lengths are to be selected such that the power of deformation becomes minimum. Mathematically speaking, L and H are variable with respect to the deformation power is minimized.

In terms of the co-ordinates of the vertices, the equations of the three bounding lines are given by

Line AB :[((W-a)/H).x] +[y-a] = 0 (2.20)

Line BO: [(W / (H-L)).x] +y+ W.L/ (H-L) = 0 (2.21)

Line OA = ((a/l).x) +y-a = 0 (2.22)

If the billet velocity V_b is prescribed, there are three unknown velocity component in this case. These components are V_p, the product velocity, and V_x and V_y, the x-and y- components of the velocity vector in the elementary rigid region.

The line AB in Fig 2.6 is the limiting line for the dead metal zone. Material enters the deformation zone across line BO and the product leaves the deformation zone through line AB . Table 2.2 shows these lines and the corresponding velocity vectors on both side of the line. The physical description of side of each line is also given in the same table.

Employing the mass continuity condition given equation (2.20) and (2.21) as appropriate to these lines, the three velocity equations are obtained as given below:

[(W-a) / H]. V x +V y =0 (2.23)

[W (H-L)] .V x + V y = [W / (H-L)] .V b (2.24)

Table 2.2 Lines, the zone they separated and velocity vector on their sides

Line and their equations	Side 1	Velocity vector on side 1	Side 1	Velocity vector on side 1
AB Φ=[(w-a).x]/L+[y-a]	Deformation zone	$_iV_x + _jV_y$	Dead metal zone	0
BO Φ= Wx/(H-L)+y+WL/(H-L)=0	Deformation zone	$_iV_x + _jV_y$	Billet	iV_b
OA Φ=[ax/L]+y-a=0	Deformation zone	$_iV_x + _jV_y$	Product	iV_p

(-a/ L). V x + V y = - (a/L) 0. V p (2.25)

On solving this set of linear equation V x , V y and V p, the velocity vectors are obtained as shown in equations (2.26) (2.27) (2.28).

$$V_x = (H.\ W.\ V_b) / (H.\ a + L.W - a.\ L) \quad (2.26)$$

$$V_y = [(W-a)\ W.\ V_b)\ ] /[H.\ a = L.\ W-a.\ L) \quad (2.27)$$

$$V_p = W\ V_b/a \quad (2.28)$$

Since the elementary region is rigid, strain rate tensor in region is zero. Therefore the power for internal deformation, J_1 is not zero. Further, the dead metal zone separates the deformation zone from the die surface and as such, there is no relative motion between the two. Therefore there is no dissipation power due to the friction at the diameter faces i.e. (J_3 =0). Thus the power consumed for deformation is dissipated only at the lines of velocity discontinuity. Therefore in this case, equation (2.1) reduces to the following form.

$$J = J_1 + J_2 \quad (2.29)$$

In the present analysis, all the lines of velocity discontinuity separate rigid regions. Hence the absolute values of the velocity discontinuities at each line are constant.

$$J = \left(\frac{2\sigma_0}{\sqrt{3}}\right)\int \sqrt{(\varepsilon_{ij}\varepsilon_{ij})}dV + \left(\frac{\sigma_0}{\sqrt{3}}\right)\int |\Delta V|_s\, dS + \left(\frac{m\sigma_0}{\sqrt{3}}\right)\int |\Delta V|_{s_f}\, ds_f \quad (2.30)$$

The upper bound to the deforming power can be calculated using equation. (2.29), the upper bound so obtained can be optimized with respect to the parameter H and L and the minimum upper bound (J_{min}) , to the deformation power can be obtained corresponding to this velocity field. The average non-dimensional extrusion pressure is determined from the relation: that can be calculated from the equation.

$$\frac{P_{avg}}{\sigma_0} = \frac{J_{\min}}{WV_b\sigma_0} \quad (2.31)$$

It may be noted that the solution is similar to that presented by Johnson [74] using the hodograph method. This solution is given here only as a demonstration of the planer elementary rigid region (PERR) technique which is the two-dimensional representation of the reformulated SERR technique.

CHAPTER -3

3D Upper-Bound Modeling for Round-to-Triangular and Rhomboidal Section Extrusion using the SERR Technique through Linear Converging dies.

3.1 Introduction

Extrusion is a massive deformation process not only to produce cylindrical bars or hollow tubes but a large variety of irregular cross sections. It is one of the fastest growing metal working methods having definite advantages over other metal deformation process like rolling for the production of complicated and re-entrant sections. For the extrusion of sections, linearly converging dies with lubricants are more preferred to square dies, as the former provide a gradual change in shape and reduction of area simultaneously resulting uniform microstructure. It is highly desirable to study the mechanics of metal deformation in order to optimize the process. Very often, many empirical rules are followed to determine process parameters, extrusion load and geometries of die profile. However, empirical relations have limited applications and can not be applied universally under various conditions. The upper-bound technique appears to be an approximate tool for investigating 3D metal forming problems which is having some specific advantage over finite element method as well as slip-line field method.

Amongst the different metal forming processes, extrusion has definite advantages over others for the production of three-dimensional section shapes. Now it is becoming essential to pay greater attention to the extrusion of section rod from round stock, as this operation offers the promise of an economic production route. The process is also attractive because press machines are readily available and the necessity to purchase expensive section stock corresponding to a multiplicity of required sections is eliminated. Theoretical consideration of this process has been become now of prime concern as simple analytical techniques can not yield valid

---

Based on the papers, entitled

1 A Numerical Application of SERR Technique for extrusion of Round-to-Triangle sections with unequal sides through linearly converging dies, accepted to be published in an International Journal of Manufacturing Technology and Research.

relationships. It has been very difficult to determine the appropriate working conditions of extrusion and to design the optimum die shape and dimensions for the required product. For a long time, those matters have been based on empirical knowledge. For the extrusion of sections, converging dies with lubricants are preferred to flat-faced square dies, as these dies provide a gradual change in shape and a reduction in area simultaneously. Again, the flat-faced or so-called square die has the disadvantages of enhancing the work-hardening effect, requiring high extrusion force and limited extrusion speed. Despite the advantage of converging dies, only a few theoretical approaches to extrusion or drawing processes have been published for three dimensional extrusions.

The present investigation is based on 3D upper bound method using SERR (spatial elementary rigid region) technique for the analysis of extrusion of round-to-triangular sections of different geometry through a linear converging die. The linear converging die is having some specific advantage over the flat faced die in respect of low friction, less redundant work and more uniform grain structure. For the sake of the present analysis, it is assumed that the centroid of die aperture lies on the billet axis. This assumption is necessary so that the product remains straight as it comes out of the die orifice. The curved surfaces are approximated to the planar surfaces to apply SERR technique. A comprehensive computational model was developed to determine the normalized extrusion pressure using a multivariate unconstrained optimization technique by Kuester and Mize [87]. The extrusion pressure has been computed for various semi-cone angles with different reductions and friction factors.

3.2 The SERR method analysis

In the SERR (spatial elementary rigid region) method of analysis, the deformation zone is discretized into rigid region thus leading to a discontinuous velocity field. When these rigid regions are in shape of tetrahedron, a determinate set of equation is obtained (by application of continuity condition to individual faces defining the rigid region) from which the velocity component in such rigid region can be calculated. It is appropriate to mention that friction surface zone are part of proposed velocity field (zone of zero velocity) and upper bound theorem admits any velocity field as long as it is kinematically admissible.

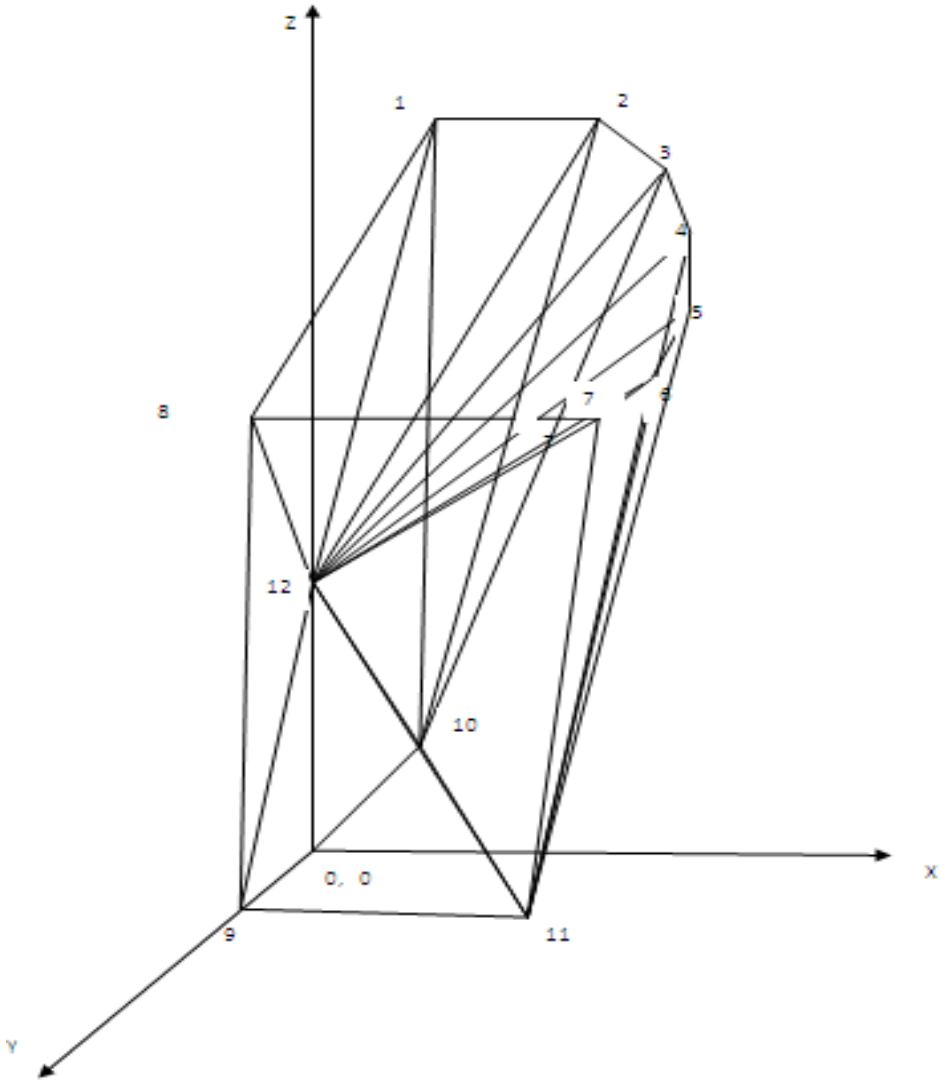

Fig. 3.1 (a) One half of the deformation zone of 12 sided polygon with single floating point

One half of the deformation geometry for triangular section is considered as shown in Fig. 3.1(a), because of symmetry about one plane. The sub zones of deformation are delineated in domain of interest by taking suitable located floating points. Referring to Fig.3.1 (a) analysis is done by taking one floating for the domain as interest for discretization. The deformation zone is to be discritized into two pyramidal subzones (12-3-4-10-11) (Fig. 3.1(b)) and (12-7-8-9-11) (Fig. 3.1 (c)) and

five tetrahedral subzones (Fig. 3.1 (d)). Hence it results in nine tetrahedrons and the number of global schemes of discretizing of different zones being four. Table 3.1 describes different planes with normal velocity for Fig. 3.1 (b) for scheme 2. It can also be defined similarly for scheme 1 and Table- 3.2 for fig. 3.1 (c). The deformation zone is to be discritized into two pyramidal subzones (12-3-4-10-11and 12-7-8-9-11) and five tetrahedral subzones (12-1-2-10, 12-2-3-10, 12-4-5-11, 12-5-6-11 and 12-6-7-11). Similarly Table (3.3 -3.7) describes different planes with normal velocity for five different tetrahedrons. Table (3.8) defines number of planes of two pyramids and five tetrahedrons.

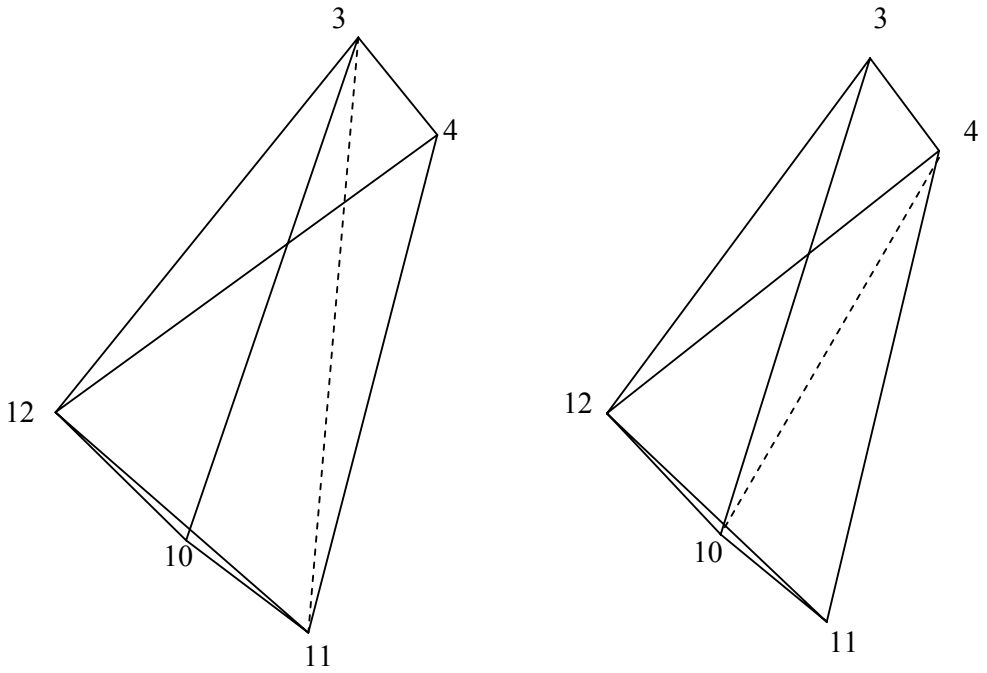

Scheme 1
Tetrahedrons
1. 12-3-4-11
2. 12-3-11-10

Scheme 2
Tetrahedrons
1. 12-3-4-10
2. 12-4-10-11

Fig. 3.1 (b) Schemes of discretization for the pyramidal subzone 12-3-4-10-11

Table-3.1 Various surfaces, types and their normal velocity (Pyramid 12-3-4-10-11, Scheme2)

Surface	Category	Normal velocity on that surface
12-3-4	Entry surface	Billet velocity (V_b)
12-3-10	Internal plane	Unknown velocity
12-4-10	Internal plane	Unknown velocity
4-10-11	Friction surface	0
3-4-10	Friction surface	0
12-11-10	Exit plane	Product velocity (V_P)
12-4-11	Internal plane	Unknown velocity

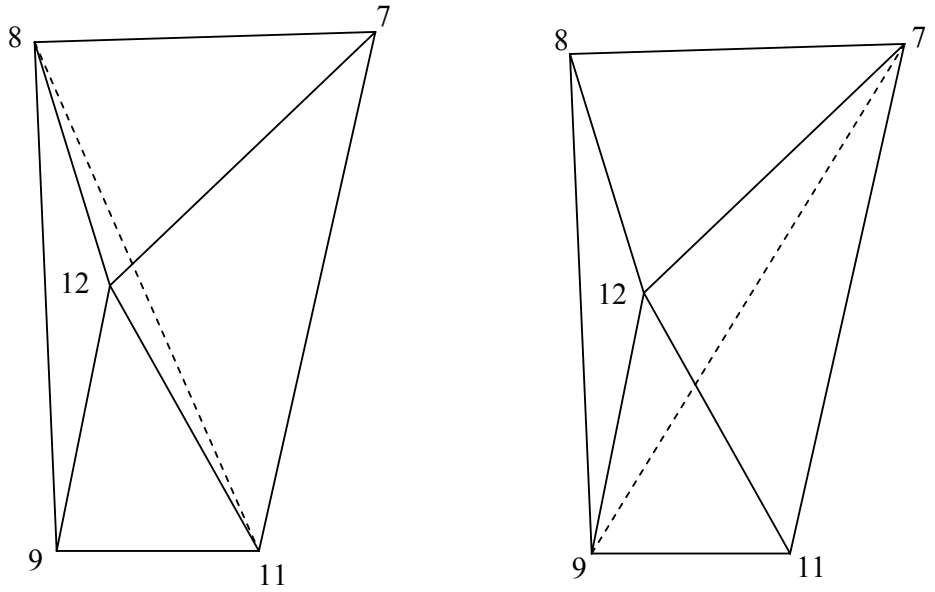

Scheme 1
Tetrahedrons
1. 12-8-9-11
2. 12-7-8-11

Scheme 2
Tetrahedrons
1. 12-8-7-9
2. 12-9-7-11

Fig. 3.1 (c) Schemes of discretization for the pyramidal subzone 12-7-8-9-11

Table-3.2 Various surfaces, types and their normal velocity (Pyramid 12-7-8-9-11, Scheme2)

Surface	Category	Normal velocity on that surface
12-7-8	Entry surface	Billet velocity (V_b)
12-8-9	Symmetry surface	Unknown velocity
12-7-9	Internal plane	Unknown velocity
7-8-9	Friction surface	0
7-9-11	Friction surface	0
12-7-11	Internal plane	Unknown velocity
12-9-11	Internal plane	Unknown velocity

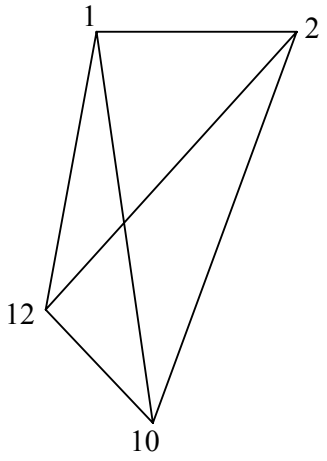

Tetrahedron: 12-1-2-10

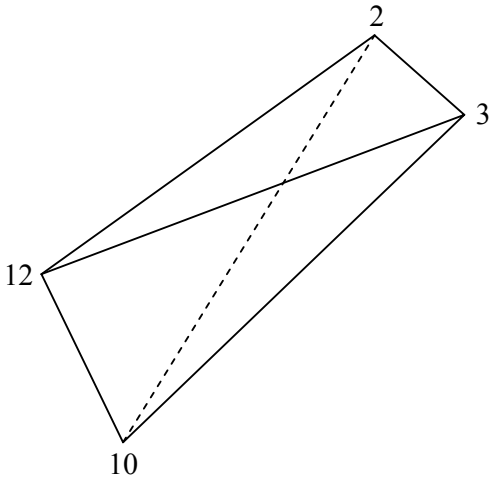

Tetrahedrons: 12-2-3-10

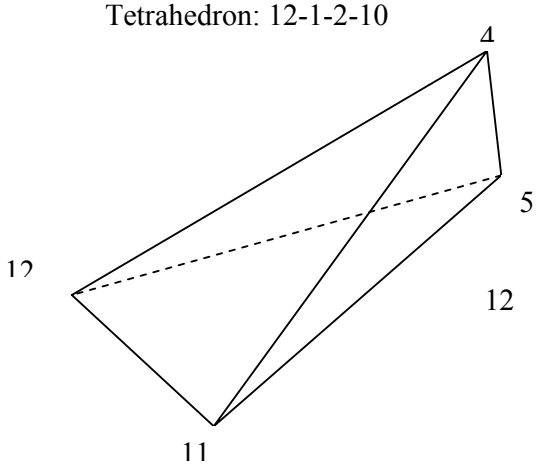

Tetrahedron: 12-4-5-11

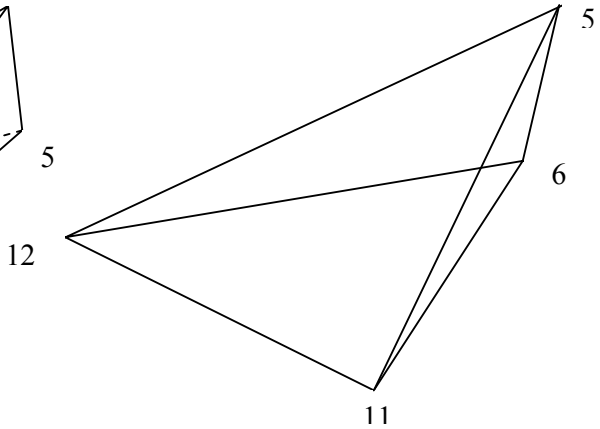

Tetrahedron: 12-5-6-11

Continue in the next page

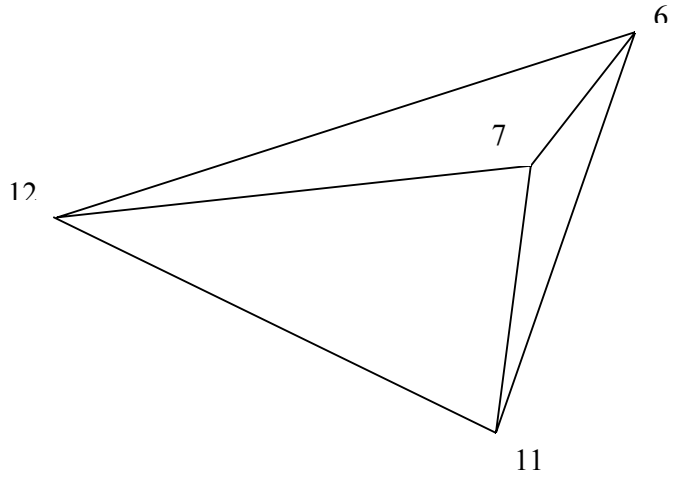

Tetrahedron: 12-6-7-11

Fig. 3.1 (d) Discretization for the tetrahedral subzone.

Table-3.3 Various surfaces, types and their normal velocity (Tetrahedron: 12-1-2-10)

Surface	Category	Normal velocity on that surface
12-1-10	Internal plane	Unknown velocity
1-10-12	Friction surface	0
12-2-10	Internal plane	Unknown velocity
12-1-2	Internal plane	Unknown velocity

Table-3.4 Various surfaces, types and their normal velocity (Tetrahedron: 12-2-3-10)

Surface	Category	Normal velocity on that surface
12-2-3	Entry surface	Billet velocity (V_b)
12-3-10	Internal plane	Unknown velocity
2-3-10	Friction surface	0
12-2-10	Internal plane	Unknown velocity

Table-3.5 Various surfaces, types and their normal velocity (Tetrahedron: 12-4-5-10)

Surface	Category	Normal velocity on that surface
12-4-11	Internal plane	Unknown velocity
4-5-11	Friction surface	0
12-5-11	Internal plane	Unknown velocity
12-4-5	Entry surface	Billet velocity (V_b)

Table-3.6 Various surfaces, types and their normal velocity (Tetrahedron: 12-5-6-11)

Surface	Category	Normal velocity on that surface
12-5-11	Internal plane	Unknown velocity
12-5-6	Entry surface	Billet velocity (V_b)
5-6-11	Friction surface	0
12-6-11	Internal plane	Unknown velocity

Table-3.7 Various surfaces, types and their normal velocity (Tetrahedron: 12-6-7-11)

Surface	Category	Normal velocity on that surface
12-6-7	Entry surface	Billet velocity (V_b)
6-11-7	Friction surface	0
12-7-11	Internal plane	Unknown velocity
12-6-11	Internal plane	Unknown velocity

Table- 3.8 Half extrusion zone (domain of interest) divided into pyramid and tetrahedron

Sub-zones	Model numbering system	No. of plane faces
1. Pyramid	12-4-5-11-10	8
2. Pyramid	12-7-8-9-11	8
3. Tetrahedron	11-12-10-2	4
4. Tetrahedron	2-12-10-3	4
5. Tetrahedron	3-12-10-4	4
6. Tetrahedron	5-12-11-6	4
7. Tetrahedron	6-12-11-7	4

Each pyramid can be divided into two tetrahedrons in two different ways as discussed in earlier chapter. Hence the total deformation zone can be subdivided into 9 numbers of tetrahedrons in 4 different ways i. e. (2x2) shown in below Table (3.9) and the total number of plane derived from the pyramid and tetrahedron shown in Table (3.10).

Table-3.9 Number of planes and ways of discretization

No. of Tetrahedrons	No. of planes	No. of ways
2x2+1+1+1+1+1=9	9x4- (8)(common plane) = 28	2x2

Table 3.10 Total number of planes of Pyramids and Tetrahedrons

Subzones	Model numbering system	Numbering of different planes	No. of planes	Total no. of common planes	Total no. of planes
Pyramid	12-3-4-10-11	12-3-4 12-3-10 12-4-10 4-10-11 3-4-10 12-11-10 12-4-11	7	12-3-4 3-10-12 12-11-10 12-4-11 12-7-11 12-2-10 12-11-6 12-11-5 (8 common planes)	(8+8+4+4+4+4+4)-8= 28
Pyramid	12-7-8-9-11	8-7-12 8-9-12 12-9-11 12-7-11 12-7-9 7-9-11 7-8-9	7		
Tetrahedran	12-1-2-10	1-12-10 12-1-2 2-12-10 10-1-12	4		
Tetrahedran	12-2-3-10	12-2-3 12-3-10 2-3-10 2-10-12	4		
Tetrahedran	12-4-5-11	12-4-11 4-5-11 12-5-11 12-4-5	4		
Tetrahedran	12-5-6-11	12-5-6 5-6-11 6-11-12 5-11-12	4		
Tetrahedran	12-6-7-11	6-12-11 12-7-11 6-7-11 6-7-12	4		

3.3 Formulation of the Present Solution

As mentioned earlier, the SERR technique can be applied where there are plane boundaries. Hence, the curved surface is to be replaced by planar surfaces so as to accommodate the SERR analysis**.**

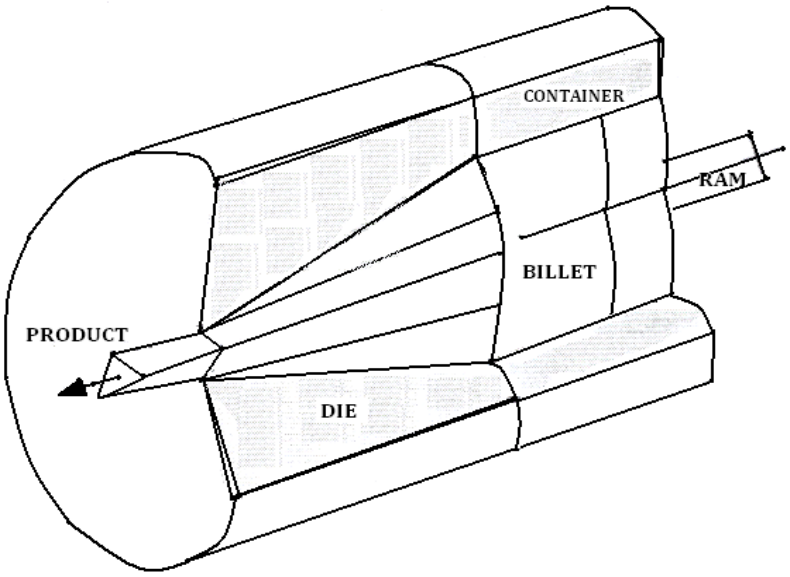

Fig. 3.2 Direct extrusion of a Triangular section from a round billet

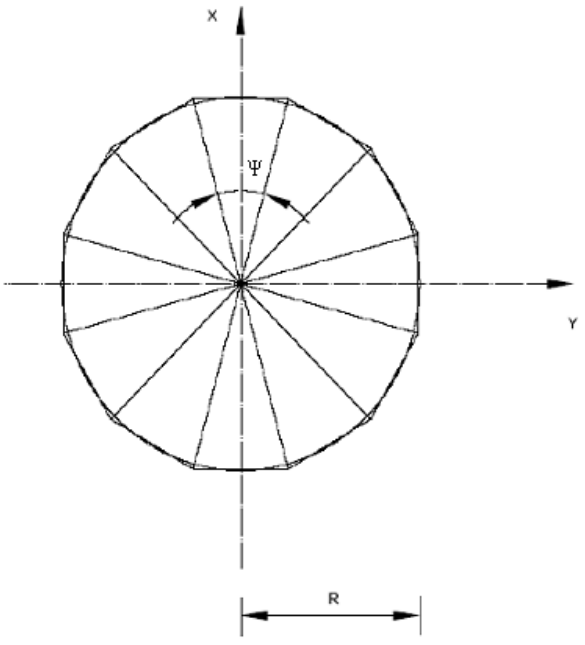

Fig 3.3 Approximation of a circular section into regular polygon of 12 sides

Fig. 3.2 shows the die geometry bounded by curved surfaces due to the round billet. For the present analysis the round billet is approximated by a regular polygon with 12 sides (as there is a negligible change of computed value by further increasing the sides**).** To approximate the circular cross-section of the billet into a regular polygon, the cross-sectional areas of the billet and the approximating polygon must be maintained equal as shown in Fig. (3.3), this condition being written as:

$$\Pi \; R^2 = \frac{1}{4} M \; L_1^{\,2} \; Cot \left(\frac{\psi}{2} \right) \qquad (3.1)$$

where R= radius of the round billet; M= number of polygon sides; L_1=length of each side of the approximating polygon; Ψ= internal angle of the regular polygon. From the die symmetry, only one half of the deformation zone is considered for analysis as seen in Fig.3.1 (a) and Fig. 3.5.

The upper bound load has been computed using discontinuous velocity field. The discontinuous velocity field has been obtained by discretizing the deformation zone into tetrahedral blocks using reformulated SERR technique. The reformulated SERR technique is applied to find out the optimum kinematically velocity field to get the upper bound solution.

As per the principles laid down in reference by Kar and Das [93], the sub-zones of deformation are delineated in the domain of interest by taking a suitably located floating point. For illustration, Fig. 3.1(a) shows one-half of the deformation zone with a single floating point on the extrusion axis at a distance from origin, all the corner points being joined to it. The resulting pyramid and tetrahedrons are the ultimate deformation sub-zone for the SERR formulation.

All these sub-zones are interconnected and have common triangular faces. Thus the basic SERR blocks in their totality have 28 bounding faces, so that as all these bounding faces are triangular in shape, by applying equation (2.12 of chapter-2), 28 velocity equations can be obtained. When these equations are solved, an equal number of velocity components can be obtained for this formulation (the discretisation details are summarized in Table 3.11).

Table 3.11 Summary of discretisation schemes

Type of sub-zones	2 pyramids 5 tetrahedrons
Total number of SERR blocks	2+2+5x1=9
Number of discretisation schemes	2x2=4
Number of triangular faces	28
No. of velocity components	9x3=27 for 9 SERR and 1 at exit Total=28

3.4 Definition of the equivalent semi cone angle

The description of the cone angle (2θ) and equivalent semi cone angle (θ) is shown in figure 3.4. D is the diameter of the round billet. The area of extruded product is made equivalent to a circular cross-section with a diameter equal to D_1. L is the die length. The 'θ' (Theta) as shown in the figure is the semi-cone angle. Here the equivalent semi-cone angle is defined as the semi-cone angle of a conical die where the reduction in area is the same, as that of a polygonal section.

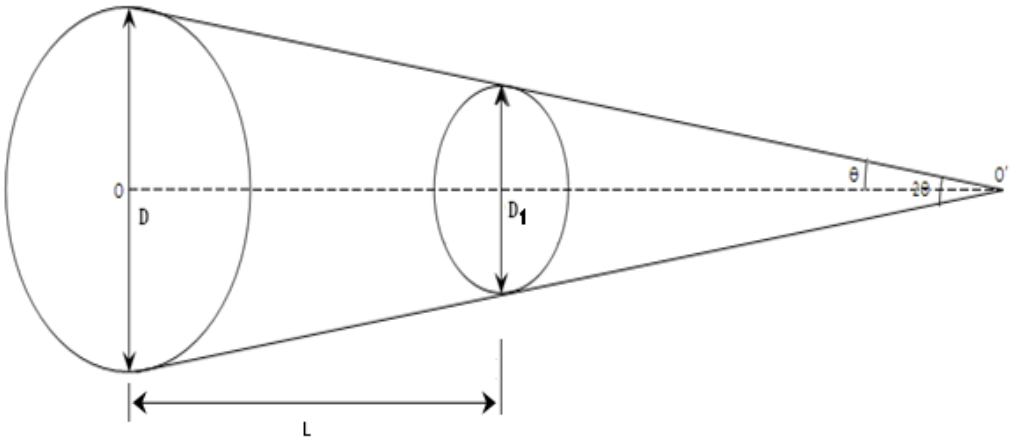

Fig 3.4 Diagram for equivalent semi cone angle.

3.5 Calculation of velocity components

Each tetrahedron move with a unique velocity. The internal velocity of each tetrahedron is V_1, V_2, and V_3 …….. V9 (as there are 9 numbers of tetrahedrons) when resolved into components along the co-ordinate axis V_1, V_2, V_3 ……..V_9 together have 28. The billet and product velocity vector, V_b, V_p along the extrusion axis (z-axis) are the nonzero component each. With prescribed billet velocity V_b, the product velocity V_p is taken as unknown. Thus, there are 28 unknown velocity components. When mass continuity condition is applied to all 28 bounding faces of these 9 tetrahedrons, then 28 equations are obtained. These 28 equations being a determinate set are solved simultaneously to give all the unknown velocity components.

Here the floating point (12) has 2 unknown co-ordinates. Using these co-ordinates, the equation of plane containing 28 triangular faces under consideration can be determined. Since a velocity discontinuity is permissible only along the tangential direction, the normal component on side of faces must be equal. A validity of equation is carried out under following consideration.

(a) Normal velocity at the die billet interface (friction-surface) is zero.

(b) Normal velocity in symmetry plane is same.

$$V_1 = \sqrt{\left[V_{1x^2} + V_{1y^2} + V_{1z^2}\right]} \tag{3.2}$$

$$V_2 = \sqrt{\left[V_{2x^2} + V_{2y^2} + V_{2z^2}\right]} \tag{3.3}$$

$$V_9 = \sqrt{\left[V_{9x^2} + V_{9y^2} + V_{9z^2}\right]} \tag{3.4}$$

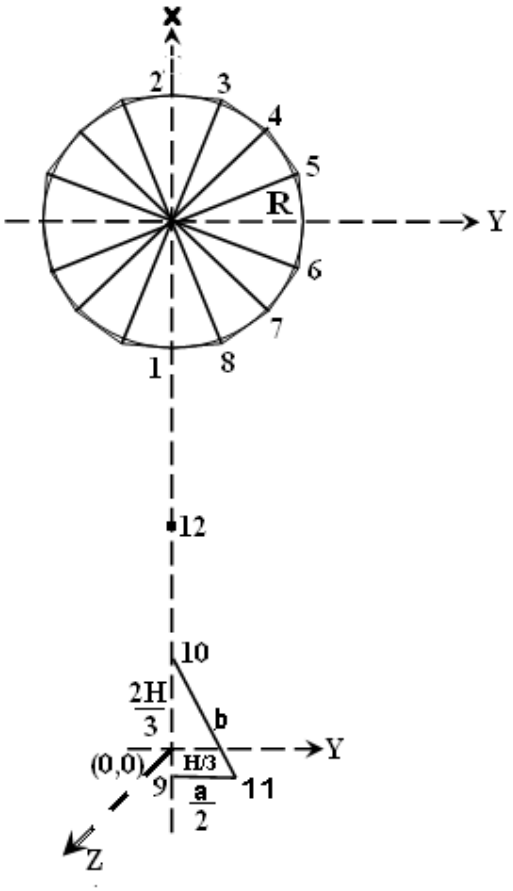

Fig 3.5 Co-ordinates of the half of the Triangular section

Table 3.12 Co-ordinates of points in deformation zone

Points	X-co-ordinate	Y-co-ordinate	Z-co-ordinate
1	-R Cos(11π/12)	0	L
2	R Cos(π/12)	0	L
3	R Cos(π/12)	R Sin(π/12)	L
4	R Cos(π/4)	R Sin(π/4)	L
5	R Cos(5π/12)	R Sin(5π/12)	L
6	R Cos(7π/12)	R Sin(7π/12)	L
7	R Cos(9π/12)	R Sin(9π/12)	L
8	R Cos(11π/12)	R Sin(11π/12)	L
9	-H/3	0	0
10	2H/3	0	0
11	-H/3	a/2	0
12	0	Y_{12}	Z_{12}

Knowing the co-ordinates of points, equation of all triangular faces 28 can be found out. But for simplicity a mathematical approach for equation of triangular face 4-5-10 can be expressed

$$\begin{vmatrix} X & Y & Z & 1 \\ R\,Cos(\pi/4) & R\,Sin(\pi/4) & L & 1 \\ R\,Cos(5\pi/12) & R\,Sin(5\pi/12) & L & 1 \\ 2H/3 & 0 & 0 & 1 \end{vmatrix} \qquad (3.5)$$

Similarly equation for all 28 planes can be set up. With this theoretical approach a matrices of (28x29) with suitable sub-program is solved to get required unknown velocity components (V_{1x}, $V_{1y,}$ V_{1z}) …….. ($V_{9x,}$ $V_{9y,}$ V_{9z}) and V_p along Z-direction. After getting the velocity components, the resultant velocity at each plane faces are then carried out.

3.6 Calculation of area of triangular faces in deformation zone

Knowing the co-ordinates of each plane face in deformation zone then area of triangle is calculated. Co-ordinate of these vertices of triangle in the space are ($X_{1,}$ $Y_{1,}$ Z_1), ($X_{2,}$ $Y_{2,}$ Z_2) , ($X_{3,}$ $Y_{3,}$ Z_3)

Area of the triangle is

$$A = \sqrt{\left(A_{x^2} + A_{y^2} + A_{z^2}\right)} \qquad (3.6)$$

$$A_x = \tfrac{1}{2}\left(y_1z_2 - y_2z_1 + y_2z_3 - y_3z_2 + y_1z_3\right) \qquad (3.7)$$

$$A_y = \tfrac{1}{2}\left(x_1z_2 - x_2z_1 + x_2z_3 - x_3z_2 + x_1z_3\right) \qquad (3.8)$$

$$A_z = \tfrac{1}{2}\left(x_1y_2 - x_2y_1 + x_2y_3 - x_3y_2 + x_1y_3\right) \qquad (3.9)$$

Using the above equation the area of the bounding faces is calculated,

$$A_n = \left(A_{1+}A_2 + A_3 + A_4 + A_5 + \ldots\ldots\ldots\ldots\ldots + A_{28}\right)\ldots\ldots\ldots\ldots\ldots \qquad (3.10)$$

when A_n is the total area of bounding faces and n is the number of bounding faces of triangular shape which is taken as 28 in our problem. Table- 3.1 to Table-3.7 shows the various surfaces, types and their velocities for deformation zone of Fig.3.1.

3.7 Calculation of non-dimensional extrusion pressure

Deformation power consists of power of shear deformation at the plane of velocity discontinuity and friction power at die/workpiece interface can be determined using relation.

$$J = \frac{\sigma_0}{\sqrt{3}} \sum \left|\nabla V_n\right| A_n + \frac{m\sigma_0}{\sqrt{3}} \sum \left|\nabla V_n\right| A_n \qquad (3.11)$$

where n=total no. of bounding faces; $\left|\nabla V_n\right|$ = the velocity discontinuity at nth faces whose area is A_n. The non-dimensional extrusion pressure (P_{av}/σ_0) is optimized with respect to seven unknown adjustable or variable parameter of deformation zone and written as

$$\frac{P_{avg}}{\sigma_0} = \frac{J}{A_b V_b \sigma_0} \qquad (3.12)$$

where A_b =area of billet; V_b = billet velocity; σ_0 = uniaxial stress in compression

3.8 Solution process

Using a suitable analysis model, computation is carried out. It consists of following steps:

(i) Determination of the co-efficient of equation of the planes containing bounding faces of tetrahedral block;

(ii) Determination of the co-efficient of velocity of equation by applying the mass continuity condition to respective planes

(iii) Magnitude of velocity discontinuity is found out by algorithim. This solution also determines exit velocity, which serves as check on computation, since exit velocity can be independently calculated using billet velocity and the area reduction.

(iv) Computation of deformation work by equation (3.11) and non-dimensional extrusion pressure by equation (3.12)

(v) Optimization of non-dimensional extrusion pressure with respect to variable parameter L, Y_{12}, $Z_{12,}$ multivariable unconstraint routine.

(vi) All the computation are carried out with a suitable subroutine of tetrahedron, and pyramid, imposed with different alternatives.

3.9 Optimization parameter

For a single point formulation, one floating point lies on plane of symmetry having two undetermined co-ordinates Y_{12} and Z_{12}. Height of deformation zone is an additional optimizing parameter. For the single-point formulation, the floating point lies on the extrusion axis. Thus, the formulation has one undetermined co-ordinate, which serves as the optimization parameter to minimize the extrusion pressure for this formulation. Here, it is to be noted that the length of the die is taken as per the equivalent semi cone angle.

3.10 Results and Discussion

The analysis was carried out for all four schemes of triangular section both for general isosceles and right angled isosceles. The discretised deformation zone corresponding to the least upper-bound is named here as the optimum configuration. The least upper bound was identified using a multivariable optimization by Kuester and Mize [87] This optimum configuration is utilized for computation of the variation of the normalized extrusion pressure with the equivalent semi-cone angle (in degrees) and the percentage area reduction, for different friction factors as shown in Fig. 3.6 & Fig. 3.7 respectively. First analyses are being carried out for extrusion of isosceles triangular section from round billet. It is clear from these figure 3.6 that the optimal semi-cone angle that secures the minimal extrusion pressure is around 10 degree for 40% reduction, though it increases slightly with the increase of friction. The variation of extrusion pressure for different frictional boundary conditions is shown in Fig.3.7 with respect to different reductions for an equivalent semi-cone angle 10 degree. These results can be used to predict the forming stress and optimal die shape for designing the sectioned die, assessing the frictional condition either in an empirical way or by means of a simulation test. As can be observed, the present method can also be used to obtain a solution for non-axisymmetric extrusion through linearly converging dies. Referring to Fig. 3.7, it is seen that there is substantial reduction of

extrusion pressure for linear converging die when compared to flat-faced square die. As seen in Fig. 3.8, the reduction in extrusion pressure of linear converging die with lubrication (m=0.38) is 34.78% and 13.04% for dry condition (m=0.75) compared to flat-faced square die. To check the accuracy of the results the extrusion pressure for different reductions is compared with homogenous compression as shown in Fig.3.7. It is observed that the extrusion pressure due to homogenous compression is the least one.

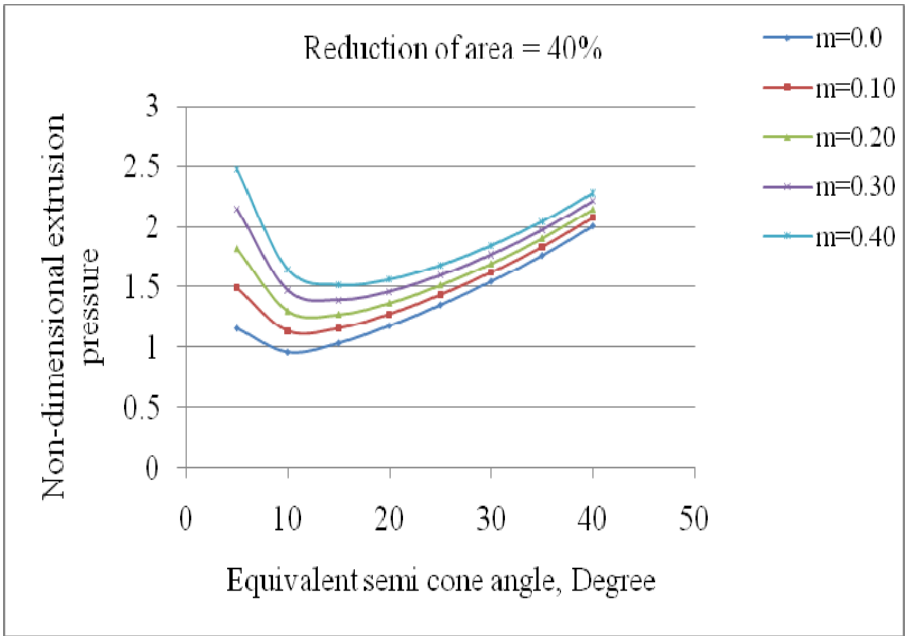

Fig. 3.6 Variation of extrusion pressure with equivalent semi-cone angle (Isosceles triangle)

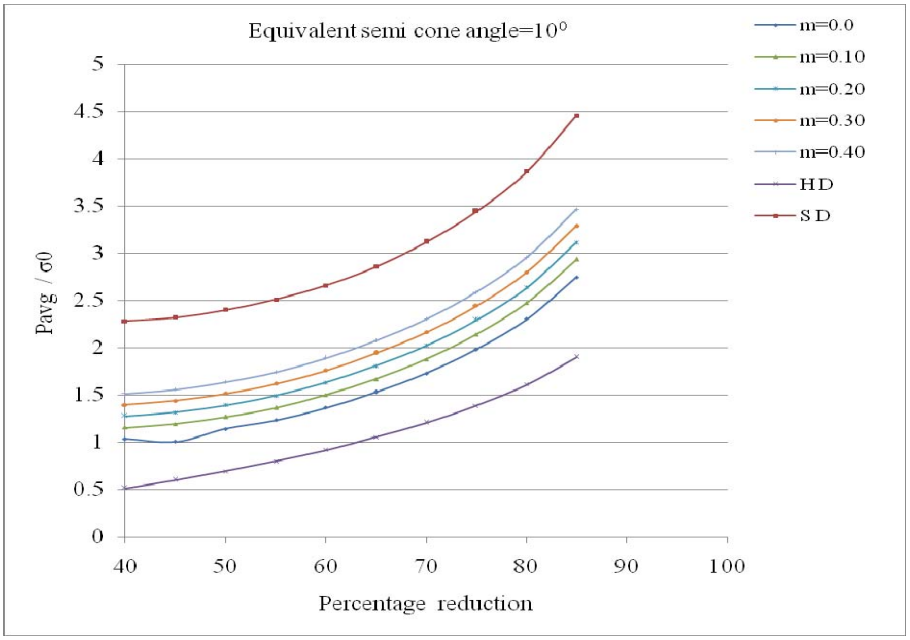

Fig. 3.7 Variation of extrusion pressure with respect to reduction.(Isosceles triangle)

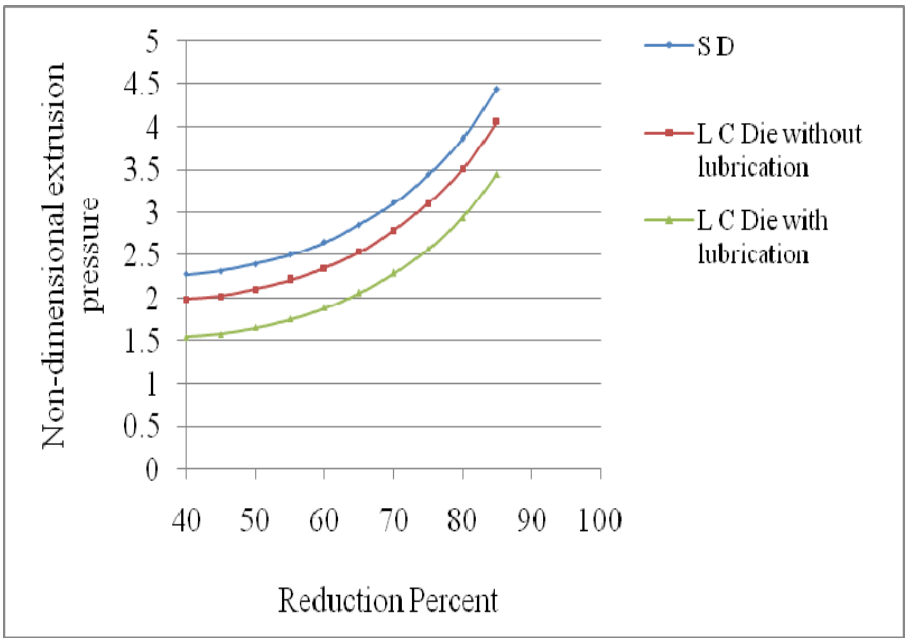

Fig. 3.8 Comparison of extrusion pressure of Square die with Linear converging die.

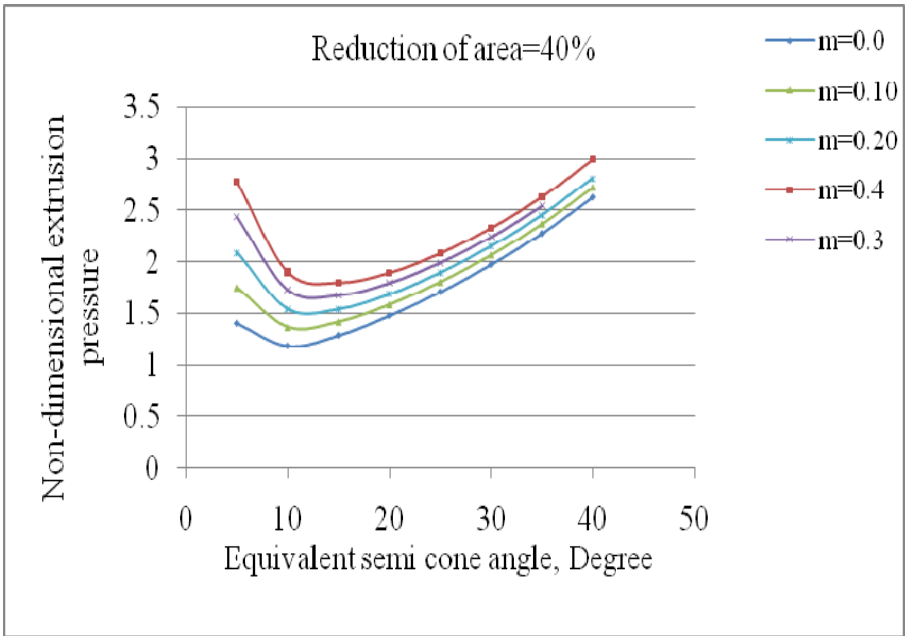

Fig. 3.9 Variation of extrusion pressure with equivalent semi-cone angle for right angled isosceles triangular section.

The variation of extrusion pressure for right angled isosceles triangle with respect to semi cone angles for 40% reduction are shown in Fig.3.9.for different friction condition at the die-billet interface of converging dies. It is evident that from the above results the equivalent semi cone angle is 12^0 for extrusion of right angled isosceles triangular section. The extrusion pressure increases with increase in friction.

The variation of non-dimensional extrusion pressure with respect to reduction for right angled isosceles triangles is shown in Fig. 3.10 for an equivalent semi cone angle 12^0. It is seen that the extrusion pressures increases with increase in reduction and friction factor. The variation of extrusion pressure with respect to semi cone angles for 40% reduction are shown in Fig.3.11 and Fig. 3.12 for different friction condition for equilateral, general isosceles, and right angled isosceles for an equivalent angle of 12^0 at the die-billet interface of converging dies. Referring to Fig. 3.11, it is evident that at m=0.1, the minimum extrusion pressure is obtained for isosceles triangle, where as equilateral triangle gives minimum pressure when m=0.4 as seen in Fig. 3.12. The comparison of non-dimensional extrusion pressure with respect to percentage area of reduction and friction factor for equilateral, general isosceles, and right angled isosceles are given for an equivalent angle of 12^0 which is

shown in Fig. 3.13 and Fig. 3.14 for different friction factors. It is evident that right angled isosceles section gives the maximum extrusion pressure where as the general isosceles yields the minimum pressure.

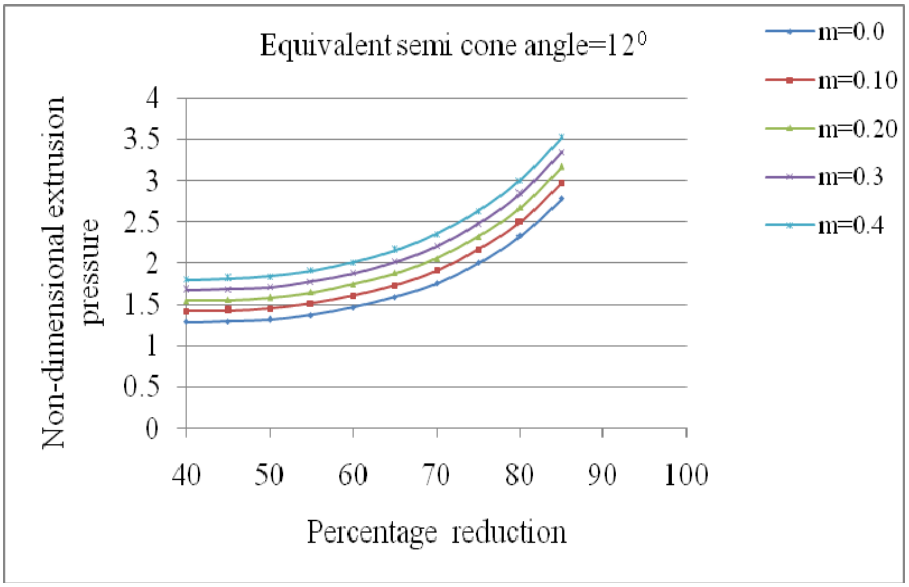

Fig. 3.10 Variation of extrusion pressure with respect to reduction.

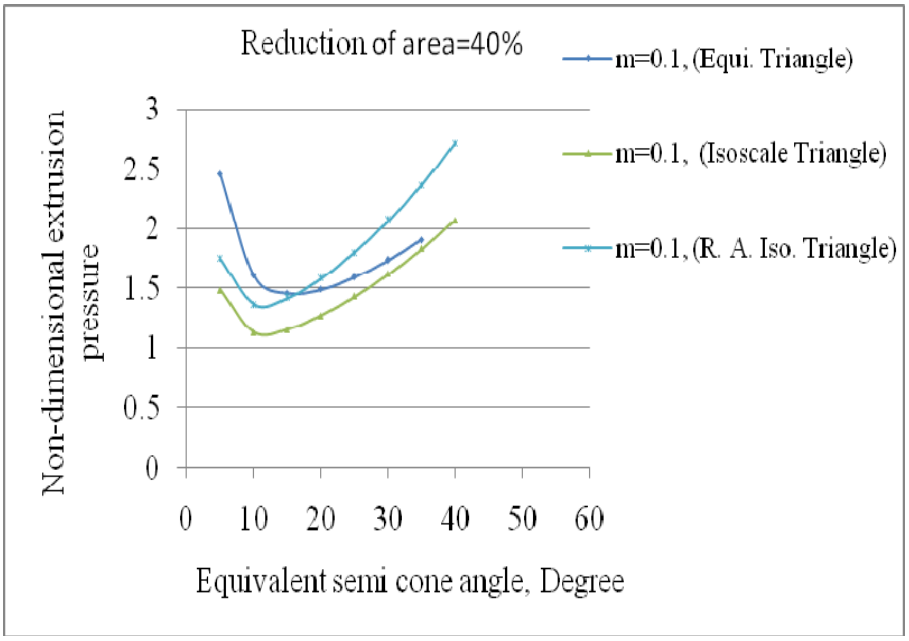

Fig. 3.11 Comparison of the extrusion pressure with equivalent semi-cone angle for equilateral, general isoscales and right angled isosceles triangular section (m=0.1).

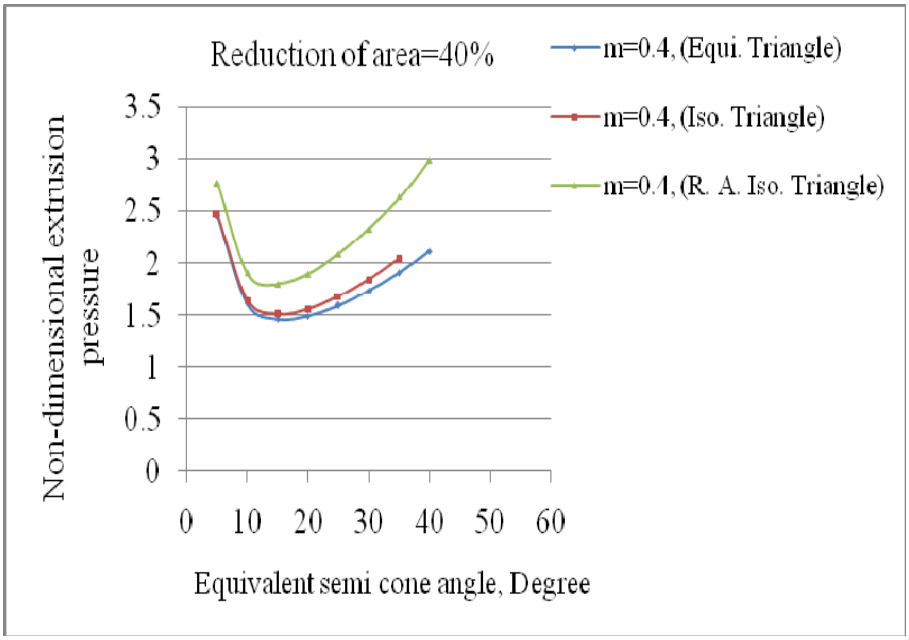

Fig. 3.12 Comparison of the extrusion pressure with equivalent semi-cone angle for equilateral, general isoscales and right angled isosceles triangular section (m=0.4).

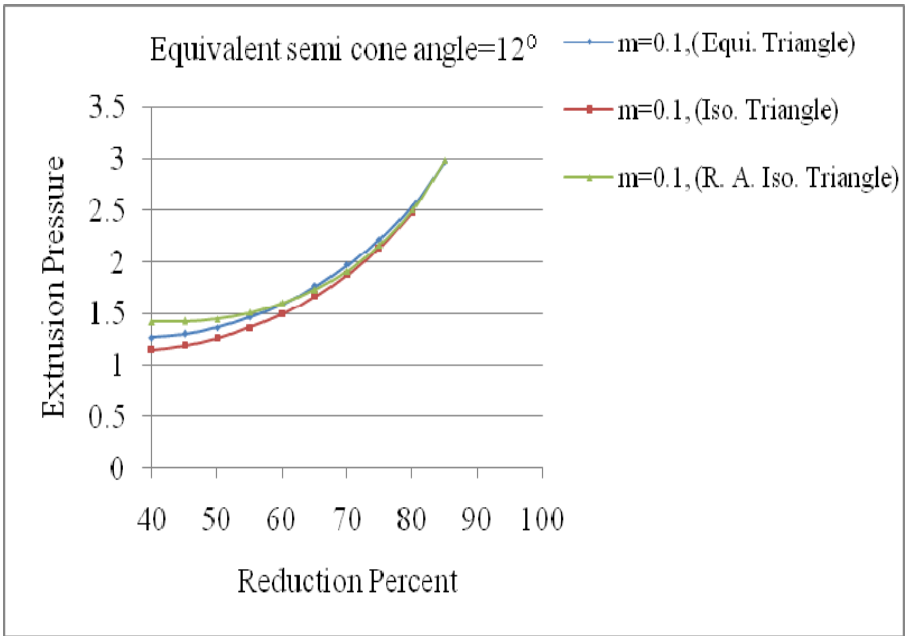

Fig. 3.13 Comparison of the extrusion pressure with respect to reduction for equilateral, general isosceles and right angled isosceles triangular section for semi-cone angle $=12^0$(m=0.1).

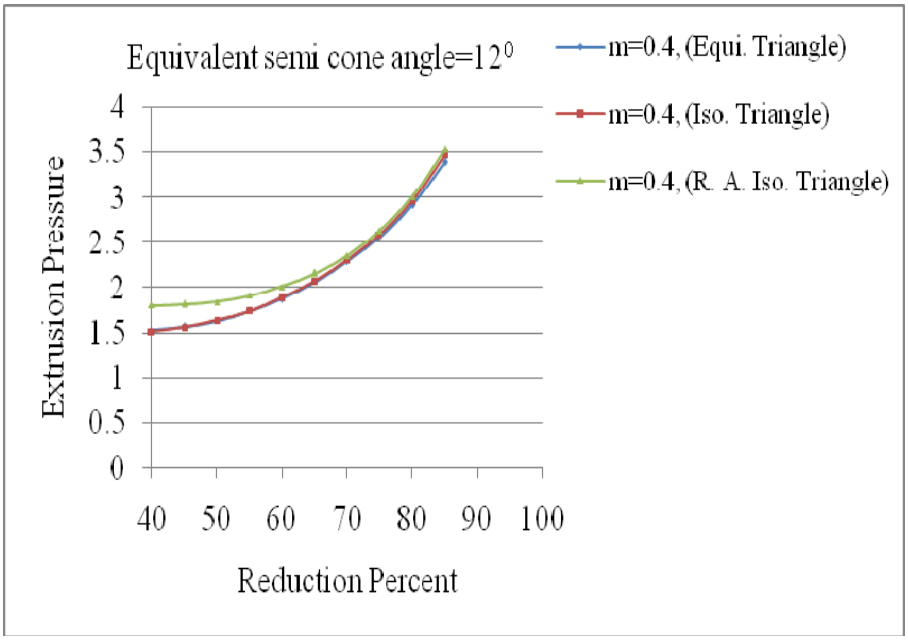

Fig. 3.14 Comparison of the extrusion pressure with respect to reduction for equilateral, general isosceles and right angled isosceles triangular section for semi cone angle is 12^0 (m=0.4).

3.11 Upper Bound Analysis of Round-to-Rhomboidal section Extrusion

Very often the bars of rhomboidal sections are in use for different structural components to satisfy the requirement of mechanical strength as well as the aesthetic appearance. The rhomboidal extruded products are strong and rigid with improved surface integrity.

The present investigation is based on 3D upper bound method using SERR technique for the analysis of round-to-rhombus section extrusion through a converging die. The curved surfaces are again approximated to the planar surfaces in the similar manner to apply SERR technique as in section 3.3. A comprehensive computational model was developed to determine the normalized extrusion pressure using a multivariate unconstrained optimization technique by Kuester and Mize [87]. The extrusion pressure has been computed for various semi-cone angles with different reductions and friction factors. These results can be used to predict the extrusion load and optimal die shape for designing the sectioned die for different frictional conditions. The geometry of rhomboidal section is also optimized to reduce the extruded power.

3.12 Formulation of the present problem

For the present analysis the round billet is approximated by a regular polygon. Fig. 3.15 shows the deformation zone, where the round billets are approximated to a 12 sided regular polygon for clear demonstration, though it was actually approximated to 16 sided polygon in solution.

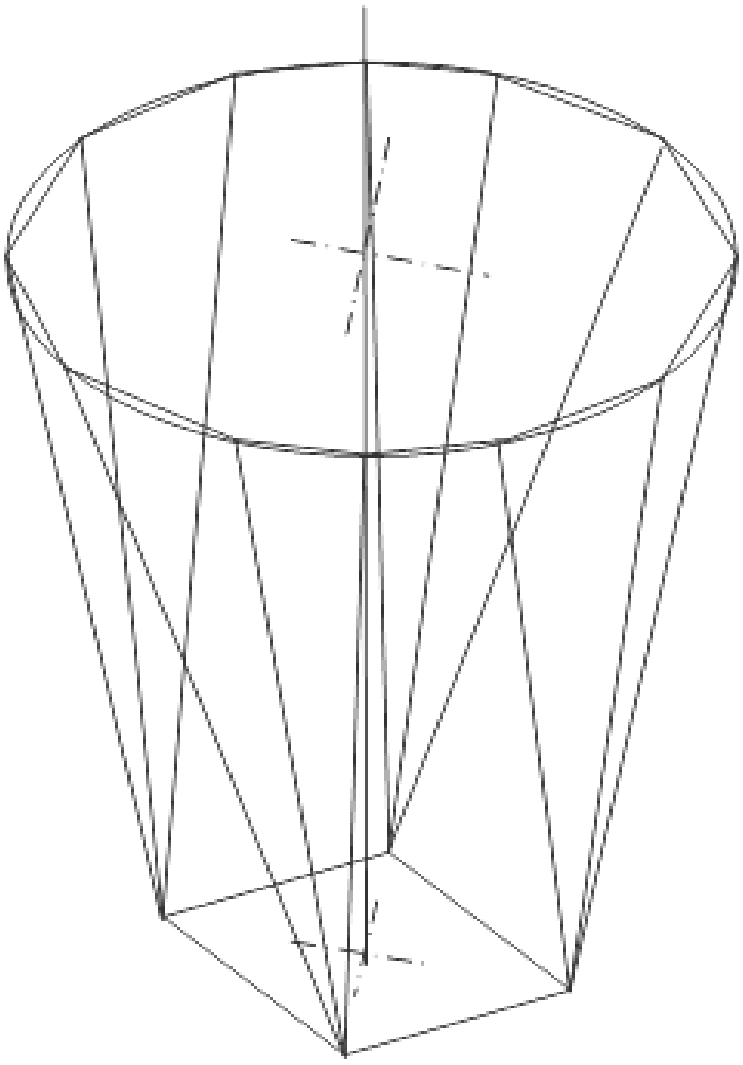

Fig. 3.15 Deformation zone, for extrusion of rhomboidal section from round billet.

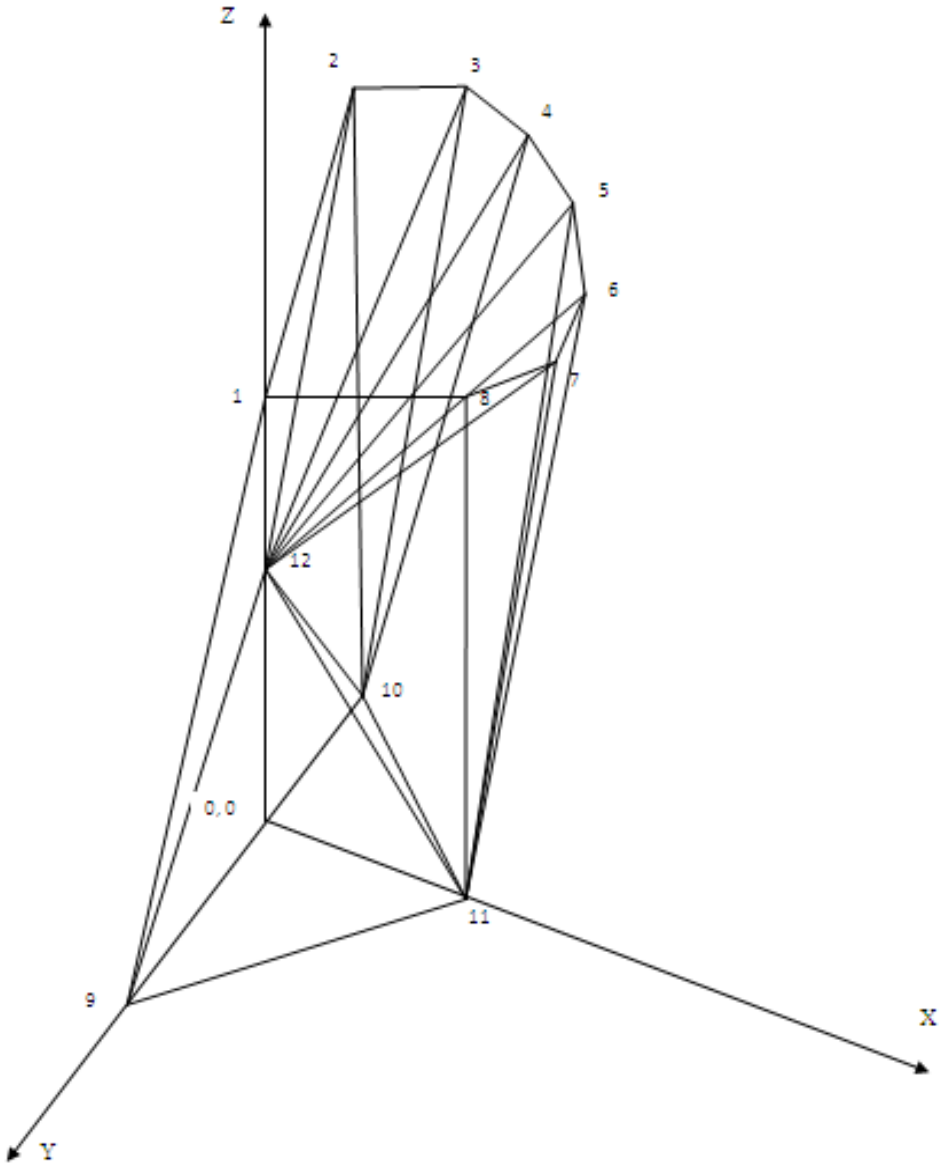

Fig. 3.16(a) One half of the deformation zone of 12 sided polygon with single floating point

In Fig.3.16 (a), analysis is done by taking one floating point for the domain as interest for discretization. The deformation zone is to be discritized into two pyramidal subzones (12-1-8-9-11 and 12-4-5-10-11) and five tetrahedral subzones (12-2-3-10, 12-3-4-10, 12-5-6-11, 12-6-7-11 and 12-7-8-11). Hence it results in nine

tetrahedrons and the number of global schemes of discretizing of different zones being four. The discretisation of pyramidal subzone 12-1-8-9-11 into tetrahedrons under scheme-1and scheme-2 is shown in Fig. 3.16(b). Table 3.13 identifies different planes for scheme-2. The similar discretisation of pyramidal subzone 12-4-5-10-11 into tetrahedrons for scheme-1 and scheme-2 are shown in Fig. 3.16(c) along with the table 3.14, for specifying different planes. Five tetrahedrons are shown in Fig. 3.16(d) with different planes specified as from Table 3.15 to 3.19. Table-3.20 summarizes the specification of all the planes in pyramids and tetrahedrons along with the common planes. The co-ordinates of the deformation zone are shown in Table-3.21.

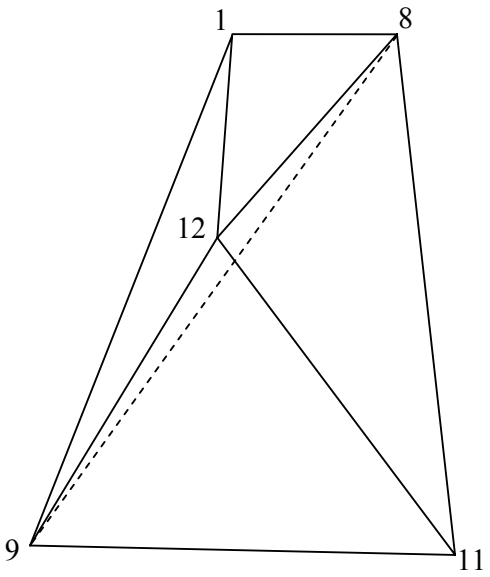

Scheme 1

Tetrahedrons

1. 12-1-8-9
2. 12-8-11-9

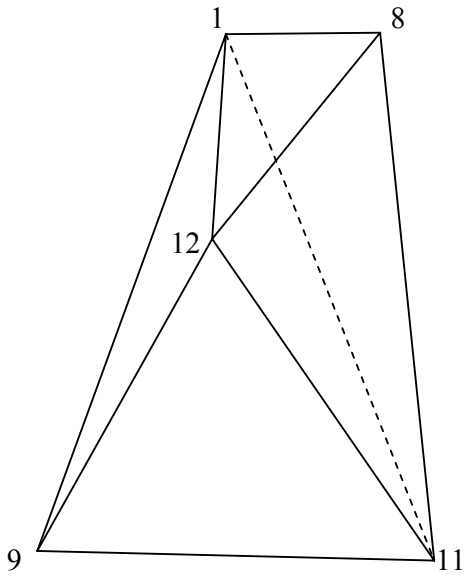

Scheme 2

Tetrahedrons

1. 12-1-9-11
2. 12-1-8-11

Fig. 3.16 (b) Schemes of discretization for the pyramidal subzone 12-1-8-9-11

Table-3.13 Various surfaces, types and their normal velocity (Pyramid 12-1-8-9-11, Scheme 2)

Surface	Category	Normal velocity on that surface
12-1-8	Entry surface	Billet velocity (V_b)
12-8-11	Internal plane	Unknown velocity
12-9-11	Exit plane	Product velocity (V_P)
12-1-11	Internal plane	Unknown velocity
12-1-9	Internal plane	Unknown velocity
1-9-11	Friction surface	0
1-8-11	Friction surface	0

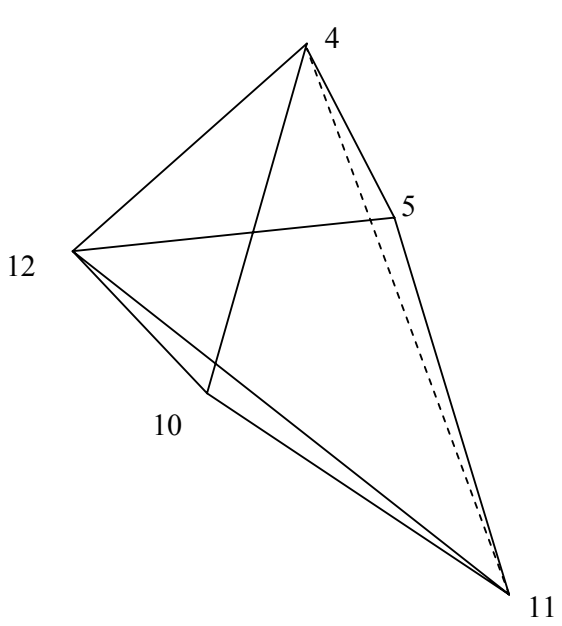

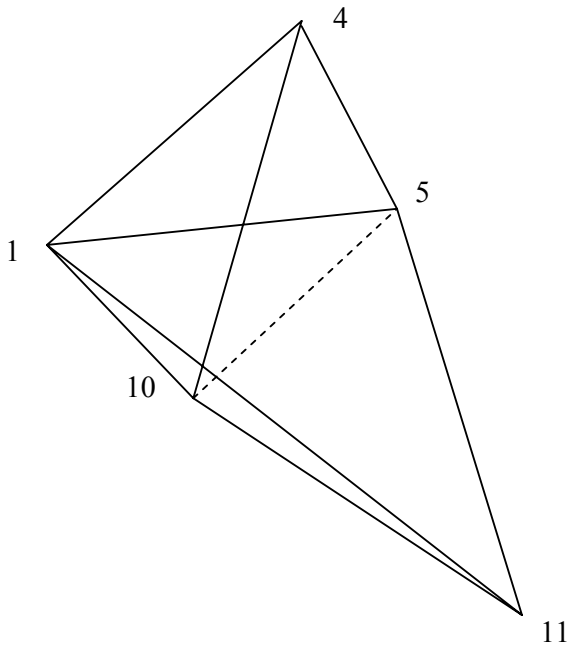

Scheme 1

Tetrahedrons

1. 12-4-5-11
2. 12-4-11-10

Scheme 2

Tetrahedrons

1. 12-4-5-10
2. 12-5-11-10

Fig. 3.16 (c) Schemes of discretization for the pyramidal subzone 12-4-5-10-11

Table-3.14 Various surfaces, types and their normal velocity (Pyramid 12-4-5-10-11, Scheme 2)

Surface	Category	Normal velocity on that surface
12-4-5	Entry surface	Billet velocity (V_b)
12-5-10	Internal plane	Unknown velocity
12-4-10	Internal plane	Unknown velocity
12-5-11	Internal plane	Unknown velocity
12-10-11	Exit plane	Product velocity (V_P)
5-10-11	Friction surface	0
4-5-10	Friction surface	0

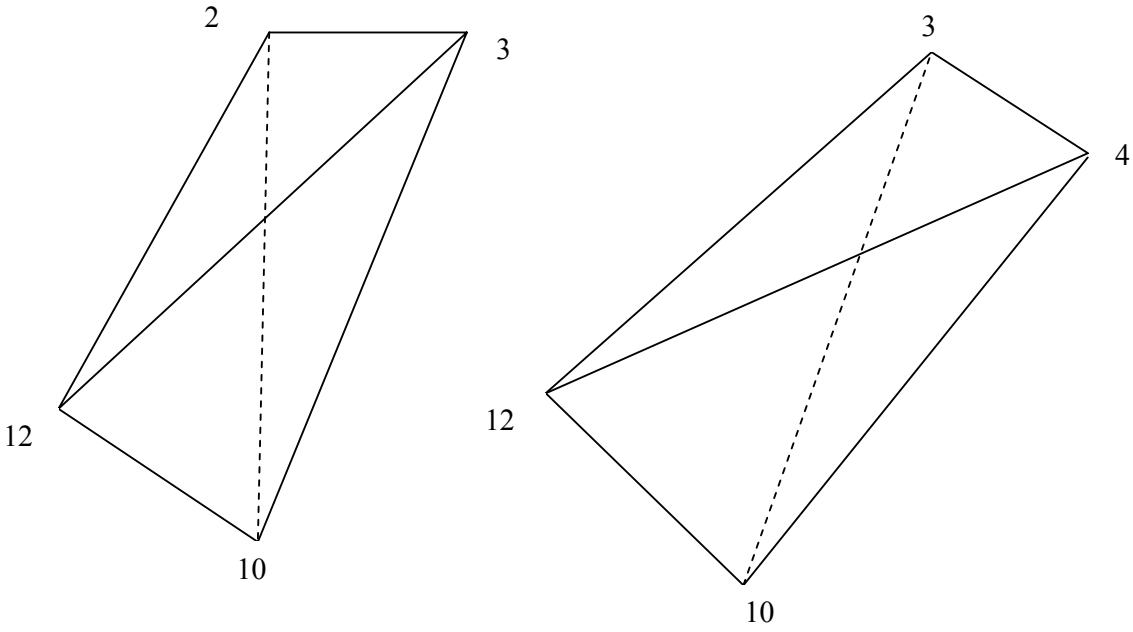

Tetrahedron: 12-2-3-10 Tetrahedrons: 12-3-4-10

Continue in the next page

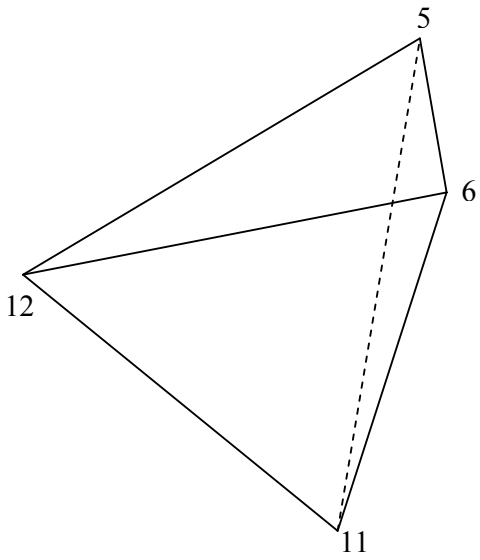

Tetrahedron: 12-5-6-11

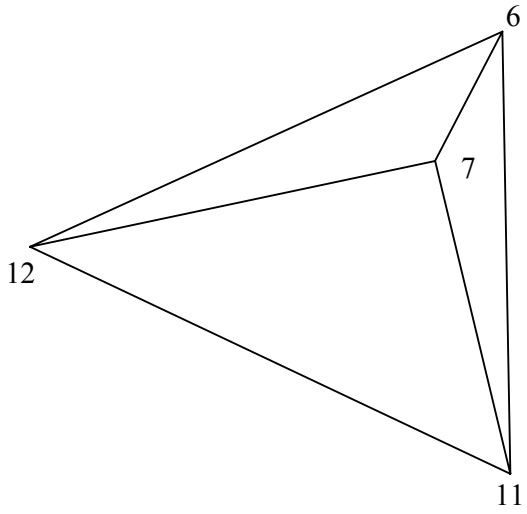

Tetrahedrons: 12-6-7-11

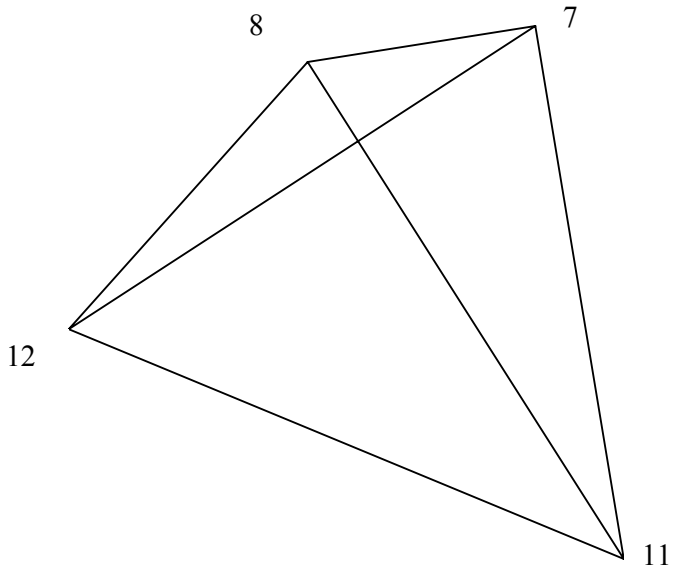

Tetrahedron: 12-7-8-11

Fig. 3.16 (d) Discretization for the tetrahedral subzone

Table-3.15 Various surfaces, types and their normal velocity (Tetrahedron: 12-2-3-10)

Surface	Category	Normal velocity on that surface
12-2-3	Entry surface	Billet velocity (V_b)
12-3-10	Internal plane	Unknown velocity
12-2-10	Internal plane	Unknown velocity
2-3-10	Friction surface	0

Table-3.16 Various surfaces, types and their normal velocity (Tetrahedron: 12-3-4-10)

Surface	Category	Normal velocity on that surface
3-4-12	Entry surface	Billet velocity (V_b)
3-4-10	Friction surface	0
12-4-10	Internal plane	Unknown velocity
12-3-10	Internal plane	Unknown velocity

Table-3.17 Various surfaces, types and their normal velocity (Tetrahedron: 12-5-6-11)

Surface	Category	Normal velocity on that surface
12-5-6	Entry surface	Billet velocity (V_b)
5-6-11	Friction surface	0
12-6-11	Internal plane	Unknown velocity
12-5-11	Internal plane	Unknown velocity

Table-3.18 Various surfaces, types and their normal velocity (Tetrahedron: 12-6-7-11)

Surface	Category	Normal velocity on that surface
6-7-12	Entry surface	Billet velocity (V_b)
6-7-11	Friction surface	0
12-7-11	Internal plane	Unknown velocity
12-6-11	Internal plane	Unknown velocity

Table-3.19 Various surfaces, types and their normal velocity (Tetrahedron: 12-7-8-11)

Surface	Category	Normal velocity on that surface
12-7-8	Entry surface	Billet velocity (V_b)
7-8-11	Friction surface	0
12-7-11	Internal plane	Unknown velocity
12-8-11	Internal plane	Unknown velocity

Table 3.20 Total number of planes of Pyramids and Tetrahedrons

Subzones	Model numbering system	Numbering of different planes	No. of planes	Total no. of common planes	Total no. of planes
Pyramid	12-1-8-9-11	12-1-8 12-8-11 12-9-11 12-1-11 12-1-9 1-9-11 1-8-11	7	(8 common planes)	(8+8+4+4+4+4+4)-8= 28
Pyramid	12-4-5-10-11	12-4-5 12-5-10 12-4-10 12-5-11 12-10-11 5-10-11 4-5-10	7		
Tetrahedran	12-2-3-10	12-2-3 12-3-10 12-2-10 2-3-10	4		
Tetrahedran	12-3-4-10	3-4-12 3-4-10 12-4-10 12-3-10	4		
Tetrahedran	12-5-6-11	12-5-6 5-6-11 12-6-11 12-5-11	4		
Tetrahedran	12-6-7-11	6-7-12 6-7-11 12-7-11 12-6-11	4		

Tetrahedran	12-7-8-11	12-7-8 7-8-11 12-7-11 12-8-11	4		

Table-3.21 Co-ordinates of points in deformation zone

Points	X-co-ordinate	Y-co-ordinate	Z-co-ordinate
1	-R Cos(11π/12)	0	L
2	R Cos(π/12)	0	L
3	R Cos(π/12)	R Sin(π/12)	L
4	R Cos(π/4)	R Sin(π/4)	L
5	R Cos(5π/12)	R Sin(5π/12)	L
6	R Cos(7π/12)	R Sin(7π/12)	L
7	R Cos(9π/12)	R Sin(9π/12)	L
8	R Cos(11π/12)	R Sin(11π/12)	L
9	-d/2	0	0
10	d/2	0	0
11	0	c/2	0
12	0	0	L0

All these sub-zones are interconnected and have common triangular faces. Thus the basic SERR blocks in their totality have 28 bounding faces, so that as all these bounding faces are triangular in shape, by applying equation (2.12 of chapter-2). 28 velocity equations can be obtained. When these equations are solved, an equal number of velocity components can be obtained for this formulation (the discretisation details are summarized in Table 3.22).

Table 3.22 Summary of discretisation schemes

Type of sub-zones	2 pyramid 5 tetrahedrons
Total number of SERR blocks	2+2+1+1+1+1+1= 9
Number of discretisation schemes	2x2 = 4
Number of triangular faces	28
No. of velocity components	9x3=27 for 9 SERR and 1 at exit Total=28

3.13 Solution process

A comprehensive computational model was developed to make an upper-bound analysis for the extrusion of rhomboidal section. The special feature of the proposed section is incorporated in this model and computations are carried out. The solution process for rhomboidal section is similar like triangular section which described in earlier section 3.7. The optimization parameters are similar as described in section 3.8.

3.14 Results and Discussion

Computations were carried out for all four schemes of rhombus section and the scheme giving the least upper-bound was identified using a multivariable optimization technique by Kuester and Mize [87]. The dimension of the die orifice to extrude rhomboidal section is shown in Fig. 3.17, where c and d are the major and minor axes of the rhomboidal section respectively. The discretised deformation zone corresponding to the least upper-bound is named here as the optimum configuration. The variation of non-dimensional extrusion pressure with the equivalent semi-cone angle for different friction factors is shown in Fig. 3.18 for rhomboidal section with $\varphi=60^0$. It is evident that the minimum average equivalent semi-cone angle is around 12^0, though there is slight increase in equivalent angle with increase in friction factor. The variation of non-dimensional extrusion pressure with reductions for different friction factors are shown in Fig. 3.19 for 12^0 semi-cone angles. Referring to Fig.3.19, the extrusion pressures are compared with that of homogenous compression. It is seen that the extrusion pressure due to homogeneous compression is the least one

similar to earlier case. It is also a check for accuracy of the present solution. The variation of extrusion pressure with the percentage area reduction and equivalent semi-cone angle (in degrees) for different rhombus angle (φ) is shown in Fig. 3.20 and Fig. 3.21 respectively. It is seen that the extrusion pressure for rhomboidal section is minimum when angle (φ) is 60^0. It is also observed that the extrusion pressure is minimum when equivalent semi-cone angle is 12^0.

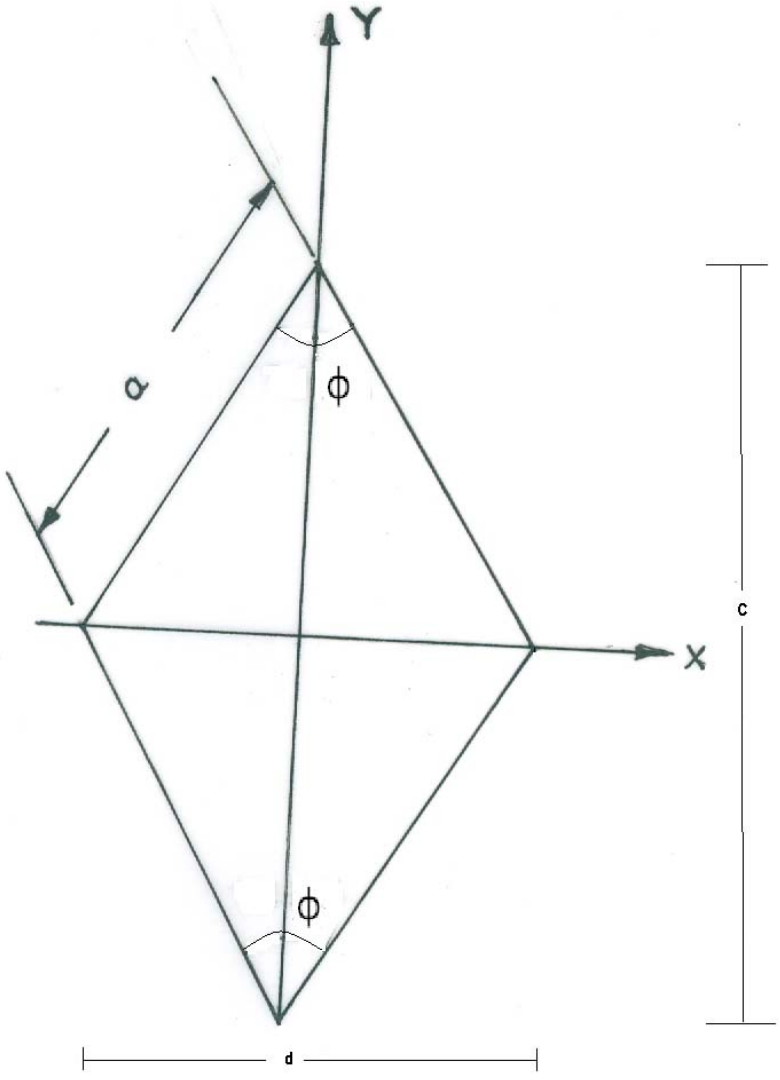

Fig.3.17 Die orifice dimensions used to extrude rhomboidal section

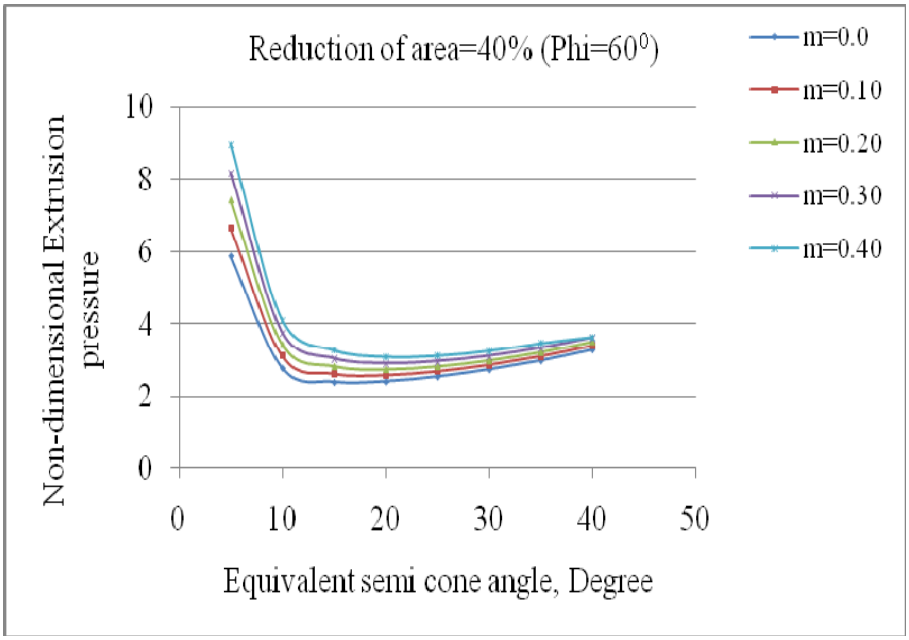

Fig.3.18 Variation of extrusion pressure with equivalent semi-cone angle for (Phi=60^0).

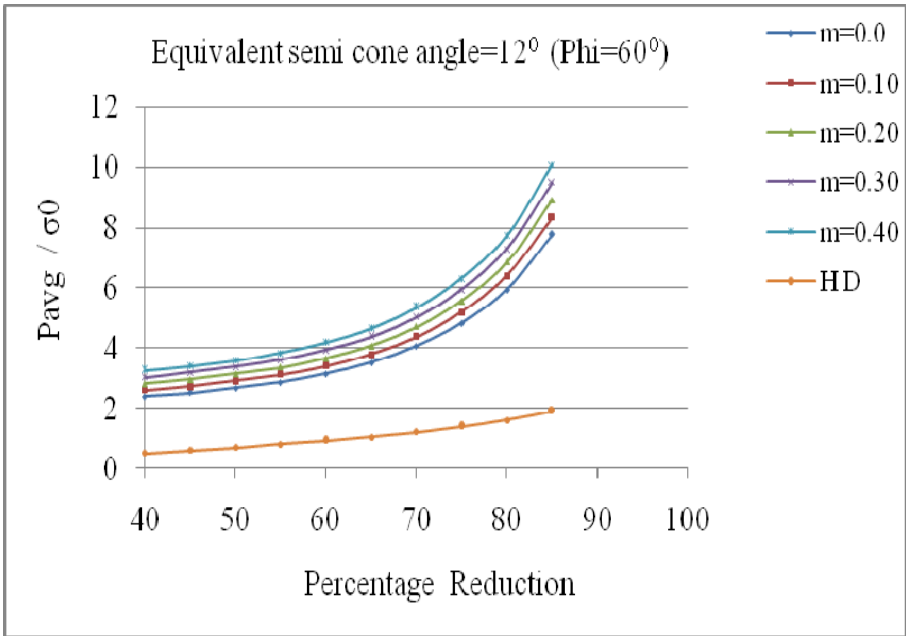

Fig.3.19 Variation of extrusion pressure with respect to reduction for (Phi = 60^0)

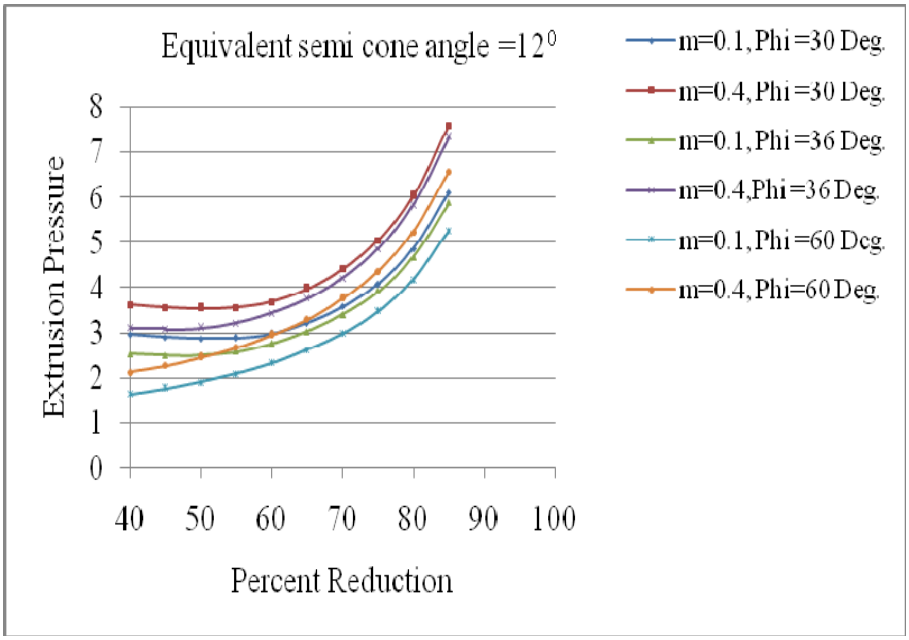

Fig.3.20 Variation of extrusion pressure with respect to reduction with different rhombus angle, Phi (φ)

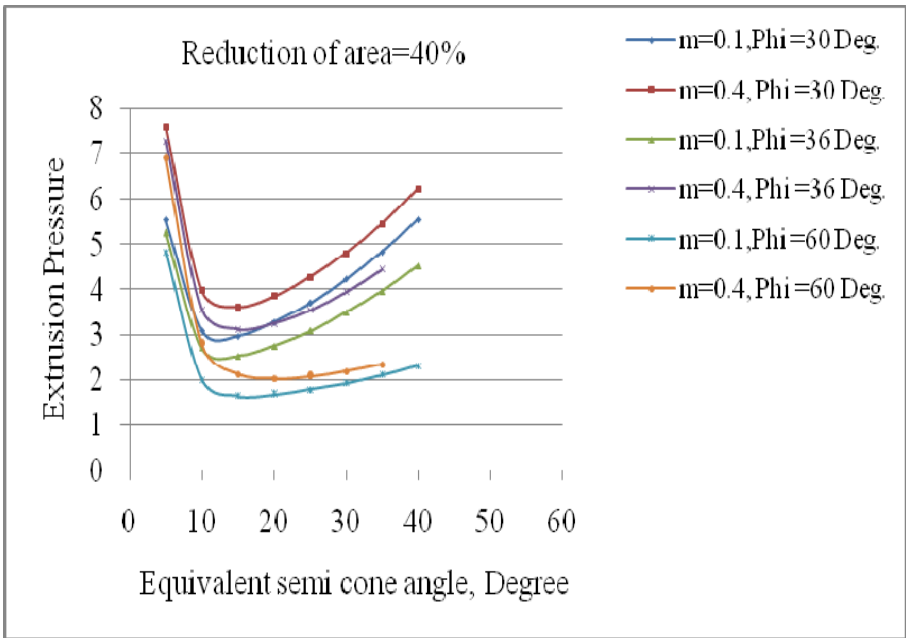

Fig. 3.21 Comparison of the extrusion pressure with equivalent semi-cone angle for different rhombus angle.

3.15 Conclusions

(i) The optimum semi cone angle is obtained to be 10^0 for general isosceles and for 12^0 right angled isosceles triangle section, where as it is 15^0 for equilateral triangular section for 40% reduction.

(ii) The extrusion pressure is maximum for right angled section, where as it is minimum for general isosceles triangle section.

(iii) The optimum equivalent semi-cone angle is 12^0 for extrusion of rhomboidal section

(iv) The extrusion pressure for rhomboidal section with $\Phi=60^0$ is found to be minimum

(v) The extrusion pressure increases with increase in reduction and friction factor.

(vi) There is a reduction in extrusion pressure for linear converging die compared to flat face square die.

Analysis of Round-to-Pentagonal and Octagonal Section Extrusion through Linearly Converging Dies using SERR Technique

4.1 Introduction

A number of analytical studies have been carried out during the past few years to compute the deformation load for extrusion/drawing of sections from round billets through square dies using three-dimensional (3D) upper bound theorem. The greatest difficulty in upper bound method is to obtain a kinematically admissible velocity field. A number of investigations have been reported for extrusion of different sections from round and square billet using flat faced square dies. But adequate investigations have not been carried out for the extrusions of section from round/square billet using linearly converging die. The linear converging die is having some specific advantage over the flat faced die in respect of low friction, less redundant work and more uniform grain structure. In view of the advantage of linearly converging die a great deal of investigations are yet to be carried out to standardize the process parameter and to optimize the die design for extrusion of different sections. In the present investigation a reformulated SERR (spatial elementary rigid region)

- *Based on the paper published by the author, entitled*

1. *Analysis of Round-to-Pentagon extrusion through linearly converging dies using SERR Technique. Published in the International Journal of Modern Manufacturing Technology (JMMT), Vol. 2, (N2), p p. , (2010)*

2. *Three Dimensional Upper Bound Modeling For Extrusion Of Round-To-Octagon Section Using Linearly Converging Die". Published in the International Journal Key Engineering Materials, Vol. 424, (2010), pp. 189-196. (2010)*

technique has been used for extrusion of pentagonal section from round billet. The round billet has been approximated by regular polygon. The optimum die geometry has been designed. The extrusion pressure has been determined for different reductions and friction factor. The constant friction factor has been considered at the die-billet interface.

4.2 Formulation of the present problem

For the sake of the present analysis, it is assumed that the centroid of the die aperture lies on the billet axis, this assumption being necessary so that the product remains straight as it comes out of the die orifice. As mentioned earlier, the SERR (spatial elementary rigid region) technique can be applied where there are plane boundaries. Hence, the curved surface is to be replaced by planar surfaces so as to accommodate the SERR analysis**.** Fig. 4.1 shows the die geometry bounded by curved surfaces due to the round billet. For the present analysis the round billet is approximated by a regular polygon with 10 sides (as there is a negligible change of final result computed value by further increasing the sides). Fig.4.2 shows the deformation zone, where the round billets is approximated to a 10-sided regular polygon for clear demonstration.

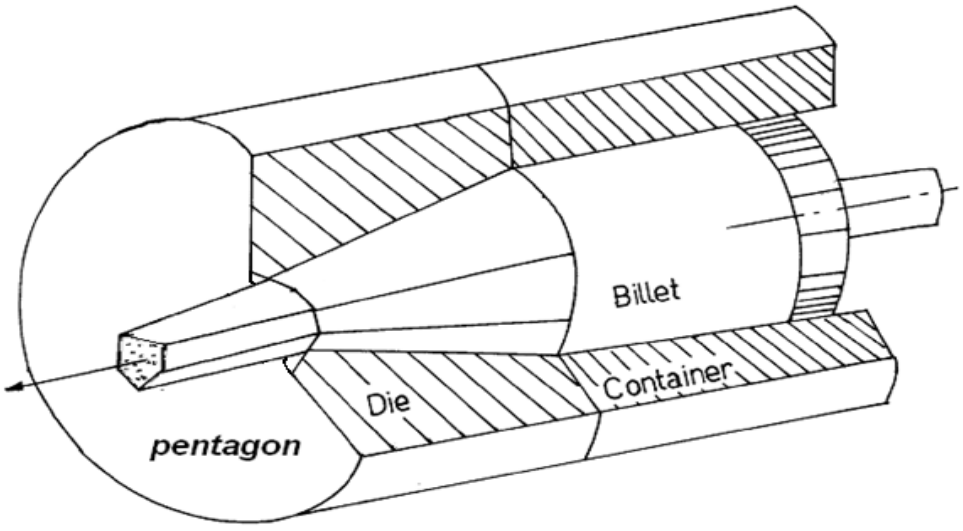

Figure 4.1 Direct extrusion of a pentagonal section from a round billet

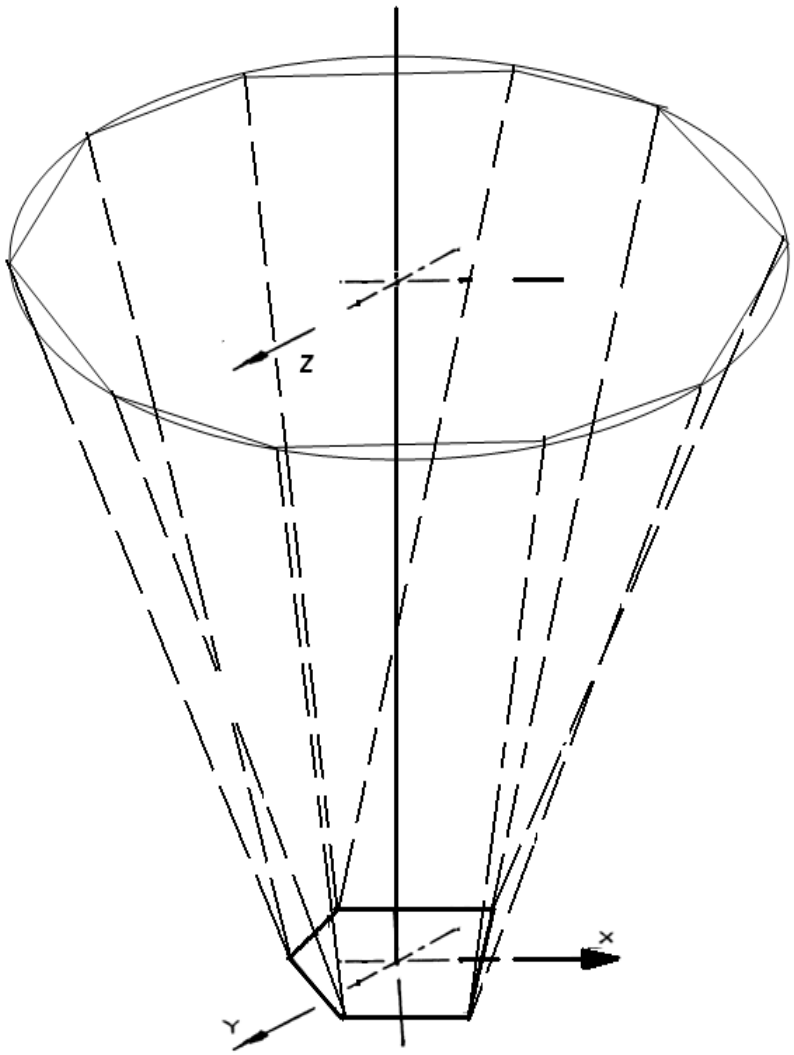

Fig. 4.2 Deformation zone, where the round billets is approximated by a 10 sided regular pentagon.

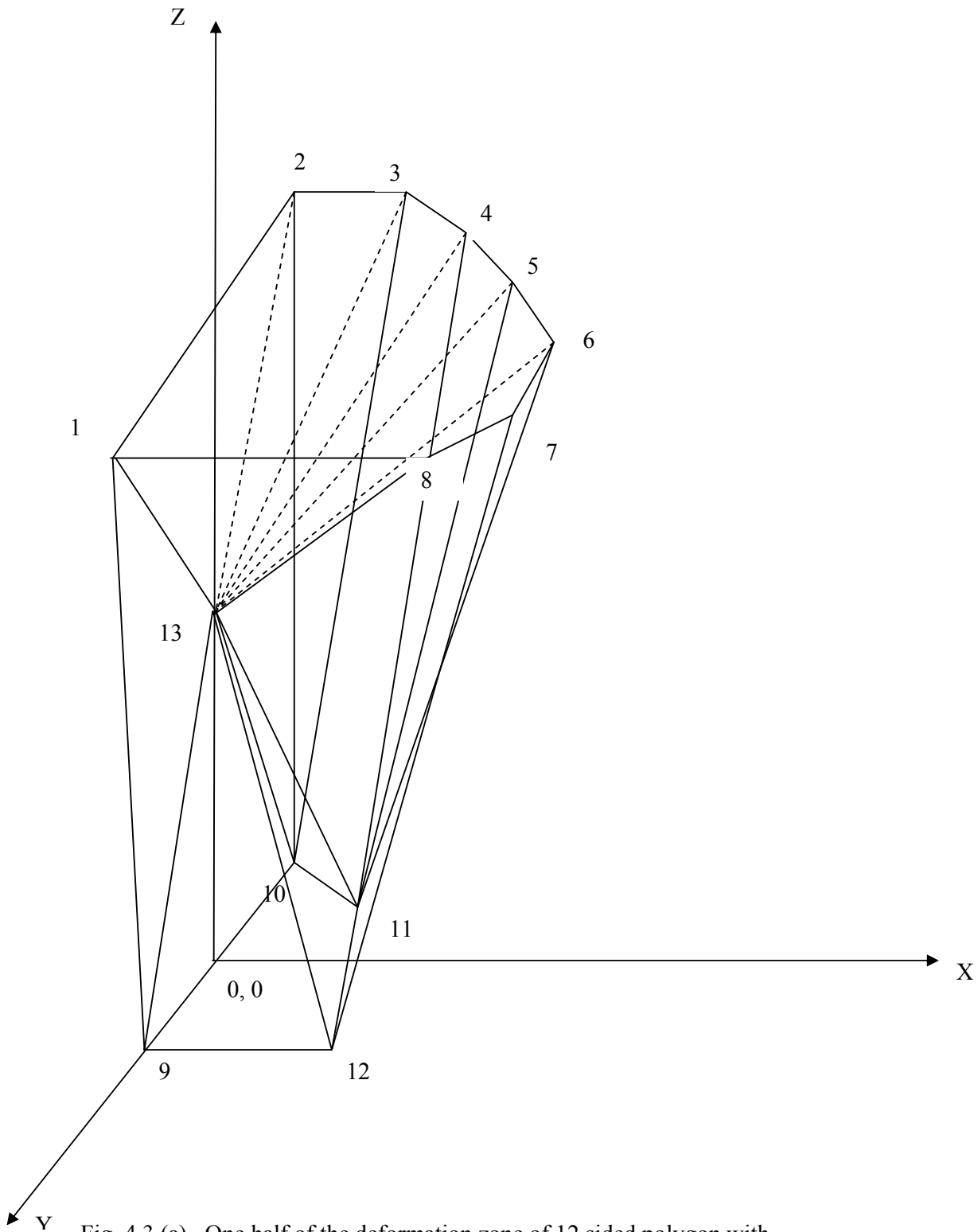

Fig. 4.3 (a) One half of the deformation zone of 12 sided polygon with single floating point

In Fig. 4.3(a) analysis is done by taking one floating point for the domain as interest for discretization. The deformation zone is to be discritized into three pyramidal subzones (13-1-8-9-12, 13-3-4-10-11 and 13-6-7-11-12 and four tetrahedral subzones (13-2-3-10, 13-4-5-11, 13-5-6-11 and 13-7-8-11). Hence it results in ten tetrahedrons and the number of global schemes of discretizing of different zones being eight. Fig. 4.3 (b) indicates the scheme of discretization for the pyramidal subzone (13-3-4-10-11), where as Fig. 4.3 (c) and Fig 4.3 (d) represent for pyramidal subzone (13-6-7-11-12) and (13-1-8-9-12) respectively. Fig. 4.3(e) shows the tetrahedral subzone (13-2-3-10, 13-4-5-11, 13-5-6-11, 13-8-7-11).

Table 4.1 to 4.7 specifies different planes with normal velocities. Table 4.8 indicates number of planes with the ways of discretization. Table 4.9 gives the list of the total number of planes in pyramids and tetrahedrons. Table 4.10 gives the co-ordinates of the points of the deformation zone as indicated in Fig. 4.3 (a). L, L_0, R, a and e are the different parameters. L and L_0 are the die length and the position of floating point (13). R is the radius of the billet and 'a' is the side of product. 'e' is the distance of the vertices from the center in the exit plane.

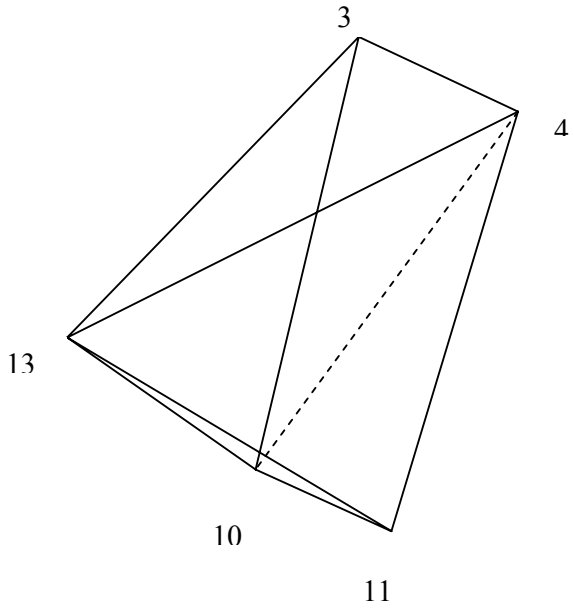

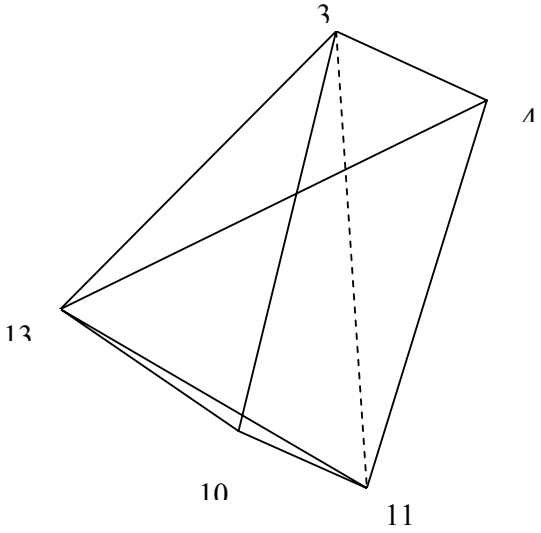

Scheme 1

Tetrahedrons

1. 13-3-4-10
2. 13-4-10-11

Scheme 2

Tetrahedrons

1. 13-3-4-10
2. 13-4-10-11

Fig. 4.3 (b) Schemes of discretization for the pyramidal subzone 13-3-4-10-11

Table-4.1 Various surfaces, types and their normal velocity (Pyramid 13-3-4-10-11, Scheme2)

Surface	Category	Normal velocity on that surface
13-3-4	Entry surface	Billet velocity (V_b)
13-4-11	Internal plane	Unknown velocity
13-3-10	Internal plane	Unknown velocity
3-4-11	Friction surface	0
13-10-11	Exit plane	Product velocity (V_P)
13-3-11	Internal plane	Unknown velocity
10-3-11	Friction surface	0

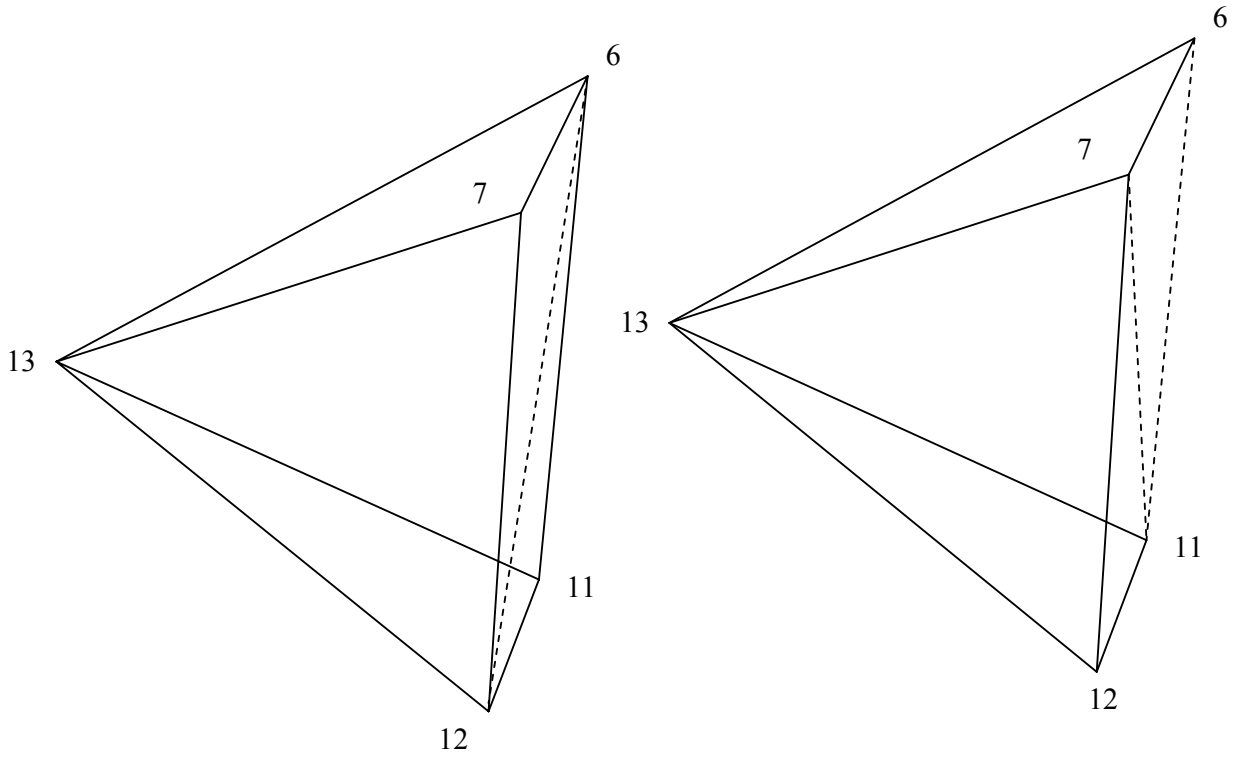

Scheme 1 Scheme 2

Tetrahedron

Tetrahedrons

1. 13-12-6-7 1. 13-6-7-11
2. 13-6-11-12 2. 13-7-11-12

Fig. 4.3 (c) Schemes of discretization for the pyramidal subzone 13-6-7-11-12

Table-4.2 Various surfaces, types and their normal velocity (Pyramid 13-6-7-11-12, Scheme2)

Surface	Category	Normal velocity on that surface
13-6-7	Entry surface	Billet velocity (V_b)
6-7-11	Friction surface	0
7-11-12	Friction surface	0
13-7-11	Internal plane	Unknown velocity
13-11-12	Exit plane	Product velocity (V_P)

13-6-11	Internal plane	Unknown velocity
13-7-12	Internal plane	Unknown velocity

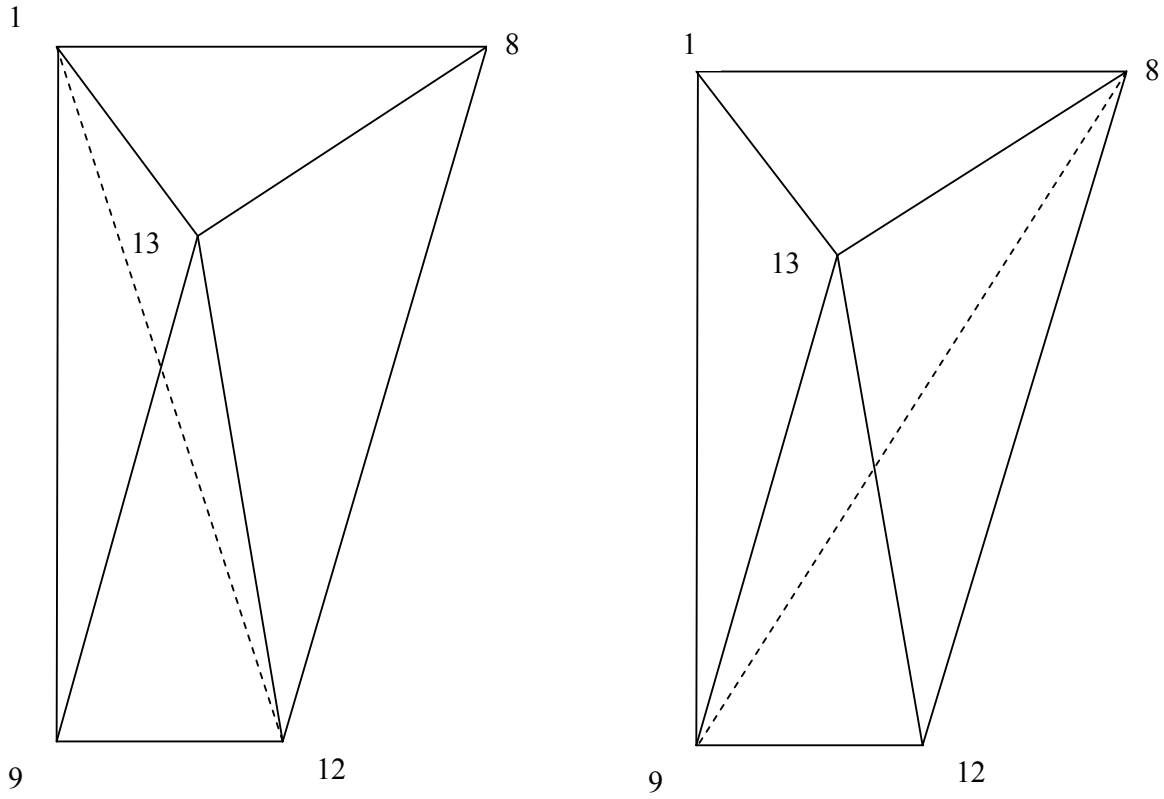

Scheme 1

Tetrahedron

1. 13-1-8-12
2. 13-1-9-12

Scheme 2

Tetrahedrons

1. 13-1-8-9
2. 13-8-9-12

Fig. 4.3 (d) Schemes of discretization for the pyramidal subzone 13-1-8-9-12

Table-4.3Various surfaces, types and their normal velocity (Pyramid 13-1-8-9-12, Scheme2)

Surface	Category	Normal velocity on that surface
13-1-8	Entry surface	Billet velocity (V_b)
13-1-9	Internal plane	Unknown velocity
13-8-12	Internal plane	Unknown velocity
13-8-9	Internal plane	Unknown velocity
12-8-9	Friction surface	0
1-8-9	Friction surface	0
13-9-12	Exit plane	Product velocity (V_P)

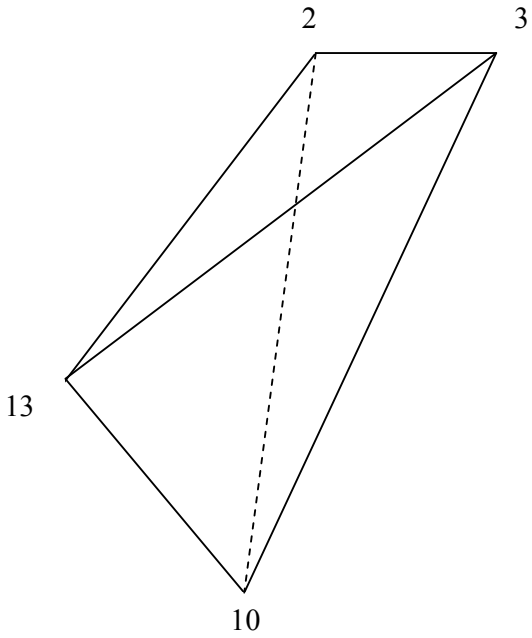

Tetrahedron: 13-2-3-10

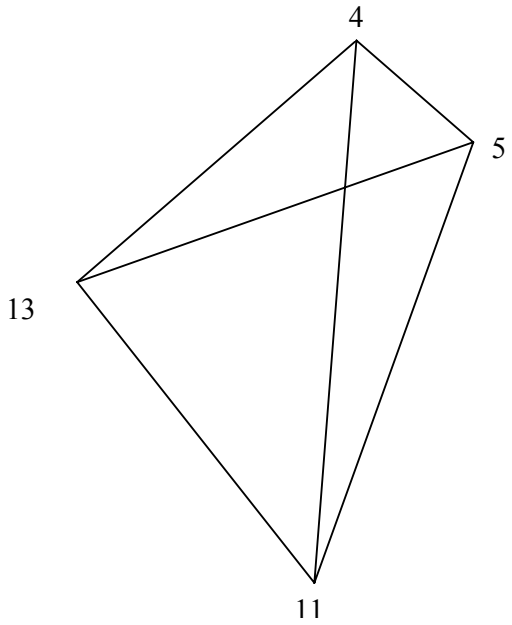

Tetrahedrons: 13-4-5-11

Continue in the next page

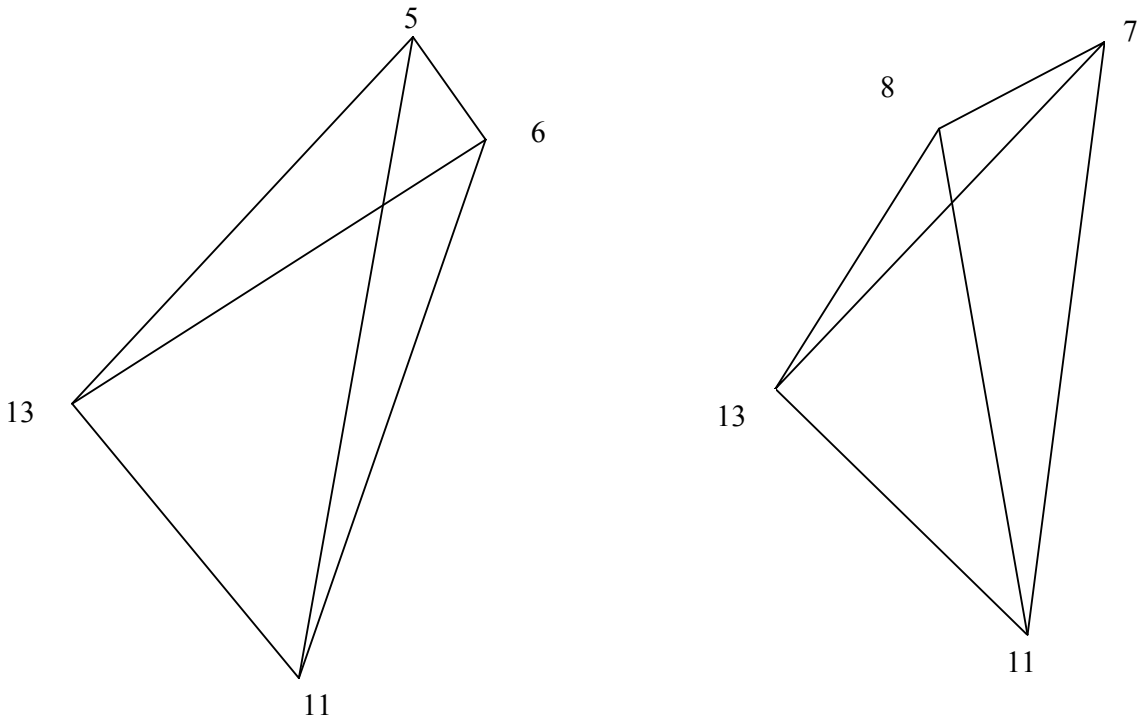

Tetrahedron: 13-5-6-11 Tetrahedrons: 13-8-7-11

Fig. 4.3 (e) Discretization for the tetrahedral subzone

Table-4.4 Various surfaces, types and their normal velocity (Tetrahedron: 13-2-3-10)

Surface	Category	Normal velocity on that surface
13-2-3	Entry surface	Billet velocity (V_b)
2-3-10	Friction surface	0
13-2-10	Internal plane	Unknown velocity
13-3-10	Internal plane	Unknown velocity

Table-4.5 Various surfaces, types and their normal velocity (Tetrahedron: 13-4-5-11)

Surface	Category	Normal velocity on that surface
13-4-5	Entry surface	Billet velocity (V_b)
4-5-11	Friction surface	0
13-4-11	Internal plane	Unknown velocity
13-5-11	Internal plane	Unknown velocity

Table-4.6 Various surfaces, types and their normal velocity (Tetrahedron: 13-5-6-11)

Surface	Category	Normal velocity on that surface
5-6-13	Entry surface	Billet velocity (V_b)
13-6-11	Internal plane	Unknown velocity
5-6-11	Friction surface	0
13-5-11	Internal plane	Unknown velocity

Table-4.7 Various surfaces, types and their normal velocity (Tetrahedron: 13-8-7-11)

Surface	Category	Normal velocity on that surface
13-8-7	Entry surface	Billet velocity (V_b)
8-7-11	Friction surface	0
13-8-11	Internal plane	Unknown velocity
13-7-11	Internal plane	Unknown velocity

To approximate the circular cross-section of the billet into a regular polygon, the cross-sectional areas of the billet and the approximating polygon must be maintained equal as shown in Fig. 3.3 (previous chapter), this condition being written as:

$$\Pi \; R^2 = \frac{1}{4} M \; L_1^{\,2} \; Cot \left(\frac{\psi}{2} \right) \qquad (4.1)$$

where R= radius of the round billet; M= number of polygon sides; L_1=length of each side of the approximating polygon; Ψ= internal angle of the regular polygon. From considerations of symmetry, only one half of the deformation zone as shown 4.3(a) has been considered for this analysis. Here single point formulation with one floating point has been considered, since it is observed earlier that single point formulation gives the best result for extrusion of this type of sections in case of flat faced or square dies.

The upper bound load has been computed using discontinuous velocity field. The discontinuous velocity field has been obtained by discretizing the deformation zone into tetrahedral blocks using reformulated SERR technique.

Fig. 4.3 shows one-half of the deformation zones with a single floating point on the extrusion axis at a distance from origin, all the corner points being joined to it. The resulting pyramid and tetrahedrons are the ultimate deformation sub-zones for the SERR analysis.

The single-point formulation (round cross-section approximated by 12 sides) gives rise to three pyramidal sub-zones and four tetrahedral sub-zones. Hence, it results in ten tetrahedrons, with the number of global schemes of discretisation being eight.

All these sub-zones are interconnected and have common triangular faces. Thus the basic SERR blocks in their totality have 31 bounding faces, so that as all these bounding faces are triangular in shape, by applying equation (2.12 of chapter-2), 31 velocity equations can be obtained. When these equations are solved, an equal number of velocity components can be obtained for this formulation (the discretisation details are summarized in Table 4.11).

Table-4.8 Number of planes and ways of discretization

No. of Tetrahedrons	No. of planes	No. of ways
2x3+1+1+1+1+1=10	10x4- (9)(common plane) = 31	2x2x2

Table 4.9 Total number of planes of Pyramids and Tetrahedrons

Subzones	Model numbering system	Numbering of different planes	No. of planes	Total no. of common planes	Total no. of planes
Pyramid	13-3-4-10-11	13-3-4 13-4-11 13-3-10 3-4-11 13-10-11 10-3-11 13-3-11	7	(9 common faces)	(8+8+8+4+4+4+4)-9 = 31
Pyramid	13-6-7-11-12	13-6-7 6-7-11 7-11-12 13-7-11 13-11-12 13-6-11 13-7-12	7		
Pyramid	13-1-8-9-12	1-8-13 1-13-9 13-8-12 13-8-9 8-9-12 1-8-9 13-9-12	7		
Tetrahedran	13-2-3-10	13-2-3 2-3-10 13-2-10 13-3-10	4		

Tetrahedran	13-4-5-11	13-4-5 4-5-11 13-4-11 13-5-11	4		
Tetrahedran	13-5-6-11	13-5-6 13-6-11 5-6-11 13-5-11	4		
Tetrahedran	13-7-8-11	13-8-7 8-7-11 13-8-11 13-7-11	4		

Table-4.10 Co-ordinates of points in deformation zone

Points	X-co-ordinate	Y-co-ordinate	Z-co-ordinate
1	0	-R Cos(11π/12)	L
2	0	R Cos(π/12)	L
3	R Sin(π/12)	R Cos(π/12)	L
4	R Sin(π/4)	R Cos(π/4)	L
5	R Sin(5π/12)	R Cos(5π/12)	L
6	R Sin(7π/12)	R Cos(7π/12)	L
7	R Sin(9π/12)	R Cos(9π/12)	L
8	R Sin(11π/12)	R Cos(11π/12)	0
9	0	-e Sin(3π/10)	0
10	0	e	0
11	e Cos(π/5)	e Sin(3π/10)	0
12	a/2	-e Sin(3π/10)	0
13	0	0	L0

Table 4.11 Summary of discretisation schemes

Type of sub-zones	3 pyramids , 4 tetrahedrons
Total number of SERR blocks	2+2+2+1+1+1+1=10
Number of discretisation schemes	2x2x2= 8
Number of triangular faces	31
No. of velocity components	10x3=30 for 10 SERR and 1 at exit; Total=31

4.3 Solution process

A comprehensive computational model was developed to make an upper-bound analysis for the extrusion of pentagonal section. The special feature of the proposed section is incorporated in this model and computations are carried out. The details of the solution process are described in the earlier section 3.8 of chapter-3.

4.4 The optimization parameters

For the single-point formulation, the floating point lies on the extrusion axis. Thus, the formulation has one undetermined co-ordinate, which serves as the optimization parameter to minimize the extrusion pressure for this formulation. Here, it is to be noted that the length of the die is taken as per the equivalent semi cone angle.

4.5 Results and Discussion

Computations were carried out for all eight schemes of pentagonal section and the scheme giving the least upper-bound was identified using a multivariable optimization technique. The discretised deformation zone corresponding to the least upper-bound is named here as the optimum configuration. This optimum configuration is utilized for computation of the variation of the normalized extrusion pressure with equivalent semi-cone angle (in degree) and the percentage area reduction, for different friction factors. The variation of extrusion pressure with respect to equivalent angles is given in Fig. 4.4. It is observed that extrusion pressure first decreases and then increases. It is noticed that the minimum extrusion pressure

corresponds to around 15^0 semi-cone angle for 40% reduction. Fig 4.5 represents the variation of extrusion pressure with respect to reduction for a equivalent semi-cone angle is 15^0. It is observed that extrusion pressure increases with increase in reduction as well as friction factor. Referring to Fig.4.4, it is noted that the optimal semi-cone angle that secures the minimal extrusion pressure increases slightly with the increase of friction.

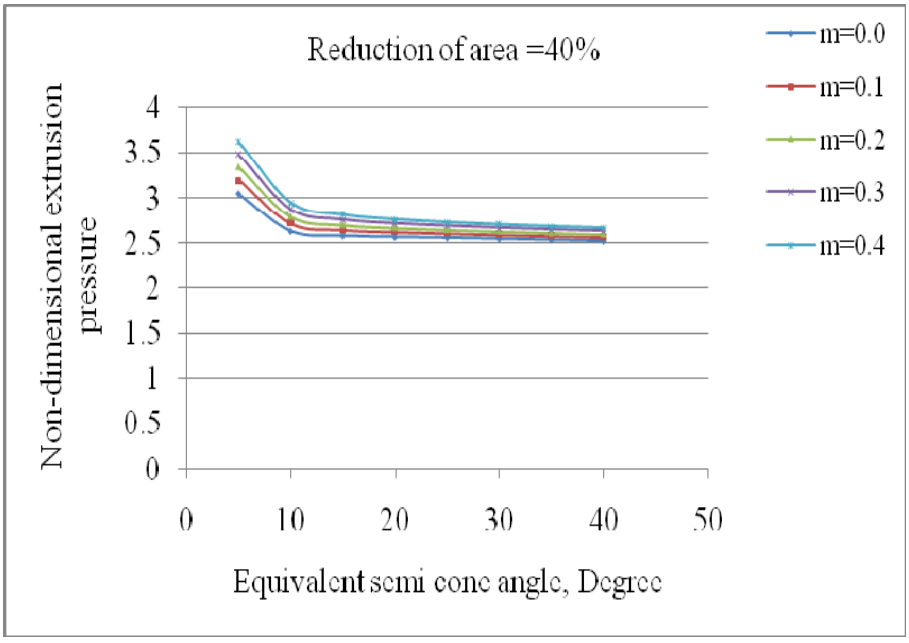

Figure 4.4 Variation of extrusion pressure with equivalent semi cone angle

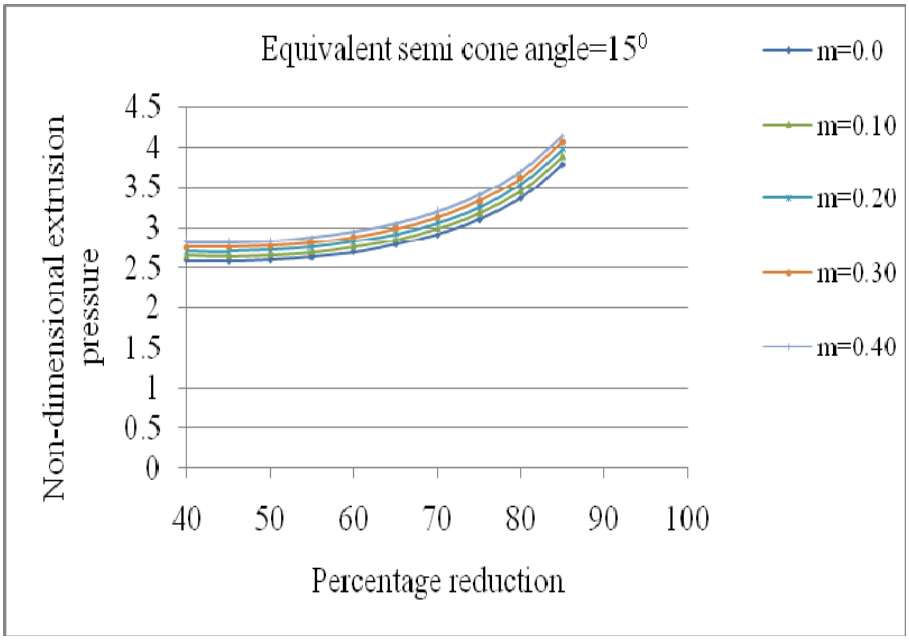

Figure.4.5 Variation of extrusion pressure with percentage of reduction.

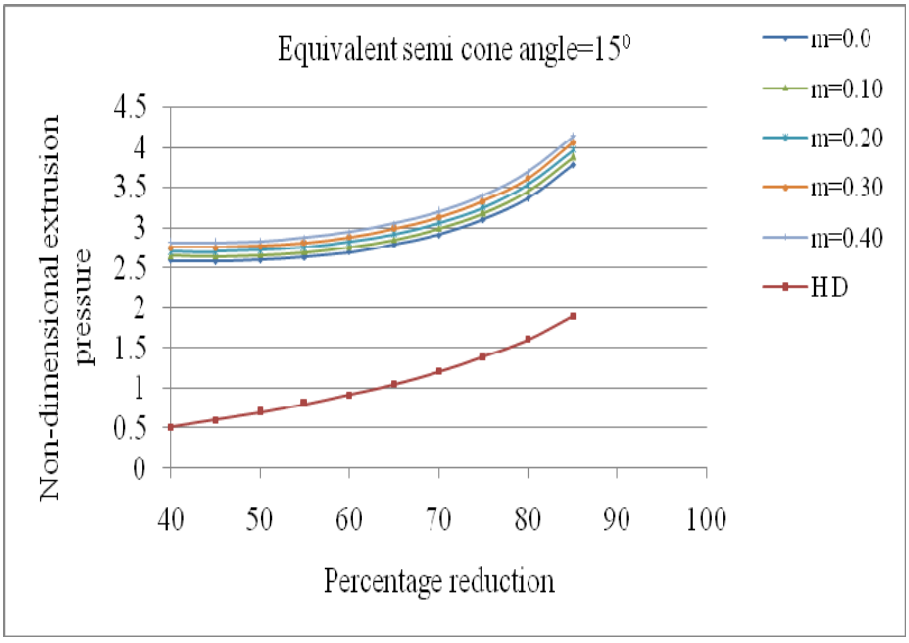

Fig. 4.6 Comparison of extrusion pressure for m=0.0 with homogeneous deformation

Referring to Fig. 4.6, the extrusion pressure due to homogeneous deformation is lower than the extrusion pressure due to friction factor m=0.0 (smooth condition). It is a check for accuracy of the results of the present investigation.

4.6 Upper Bound Analysis of Round-to-Octagonal section Extrusion

The present investigation is based on 3D upper bound method using SERR technique for the analysis of round-to-octagonal section extrusion through a converging die. The curved surfaces are approximated to the planar surfaces to apply SERR technique. A comprehensive computational model was developed to determine the normalized extrusion pressure using a multivariate unconstrained optimization technique by Kuester and Mize [87]. The extrusion pressure has been computed for various semi-cone angles with different reductions and friction factors. These results can be used to predict the forming load and optimal die shape for designing the sectioned die assuming the frictional condition.

4.7 Formulation of the present problem

As mentioned earlier, the SERR technique can be applied where there are plane boundaries. Hence, the curved surface is to be replaced by planar surfaces so as to accommodate the SERR analysis**.** Fig.4.7 shows the die geometry bounded by curved surfaces due to the round billet. For the present analysis the round billet is approximated by a regular polygon with 24 sides. Fig. 4.8 shows the deformation zone, where the round billet is approximated to a 16 sided regular polygon for clear demonstration. The circular cross section of the billet is converted into an equivalent polygon of equal area as similar to Fig. (3.3) using equations (3.1 and 4.1) to satisfy the requirement of three dimensional upper bound method based on SERR technique.

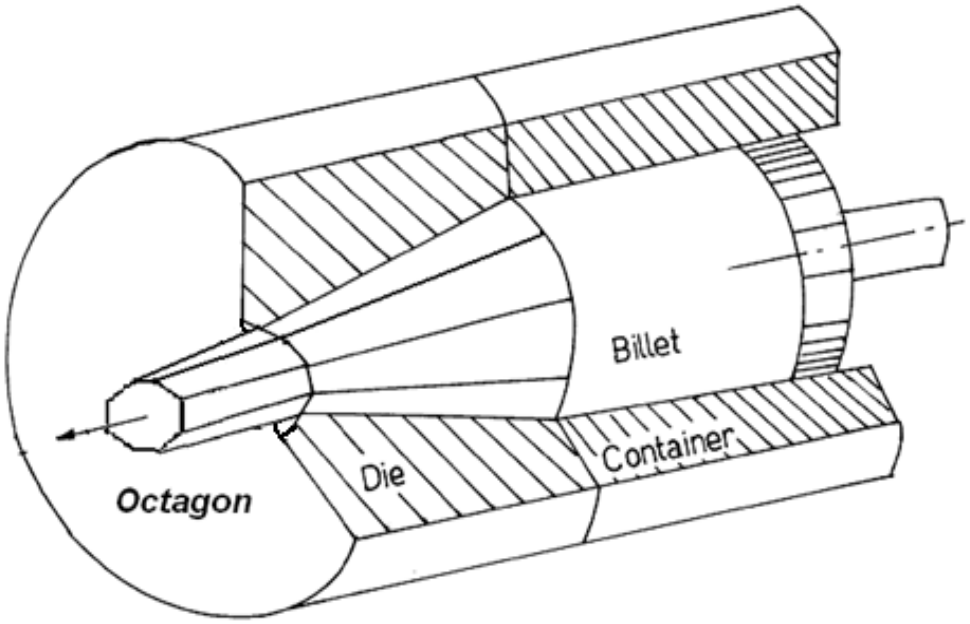

Fig. 4.7 Direct extrusion of an octagonal section from a round billet

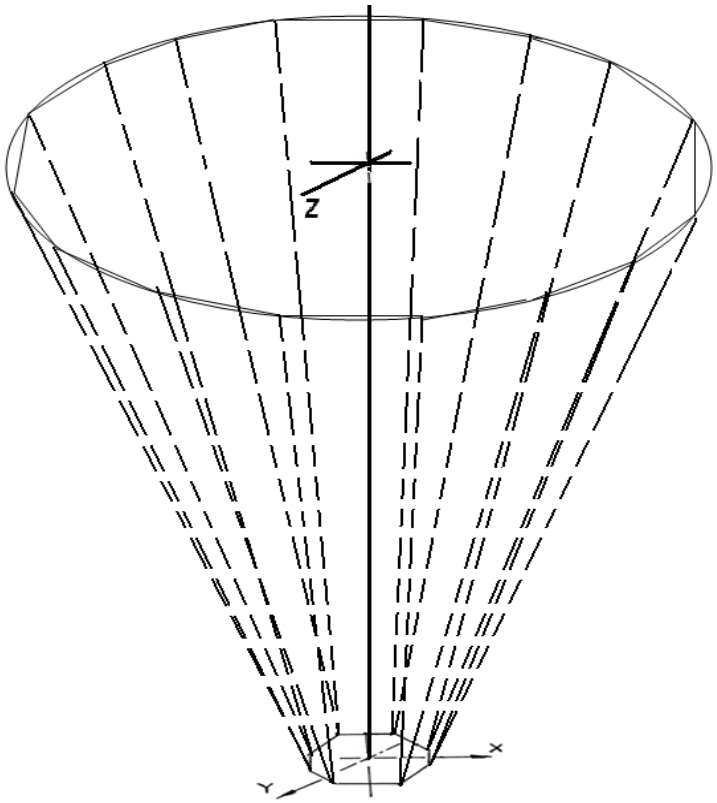

Fig. 4.8 Deformation zone, where the round billet is approximated by a 16-sided regular octagon.

Analysis is done by taking one floating point for the domain as interest for discretization. The deformation zone is to be discritized into three pyramidal subzones (13-1-2-9-10, 13-3-4-10-11 and 13-5-6-11-12), which are shown in Fig. 4.9(b), Fig. 4.9(c) and Fig. 4.9(d) respectively.

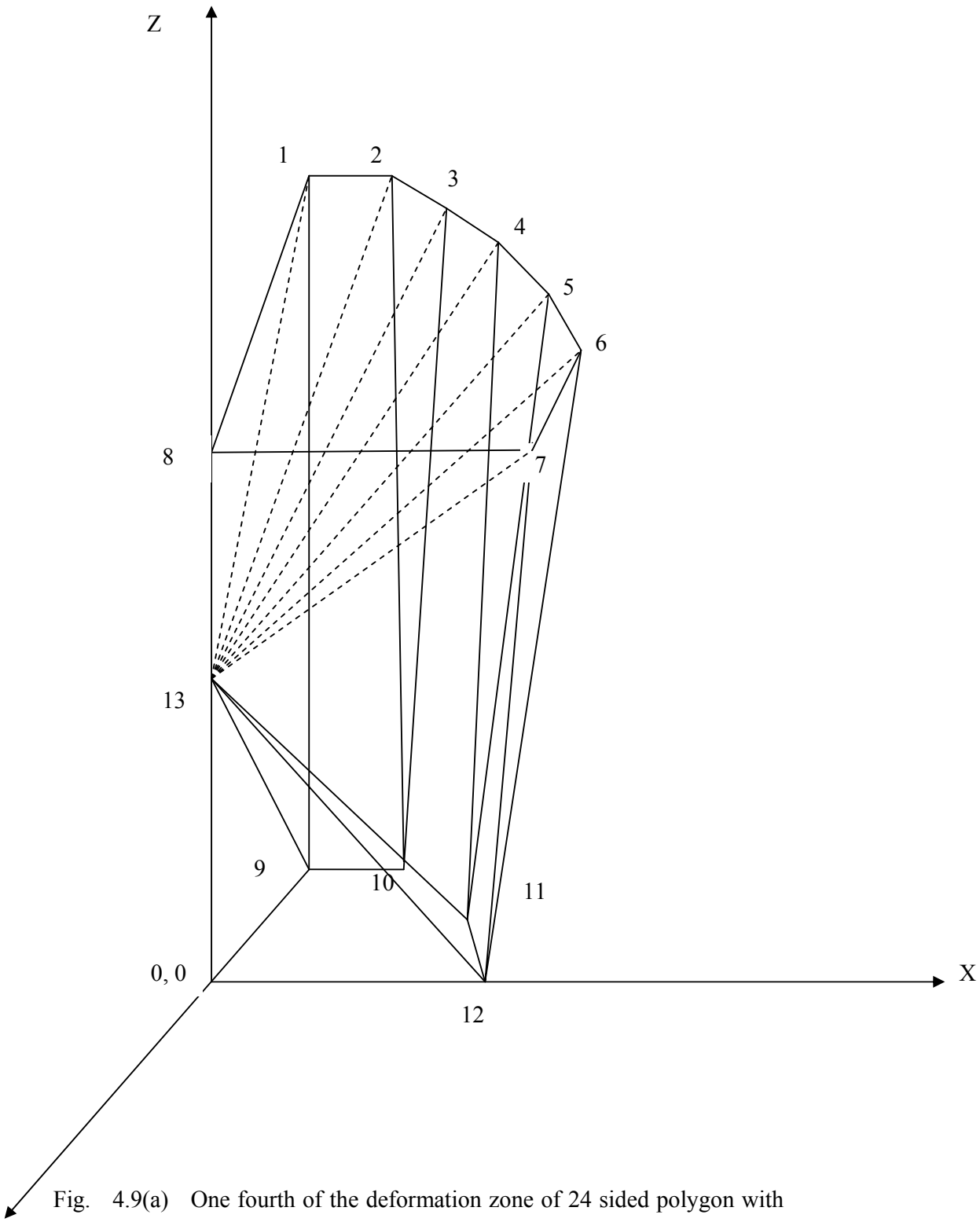

Fig. 4.9(a) One fourth of the deformation zone of 24 sided polygon with single floating point

The three tetrahedral subzones (13-2-3-10, 13-4-5-11 and 13-6-7-12), which are shown in Fig 4.9(e). Hence it results in nine tetrahedrons and the number of global schemes of discretizing of different zones being eight. The different planes are also specified in Table 4.12 to 4.17 with the normal component of velocities. Table 4.18 indicates the nature of tetrahedrons with the number of discretisation of planes. Table 4.19 summarizes the total number of planes in the deformation zone indicating the total number of planes with number of common planes. Table 4.20 specifies the co-ordinate of the deformation zone.

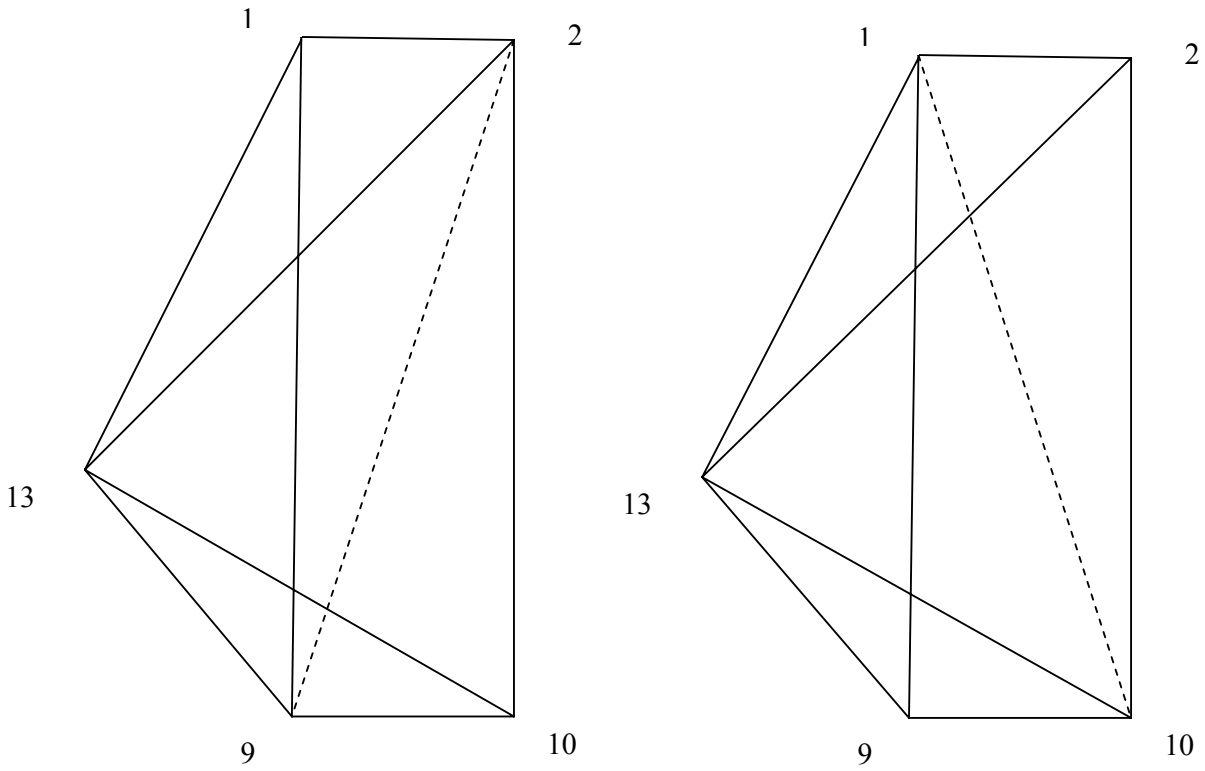

Scheme 1

Tetrahedrons

1. 13-1-2-9
2. 13-2-10-9

Scheme 2

Tetrahedrons

1. 13-1-2-10
2. 13-1-9-10

Fig. 4.9 (b) Schemes of discretization for the pyramidal subzone 13-1-2-9-10

Table-4.12 Various surfaces, types and their normal velocity (Pyramid 13-1-2-9-10, Scheme2)

Surface	Category	Normal velocity on that surface
13-1-2	Entry surface	Billet velocity (V_b)
13-2-10	Internal plane	Unknown velocity
13-1-10	Internal plane	Unknown velocity
13-1-9	Friction plane	0
13-9-10	Exit plane	Product velocity (V_P)
1-9-10	Friction plane	0
1-2-10	Friction plane	0

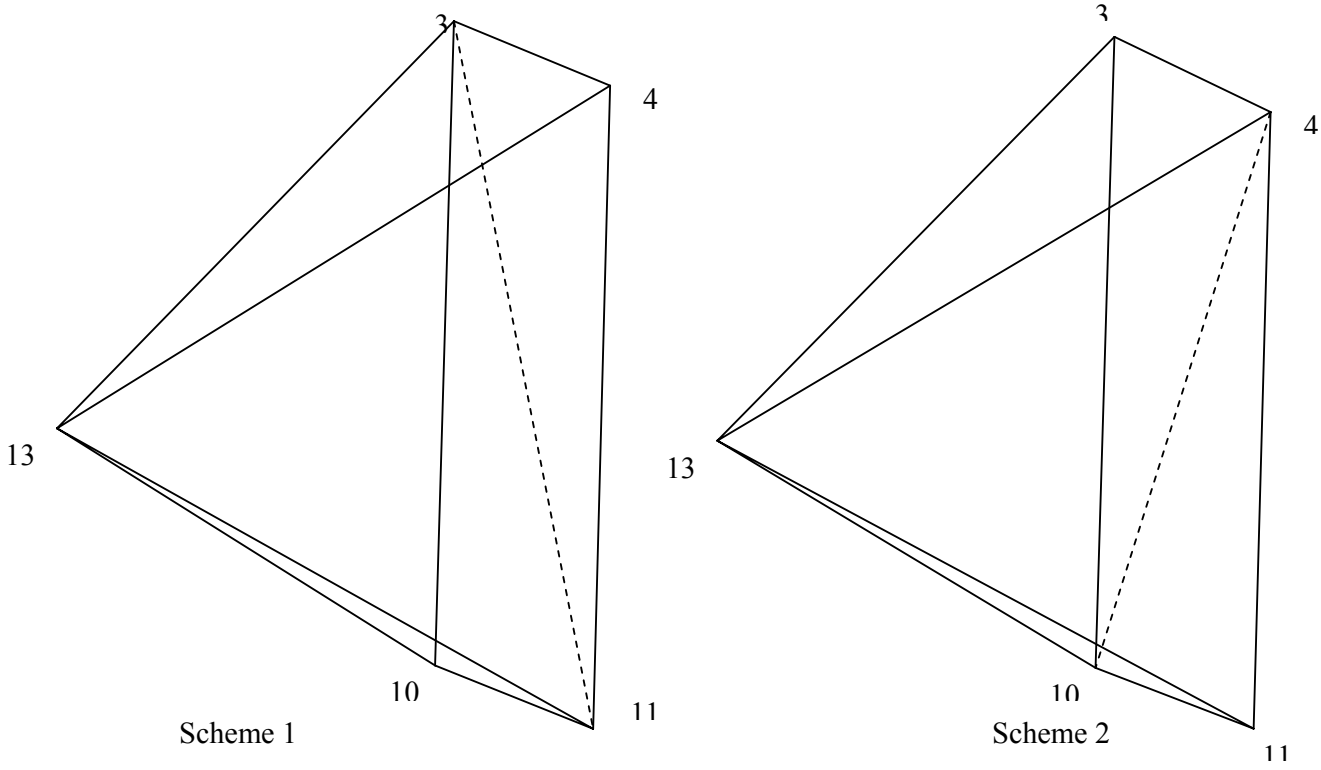

Scheme 1

Tetrahedrons

1. 13-4-10-11
2. 13-3-10-11

Scheme 2

Tetrahedrons

1. 13-3-4-10
2. 13-4-10-11

Fig. 4.9 (c) Schemes of discretization for the pyramidal subzone 13-3-4-10-11

Table-4.13 Various surfaces, types and their normal velocity (Pyramid 13-3-4-10-11, Scheme2)

Surface	Category	Normal velocity on that surface
13-3-4	Entry surface	Billet velocity (V_b)
3-4-10	Friction plane	0
13-4-10	Internal plane	Unknown velocity
13-4-11	Internal plane	Unknown velocity
13-10-11	Exit plane	Product velocity (V_P)
4-10-11	Friction plane	0
13-3-10	Internal plane	Unknown velocity

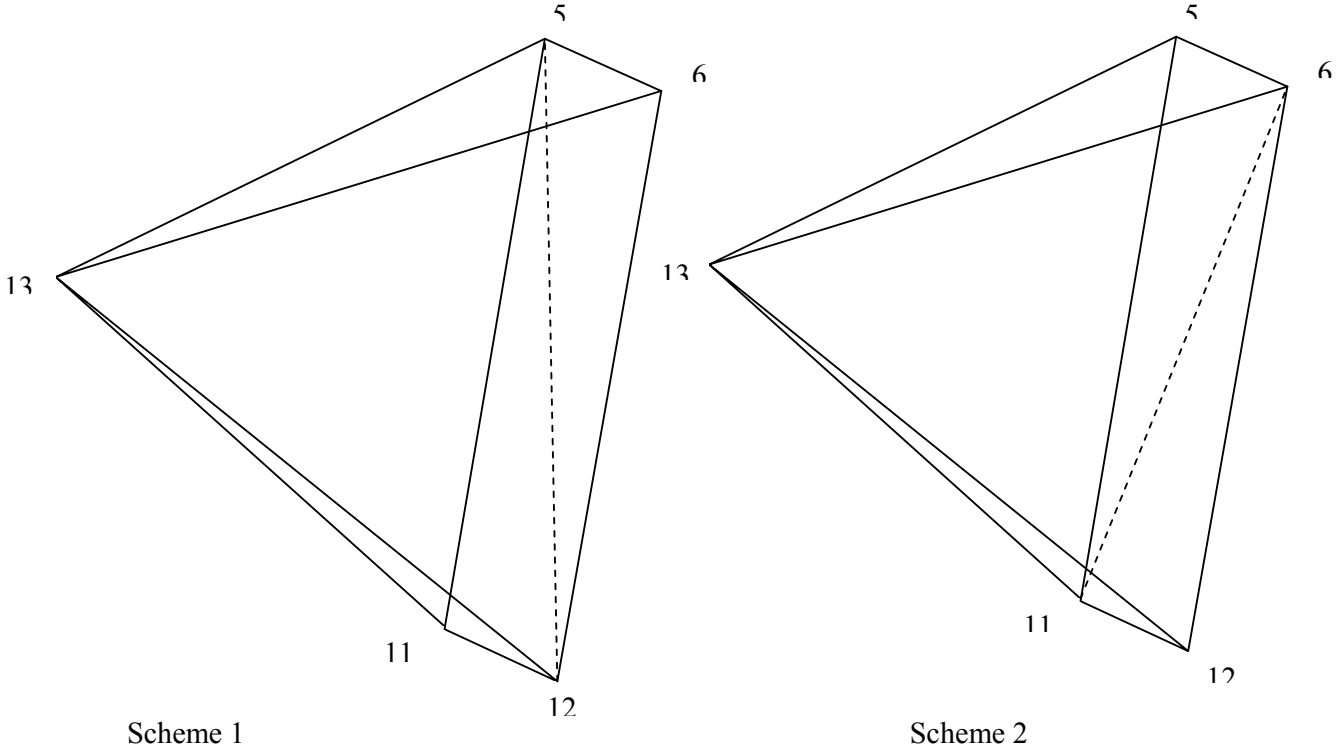

Scheme 1

Tetrahdrons

1. 13-5-11-12
2. 13-6-11-12

Scheme 2

Tetrahedrons

1. 13-6-11-12
2. 13-5-6-11

Fig. 4.9 (d) Schemes of discretization for the pyramidal subzone 13-5-6-11-12

Table-4.14 Various surfaces, types and their normal velocity (Pyramid 13-5-6-11-12, Scheme2)

Surface	Category	Normal velocity on that surface
13-5-6	Entry surface	Billet velocity (V_b)
5-6-11	Friction plane	0
6-11-12	Friction plane	0
13-6-11	Internal plane	Unknown velocity
13-11-12	Exit plane	Product velocity (V_P)
13-5-11	Internal plane	Unknown velocity
13-6-12	Internal plane	Unknown velocity

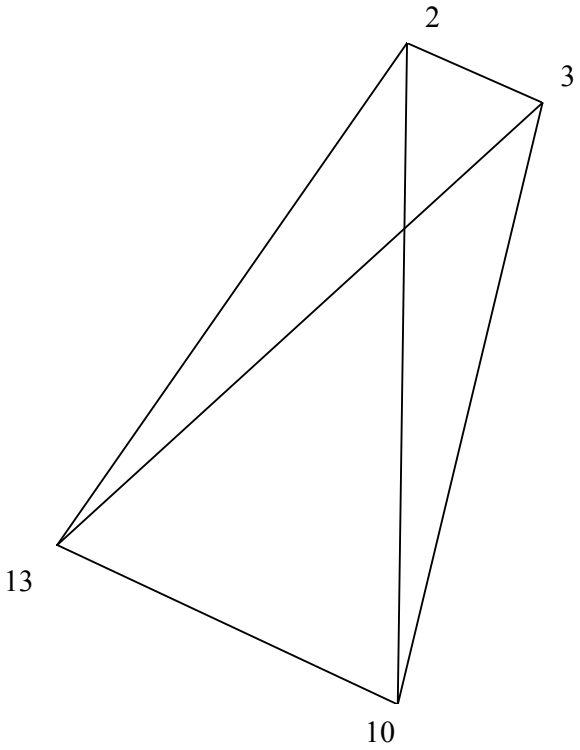

Tetrahedron: 13-2-3-10

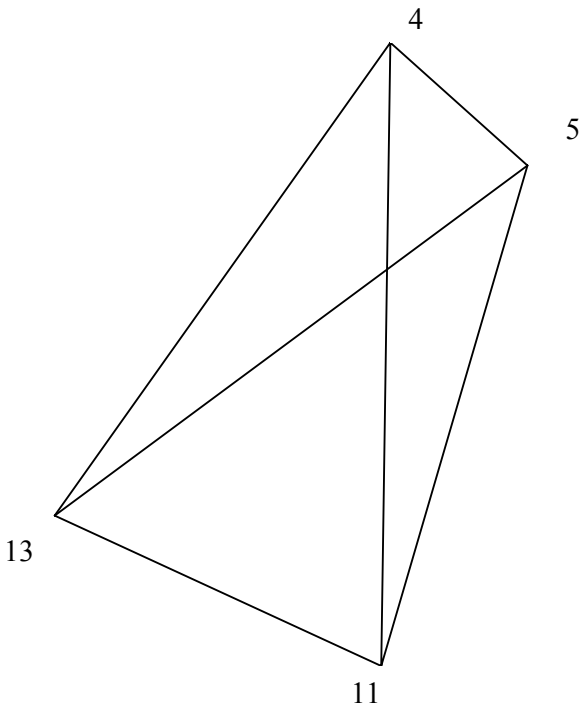

Tetrahedrons: 13-4-5-11

Continue in the next page

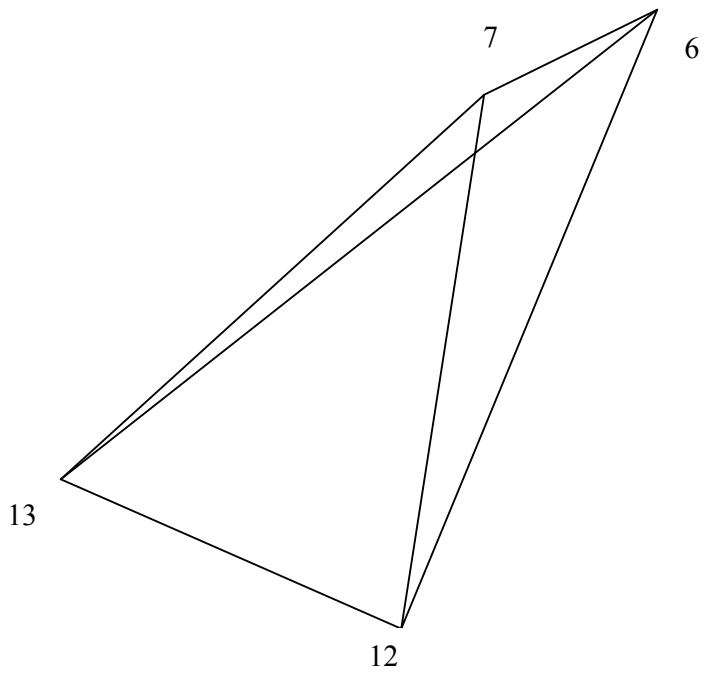

Tetrahedron: 13-6-7-12

Fig. 4.9 (e) Discretization for the tetrahedral subzone

Table-4.15 Various surfaces, types and their normal velocity (Tetrahedron: 13-2-3-10)

Surface	Category	Normal velocity on that surface
13-2-3	Entry surface	Billet velocity (V_b)
2-3-10	Friction plane	0
13-3-10	Internal plane	Unknown velocity
13-2-10	Internal plane	Unknown velocity

Table-4.16 Various surfaces, types and their normal velocity (Tetrahedron: 13-4-5-11)

Surface	Category	Normal velocity on that surface
13-4-5	Entry surface	Billet velocity (V_b)
4-5-11	Friction plane	0
13-5-11	Internal plane	Unknown velocity
13-4-11	Internal plane	Unknown velocity

Table-4.17Various surfaces, types and their normal velocity (Tetrahedron: 13-6-7-12)

Surface	Category	Normal velocity on that surface
13-6-7	Entry surface	Billet velocity (V_b)
6-7-12	Friction plane	0
13-7-12	Internal plane	Unknown velocity
13-6-12	Internal plane	Unknown velocity

Since the octagonal section has four-fold symmetry, only one-fourth of the deformation zone is considered for the analysis. For illustration, Fig. 4.8(a) shows one-fourth of the deformation zone with a single floating point on the extrusion axis at a distance from origin, all the corner points being joined to it. The resulting pyramid and tetrahedrons are the ultimate deformation sub-zone for the SERR formulation.

All these sub-zones are interconnected and have common triangular faces. Thus the basic SERR blocks in their totality have 28 bounding faces, so that as all these bounding faces are triangular in shape by applying equation (2.12 of chapter-2), 28 velocity equations can be obtained. When these equations are solved, an equal number of velocity components can be obtained for this formulation, which is mentioned in Table 4.21.

Table-4.18 Number of planes and ways of discretization

No. of Tetrahedrons	No. of planes	No. of ways
2+2+2+1+1+1=9	9x4- (8)(common plane) = 28	2x2x2

Table 4.19 Total number of planes of Pyramids and Tetrahedrons

Subzones	Model numbering system	Numbering of different planes	No. of planes	Total no. of common planes	Total no. of planes
Pyramid	13-1-2-9-10	13-1-2 13-2-10 13-1-10 13-1-9 13-9-10 1-9-10 1-2-10	7	(8 common planes)	(8+8+8+4+4+4)-8 = 28
Pyramid	13-3-4-10-11	13-3-4 3-4-10 13-4-10 13-4-11 13-10-11 4-10-11 13-3-10	7		
Pyramid	13-5-6-11-12	13-5-6 5-6-11 6-11-12 13-6-11 13-11-12 13-5-11 13-6-12	7		
Tetrahedran	13-2-3-10	13-2-3 2-3-10 13-3-10 13-2-10	4		
Tetrahedran	13-4-5-11	13-4-5 4-5-11 13-5-11	4		

		13-4-11			
Tetrahedran	13-6-7-12	13-6-7 6-7-12 13-7-12 13-6-12	4		

Table-4.20 Co-ordinates of points in deformation zone

Points	X-co-ordinate	Y-co-ordinate	Z-co-ordinate
1	0	R Cos(π/24)	L
2	R Sin(π/24)	R Cos(π/24)	L
3	R Sin(3π/24)	R Cos(3π/24)	L
4	R Sin(5π/24)	R Cos(5π/24)	L
5	R Sin(7π/24)	R Cos(7π/24)	L
6	R Sin(9π/24)	R Cos(9π/24)	L
7	R Sin(11π/24)	R Cos(11π/24)	L
8	R Sin(11π/24)	0	L
9	0	e	0
10	a/2	e Cos(3π/24)	0
11	e Cos(3π/24)	a/2	0
12	e Cos(3π/24)	0	0
13	0	0	L0

Table 4.21 Summary of discretisation schemes

Type of sub-zones	3 pyramids 3 tetrahedrons
Total number of SERR blocks	2+2+2+1+1+1=9
Number of discretisation schemes	2x2x2=8
Number of triangular faces	28
No. of velocity components	9x3=27 for 9 SERR and 1 at exit Total=28

4.8 Results and Discussion

The solution process and the calculation of the optimizing parameters are described in the sections 3.7 and 3.8 of the chapter-3. Computations were carried out for all eight schemes of octagonal section and the scheme giving the least upper-bound was identified. The discretised deformation zone corresponding to the least upper-bound is named here as the optimum configuration. This optimum configuration is utilized for computation of the variation of the normalized extrusion pressure with equivalent semi-cone angle (in degrees) and the percentage area reduction, for different friction factors. The variation of non-dimensional extrusion pressure with equivalent semi-cone angles is given in Fig. 4.10 for 40% reduction. It is observed that the minimum extrusion pressure corresponds nearly to semi-equivalent angle of 15^0, though there is some change in equivalent angle with change in friction factor. The variation of non-dimensional extrusion pressure with respect to percentage of area reduction and friction factors are shown in Fig. 4.11 for a constant die length corresponding to semi-equivalent angle of 15^0. The extrusion pressure increases with increase in reduction and friction factor. It is also observed that the effect of friction factor on extrusion pressure is more predominant at high friction.

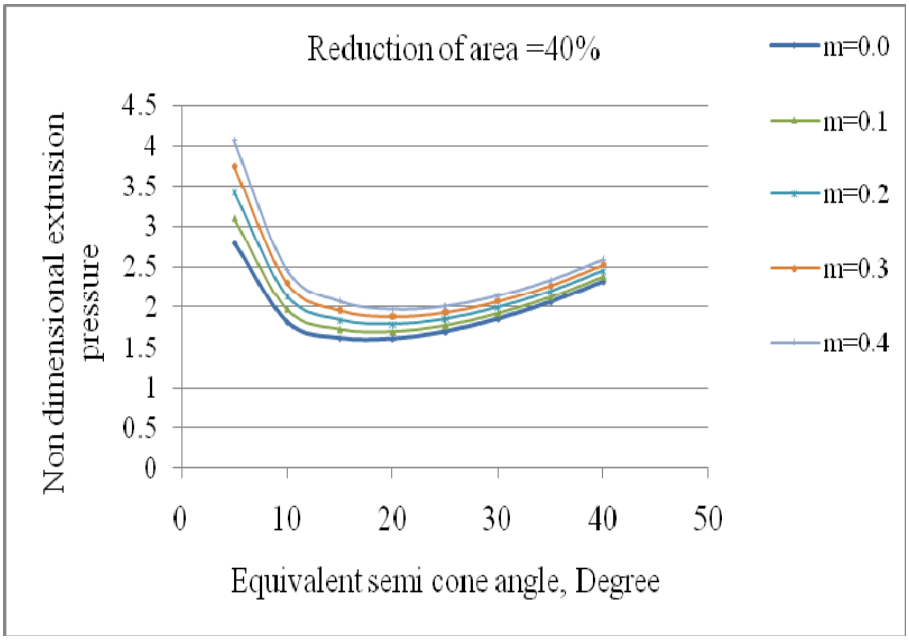

Fig.4.10 Variation of extrusion pressure with equivalent semi cone angle

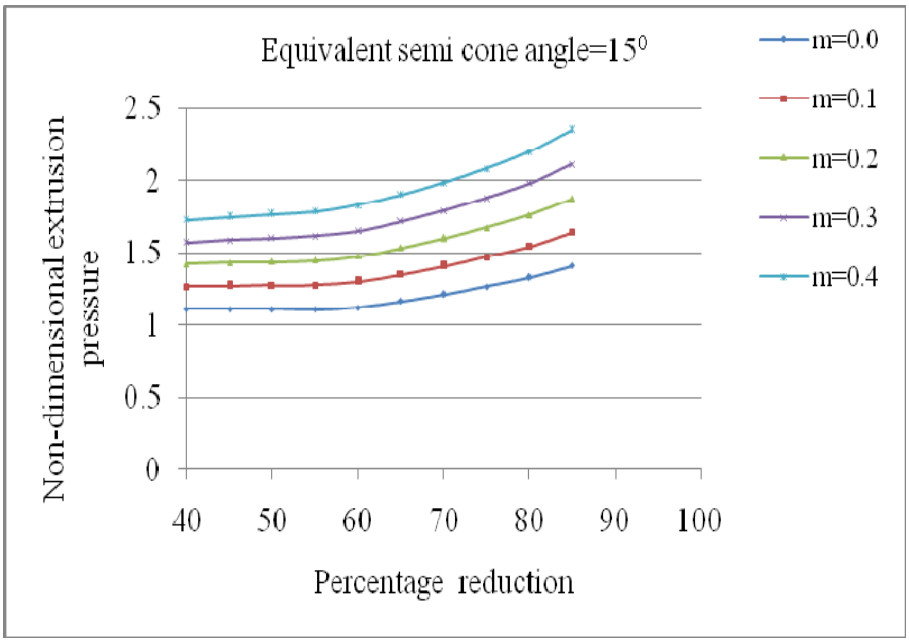

Fig.4.11 Variation of extrusion pressure with percentage of reduction.

4.9 Conclusions

(i) The extrusion pressure increases with increase in reduction and friction factor.

(ii) The extrusion pressure is minimum, when the equivalent semi cone angle is 15^0 for pentagonal as well as octagonal section.

(iii) Using the solution, the optimal die geometry (the equivalent semi-cone angle) that requires the minimum extrusion pressure can be obtained for different reductions of area and friction condition.

A Class of Solution to Extrusion of Square Section from Square Billet through Cosine, Polynomial and Bezier Shaped Curved Die

5.1 Introduction

A great deal of work has been carried out for the extrusion of different sections using flat faced die and converging dies. The converging dies are having some specific advantages over flat faced dies in terms of reduction in extrusion load and gradual flow of material. In all the previous chapters, upper bound analysis has been carried out for extrusion of different sections from round billet using discontinuous velocity field based on SERR technique. In the following sections upper bound analysis is being carried out using continuous velocity field based on dual stream function method.

- ***Based on the paper published by the author, entitled,***

1. *Numerical and Experimental study on the three-dimensional extrusion of square section from square billet through a polynomial shaped curved die, communicated to an Int. J. of Advanced Manufacturing Technology (A-M-T), (Springer publication)* ***(Under third final review)***

2. *An Upper Bound solution to Three-Dimensional extrusion through a Bezier shaped curved die, published in an International Journal of Manufacturing Technology and Research,* ***Vol. 5, (1-2)****, 2009.*

3. *Computer-Aided Simulation of Metal Flow Through Curved Die for Extrusion of Square Section From Square Billet", published in the Journal Key Engineering Materials,* ***Vol. 424, pp. 181-188****, (2010) (Trans Tech. Publications, Switzerland)*

4. *A Numerical Investigation of Extrusion through Bezier shaped curved Profile, published in the Journal Key Engineering Materials* ***(with the title Advances in Materials Processing IX)****,* ***Vol. 443, (2010), pp. 93-97,*** *(Trans Tech. Publications, Switzerland).*

The geometry of die profile plays a significant role for smooth flow of material resulting in the evolution of uniform microstructure in extruded product with improved mechanical properties and reduction in extrusion pressure. Recently the process design involving mathematically contoured die profile has drawn the attention of various researchers to improve not only dimensional accuracy but also quality of products.

In the present investigation an upper bound analysis has been carried out for extrusion of square section from square billets with cosine, polynomial and Bezier die profile using dual stream function method.

5.2 Extrusion of Square Sections from Square Billets through Polynomial Shaped curved Dies

An upper bound analysis has been carried out for extrusion of square section from square billets with polynomial die profile using dual stream function method. The die profile function has been defined by a fifth order polynomial with non-zero slope at the entry and exit planes. The constant friction factor has been assumed at the die billet interface as linear boundary condition.

The upper bound theorem states that the power estimated from kinematically-admissible velocity fields (KAVF) is always higher than the actual one. Amongst all kinematically-admissible velocity fields the actual one minimizes the expression:

$$J = \left(\frac{2\sigma_0}{\sqrt{3}}\right)\int_V \sqrt{(\varepsilon_{ij}\varepsilon_{ij})}dV + \left(\frac{\sigma_0}{\sqrt{3}}\right)\int_{S_i} |\Delta V|_{S_i} dS_i + \left(\frac{m\sigma_0}{\sqrt{3}}\right)\int_{SD_i} |\Delta V|_{SDi} dS_{SD_i} \qquad (5.1)$$

where J is the power of dissipation rate, σ_0 is the flow stress; ε_{ij} is the derived strain-rate tensor, $|\Delta V|_{S_i}$ is the velocity discontinuity at the entry and exit surfaces S_i, $|\Delta V|_{SD_i}$ is the velocity discontinuity at the die-metal interfaces SD_i and m is the friction factor.

The kinematically admissible velocity field has been obtained using dual stream function method. According to Yih [192], the velocity components can be derived from these stream functions using the equations.

$$V_x = \left(\frac{\partial \psi_2}{\partial y}\right)\left(\frac{\partial \psi_1}{\partial z}\right) - \left(\frac{\partial \psi_1}{\partial y}\right)\left(\frac{\partial \psi_2}{\partial z}\right) \qquad 5.2(a)$$

$$V_y = \left(\frac{\partial \psi_2}{\partial z}\right)\left(\frac{\partial \psi_1}{\partial x}\right) - \left(\frac{\partial \psi_1}{\partial z}\right)\left(\frac{\partial \psi_2}{\partial x}\right) \qquad 5.2(b)$$

$$Vz = \left(\frac{\partial \psi_2}{\partial x}\right)\left(\frac{\partial \psi_1}{\partial y}\right) - \left(\frac{\partial \psi_1}{\partial x}\right)\left(\frac{\partial \psi_2}{\partial y}\right) \qquad 5.2(c)$$

To derive the dual stream functions for the present problem, the geometry shown in Fig.5.1 and Fig. 5.2 with prescribed reference system is considered. Because of symmetry about two mutually perpendicular axes, only one quadrant of the actual deformation zone is considered, F(z) is the die-profile function such that the die faces in the x-z and y-z planes are represented by x=F(z) and y=F(z) respectively. The function F (z) must satisfy the conditions that F (z) =W at z=0 and F(z)=A at x=L, where W and A are the semi width of billet and product respectively and L is the die length.

The dual stream functions ψ_1 and ψ_2 are chosen as shown below

$$\psi_1 = -\frac{x}{F(z)} \qquad 5.3(a)$$

$$\psi_2 = \frac{W^2 V_b\, y}{F(z)} \qquad 5.3(b)$$

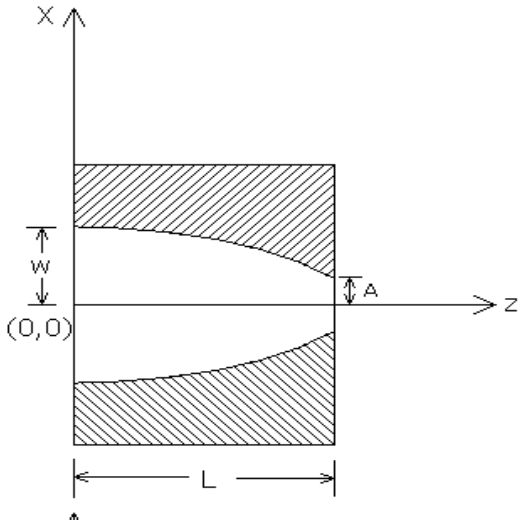

Fig. 5.1 Profile of a curved die with the axes of reference.

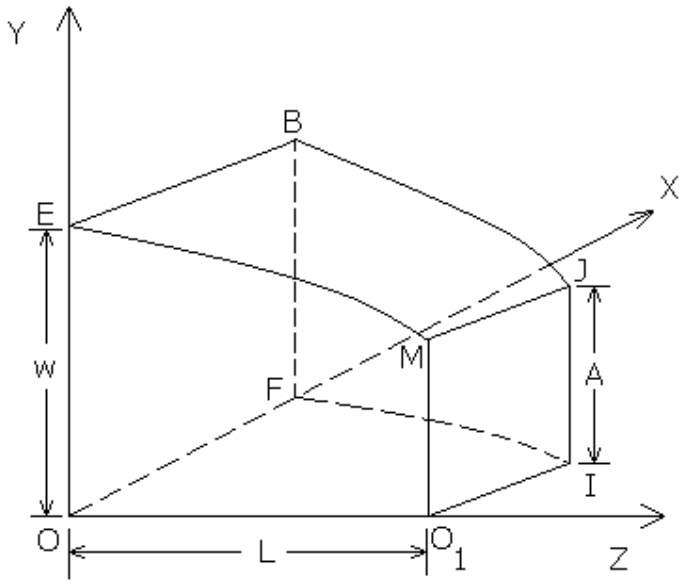

Fig. 5.2 One quadrant of the deformation zone.

where V_b is the billet velocity. It can be easily verified that (i) $\psi_1 = 0$ on the plane x=0 and $\psi_1 = -1$ on the die surface plane x=F (z); and (ii) $\psi_2 = 0$ on the plane y=0 and $\psi_2 = W^2 V_b$ (which is a constant) on the die surface y=F (z)). Such constant values ensure that surfaces x=0, x=F (z), y=0 and y=F (z) are stream surfaces, and as such velocity components normal to those surface vanish. Thus, ψ_1 *and* ψ_2 defined in the above-mentioned manner satisfy all velocity boundary conditions. Hence they are valid boundary conditions. Hence, they are valid stream functions to generate a kinematically-admissible velocity field. Substituting Eq. (5.3) into Eq. (5.2) and simplifying, the velocity components in the deformation region are:

$$V_x = \frac{W^2 V_b \, xF'}{F^3} \qquad 5.4(a)$$

$$V_y = \frac{W^2 V_b \, yF'}{F^3} \qquad 5.4(b)$$

$$V_z = \frac{W^2 V_b}{F^2} \qquad 5.4(c)$$

where F = F (z) and $F' = dF/dz$

The strain-rate components ε_{ij} are derived from the velocity components using the relationship:

$$\varepsilon_{ij} = \frac{1}{2}\left[\left(\frac{\partial V_j}{\partial x_i}\right)+\left(\frac{\partial V_i}{\partial x_j}\right)\right] \tag{5.5}$$

The strain-rate components for the proposed flow field are as follows by substituting Eq. (5.4) in Eq. (5.5)

$$\varepsilon_{xx} = \frac{\left(W^2\, V_b\, F'\right)}{F^3} \tag{5.6(a)}$$

$$\varepsilon_{yy} = \frac{\left(W^2\, V_b\, F'\right)}{F^3} \tag{5.6(b)}$$

$$\varepsilon_{zz} = \frac{\left(-2W^2\, V_b\, F'\right)}{F^3} \tag{5.6(c)}$$

$$\varepsilon_{xy} = \varepsilon_{yx} = 0 \tag{5.6(d)}$$

$$\varepsilon_{yz} = \varepsilon_{zy} = \left(\frac{1}{2}\right)W^2 V_b\, y\left[\left(\frac{F''}{F^3}\right)-\left(\frac{3\left(F'\right)^2}{F^4}\right)\right] \tag{5.6(e)}$$

$$\varepsilon_{zx} = \varepsilon_{xz} = \left(\frac{1}{2}\right)W^2 V_b\, x\left[\left(\frac{F''}{F^3}\right)-\left(\frac{3\left(F'\right)^2}{F^4}\right)\right] \tag{5.6(f)}$$

where $F'' = d^2F / dz^2$

From equation (5.6), it is evident that velocity field satisfy incompressibility condition. Using Eq. (5.1), J can be evaluated when the die-profile function, F, is known. For any reduction and friction factor m, J then can be minimized with respect to appropriate parameters to yield the best upper bound.

The mean extrusion pressure using the above upper-bound theorem is determined from the relation

$$\frac{p_{av}}{\sigma_0} = \frac{J}{W^2 V_b \sigma_0} \tag{5.7}$$

5.3 Computation

An integrated FORTRAN code was developed to compute the upper bound extrusion load using Eq. (5.1). For any reduction R and friction factor m, the program first calculates the velocity components and the strain rate components using Eq. (5.4) and (5.6) respectively and then evaluates the upper-bound power on Eq. (5.1) by numerical integration using the 5-point Gauss-Legendre quadrature algorithm. The total power of deformation has been minimized using a multivariable optimization technique [87].

5.4 Die-profile function

The die geometries examined in the present investigation are shown in Fig. 5.1-5.2, Referring to this figure, it may be seen that:

(a) the die-profile function F(z) is similar in both the x- and y-directions:

(b) $$x = b_1\left(\frac{z}{L}\right)^5 + b_2\left(\frac{z}{L}\right)^4 + b_3\left(\frac{z}{L}\right)^3 + b_4\left(\frac{z}{L}\right)^2 + b_5\left(\frac{z}{L}\right) + W \tag{5.9}$$

Where, $b_5 = A - b_1 - b_2 - b_3 - b_4 - W$

The die profile function satisfies the boundary condition such that at z=0, x=W and z=L, x=A. The exit and entry angles are non-zero angles. There are five independent variables including die length.

(c) The velocity-discontinuity surfaces are normal to the axial flow directions.

5.5 Results and Discussion

The variation of non-dimensional extrusion pressure with respect to reductions are shown in Fig.5.3 for different friction factor (m=0.0 to 1). It is observed that there is an increase in extrusion pressure with increase in reduction and friction factor. At low reduction, PR=30% the extrusion pressure varies from $0.5\sigma_0$ to $1.2\sigma_0$ whereas at high reduction PR=90%, it varies from $2.4\sigma_0$ to $6.0\sigma_0$. It is interesting to note that the effect of friction is more significant at higher reduction compared to lower reduction. Hence, the role of lubricant at larger reduction is more effective in reducing the extrusion pressure.

The variation of non-dimensional die length (L/W) with respect to different reductions and friction factors are shown in Fig.5.4. It is observed that there is increase in die length with rise in reduction, but decrease in die length with increase in friction factor at the die billet interface. At low reduction 30% the optimum die length varies from 0.4 to 0.78 times of billet width, whereas at the higher reduction 90%, it varies from 0.97 to 1.4. The variation is almost linear with respect to reduction.

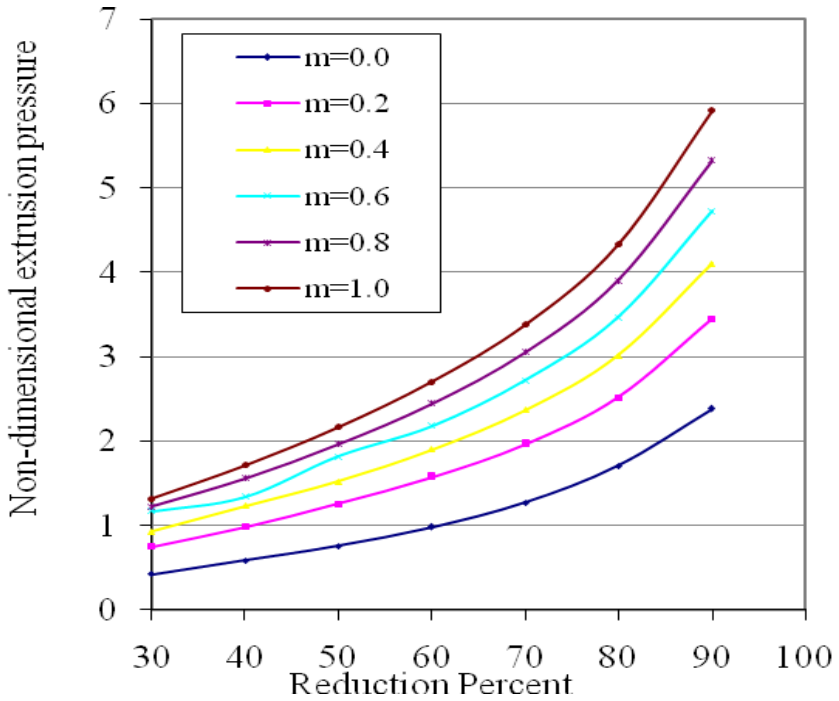

Fig. 5.3 Variation of the non-dimensional extrusion pressure with percentage reduction.

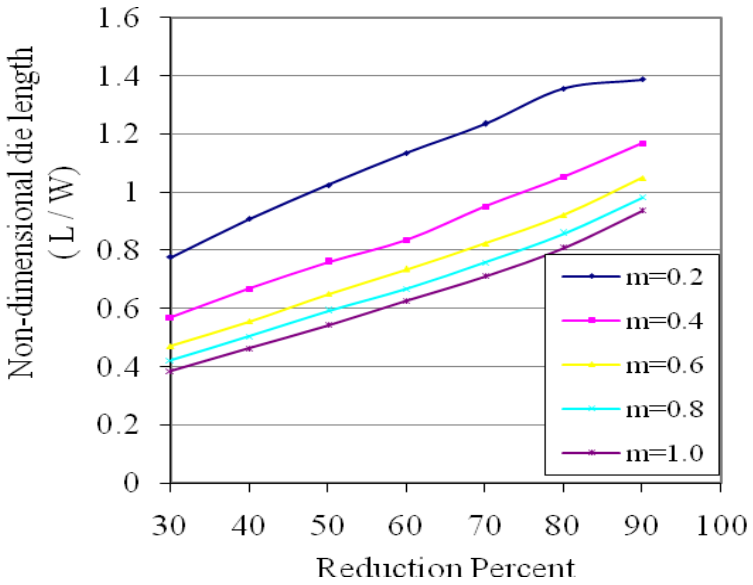

Fig. 5.4 Variation of the non-dimensional die length with percentage reduction.

For different friction factors, the power of deformation due to velocity discontinuity at the entry and exit planes with respect to reductions is presented in Fig.5.5 and Fig. 5.6 respectively. It is noted that both the power of deformation due to velocity discontinuities increase with rise in reduction as well as friction factor almost linearly in identical manner. The variation of power due to frictional work at the die-billet interface is shown in Fig.5.7. It increases with both rise in reduction and friction factor. It is also obvious that the effect of friction is more sensitive at higher reduction. The variation of internal power of deformation with reduction is presented in Fig.5.8. It is shown that variation of internal power of deformation is not sensitive to change in friction factor. Referring to Fig.5.9, it is evident that the total power of deformation as well as internal power of deformation is always higher than homogeneous deformation. It is a check for validity of the solution.

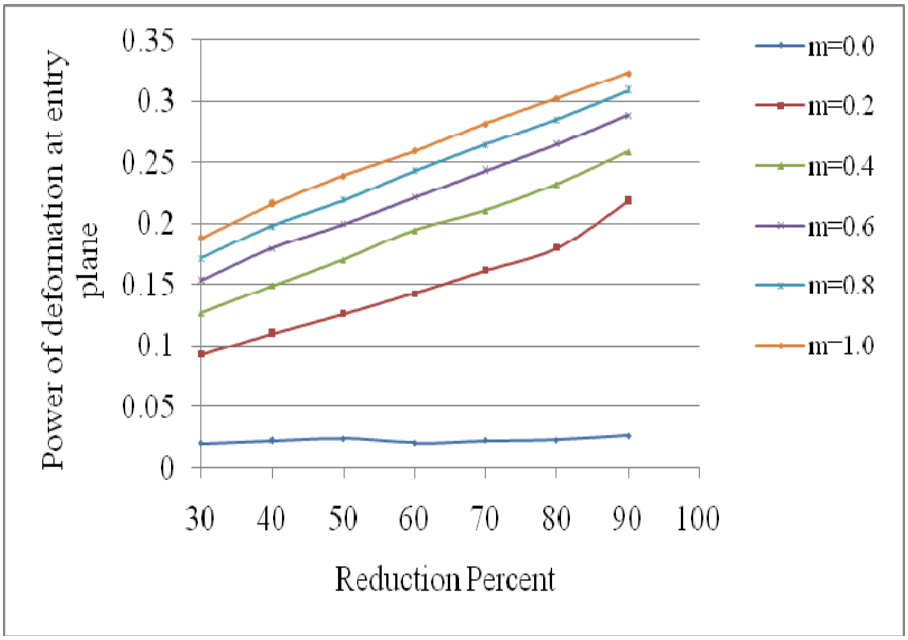

Fig. 5.5 Variation of the power of deformation at the entry plane with percentage reduction.

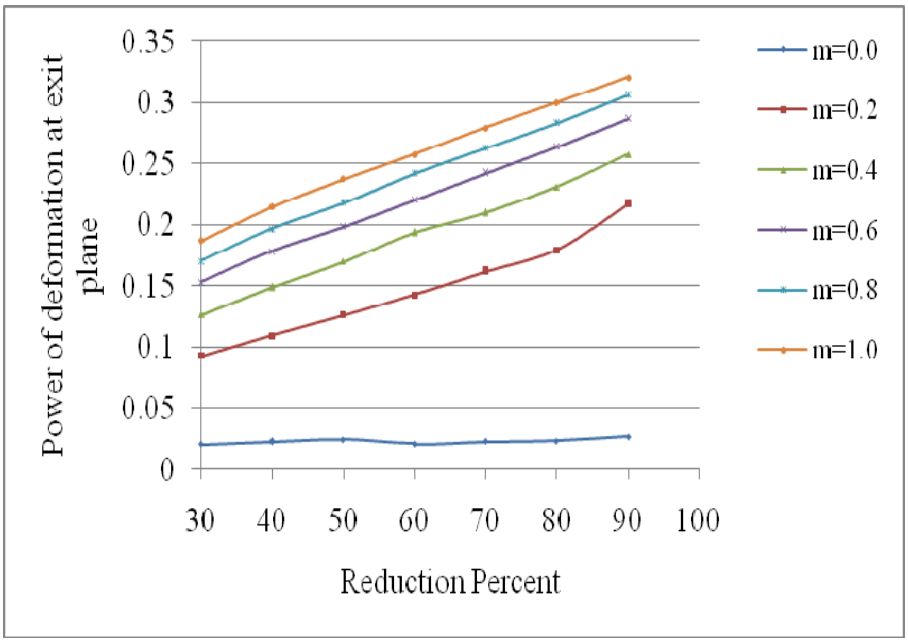

Fig.5.6 Variation of the power of deformation at the exit plane

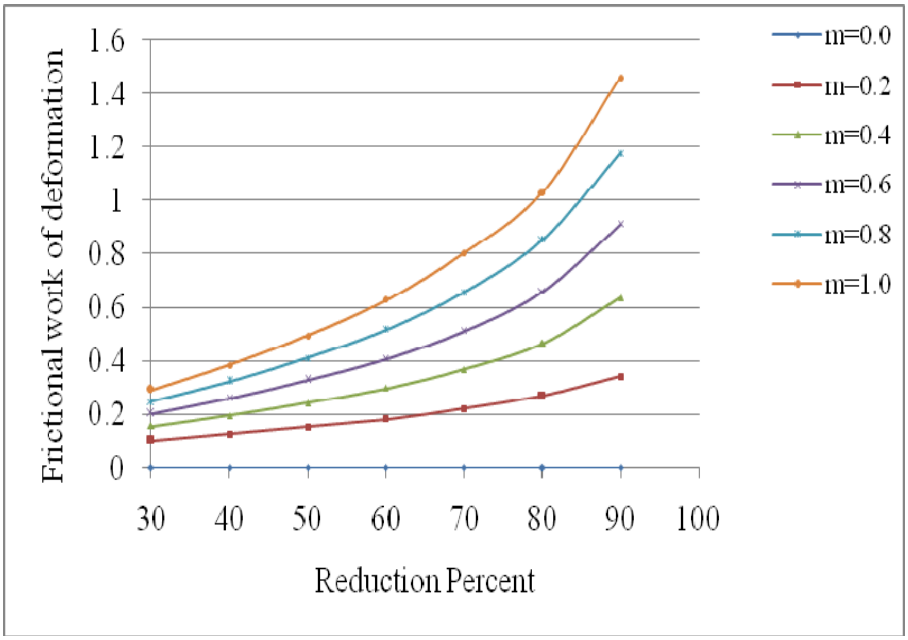

Fig. 5.7 Variation of the frictional power of deformation with percentage reduction

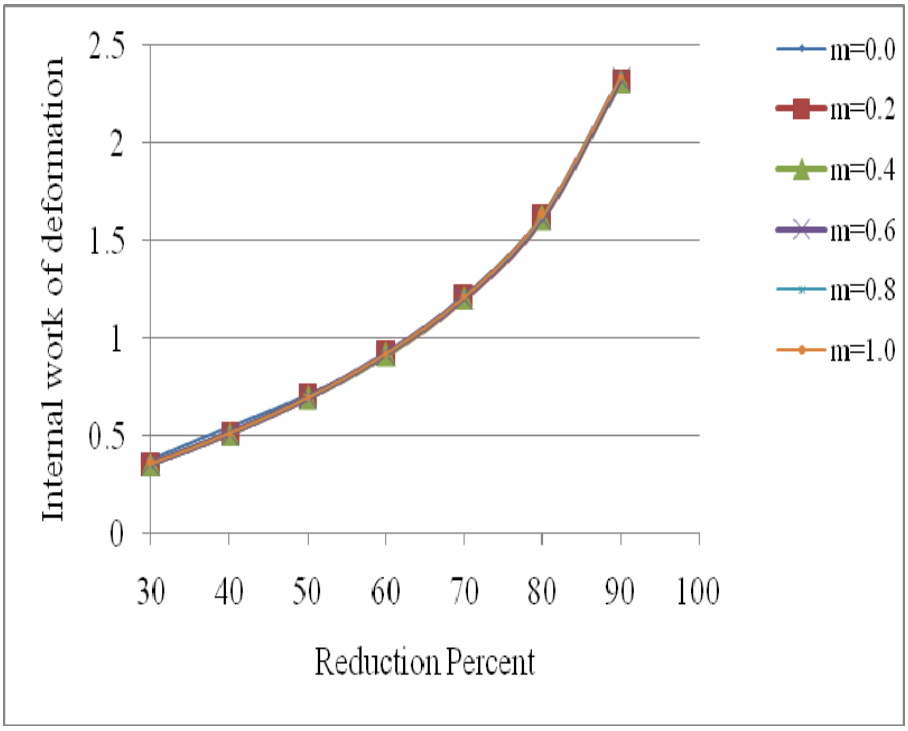

Fig. 5.8 Variation of the internal power of deformation with percentage reduction.

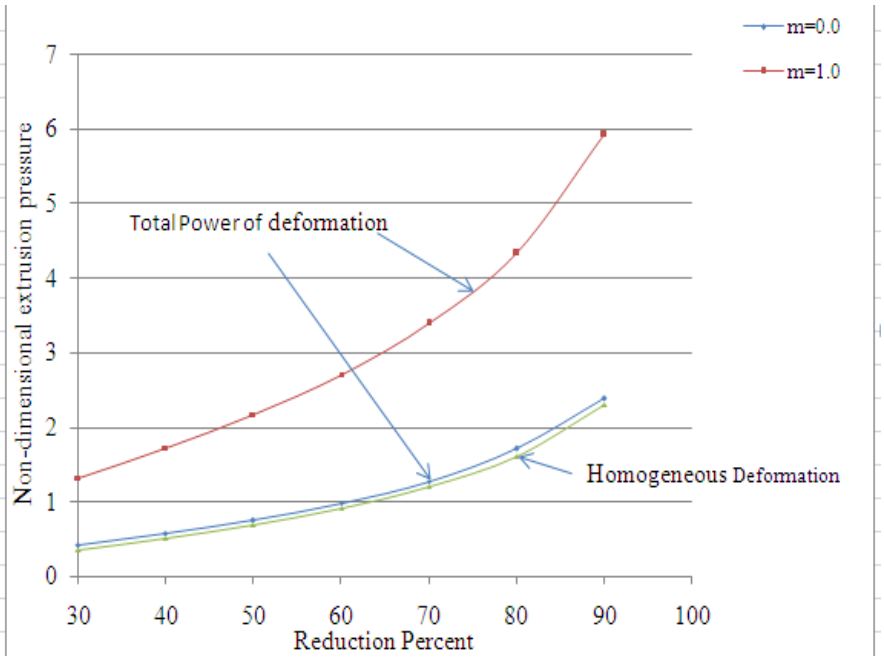

Fig. 5.9 Comparison of internal and homogeneous power of deformation with percentage reduction at m=1.0.

The extrusion pressure for polynomial shaped mathematically contoured die is compared with other conventional curved dies in lubricated condition (m=0.4) [117] in Fig.5.10. It is evident that polynomial shaped die is superior to hyperbolic, parabolic, circular and elliptic die profile [117]. However, cosine shaped die yields identical results with polynomial shaped die especially at low reduction. Referring to Fig.5.11, it is also evident that extrusion pressure required for the polynomial shaped die is the least compared to other analytic curved die for the sticking friction condition (m=1.0) [117]. Hence the performance of polynomial shaped mathematically contoured die is better than other conventional curved dies [117] for a wide range of frictional boundary conditions at the die billet interface. The above results are valid for any rigid plastic material with constant flow stress. It can also be applied for materials with strain hardening assuming average flow stress using above modeling. As reported earlier [117], the extrusion pressure of cosine die is minimum compared to elliptic, hyperbolic, parabolic and circular die profile. Referring to Fig.5.12, the variation of non-dimensional extrusion pressure with respect to reduction for

polynomial as well as cosine dies are shown in Fig. 5.12 for m=0.38 and m=0.75 respectively. The m=0.38 and m=0.75 correspond to wet and dry friction for lead material as obtained from ring compression test as done in later chapter-7. It is seen that at dry friction polynomial shaped die yields the minimum extrusion pressure, where as cosine die gives almost identical results with polynomial die. Using proper frictional boundary conditions, the extrusion pressure and optimum die geometries can be determined for different work materials

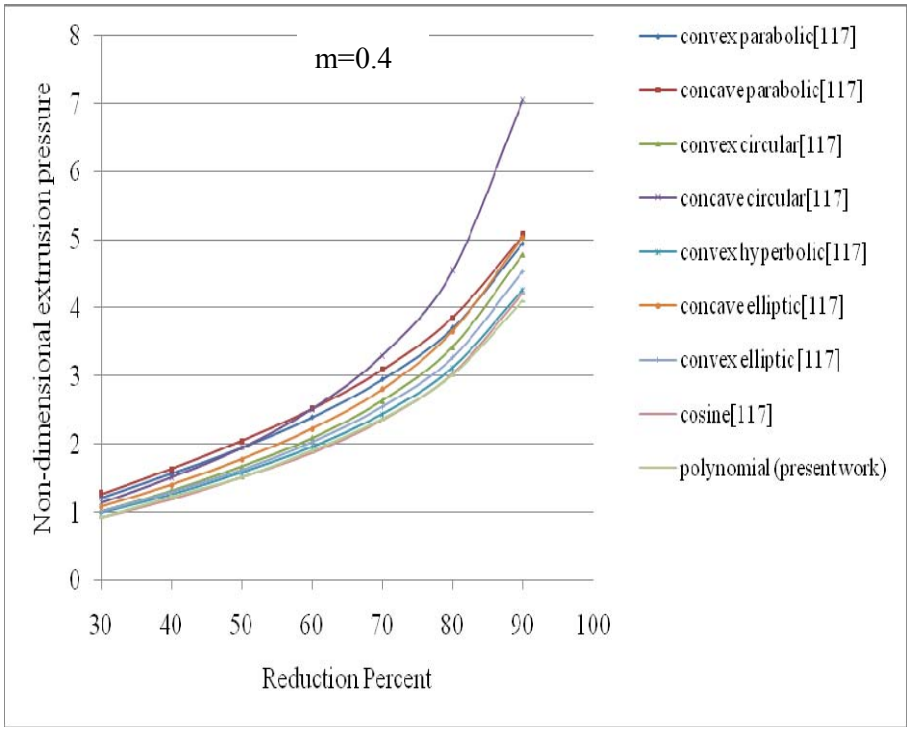

Fig. 5.10 Variation for the non-dimensional extrusion pressure with percentage reduction for dies with semi lubricated condition (m=0.4).

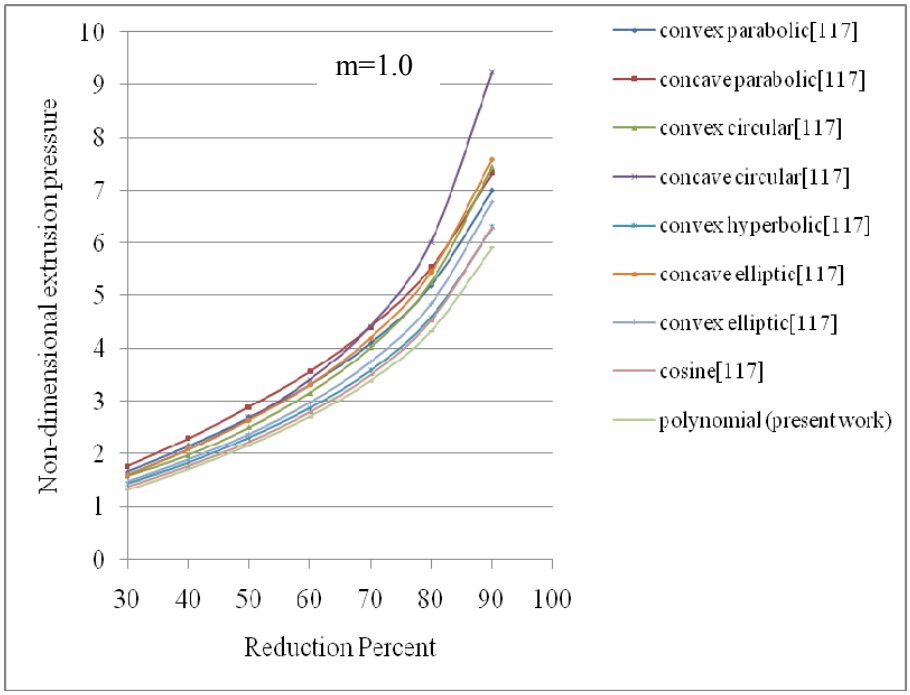

Fig. 5.11 Variation for the non-dimensional extrusion pressure with percentage reduction for dies with sticking friction (m=1.0).

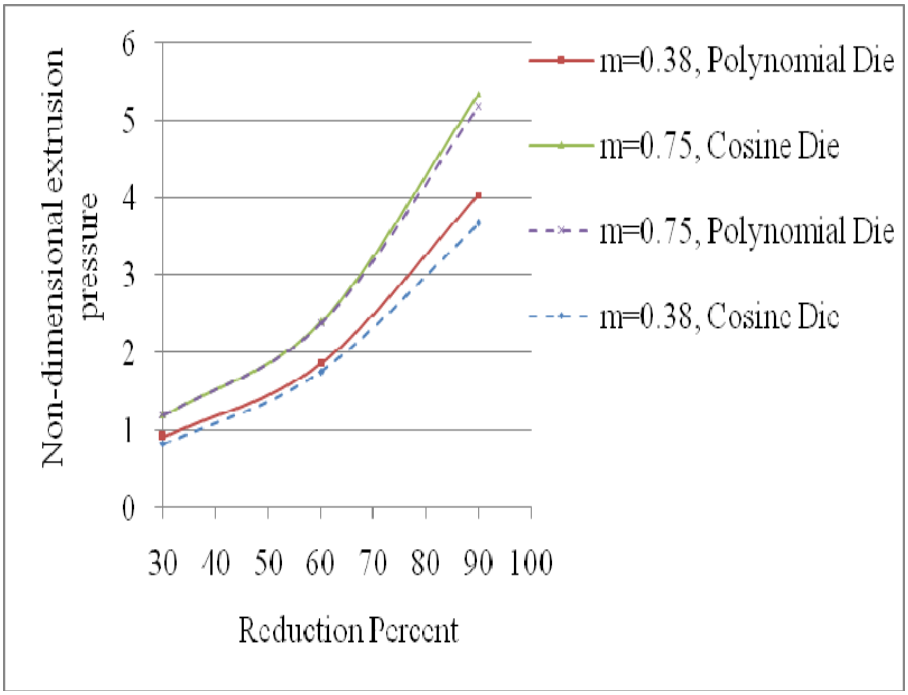

Fig. 5.12 Comparison of extrusion pressure at dry and wet friction.

The variation of extrusion pressure with respect to reduction for polynomial shaped die for fourth order, fifth order and sixth order is given in Fig. 5.13. It is evident that there is no change in extrusion pressure. In our investigation fifth order polynomial is considered.

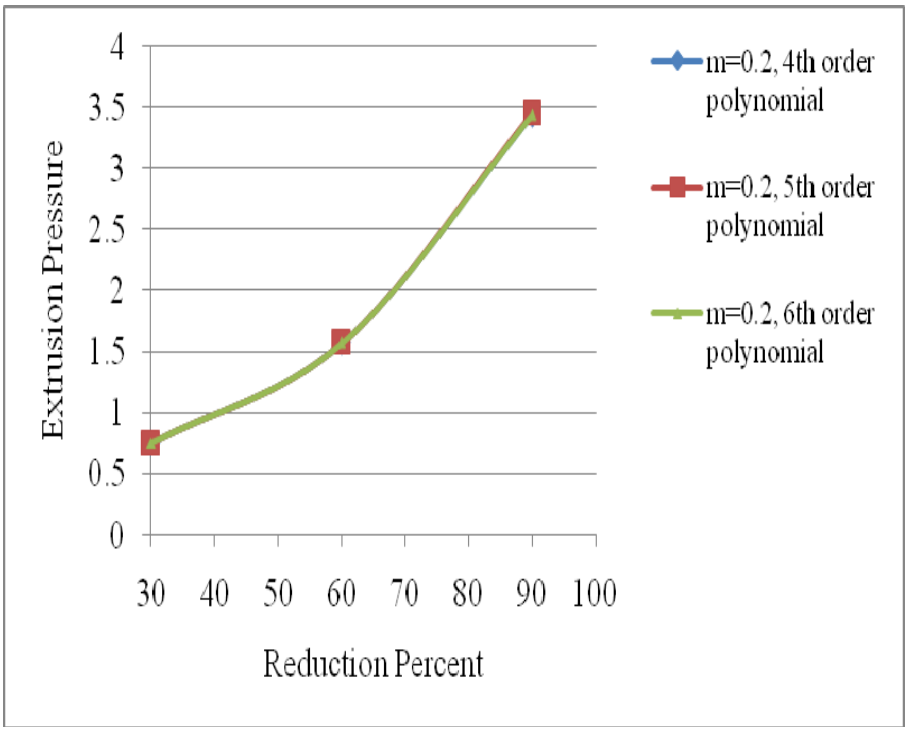

Fig. 5.13 Variation of the extrusion pressure with percentage reduction for different order polynomial profile.

5.5.1 Variation of Velocity and Strain rate

The variation of kinematically admissibility velocity field with associated strain rate along the die length is presented in Fig.5.14- 5.17. The investigations presented here are for three constant friction factors (m=0.2, 0.4, 0.6) at the die billet interface and at a distance x=10mm and y=10mm in the one quadrant of deformation zone as shown in Fig. 5.2. The billet velocity is considered one unit (1mm/sec). The variation of velocity components V_x, V_y and V_z are presented in Fig.5.14 for 30% reduction. It is seen that variation of velocity components is linear and the axial velocity component V_z is equal to billet velocity V_b at the entry plane. The velocity V_z increases linearly across the die length and becomes maximum at the exit plane equal

to product velocity. The V_z component is independent of x and y positions, where as the velocity components V_x and V_y are independent of y and x coordinates respectively. The variation of velocity components V_x and V_y is identical. It is interesting to note that the velocity component V_z is independent of friction factor at the die billet interface at lower reduction but the velocity components V_x and V_y vary with change in friction factors. Referring to equations for velocity components (5.4), it is seen that at the centre line in the deformation zone along z axis the velocity components V_x and V_y are zero and velocity V_z increases along the die length. The velocity components for 60% reduction are given in Fig. 5.15. It is observed that the velocity components V_z increases non-linearly and also influenced by friction factor. V_x and V_y components also vary non-linearly along the die length.

The variation of direct and shear strain rate component are shown in Fig.5.16 for 30% reduction. The direct strain rate $\acute{\varepsilon}_{xx}$ is equal to $\acute{\varepsilon}_{yy}$ and $\acute{\varepsilon}_{zz}$ is expressed in terms of $\acute{\varepsilon}_{xx}$ to satisfy incompressibility condition as shown in equation (5.5). From the present mode of deformation, the shear strain rate $\acute{\varepsilon}_{xy} = 0$ and the shear strain rate $\acute{\varepsilon}_{yz}$ is equal to $\acute{\varepsilon}_{zx}$. There is a variation of direct strain rate $\acute{\varepsilon}_{xx}$ along the die length and becomes maximum at the exit plane. It was found that shear strain rate $\acute{\varepsilon}_{xz}$ and $\acute{\varepsilon}_{yz}$ remain insensitive to change in friction factor at 30% reduction, where as there is change in direct strain rate $\acute{\varepsilon}_{xx}$. The strain rate for 60% reduction is given in Fig. 5.17. It is observed that the strain rate increases non-linearly and also influenced by friction factor.

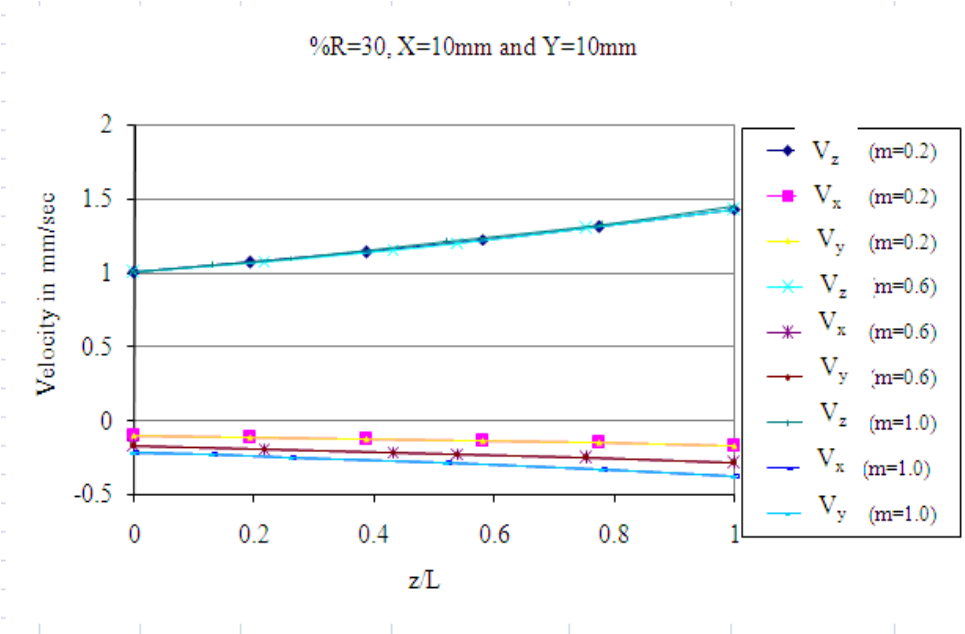

Fig. 5.14 Variation of velocity components (V_x, V_y, V_z) in the deformation zone at 30% reduction.

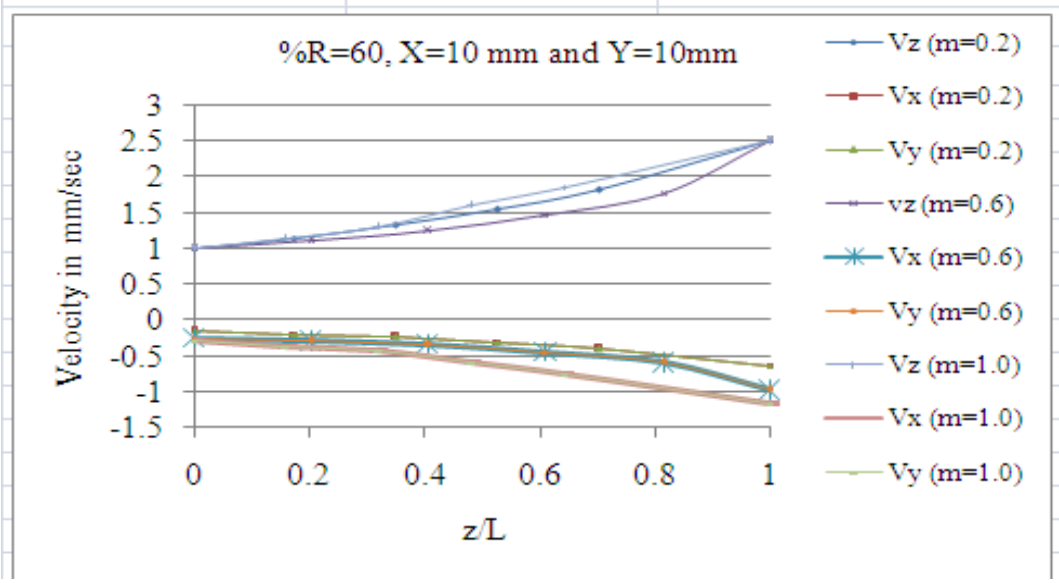

Fig. 5.15 Variation of velocity components (V_x, V_y, V_z) in the deformation zone at 60% reduction.

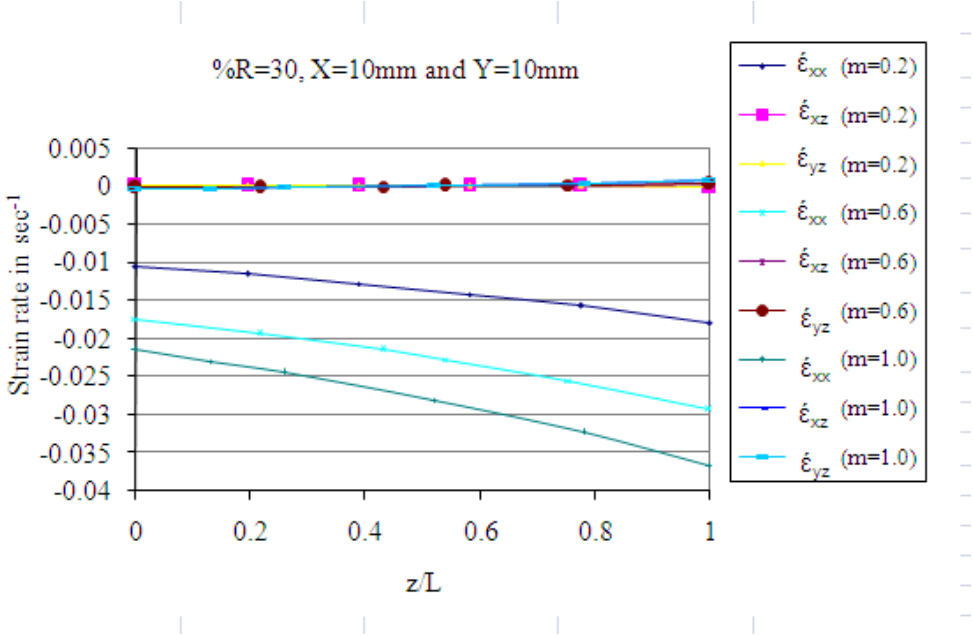

Fig. 5.16 Variation of strain rate components ($\dot{\varepsilon}_{xx}$, $\dot{\varepsilon}_{xz}$, $\dot{\varepsilon}_{yz}$) along the die length at 30% reduction

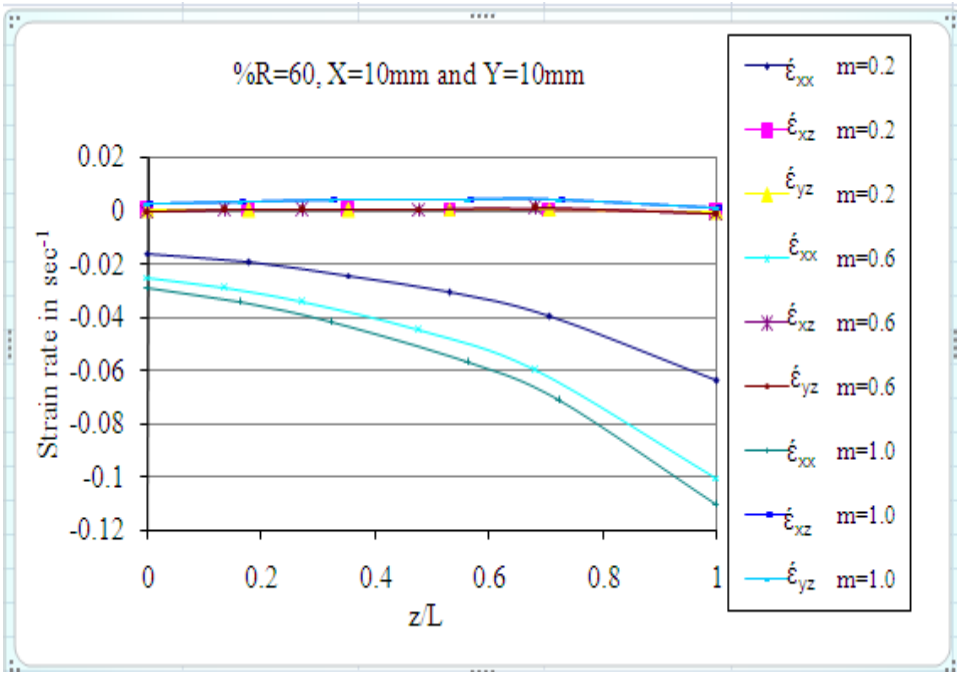

Fig. 5.17 Variation of strain rate components ($\dot{\varepsilon}_{xx}$, $\dot{\varepsilon}_{xz}$, $\dot{\varepsilon}_{yz}$) along the die length at 60% reduction

5.6 An Upper Bound Solution to Three-Dimensional Extrusion through Bezier Shaped Curved Die

An upper bound solution to three-dimensional extrusion through Bezier shaped curved die has been carried out in the similar manner as that of polynomial shaped die.

5.6.1 Die Profile Function

The curved die with Bezier die profile for extrusion of square section from square billet is shown in Fig. 5.18. Since, here again the deformation zone is similar in both x and y directions, one quadrant of deformation zone is taken for analysis. The Bezier die profile is given by

$$x = y = F(z) = b_0(1 - z/L)^3 + 3b_1(z/L)(1 - z/L)^2 + 3b_2(z/L)^2(1 - z/L) + b_3(z/L)^3 \quad (5.10)$$

where $b_0 = W$ *and* $b_3 = A$.

The b_0, b_1, b_2 and b_3 are the coefficients of bezier function. The die profile function satisfies the boundary condition such that at z=0, x=W and at z=L, x=A. The exit and entry angles are non-zero angles. The velocity-discontinuity surfaces are normal to the axial flow directions.

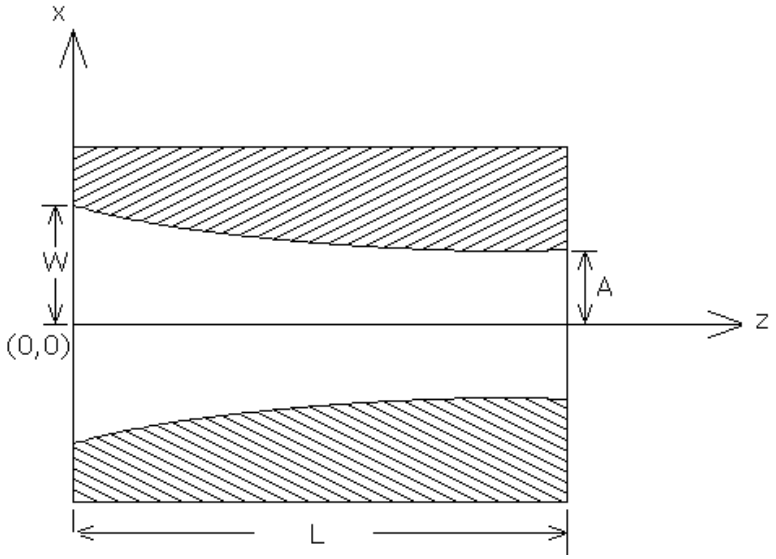

Fig. 5.18 Profile of a curved die with the axes of reference.

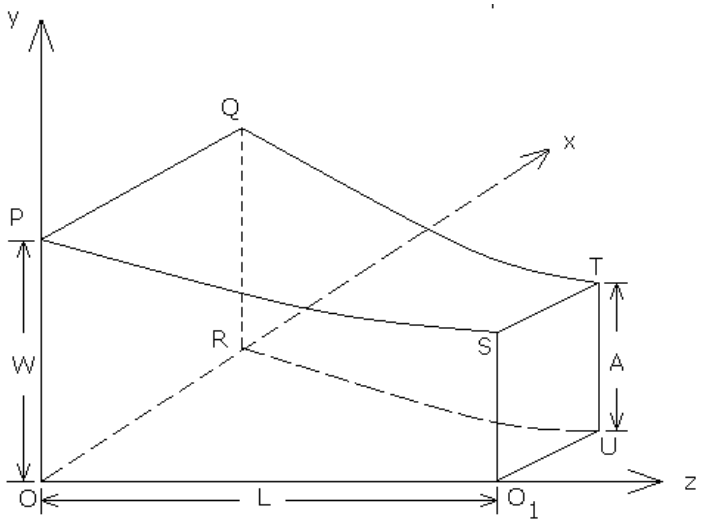

Fig. 5.19 One quadrant of the deformation zone.

5.7 Results and Discussion

The variation of non-dimensional extrusion pressure with respect to reductions are shown in Fig.5.20 for different friction factor (m=0.0 to 1). It is observed that there is an increase in extrusion pressure with increase in reduction and friction factor. At low reduction, PR=30% the extrusion pressure varies from $1.507\sigma_0$ to $1.822\sigma_0$ whereas at high reduction PR=90%, it varies from $3.445\sigma_0$ to $5.929\sigma_0$. It is interesting to note that the effect of friction is more significant at higher reduction compared to lower reduction. Hence, the role of lubricant at larger reduction is more effective in reducing the extrusion pressure.

The variation of non-dimensional die length (L/W) with respect to different reductions and friction factors are shown in Fig.5.21. It is observed that there is increase in die length with rise in reduction, but decrease in die length with increase in friction factor at the die billet interface. At low reduction 30% the optimum die length varies from 0.4 to 0.8 times of billet width, whereas at the higher reduction 90%, it varies from 0.7 to 1.3. The variation is almost linear with respect to reduction. It is interesting to note that die length increases with decrease in friction factor. For zero friction, there is no optimum length. The extrusion pressure decreases as die length increases.

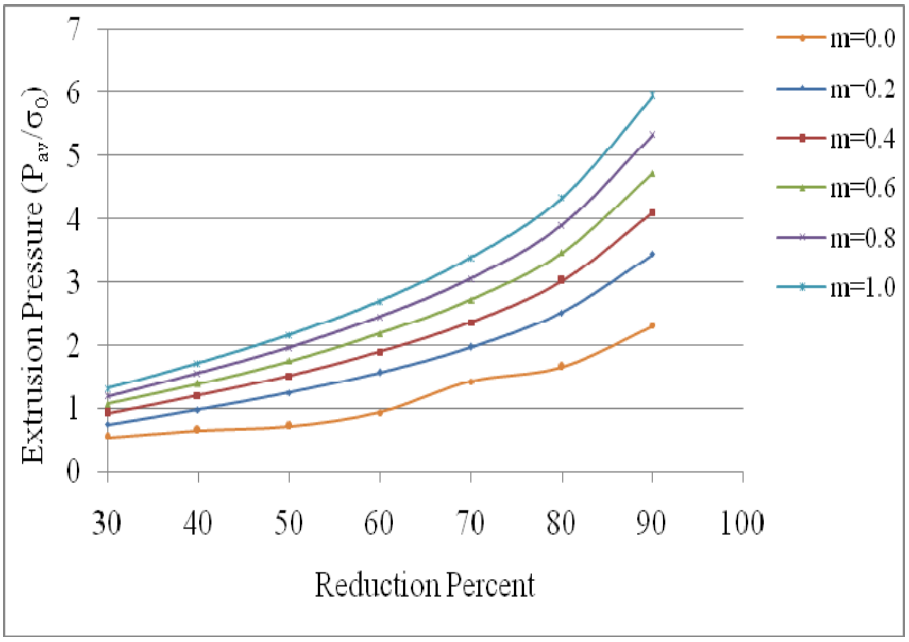

Fig. 5.20 Variation of the non-dimensional extrusion pressure with percentage reduction.

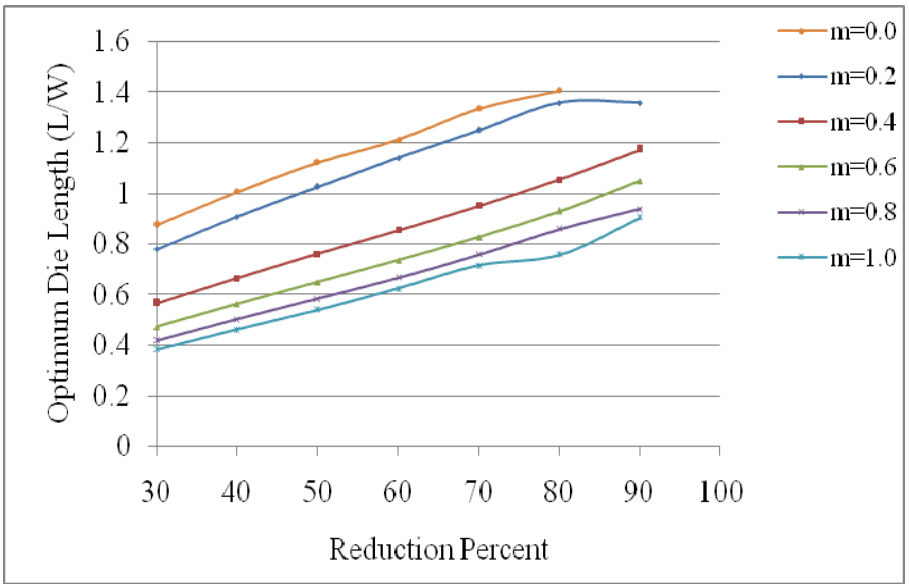

Fig. 5.21 Variation of the non-dimensional die length with percentage reduction.

The variation of the power of deformation at exit plane, at die-billet interface and internal power of deformation are shown in Fig 5.22 for a constant friction factor m=0.6. The power of deformation at the exit and entry plane is identical. The internal power of deformation contributes maximum total power of deformation. The significance of power of deformation at the exit and entry plane is the less.

It is noted that both the power of deformation due to velocity discontinuities increase with rise in reduction as well as friction factor almost linearly in identical manner. The variation of power due to frictional work at the die-billet interface increases with both rise in reduction and friction factor. It is also obvious that the effect of friction is more sensitive at higher reduction. It is shown that variation of internal power of deformation is not sensitive to change in friction factor.

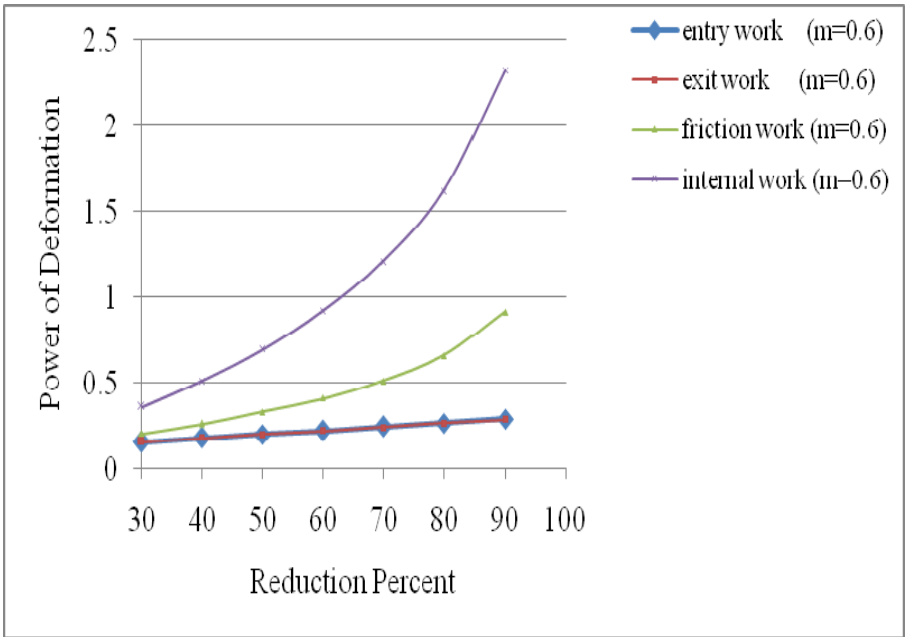

Fig. 5.22 Variation of the power of deformation at the entry, exit, frictional power of deformation and internal power of deformation with percentage reduction at constant friction factor (m=0.6)

Referring to Fig.5.23, it is evident that the total power of deformation as well as internal power of deformation is always higher than homogeneous deformation.

The extrusion pressure for Bezier shaped mathematically contoured die is compared with other conventional curved dies in lubricated condition (m=0.4) in

Fig.5.24. It is evident that Bezier shaped die is superior to hyperbolic, parabolic, circular and elliptic die profile [117]. However, cosine shaped die yields identical results with Bezier shaped die especially at low reduction. Referring to Fig.5.25, it is also evident that extrusion pressure required for the Bezier shaped die is the least compared to other analytic curved die for the sticking friction condition (m=1.0) [117]. Hence the performance of Bezier shaped mathematically contoured die is better than other conventional curved die for a wide range of frictional boundary conditions at the die billet interface. The above results are valid for any rigid plastic material with constant flow stress. It can also be applied for materials with strain hardening assuming average flow stress using above modeling. Referring to Fig. 5.26 and Fig. 5.27, it is observed that Bezier and polynomial die perform in similar manner both in lubricated and dry condition.

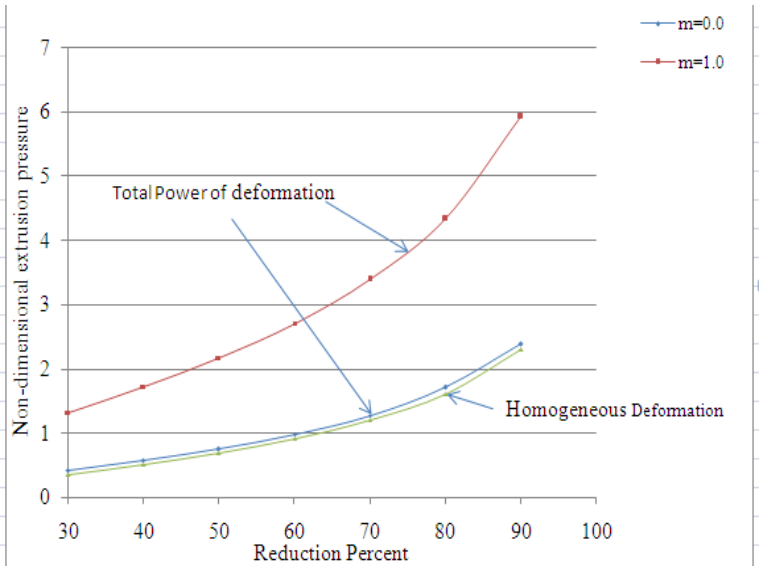

Fig. 5.23 Comparison of internal and homogeneous power of deformation with percentage reduction at m=1.0.

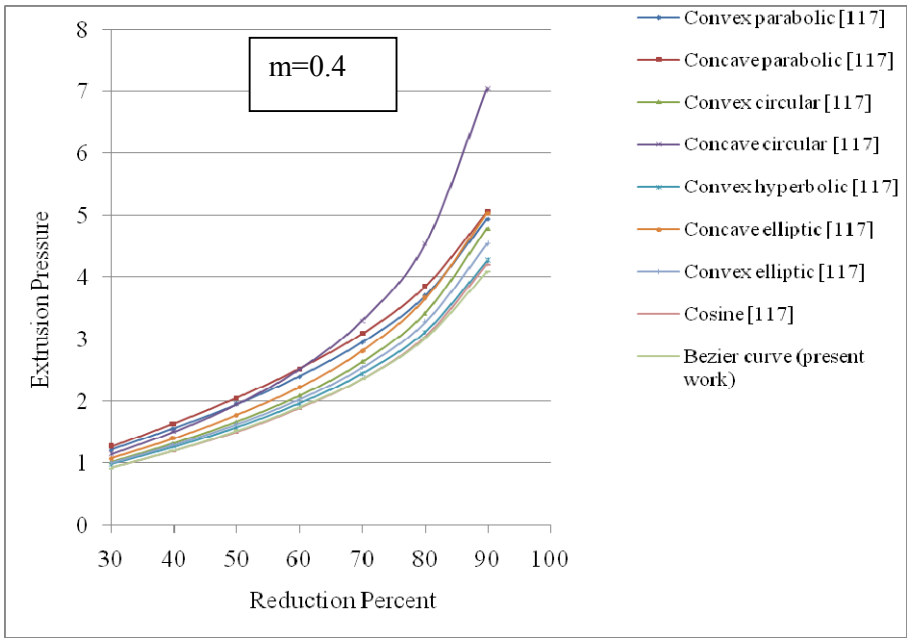

Fig 5.24 Variation for the non-dimensional extrusion pressure with percentage reduction for dies with Semi lubricated condition (m=0.4).

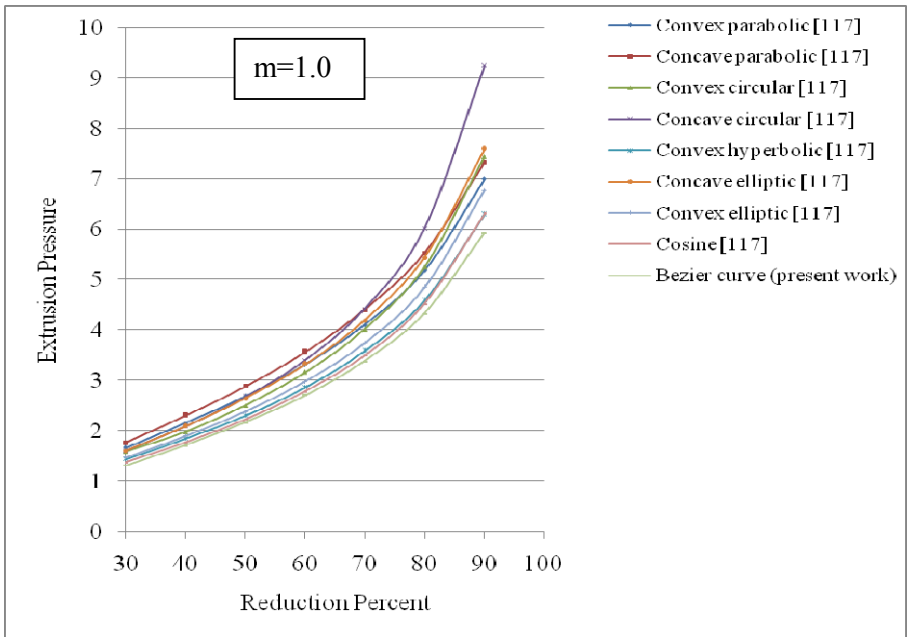

Fig. 5.25 Variation for the non-dimensional extrusion pressure with percentage reduction for dies with sticking friction (m=1.0).

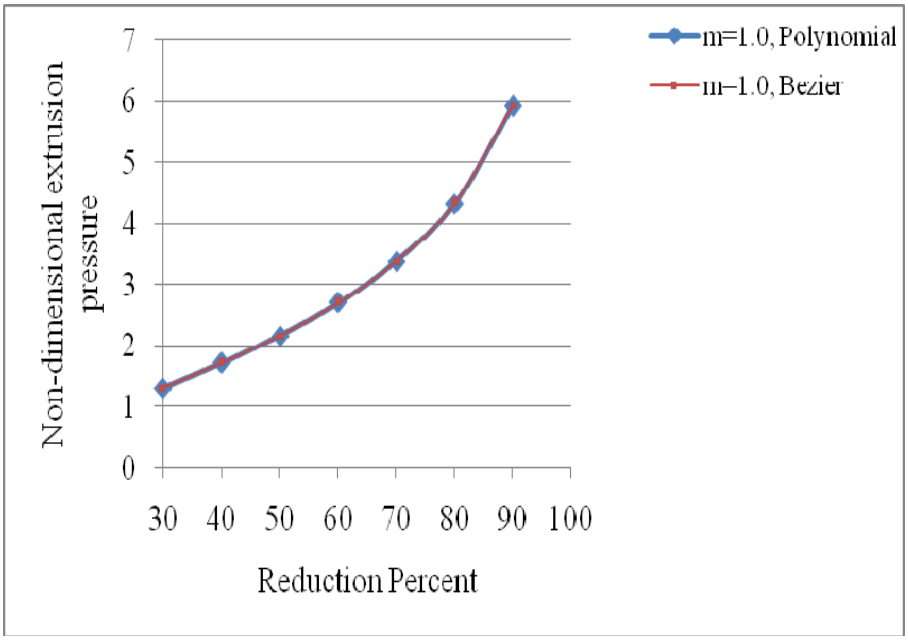

Fig. 5.26 Comparison of extrusion pressure of polynomial and Bezier die (m=1.0)

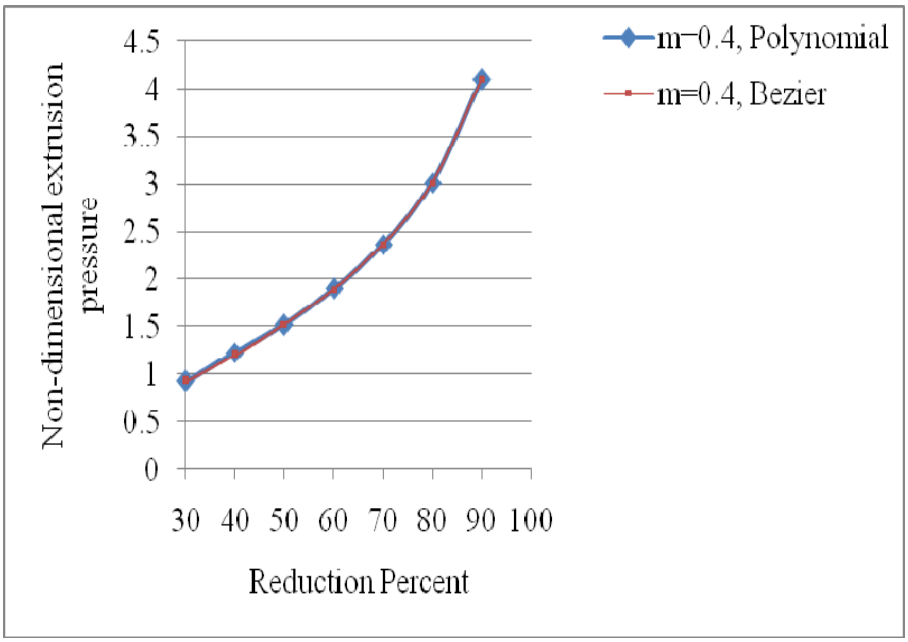

Fig. 5.2 Comparison of extrusion pressure of polynomial and Bezier die (m=0.4)

5.7.1 Variation of Velocity and Strain rate

The velocity and strain rate have also been computed for Bezier die profile. The variation of velocity and strain rate with respect to axial direction of the die is same as polynomial die profile.

5.8 Finite Element Analysis

FEM modeling is a powerful technique used for different metal deformation problems including extrusion. In the present investigation, FEM modeling has again been carried out for extrusion of square section from square billet with cosine, polynomial and Bezier die profile, using DEFORM-3D software. The optimum die length for a particular reduction as well as frictional boundary condition as obtained from previous upper bound analysis has been considered. The effective stress, strain rate, velocity and temperature distribution have been predicted. The extrusion pressure for different reduction and friction factors has been determined.

5.8.1 Die-profile function

The function for Bezier and polynomial die profile are given same as in equation (5.9) and (5.10). The die-profile function for cosine die is given as below

$$x = y = F(z) = \frac{W + A}{2} + \frac{W - A}{2} \cos\left(\frac{\pi z}{L}\right) \tag{5.11}$$

The die profile function satisfies the boundary condition such that at z=0, x=W (width of billet) and at z=L, x=A (width of product). The exit and entry angles are non-zero angles. The velocity-discontinuity surfaces are normal to the axial flow directions.

5.8.2 Finite element simulation

A FEM-based program DEFORM-3D (DEFORM ^{TM} 3D Version 6.1(sp2), 2008, is used), which consists of three special features such as Pre-processor, FEM simulation and Post-processor.

5.8.2.1 Pre-processor

The pre-processor includes (i) an input module for iterative data input verification, (ii) an automatic mesh generation program which creates a mesh by considering various process related parameters such as movement of punch, friction, material properties, die and work piece geometry; and (iii) an interpolation module that can interpolate various simulation results of an old mesh onto a newly generated mesh. The automatic mesh generation facilitates a continuous simulation without any intervention by the user. All the input data generated in the pre-processor can be saved (i) in a text form which enables the user to access the input data through any text editor; and/or (ii) in a binary form which is used by the simulation engine [42]. In preprocessing data, the length of work piece should not exceed a limiting value: Minimum work piece length = Number of simulation steps x with equal time increment x feed. Punch is also known as primary die since it has certain feed to push the work piece into the die.

Effective stress due to Von-Mises criterion

$$\sqrt{\left\{\frac{1}{2}\left[(\sigma_1-\sigma_2)^2+(\sigma_2-\sigma_3)^2+(\sigma_1-\sigma_3)^2\right]\right\}}=\bar{\sigma}$$

(5.12)

where, σ_1 , σ_2 and σ_3 are the principal stresses; $\bar{\sigma}$ is the flow stress in uniaxial compression

Effective strain rate

$$\dot{\bar{\varepsilon}}=\frac{\dot{\varepsilon}_1(\sigma_1-\sigma_m)+\dot{\varepsilon}_2(\sigma_2-\sigma_m)+\dot{\varepsilon}_3(\sigma_3-\sigma_m)}{\sqrt{\left\{\frac{3}{2}\left[(\sigma_1-\sigma_m)^2+(\sigma_2-\sigma_m)^2+(\sigma_3-\sigma_m)^2\right]\right\}}}$$

(5.13)

Where, $\dot{\varepsilon}_1, \dot{\varepsilon}_2$ *and* $\dot{\varepsilon}_3$ are the principal strain rate and σ_m = hydrostatic stress

5.8.2.2 FEM Simulation

The actual FEM-based analysis is carried out in this portion of DEFORM-3D. This simulation engine is based on a rigid-plastic FE formulation and can handle a multiple number of billets and dies with non-isothermal simulation capability. This is the programme which actually performs the numerical calculations for solution of the problem [42]. In the present investigation, square billet of rigid plastic material for extrusion of square section is modeled with a rigid curved die.

The tetrahedral solid elements are taken for analysis. The work-material is taken as tellurium lead, which is rigid-plastic in nature. The mesh is generated automatically in the model as shown in Fig. 5.28. The billet velocity is taken as 0.03 mm/sec. The properties of work material are as follows: flow stress =52.5 N/mm^2 (different values for different reduction); Young's Modulus = 14 GPa; Thermal expansion = 2.9 $e^{0.005}$ mm/mm/sec; Poisson's ratio = 0.4; Thermal conductivity =34 N/sec/C; Heat capacity = 1.36 $N/mm^2/C$; Emissivity = 0.3. The constant friction factor is assumed in the modeling. The modeling has been carried out both for dry and lubricated condition. The friction factor 'm' for dry and lubricated conditions are determined from ring compression test. The values of 'm' are 0.38 and 0.75 for wet and dry conditions respectively. The operation has been carried out at room temperature.

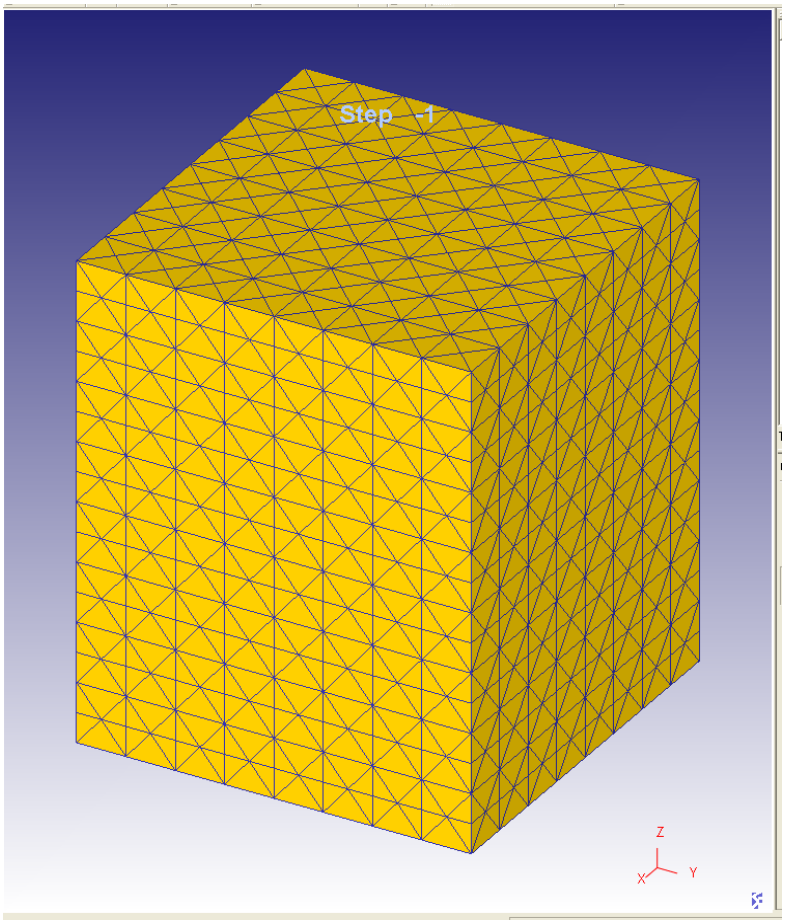

Fig. 5.28 Mess formulation (tetrahedral) for square billet (Size Ratio=1; Number of elements =10000)

5.8.2.3 Post-processor

The use of post-processor is to display the results of the simulation in graphical or alphanumeric form. Thus, available graphic representations include (i) FE mesh; (ii) contour plots of distributions of strain, stress, temperature etc., (iii) velocity vectors, and (iv) load-stroke curves. The other useful capabilities in the post-processor are 'point tracking', which provides deformation histories or microstructure of selected points in the work piece throughout the deformation.

5.9 Results and Analysis

5.9.1 The Simulation results by FEM analysis for Cosine Die Profile

From the present modeling, the effective stress, strain, strain rate, velocity and temperature distribution for cosine die profile are analyzed for different reductions as shown in Fig. 5.29 to 5.33.

Referring to fig. 5.29, the effective stress is found to be around 52.5 N/mm^2 equal to flow stress of the work material in the deformation zone, since the rigid plastic material is assumed in the model. The effective stress as estimated from von-mises criteria is given in equation (5.12). The variation of effective strain and strain rate are given in Fig. 5.30 and Fig. 5.31 respectively. It is seen that effective strain is smaller, but where as effective strain rate is greater. The effective strain rate is computed using equation (5.13). The variation of velocity and total velocity is given in Fig.5.32. It is seen from the velocity model that the velocity boundary conditions are satisfied. At the entry plane, the total billet velocity is equal to the punch velocity, where as it is equal to the product velocity at the exit plane. The product velocity is predetermined from volume constancy condition. The temperature induced in the product while being extruded is indicated in the temperature model as shown in Fig.5.33. The operation was carried out at room temperature. During the deformation, the maximum temperature increases to around 70^0C. After the FEM simulation, the variation of extrusion load with respect to ram travel for 30% reduction is shown in Fig. 5.34 in lubricated condition (m=0.38).

The wet and dry friction condition at the die-billet interface corresponds to constant friction factor m=0.38 and m=0.75 respectively, which was determined by ring compression test experimentally. Referring to the chart [8], the above friction factors are determined for dry and lubricated conditions which are obtained from the geometrical parameters of the deformed ring specimen after compression. The flow stress (σ_0=52.5 N/mm^2) has been determined using uni-axial compression test.

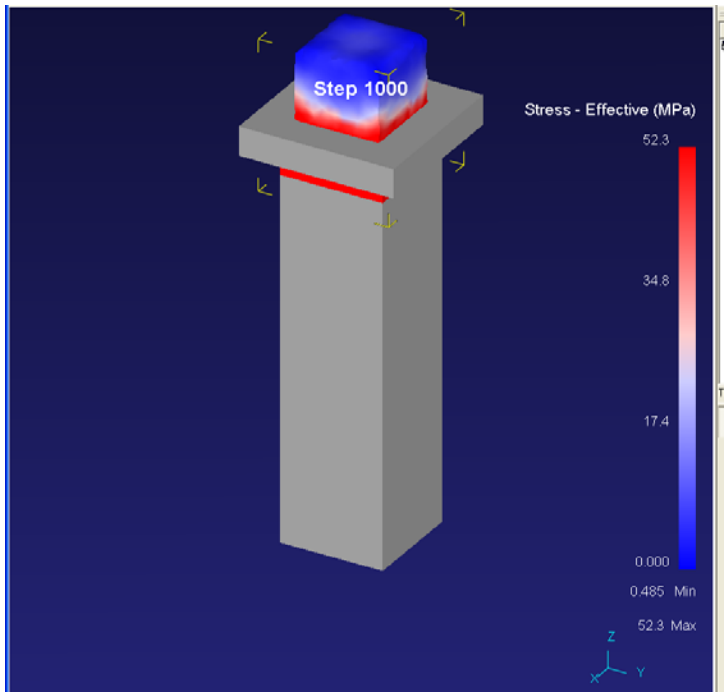

Fig. 5.29 Effective-Stress analysis for cosine curve (30%)

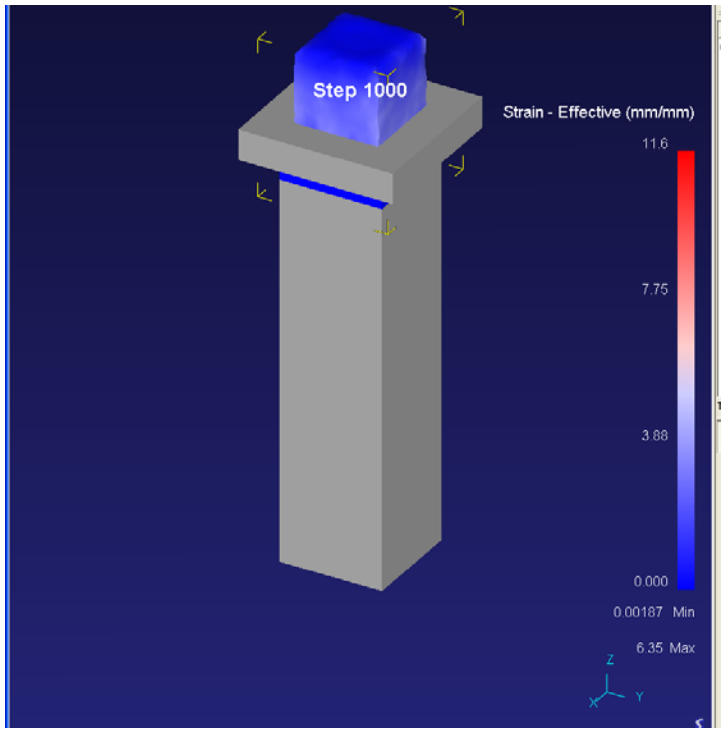

Fig. 5.30 Effective-Strain analysis for cosine curve (30% reduction)

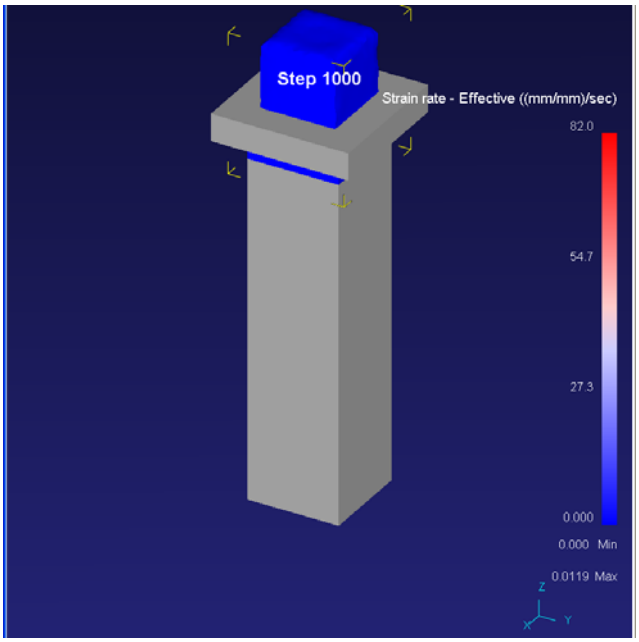

Fig. 5.31 Strain rate analysis of cosine curve (30%)

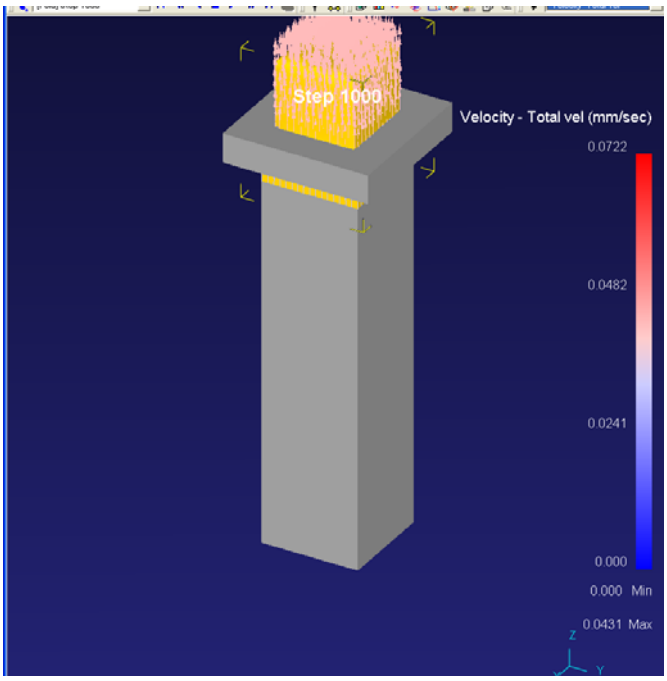

Fig. 5.32 Velocity and Total velocity analysis during extrusion of cosine curve (30%)

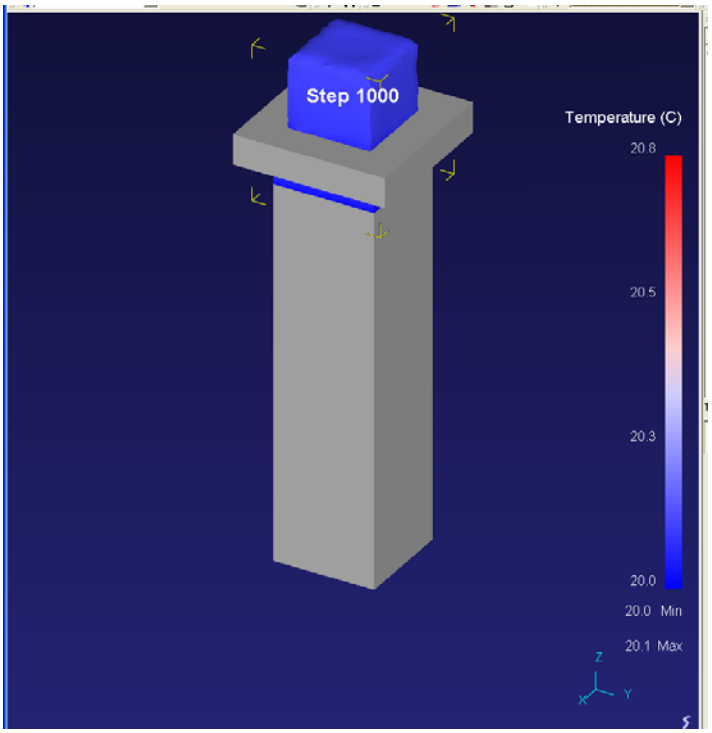

Fig. 5.33 Temperature distribution during extrusion of cosine curve (30%)

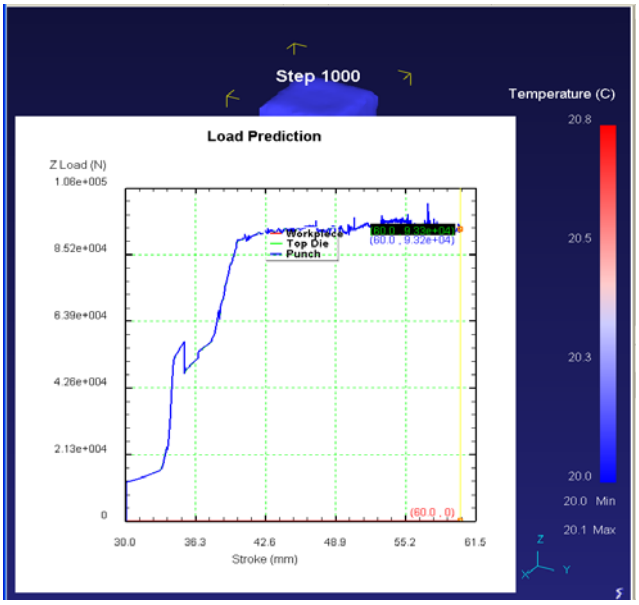

Fig. 5.34 Punch load vs. Punch travel for wet condition (After FEM simulation)

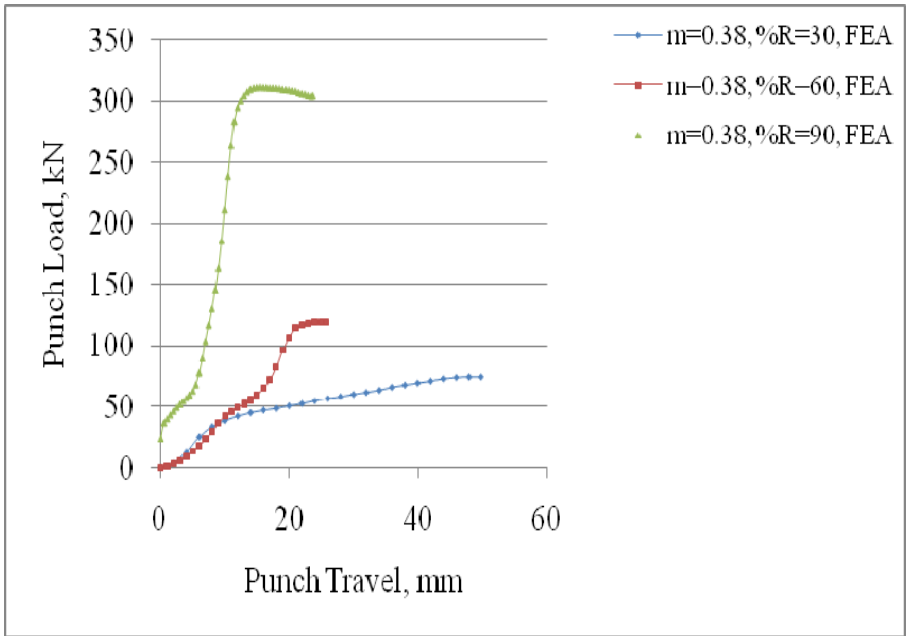

Fig. 5.35 Punch load vs. Punch travel for wet condition

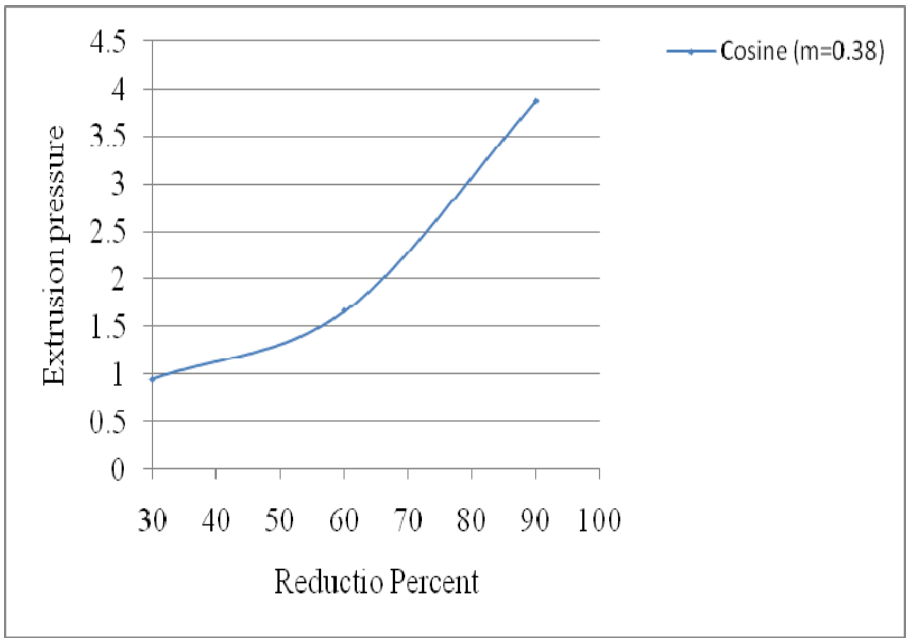

5.36 Extrusion pressure vs. percent reduction (FEM)

The variation of extrusion load with respect to ram travel for 30%, 60% and 90% reduction are shown in Fig. 5.35 in lubricated condition (m=0.38). The

extrusion load gradually increases and then becomes steady. The variation of extrusion pressure with respect to reductions are shown in Fig. 5.36 for lubricated condition (m=0.38). It is obvious from the figure that the extrusion pressure increases with increase in reduction.

5.9.2 The Simulation results by FEM analysis for polynomial die Profile

From the present modeling, the effective tress, strain, strain rate, velocity and temperature for polynomial die profile are analyzed for different reductions of die-billet interface. As similar to cosine die profile the effective stress, strain rate, temperature distribution and the velocity pattern for 60% reduction are shown in from Fig. 5.37 to 5.41. The variation of the above parameters is also found to be similar to cosine die profile. After the FEM simulation, the variation of extrusion load with respect to ram travel for 60% reduction is shown in Fig. 5.42 in lubricated condition (m=0.38). The variation of extrusion load versus ram travel for different reductions (30% to 90%) is shown in Fig. 5.43 and Fig. 5.44 for lubricated and dry conditions respectively. The variation of extrusion pressure with respect to reductions is shown in Fig. 5.45 for lubricated and dry condition. In both the cases, there is increase in pressure with increase in reduction. But there is more difference in large reduction with maximum up to 11.1%.

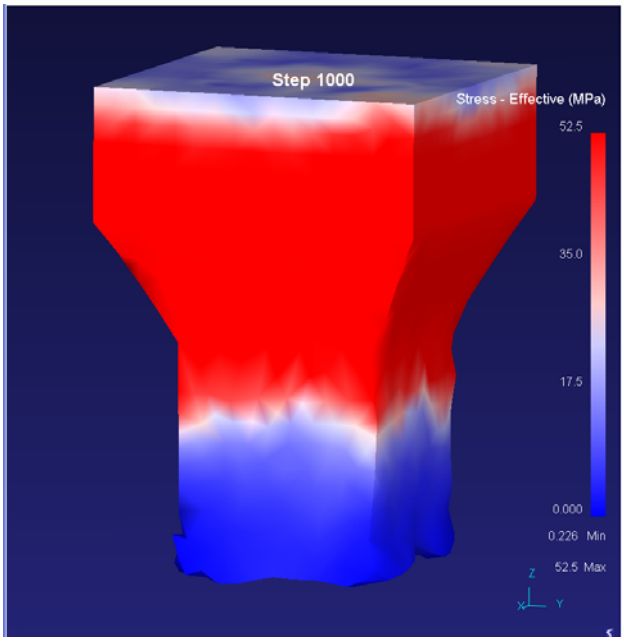

Fig. 5.37 Effective-Stress Analysis of polynomial curve (60%)

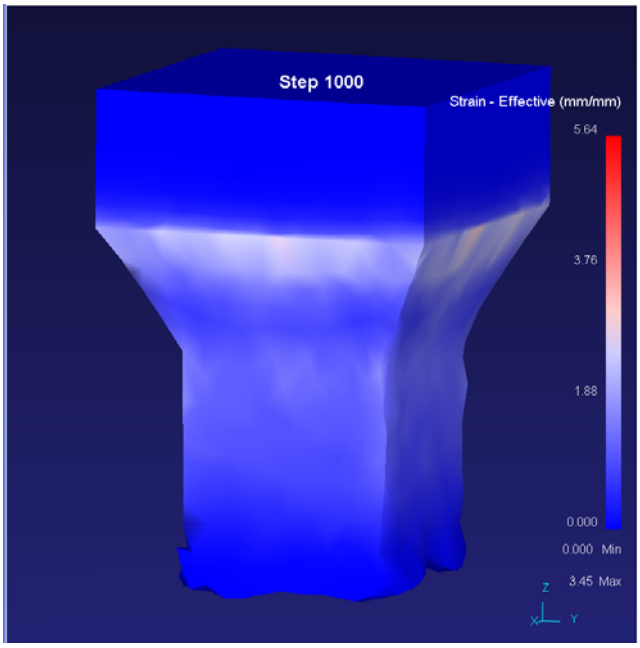

Fig. 5.38 Effective-Strain Analysis of polynomial curve (60% reduction)

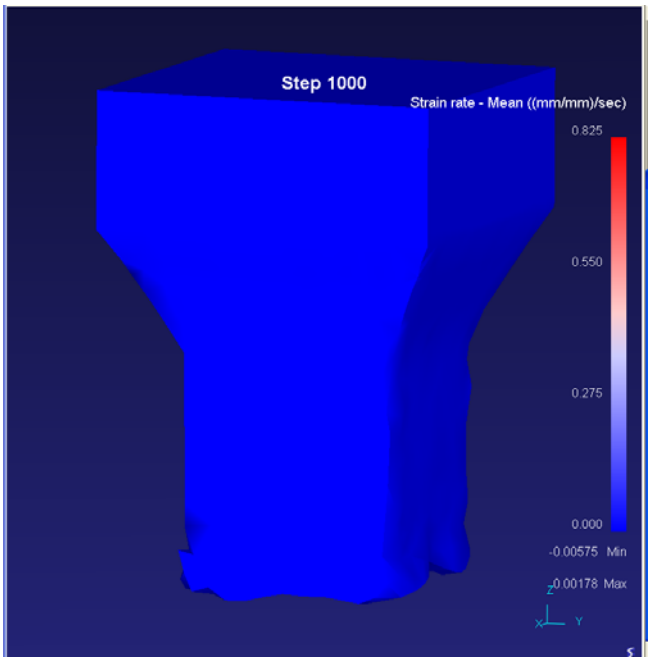

Fig. 5.39 Strain rate Analysis of polynomial curve (60%)

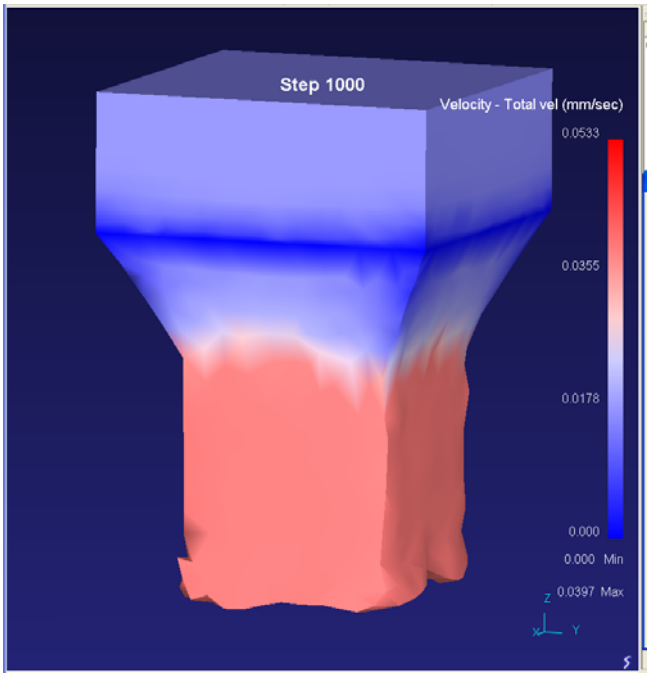

Fig. 5.40 Velocity and Total velocity analysis during extrusion of polynomial curve (60%)

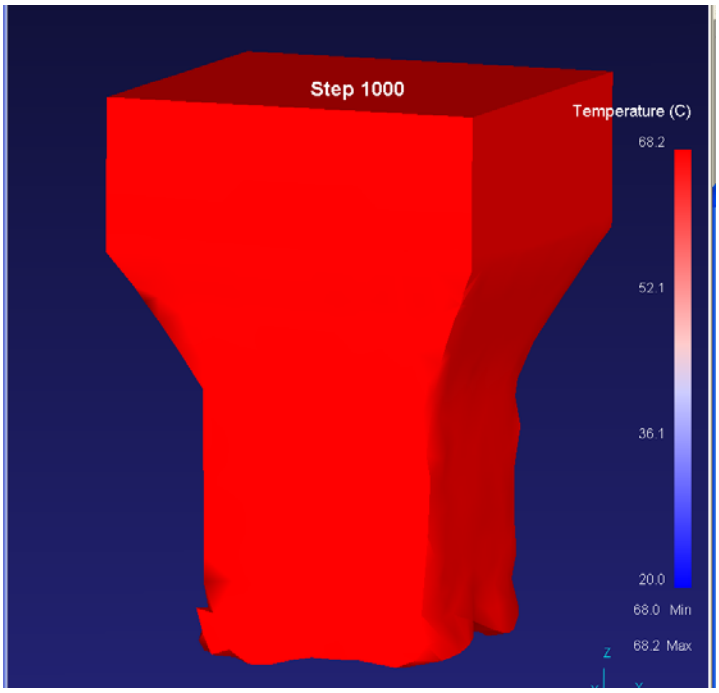

Fig. 5.41 Temperature distribution during extrusion

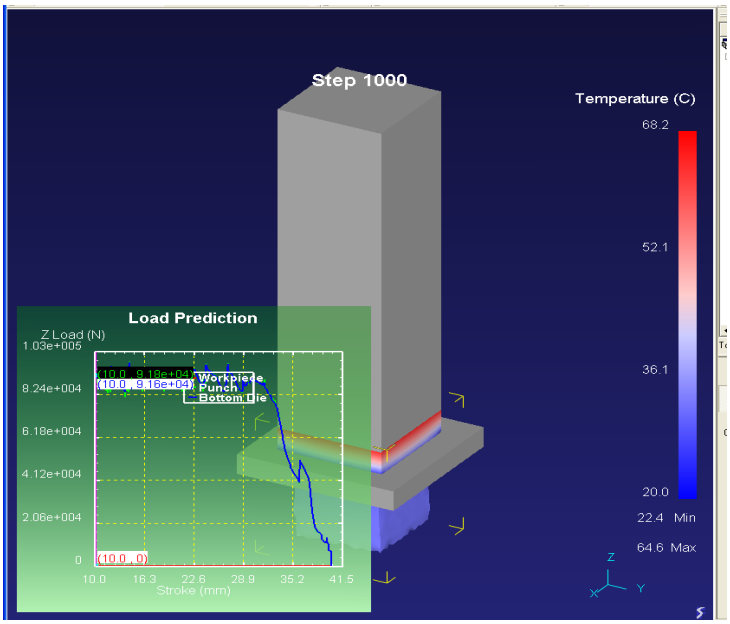

Fig. 5.42 Punch load vs. Punch travel for wet condition (After FEA simulation)

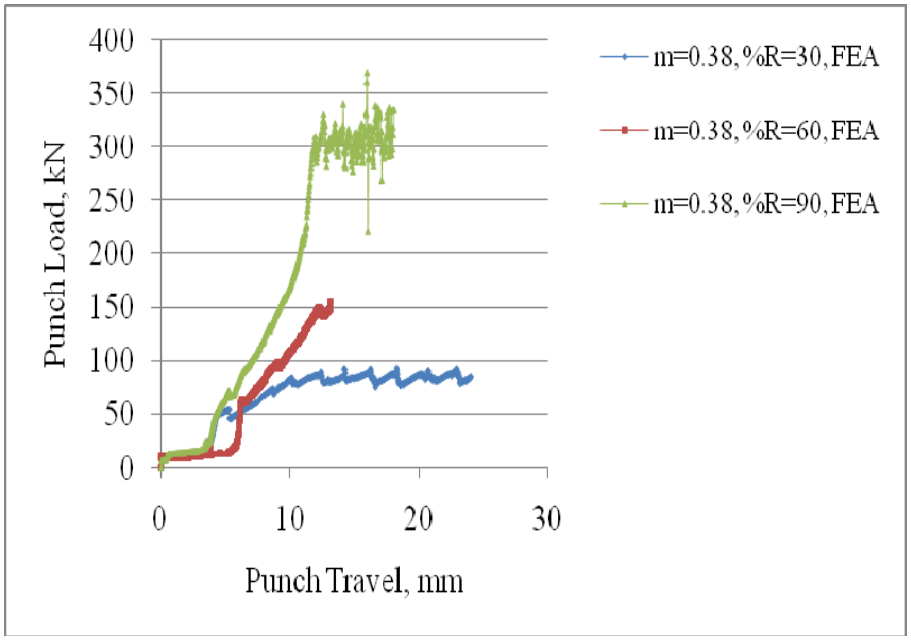

Fig. 5.43 Punch load vs. Punch travel for wet condition

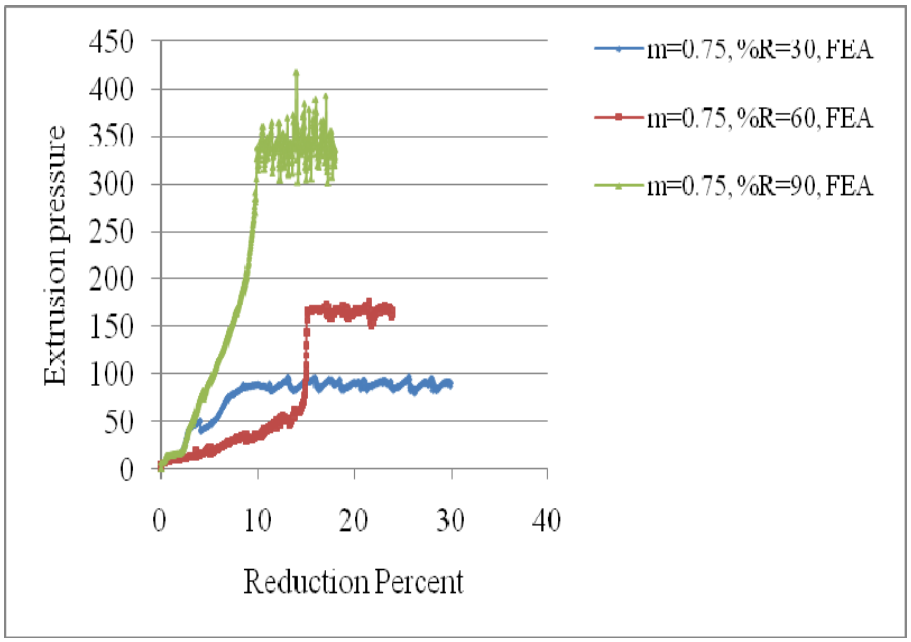

Fig. 5.44 Punch load vs. Punch travel for dry condition

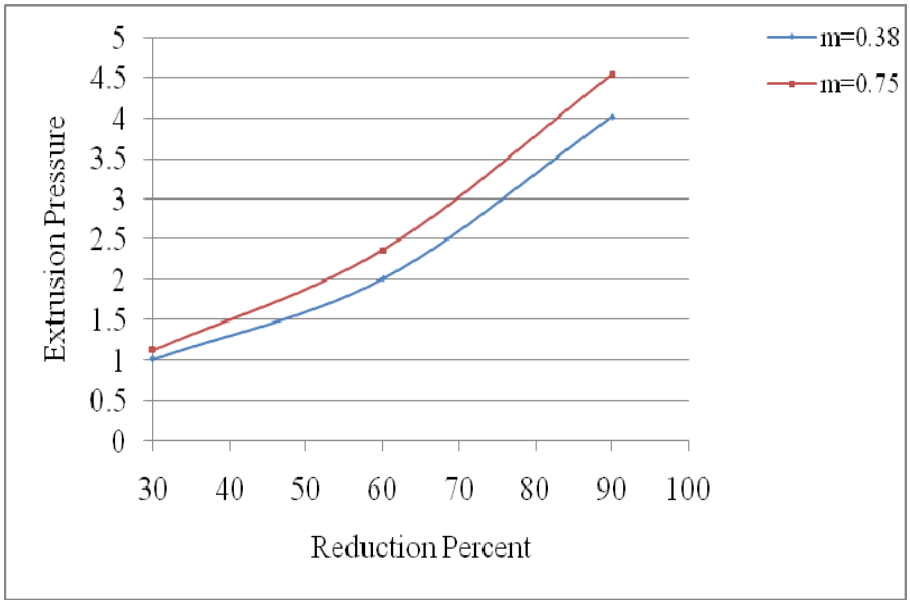

Fig. 5.45 Comparison of wet and dry extrusion pressure

5.9.3 The Simulation Results by FEM analysis for Bezier die Profile

In this case, also the effective stress, strain, strain rate, velocity and temperature for 3rd order Bezier shaped die profile are analyzed for different reductions of die-billet interface. As similar to the previous die profile the effective stress, strain, strain rate, temperature distribution and the velocity pattern for 90% reduction are shown in from Fig. 5.46 to Fig. 5.50. The variation of the above parameters is also found to be similar to polynomial profile. After the FEM simulation, the variation of extrusion load with respect to ram travel for 90% reduction is shown in Fig. 5.51 in lubricated condition (m=0.38).

The variation of extrusion load with respect to ram travel are shown in Fig. 5.52 and Fig. 5.53 for lubricated (m=0.38) and dry condition (m=0.75) respectively. The variation of extrusion pressure with respect to reductions is shown in Fig. 5.54 both for dry and wet condition. The comparison of extrusion pressure with respect to reduction for cosine, polynomial and Bezier die profile for wet conditions (m=0.38) as obtained from FEM analysis is shown in Fig. 5.55. From this figure it is observed that the cosine die gives the least extrusion pressure.

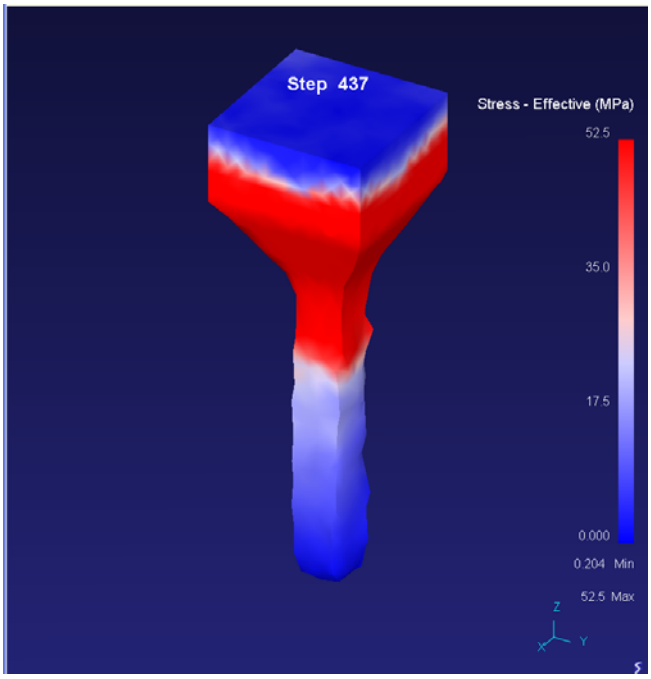

Fig. 5.46 Effective-Stress Analysis of Bezier curve (90%)

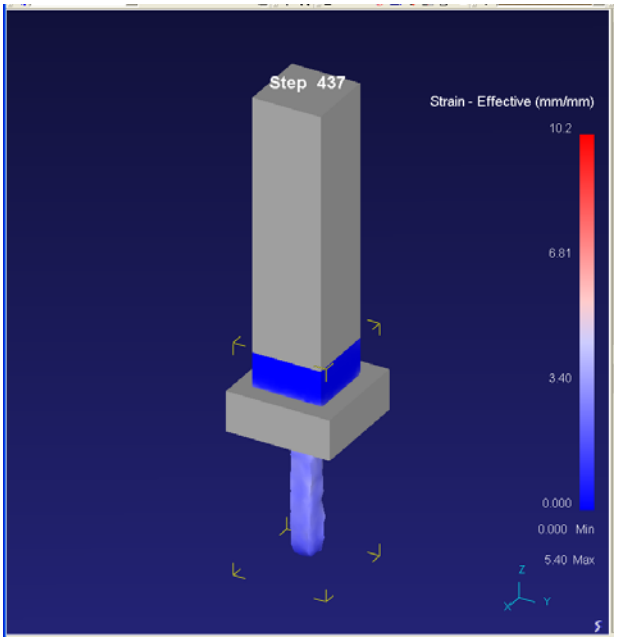

Fig. 5.47 Effective-Strain Analysis of Bezier curve (90% reduction)

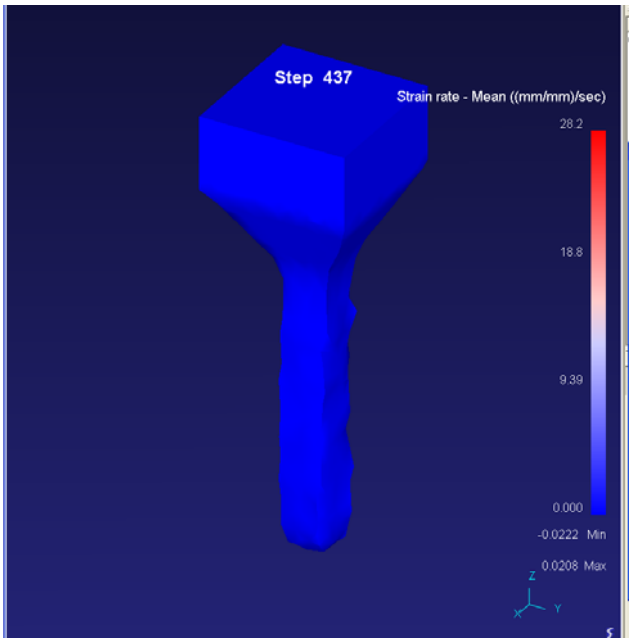

Fig. 5.48 Strain rate Analysis of Bezier curve (90%)

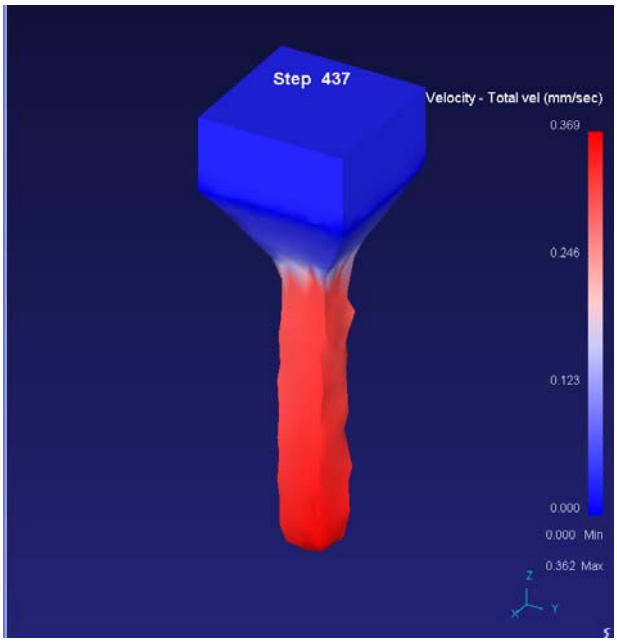

Fig. 5.49 Velocity and Total velocity analysis during extrusion of Bezier curve (90%)

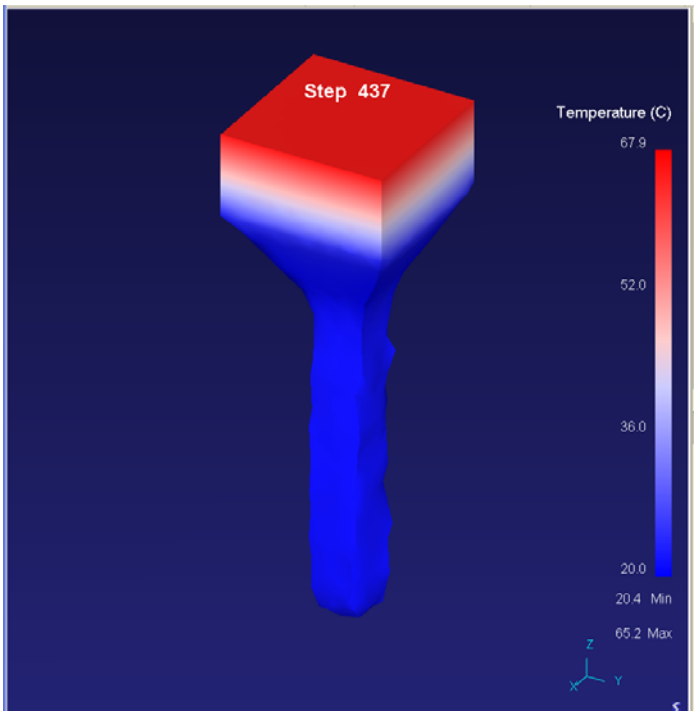

Fig. 5.50 Temperature distribution during extrusion

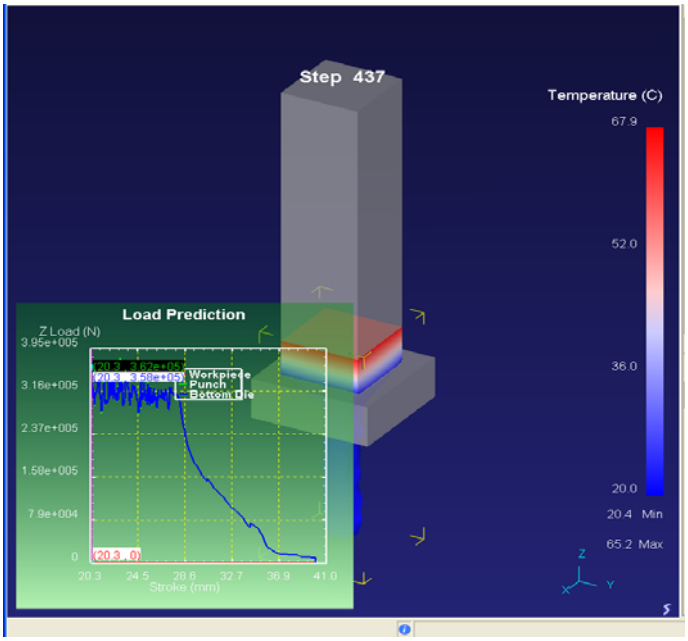

Fig. 5.51 Punch load vs. Punch travel for wet condition (After FEM simulation)

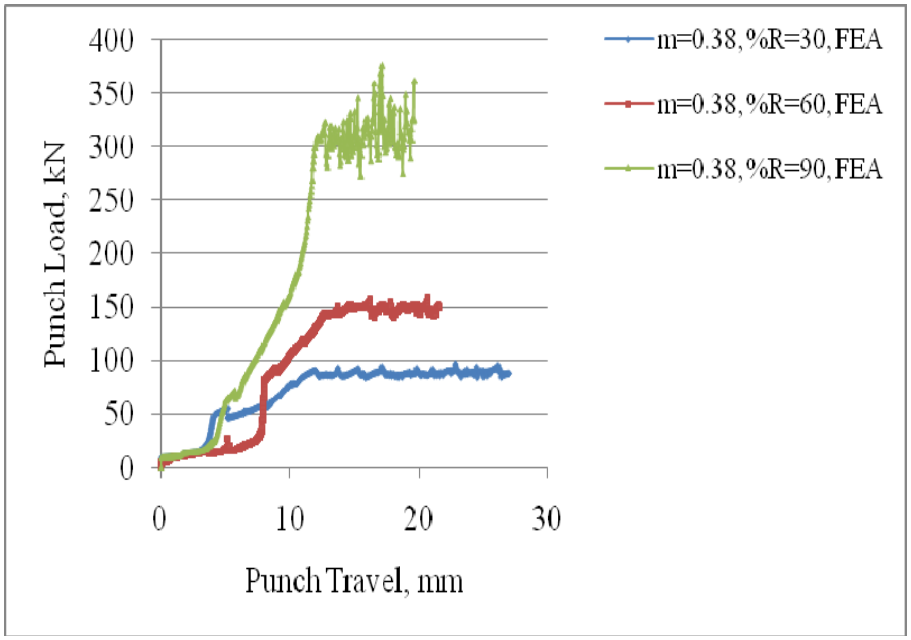

Fig. 5.52 Punch load vs. Punch travel

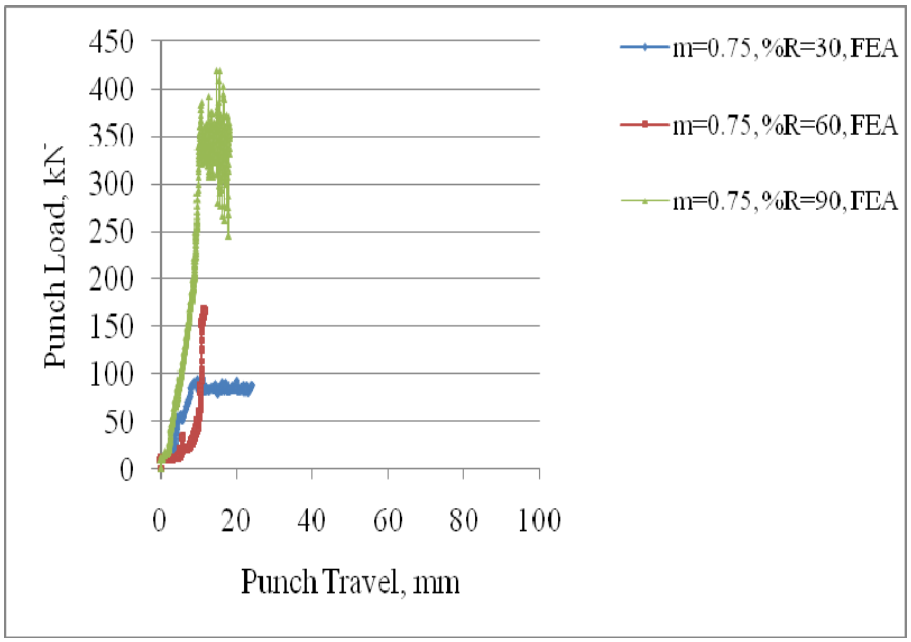

Fig. 5.53 Punch load vs. Punch travel

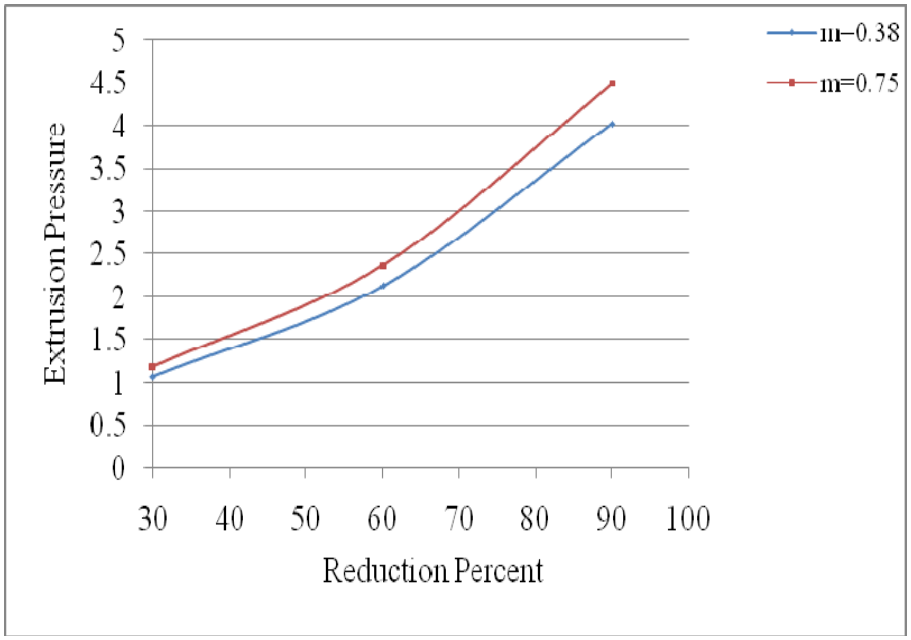

Fig. 5.54 Comparison of wet and dry extrusion pressure

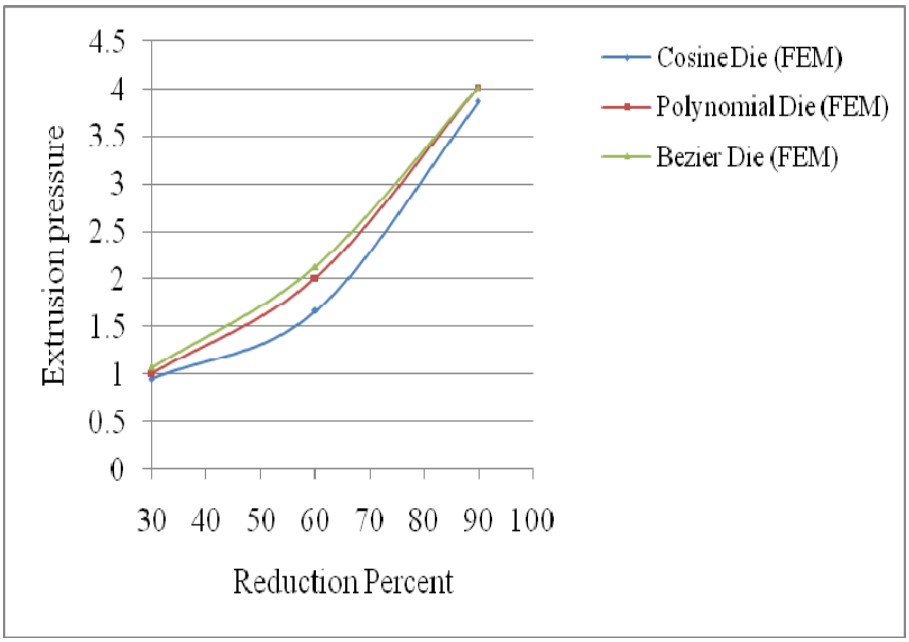

Fig. 5.55 Comparison of extrusion pressure with reduction of cosine, polynomial and Bezier shaped die in wet condition (m=0.38).

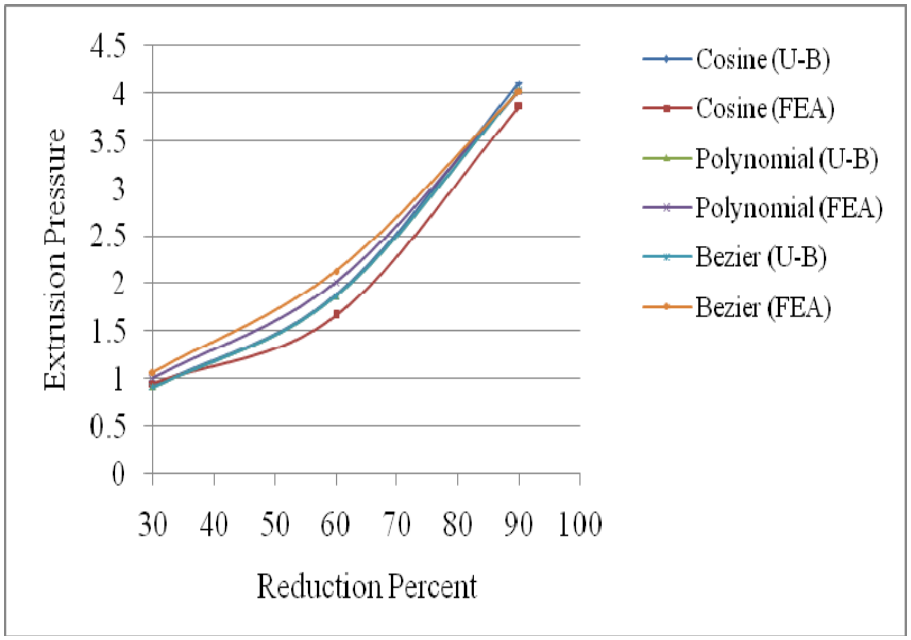

Fig. 5.56 Comparison of extrusion pressure with reduction for upper-bound and FEA in wet condition (m=0.38)

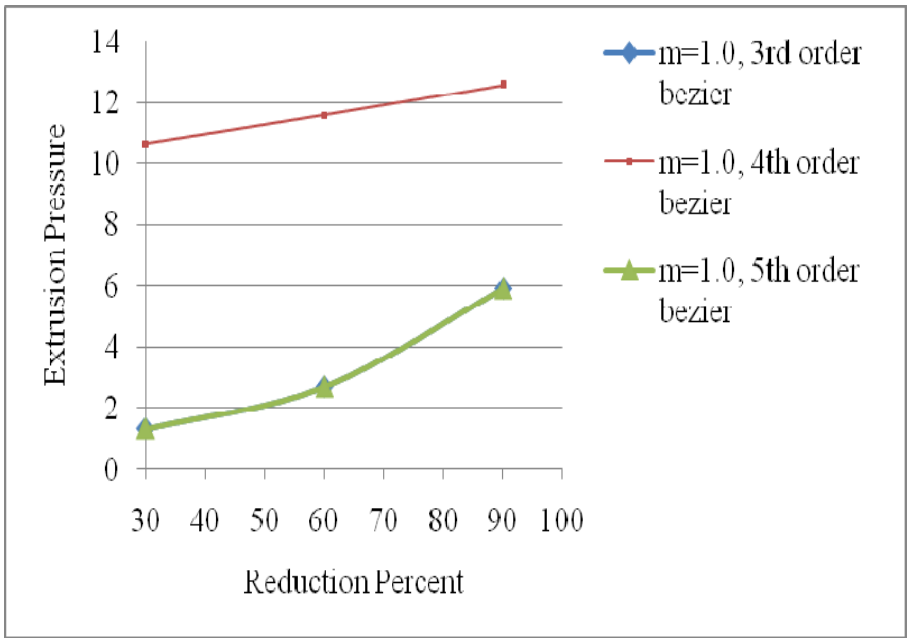

Fig. 5.57 Variation of the extrusion pressure with percentage reduction for different order bezier profile.

The variation of extrusion pressure with respect to reduction at wet condition (m=0.38) for cosine, Bezier and polynomial die both by upper bound as well as finite element analysis are given in Fig. 5.56. It is seen in the figure that extrusion pressure obtained by FEM analysis is minimum for cosine die profile. A comparison of extrusion pressure for 3^{rd} order, 4^{th} order and 5^{th} order Bezier die profile is given in Fig. 5.57. It is seen from the figure that the third order and fifth order die profile yield identical minimum results. So in the present analysis, the die profile is taken as 3^{rd} order.

5.10 Conclusions

(i) The performance of polygonal and Bezier die profile is almost identical

(ii) The polynomial and Bezier die profiles are superior to cosine, circular, elliptic and hyperbolic die profiles. But in very low friction, the cosine die is found to be the best.

(iii) The effect of friction is more predominant in high reduction.

(iv) The internal work of deformation is insensitive to the friction at the die-billet interface

(v) The extrusion pressure increases with increase in reduction and friction factor, but optimum die length increases with increase in reduction and decreases with increase in friction.

A Numerical Analysis of Extrusion of Triangular and Square Sections from Round Billet through Curved dies with design of die profile.

6.1 Introduction

The optimum geometrical parameters are very critical for smooth flow of material resulting in the evolution of uniform microstructure in extruded product with improved mechanical properties and reduction in extrusion pressure. Recently the process design involving mathematically contoured die profile has drawn the attention of various researchers to improve not only dimensional accuracy but also quality of products. The optimum die profile has been obtained by Azad et al. [2] considering work hardening of the material in cold extrusion, on the basis of minimization of stress and load in die–work piece contact surface by using a developed computer program. Knoerr et al. [89] have investigated the die fill, defect analysis and prevention, as well as for the prediction of part properties by using DEFORM FEM software. Kim et al. [94] have summarized the results of industrially relevant "work-in-progress" research with the DEFORM-2D and 3D systems. Kang et al. [90] carried out simulation of preform design using finite element modeling and validated with experimental confirmation. Kang et al. [97] have performed finite element simulation of hot extrusion for copper-clad aluminium rod to predict the distributions of temperature, effective stress, and effective strain rate and mean stress for various sheath thickness, die exit diameter and die temperature and validated with experiments. Kumar and Prasad [100] have combined rigid plastic finite element (RPFE) model for steady state axisymmetric hot extrusion with the upper bound model using the kinematically admissible velocity field for design of feature based extrusion process. Kumar and Prasad [52] have also modeled the thermal FEM model of hot and cold extrusion combined with upper bound element technique. Reinikainen et al. [144] have studied the finite-element simulation of various copper extrusion

processes under the assumption of isothermal process with two different frictional conditions. It is found that results of the FEM simulation using DEFORM software agreed well with the experimental results. Reddy et al. [145] have proposed combined upper-bound/slab method to compare eight different die shapes namely, stream-lined (third and fourth- order polynomial, cosine and modified Blazynski's CRHS), elliptical, hyperbolic, conical and Blazynski's CRHS. Reddy et al. [146] also presented the combined upper bound method/FEM to analyse four different die shapes, namely, stream-lined, cosine, hyperbolic and conical. The Galerkin FEM is used to solve the axisymmetric heat-conduction equation with convective terms to obtain the temperature distribution in the deformation zone. Reddy et al. [147] have also investigated an axisymmetric steady-state tube extrusion through a streamlined die by the finite element method (FEM) to study the influence of process variables on tool design and final product quality for a strain hardening material. Saboori et al. [169] have determined the extrusion energy for the two optimal conical and curved dies, for aluminum and lead billets, in forward and backward extrusion by using FEM with verification of experimental data. Ulysee [182] has designed the traditional die flow correctors used in flat-faced aluminum extrusion dies. Analytical sensitivities have been developed from the discretized finite-element equations in order to compute the necessary derivatives during optimization. The noncircular sections such as elliptic and clover-leaf sections through curved dies by finite element analysis for steady-state three-dimensional extrusion have been analyzed by Yang et al. [200]. Narayanasamy et al. [131] have used CAD to design streamlined extrusion dies for square cross-section.

In the present investigation mathematically contoured curved die profiles have been designed for extrusion of square and triangular sections from round billet. A numerical analysis has been carried out using DEFORM software for extrusion of the above sections from round billet. The extrusion load with respect to ram travel has been determined both for dry and lubricated condition. The extrusion pressure with respect to ram travel has been predicted. The effective stress, strain rate, strains and temperature distribution have been predicted in the deformation zone. The extrusion pressure with respect to reductions has been determined for different frictional boundary conditions.

6.2 Design of streamlined extrusion dies for extrusion of square section with curved die profile.

In the previous chapter, the design of curved die for extrusion of square sections from square billet has been considered using cosine, bezier and polynomial shaped die profile. The results have been compared with elliptical, parabolic, hyperbolic and circular die profiles. In the present investigation the curved die profiles have been designed for extrusion of square and triangular section from round billet.

6.2.1 Geometry of die profile for extrusion of square section from round billet

The die profile is designed in such a manner so that the square section is converted gradually from round billet. In order to achieve this, a parabolic function has been considered.

The billet is of circular shape with radius R and product is of square shape with half width is A.

Half diagonal of the square = √2A; R = Radius of the circle. Let N be the total number of steps required for conversion of round shape to square shape and P be the number of any intermediate steps.

Hence, P<N

After 'P' steps, the die section is a parabolic profile POM as shown in Fig. 6.1

Focal length = a = $OO' = \left(R - (R - A)\frac{P}{N} \right)$

LENGTH (OM) =OP= R – (R-√2A)*(P/N)

x and y co-ordinates are same for the above length.

x = y = OM COS45^0 = OM SIN45^0

The general equation of the parabola can be derived using three points on it as follows:

$$-y^2 = 4\alpha (x - a) \qquad (6.1)$$

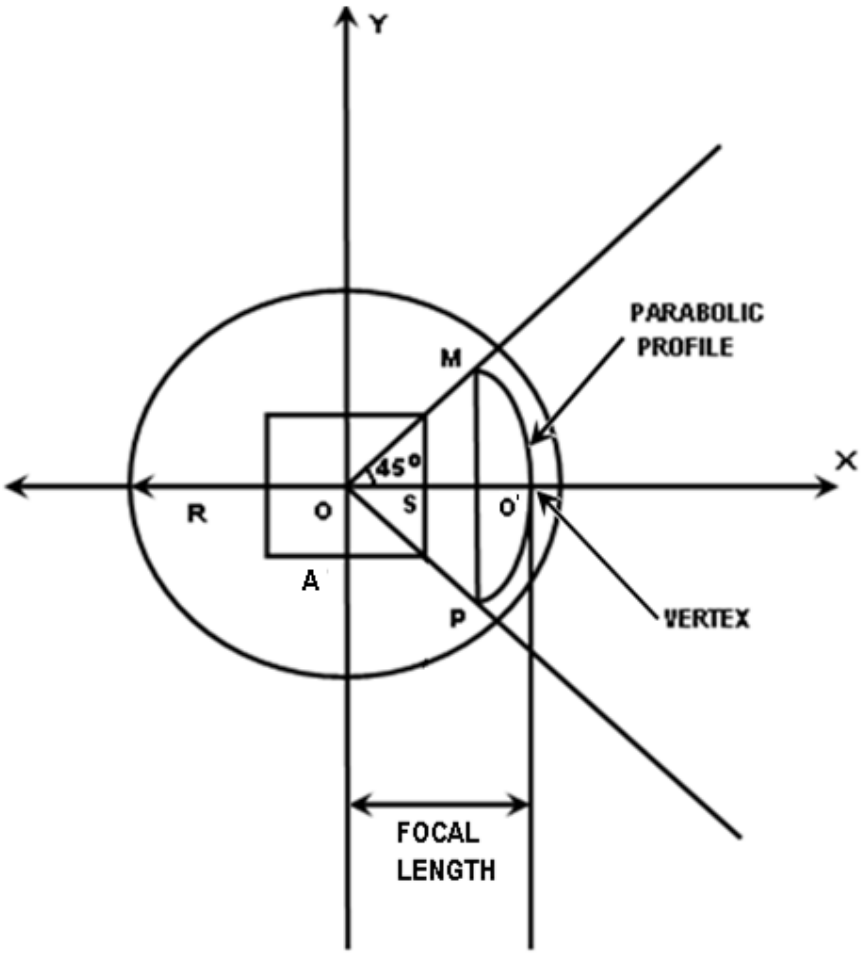

Fig. 6.1 The die profile (a sectional view) for extrusion of square section from round billet.

In the above equation; the parabola with focus (-a, 0) and axis along x-axis

The parabola is open to the right of y-axis.

To determine 4α, it is to be proceeded

The parabola $MO'P$ passes through the points (x, +/- y)

[(R- (R-√2A) *(P/N))*1/√2, +/- (R – (R-√2A)*(P/N))* 1/√2]

Putting the value of focal length 'a' in equation (6.1), the parabolic equation is given as follows:

$$-y^2 = 4\alpha\left(x-\left(R-\left(R-A\right)*\left(P/N\right)\right)\right) \tag{6.2}$$

Solving to the equation 6.2

$$-\left(1/2\right)\left(R\left(1-P/N\right)+\sqrt{2}A\left(P/N\right)\right)^2 = 4\alpha\left(\left(R-\left(R-\sqrt{2}A\right)\left(P/N\right)\right)\left(1/\sqrt{2}\right)-\left(R-\left(R-A\right)\left(P/N\right)\right)\right)$$

$$\left(1/2\right)\left(R\left(1-P/N\right)+\sqrt{2}A\left(P/N\right)\right)^2 = 4\alpha\left(\left(R\left(1-P/N\right)\left(1-1/\sqrt{2}\right)\right)\right)$$

$$4\alpha = \frac{\left(1/2\right)\left(R\left(1-P/N\right)+\left(r/\sqrt{2}\right)\left(P/N\right)\right)}{\left(R\left(1-P/N\right)\left(1-1/\sqrt{2}\right)\right)} \tag{6.3}$$

Putting the 4α value from the equation 6.2;

$$-y^2 = 4\alpha\left(x-\left(R-\left(R-A\right)\left(P/N\right)\right)\right)$$

$$-y^2 = \frac{\left(1/2\right)\left(R\left(1-P/N\right)+\sqrt{2}A\left(P/N\right)\right)}{\left(R\left(1-P/N\right)\left(1-1/\sqrt{2}\right)\right)}\left(x-\left(R-\left(R-A\right)\left(P/N\right)\right)\right)$$

$$y^2 = \frac{\left(1/2\right)\left(R\left(1-P/N\right)+\sqrt{2}A\left(P/N\right)\right)}{\left(R\left(1-P/N\right)\left(1-1/\sqrt{2}\right)\right)}\left(\left(R-\left(R-A\right)\left(P/N\right)-x\right)\right) \tag{6.4}$$

Putting P= 1, 2, 3, …….. N-1 and we will get the different parabola surfaces

Considering the die profile at different depths with parameter (t=P/N) where the total die depth is assumed to be L

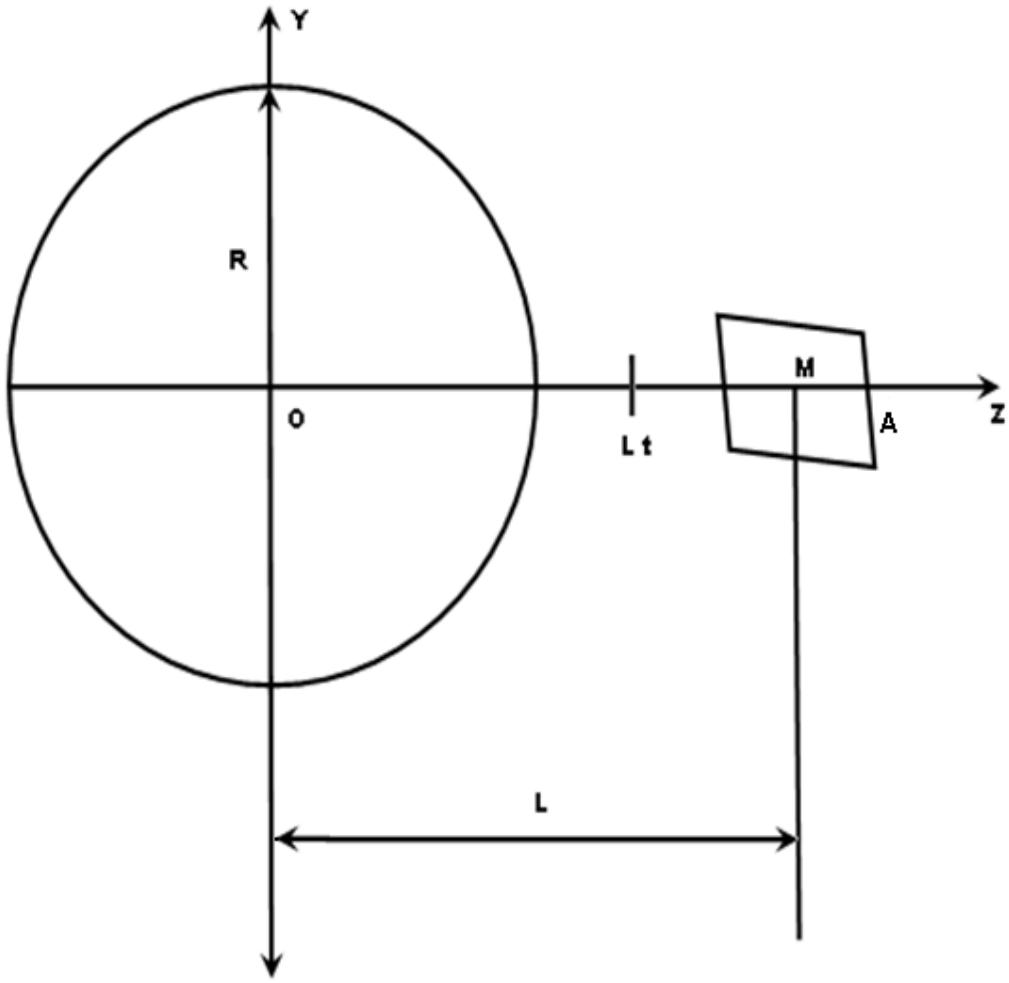

Fig. 6.2 The theoretical analysis of the die profile

when t=0 i. e. at the entrance plane of die, Z=0

when t=1, i.e. at the exit plane, Z=L (Die length(L))

If the percentage fraction of reduction is (1-P), then

$$\frac{\pi R^2 - 4A^2}{\pi R^2} = (1 - P)$$

$$4A^2 = \pi R^2 P$$

$$A = \frac{R}{2}\left(\sqrt{\pi P}\right)$$

$$2A = R\left(\sqrt{\pi\ P}\right)$$

Semi diagonal length = $A * \sqrt{2} = \frac{R}{2}\left(\sqrt{\pi\ P}\right) * \sqrt{2} = \frac{R}{\sqrt{2}}\left(\sqrt{\pi\ P}\right)$

For any value of 't' if y=0, then, the

x co-ordinate of O' is = $R\left(1 - t + t\sqrt{\pi\ P/4}\right)$

where t= P/N

The y co-ordinate of O' is = 0

The x co-ordinate of M and P is = $\left(R/\sqrt{2}\right)\left(1 - t + t\sqrt{\pi\ P/2}\right)$

The y co-ordinate of M is = $\left(R/\sqrt{2}\right)\left(1 - t + t\sqrt{\pi\ P/2}\right)$

and the y co-ordinate of P is = $-\left(R/\sqrt{2}\right)\left(1 - t + t\sqrt{\pi\ P/2}\right)$

To find the equation of the parabola

$$y^2 = 4\alpha\left(\left(R\left(1 - t + t\left(\sqrt{\pi\ P/4}\right)\right) - x\right)\right) \qquad (6.5)$$

The value of α is determined from equation (6.5) by putting the values of x and y as follows:

$$\left(R^2/2\right)\left(1 - t + t\sqrt{\pi\ P/2}\right)^2 = 4\alpha\left(\left(R\left(1 - t + t\left(\sqrt{\pi\ P/4}\right)\right) - \left(R/\sqrt{2}\right)\left(1 - t + t\left(\sqrt{\pi\ P/2}\right)\right)\right)\right)$$

Hence,

$$4\alpha = \frac{R\left(1-t+t\left(\sqrt{\pi\ P/2}\right)\right)}{2\left(1-\frac{1}{\sqrt{2}}\right)(1-t)} \tag{6.6}$$

The equation (6.5) is expressed as follows by putting the value of 4α from equation (6.6)

$$y^2 = \frac{R\left(1-t+t\left(\sqrt{\pi\ P/2}\right)\right)}{2\left(1-\frac{1}{\sqrt{2}}\right)(1-t)}\left(\left(R\left(1-t+t\left(\sqrt{\pi\ P/4}\right)\right)-x\right)\right) \tag{6.7}$$

Here t represents a depth parameter and the equation (6.7) gives the equation of the surface. This equation is called parametric equation where Z represents the absolute depth and the parameter 't' is given by

$$t = \frac{Z}{L}$$

CASE 1:

At t=0 and y=0

It should be noted that R is different from the corresponding value of 'x'. This is so because we have taken an approximation of the circle by a parabola

CASE 2:

When t=1, y=0, Z=L

$$0 = R\left(\sqrt{\pi\ P/\ 2}\right) * R\left(\sqrt{\pi\ P/4}\right) - x$$

$x = (R/2)\sqrt{\pi\ P}$ = Half length of the side of the square.

6.2.2 Geometry of die profile for extrusion of triangular (equilateral) section from round billet

The billet is of circular shape with radius R and product is of triangular shape with half width of each side is A. i. e. 2A = side of the triangle; Half side of the triangle = A; R = radius of the circular billet

The distance from CG to any vertex of the triangle = 2A/√3; P and N again represent the number of steps from extreme outer edge towards the center of the triangle as described earlier.

After (P) Steps:

P<N

OO'=Focal length = $\left(R-\left(R-\frac{A}{\sqrt{3}}\right)(P/N)\right)$

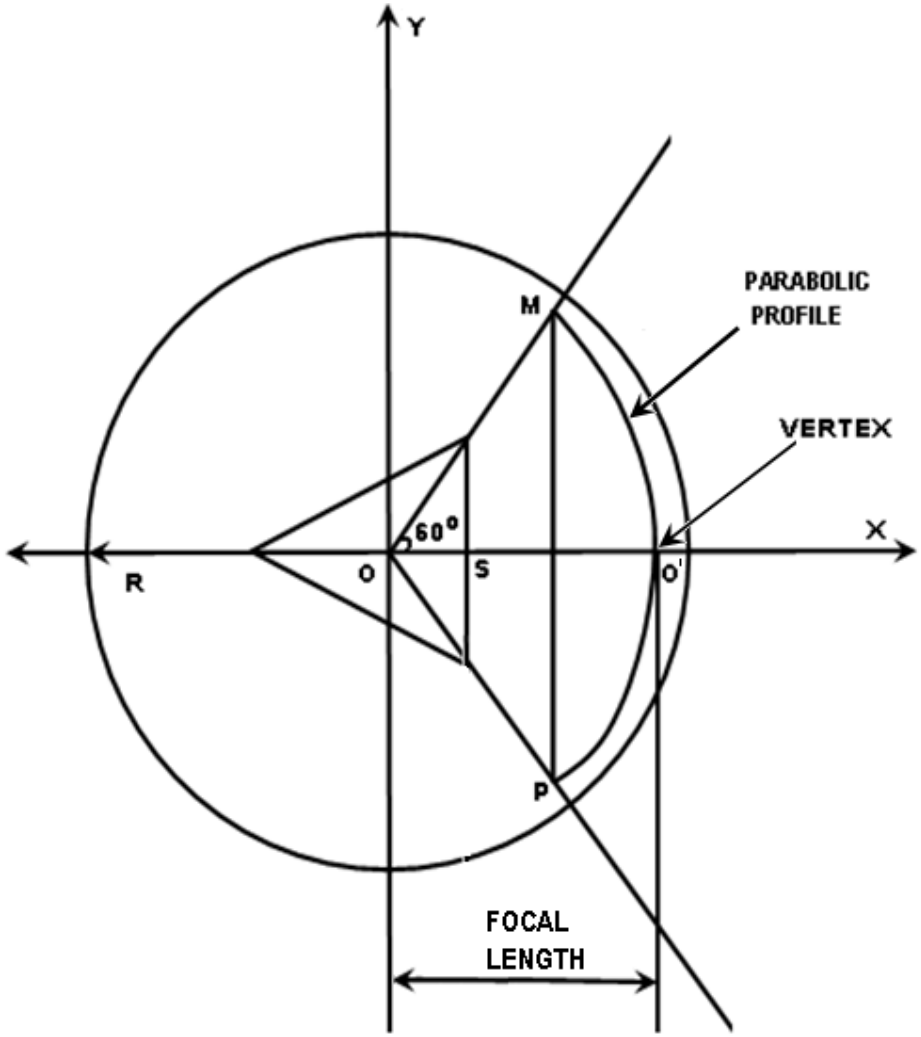

Fig. 6.3 The die profile (plan view) from round to triangular section

i. e the x-coordinate of O' is = $\left(R-\left(R-\frac{A}{\sqrt{3}}\right)(P/N)\right)$ and the y-coordinate is = 0

The x- co-ordinate of both M and P are = $\left(R-\left(R-\frac{2A}{\sqrt{3}}\right)\left(\frac{P}{N}\right)\right)\left(\frac{1}{2}\right)$.

But the y-coordinate of M is = $\left(R-\left(R-\frac{2A}{\sqrt{3}}\right)\left(\frac{P}{N}\right)\right)\left(\frac{\sqrt{3}}{2}\right)$

But the y-coordinate of P is = $-\left(R-\left(R-\frac{2A}{\sqrt{3}}\right)\left(\frac{P}{N}\right)\right)\left(\frac{\sqrt{3}}{2}\right)$

The equation of the parabola can be determined by knowing three points on as determined below.

To obtain the parameter 4α, proceeding is as follows.

The equation of the parabola passes through these points with vertex at

$\left\{\left(R-\left(R-\frac{A}{\sqrt{3}}\right)\frac{P}{N}\right), 0\right\}$ is given by

$$-y^2 = 4\alpha\left(x-\left(R-\left(R-\frac{A}{\sqrt{3}}\right)\left(\frac{P}{N}\right)\right)\right) \tag{6.8}$$

where 4α is to be determined from the knowledge that the parabola passes through the point

$$\left\{\left(R-\left(R-\frac{2A}{\sqrt{3}}\right)\left(\frac{P}{N}\right)\right)\left(\frac{1}{2}\right), \left(R-\left(R-\frac{2A}{\sqrt{3}}\right)\left(\frac{P}{N}\right)\right)\left(\frac{\sqrt{3}}{2}\right)\right\}$$

Putting these values of x and y in the equation (6.8), we get

$$-\left(R-\left(R-\frac{2A}{\sqrt{3}}\right)\left(\frac{P}{N}\right)\right)^2\left(\frac{3}{4}\right) = 4\alpha\left\{\left(R-\left(R-\frac{2A}{\sqrt{3}}\right)\left(\frac{P}{N}\right)\right)\left(\frac{1}{2}\right)-\left(R-\left(R-\frac{A}{\sqrt{3}}\right)\left(\frac{P}{N}\right)\right)\right\} \tag{6.9}$$

Solving the equation (6.9), we get

$$4\alpha = \frac{\left(\frac{3}{2}\right)\left[R - \left(1 - \frac{P}{N}\right) + \frac{2AP}{N\sqrt{3}}\right]^2}{R\left(1 - \frac{P}{N}\right)}$$

where P = 1, 2, 3 …….. N-1

Putting the value of 4α in the equation (6.8), the equation of the parabola is as follows:

$$y^2 = \frac{3\left[R\left(1 - \frac{P}{N}\right) + \frac{2AP}{N\sqrt{3}}\right]^2}{2R\left(1 - \frac{P}{N}\right)}\left(R\left(1 - \frac{P}{N}\right) + \frac{AP}{\sqrt{3}N} - x\right) \qquad (6.10)$$

Putting P= 1, 2, 3, …….. N-1 in equation (6.10) we will get the different parabola surfaces.

The die profile is considered at different depths with parameter (t=P/N) where the total die depth is assumed to be L.

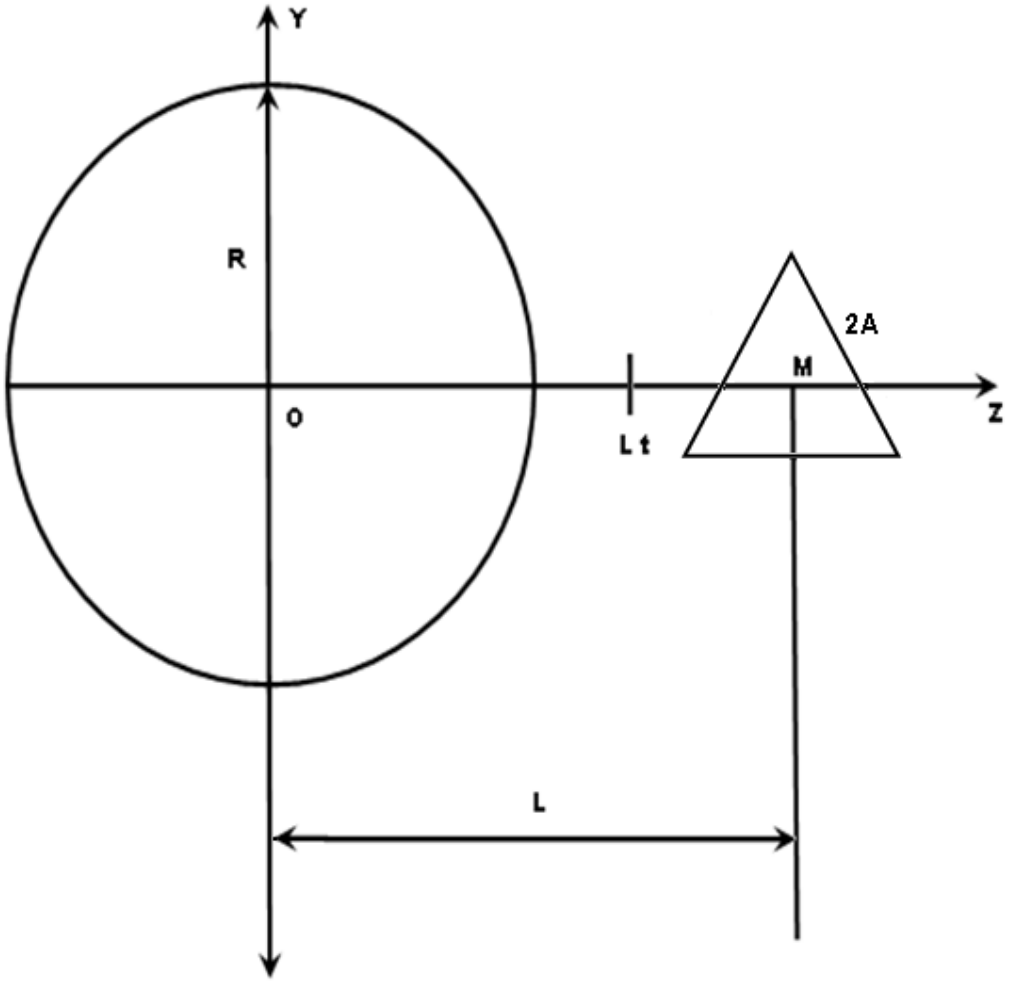

Fig. 6.4 The theoretical analysis of the die profile

When t=0 i. e. at the entrance of the die, z=0.

When t=1 i.e. at the exit plane, then z=OM= L(die length).

If the percentage fraction of reduction is (1-P), then

$$\frac{\pi R^2 - 3A^2}{\pi R^2} = (1 - P)$$

$$3A^2 = \pi R^2 P$$

$$A = R\sqrt{\pi\, P/3}$$

$$2A = 2R\sqrt{\pi\, P/3}$$

The distance of CG to any vertex of the triangle = $\frac{2A}{\sqrt{3}} = \frac{2}{3} R\sqrt{\pi\, P}$

For any value of 't' if y=0, then, the

The x-coordinate of O' is = $R\left(1 - t + \frac{t}{3}\sqrt{\pi\, P}\right)$

The y-coordinate is = 0

The x- co-ordinate of M and P are = $\frac{R}{2}\left(1 - t + \frac{2t}{3}\sqrt{\pi\, P}\right)$

But the y-coordinate of M is = $\frac{R\sqrt{3}}{2}\left(1 - t + \frac{2t}{3}\sqrt{\pi\, P}\right)$

But the y-coordinate of P is = $-\frac{R\sqrt{3}}{2}\left(1 - t + \frac{2t}{3}\sqrt{\pi\, P}\right)$

To find the equation of the parabola

$$y^2 = 4\alpha\left[\left(R\left(1 - t + \frac{t}{3}\sqrt{\pi\, P}\right)\right) - x\right] \qquad (6.11)$$

Putting the value of x and y in the equation (6.11), the value of α can be determined

$$\left\{\frac{R}{2}\left(1-t+\frac{2t}{3}\sqrt{\pi P}\right),\frac{R\sqrt{3}}{2}\left(1-t+\frac{2t}{3}\sqrt{\pi P}\right)\right\}$$

$$\frac{3R^2}{4}\left(1-t+\frac{2t}{3}\sqrt{\pi P}\right)^2=4\alpha\left[R\left(1-t+\frac{t}{3}\sqrt{\pi P}\right)-\frac{R}{2}\left(1-t+\frac{2t}{3}\sqrt{\pi P}\right)\right] \qquad (6.12)$$

The value of 4α is determined from equation (6.12) as follows:

$$4\alpha=\frac{3R\left(1-t+\frac{2t}{3}\sqrt{\pi P}\right)^2}{4\left(\frac{1}{2}-\frac{t}{2}-\frac{t}{3}\sqrt{\pi P}\right)} \qquad (6.13)$$

Putting the value of α in the equation (6.11), we get

$$y^2=\frac{3R\left(1-t+\frac{2t}{3}\sqrt{\pi P}\right)^2}{4\left(\frac{1}{2}-\frac{t}{2}-\frac{t}{3}\sqrt{\pi P}\right)}\left[\left(R\left(1-t+\frac{t}{3}\sqrt{\pi P}\right)\right)-x\right]$$

(6.14)

Here t represents a depth parameter and the equation (6.14) gives the equation of the surface. This equation is called parametric equation where z represents the absolute depth and the parameter‘t’ is given by

$t=\frac{Z}{L}$, then it becomes the equation of the die profile

CASE 1:

When t=0, y=0

R is different from x because the parabola is replacing the circular section approximately

CASE 2:

When t=1, y=0, z=L

$$0 = \frac{2A}{\sqrt{3}} - x$$

$x = \frac{2A}{\sqrt{3}} = \frac{2R}{3}\sqrt{\pi P}$ = The distance of CG to any vertex of the triangle

6.3 FEM Simulation

FEM modeling has been carried out using 3D Deform software. A solid CAD model for the curved die profile is made using solid wax software. CAD model for extrusion of square and triangular sections from round billet are given in Fig. 6.5 and Fig. 6.6 respectively. The length of die is taken as 40mm. Similar solid CAD models are developed for three reductions. The workpiece model with automatic mesh generation for extrusion of square section as well as triangular section is given in Fig. 6.7. The type of element is taken as tetrahedral. The number of elements is taken as 10,000. The material taken in the model is tellurium lead. The mechanical properties of the lead are as follow:

Young's Modulus = 14 GPa; Thermal expansion = 2.9 $e^{0.005}$ mm/mm/sec; Poisson's ratio = 0.4; Thermal conductivity =34 N/sec/C; Heat capacity = 1.36 N/mm^2/C; Emissivity = 0.3. In the modeling, the rigid plastic model for the material is assumed. The die is modeled as rigid body and stationery. The punch is also modeled as rigid body but moves with a velocity are equal to 0.03 mm/sec.

The two frictional boundary conditions are taken. In one case, no lubrication is used. It is a condition of dry friction. From ring compression test it corresponds to a

constant friction factor m=0.75. In another case, lubricant (commercial automobile grease) is used. It corresponds to a constant friction factor m=0.38.

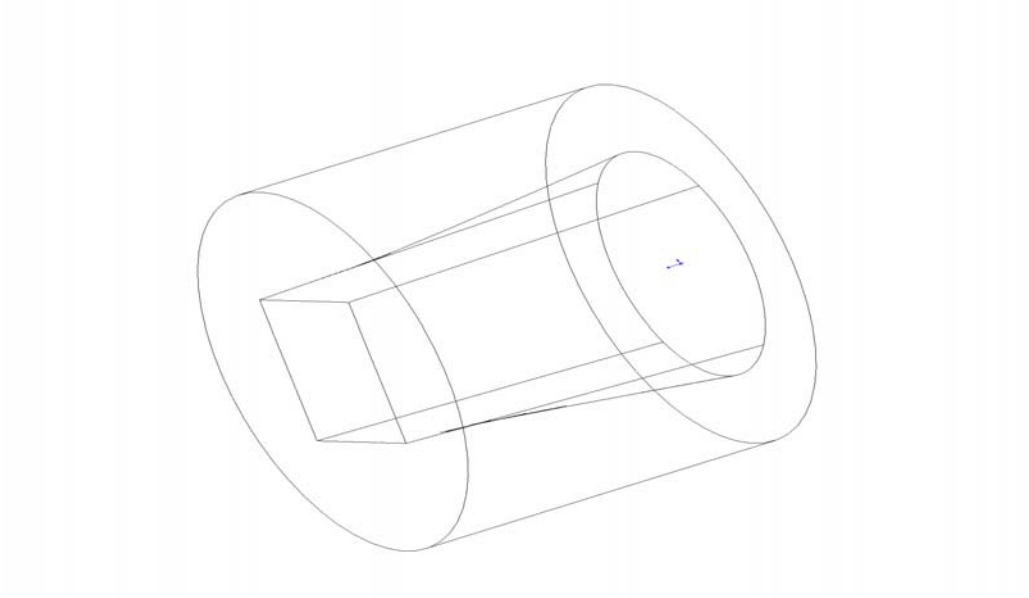

Fig. 6.5 Streamlined die for extrusion of square section (70% reduction)

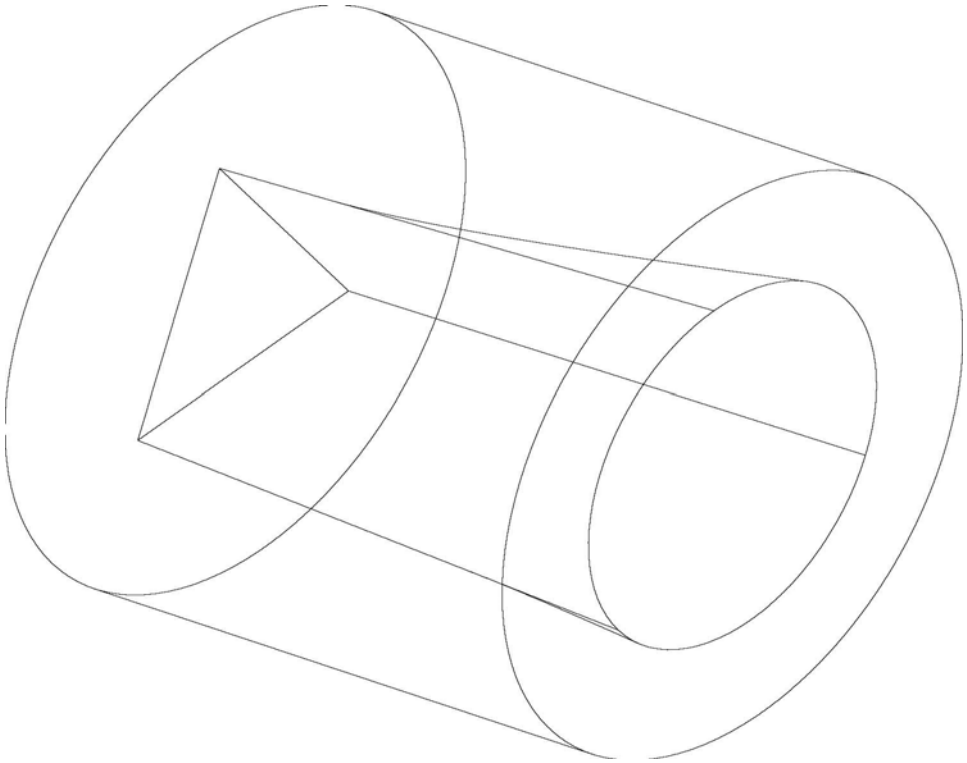

Fig. 6.6 Streamlined die for extrusion of triangular (equilateral) section (60% reduction)

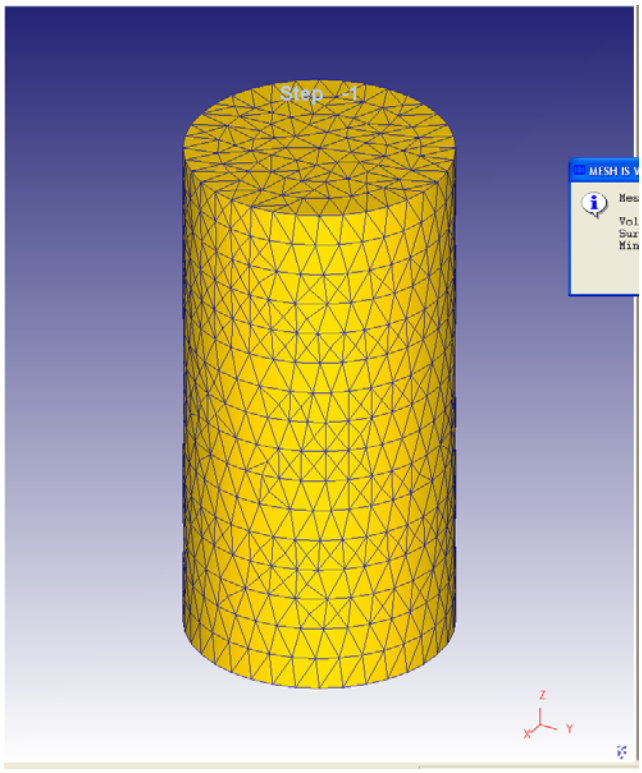

Fig. 6.7 Mess formulation (tetrahedral) for round billet (Size Ratio=1; Number of elements =10000)

6.4 Results and discussion

From the present modeling, the effective strain, stress, strain rate, velocity and temperature are determined for different reductions as well as frictional boundary conditions. The above parameters are indicated in Fig.6.8 to Fig. 6.12 for 90% reduction for extrusion of square section from round billet corresponding to m=0.38 as computed from FEM modeling. Similarly the results are shown for extrusion of triangular section in Fig. 6.13 to Fig. 6.17. The equations of effective stress and strain are given as follows:

Effective stress due to Von-Mises criterion

$$\sqrt{\left\{\frac{1}{2}\left[(\sigma_1-\sigma_2)^2+(\sigma_2-\sigma_3)^2+(\sigma_1-\sigma_3)^2\right]\right\}}=\bar{\sigma} \qquad (6.14)$$

where, σ_1, σ_2 and σ_3 are the principal stresses; $\dot{\sigma}$ is the flow stress in uniaxial compression

Effective strain rate

$$\dot{\varepsilon} = \frac{\dot{\varepsilon}_1(\sigma_1 - \sigma_m) + \dot{\varepsilon}_2(\sigma_2 - \sigma_m) + \dot{\varepsilon}_3(\sigma_3 - \sigma_m)}{\sqrt{\left\{\frac{3}{2}\left[(\sigma_1 - \sigma_m)^2 + (\sigma_2 - \sigma_m)^2 + (\sigma_3 - \sigma_m)^2\right]\right\}}} \quad (6.15)$$

where $\dot{\varepsilon}_1$, $\dot{\varepsilon}_2$ *and* $\dot{\varepsilon}_1$ are the principal strain rates and σ_m = hydrostatic stress. The effective stress distribution is given in Fig. 6.8. It is observed that the effective stress is mostly equal to 52.5 N/mm^2, which is the flow stress of the material. This is because the material is almost rigid plastic. Similarly the effective strain and the effective strain rate distribution is given in Fig. 6.9 and Fig. 6.10 respectively. The total velocity distribution is given in Fig. 6.11. It is observed that at entry plane the velocity is equal to the billet velocity and at the exit plane, the velocity is equal to the product velocity. The temperature analysis is again given Fig. 6.12. The operation was carried out at room temperature. There is some rise in temperature in the deformation model. The maximum temperature is around 70^0C. Similarly analysis has been carried out for triangular section.

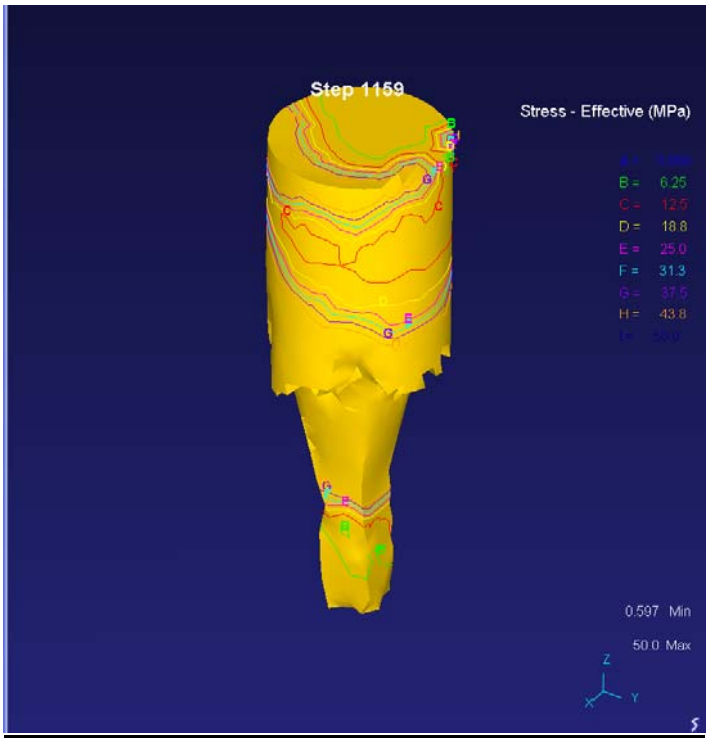

Fig. 6.8 Effective-Stress analysis for square section, m=0.75

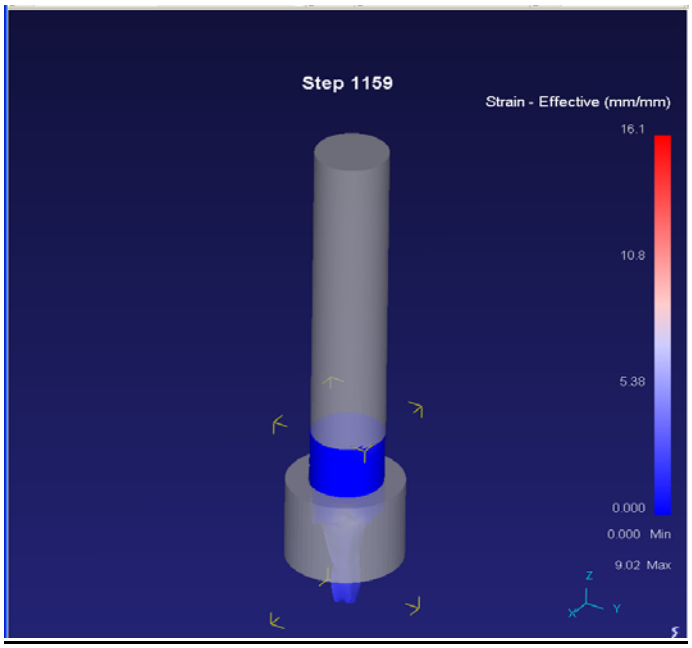

Fig. 6.9 Effective-Strain analysis for square section for 90% reduction, m=0.75

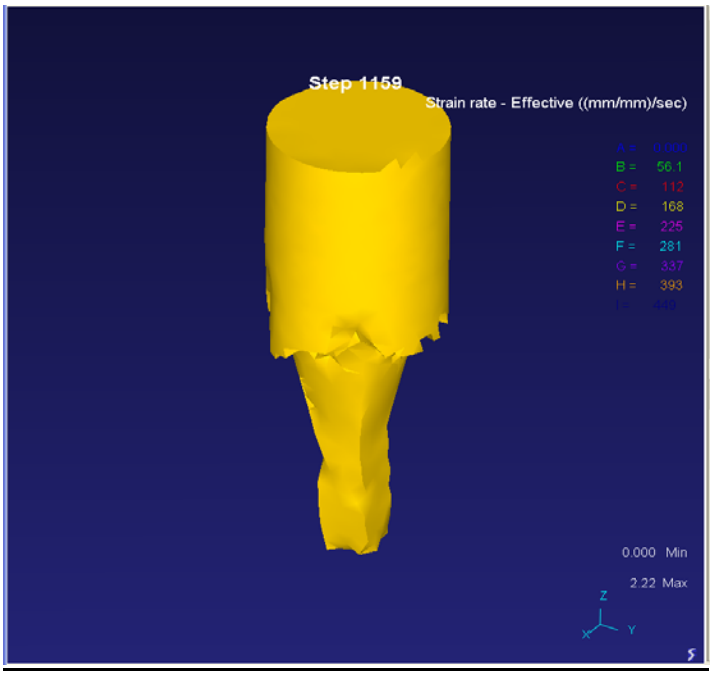

Fig. 6.10 Strain rate analysis for square section, m=0.75

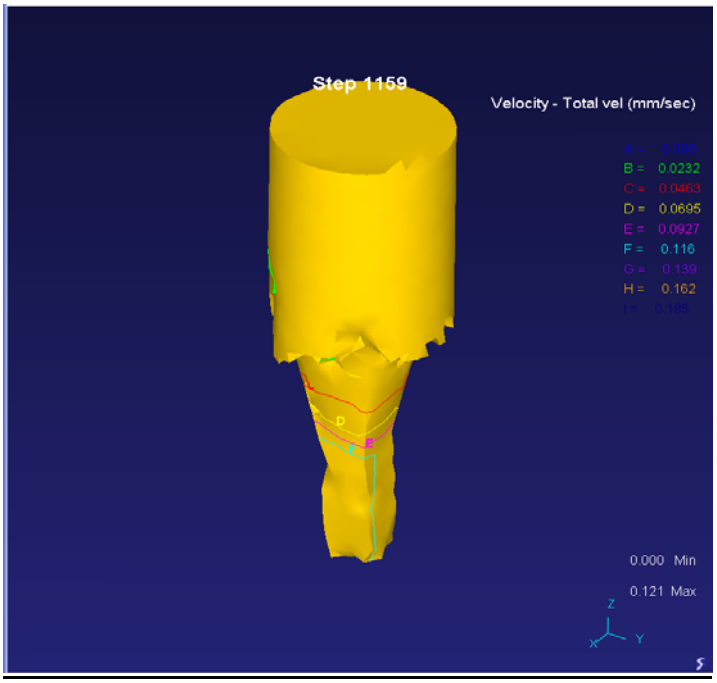

Fig. 6.11 Velocity and Total velocity pattern for square section, m=0.75

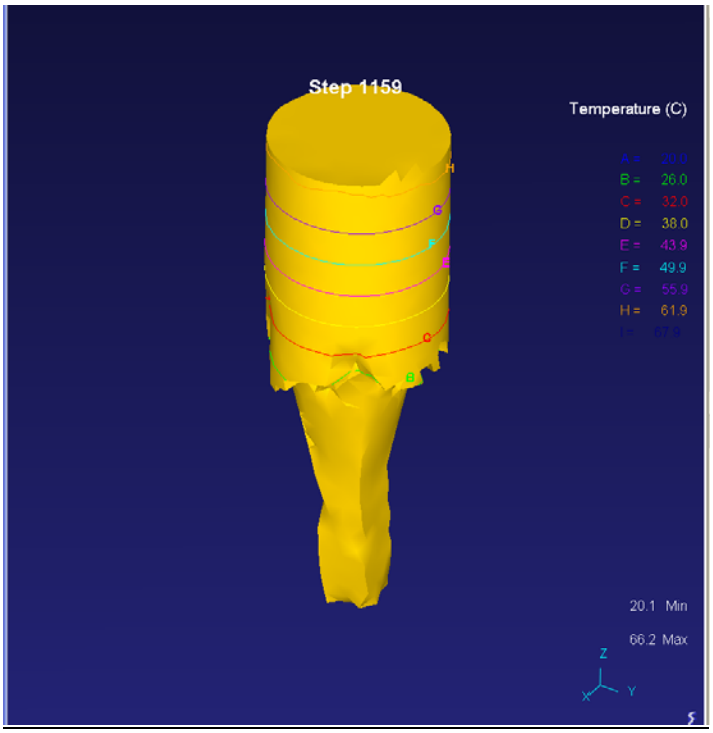

Fig. 6.12 Temperature distribution for square section

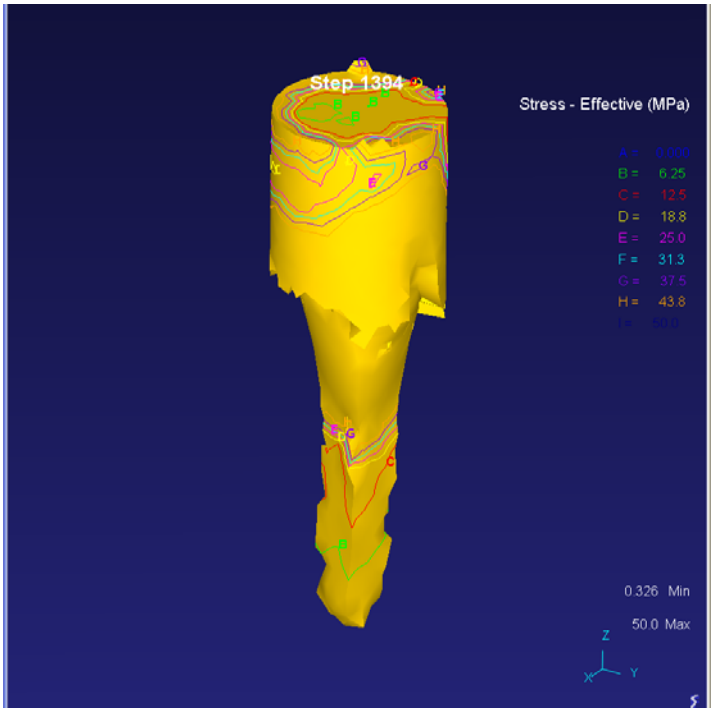

Fig. 6.13 Effective-Stress analysis for triangular section (m=0.38)

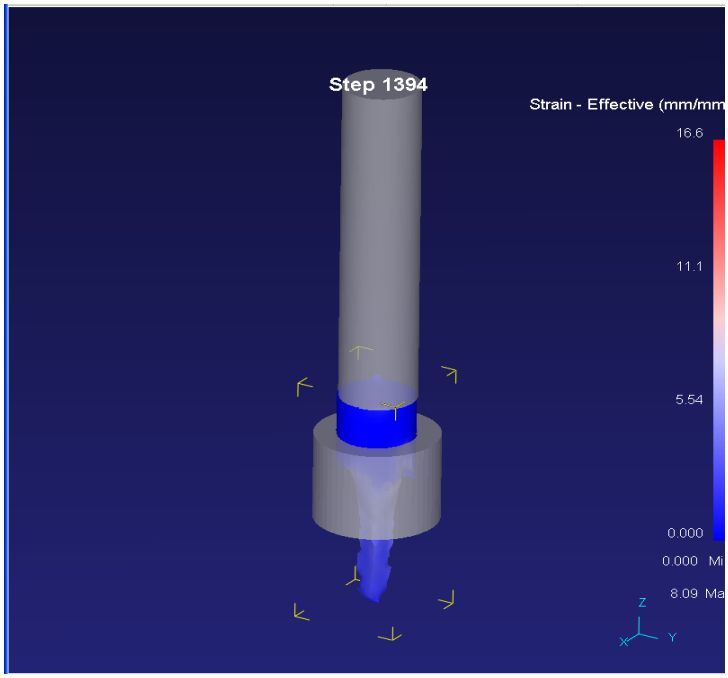

Fig. 6.14 Effective-Strain analysis for triangular section for 90% reduction and m=0.38.

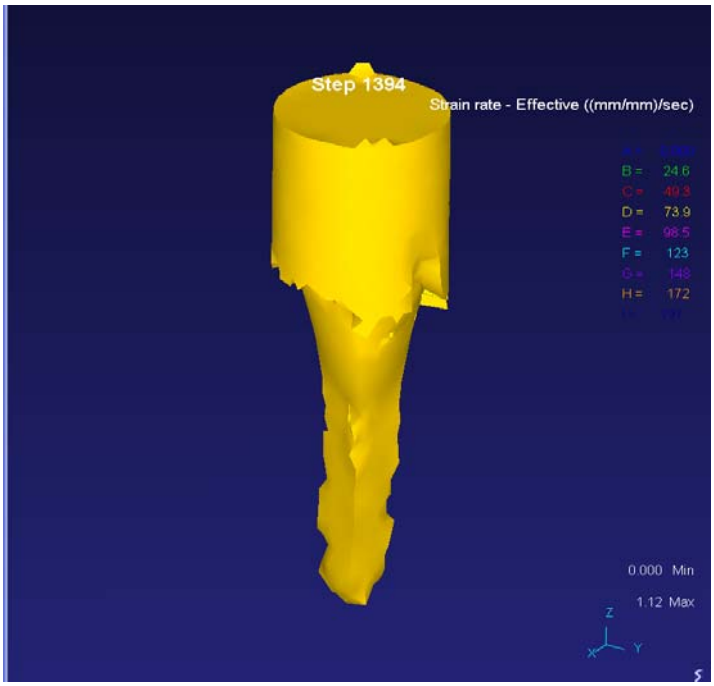

Fig. 6.15 Strain rate analysis for triangular section (m=0.38)

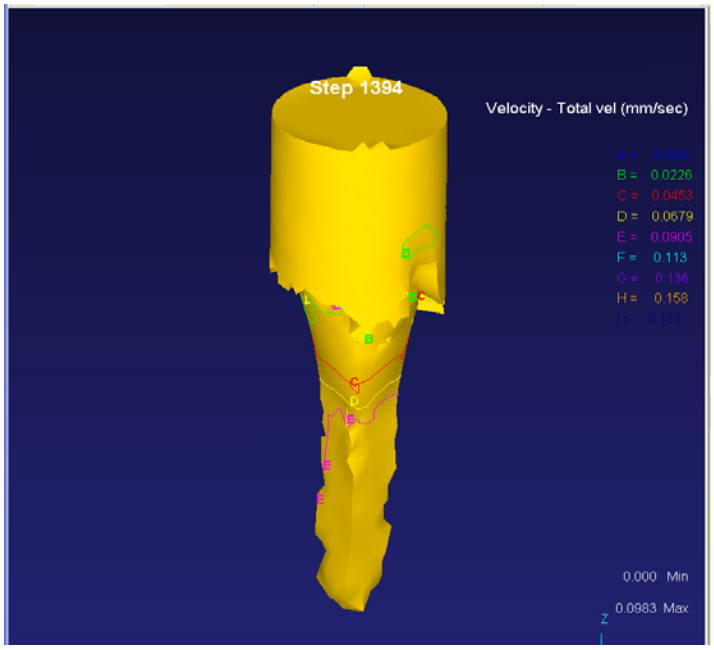

Fig. 6.16 Velocity -Total velocity pattern for triangular section, m=0.38

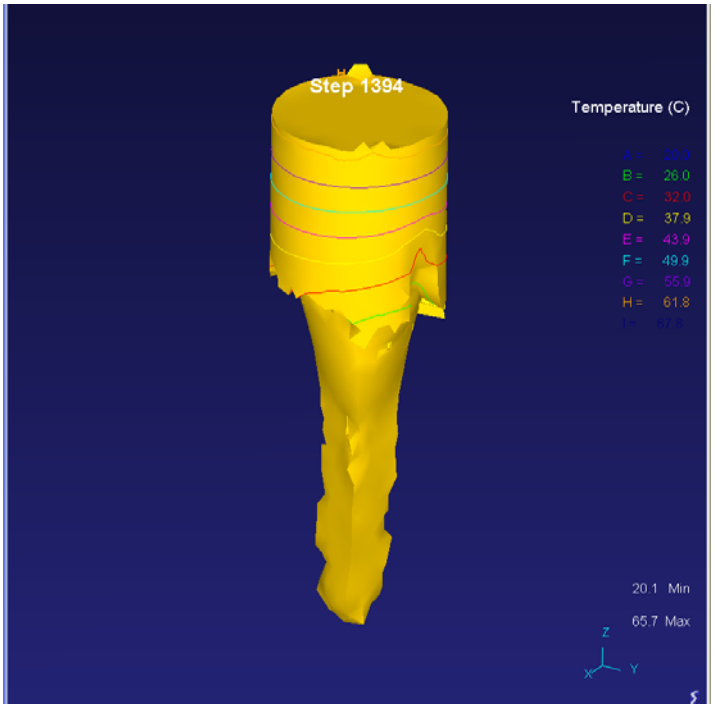

Fig. 6.17 Temperature distribution for triangular section, m=0.38

The variation of punch load versus ram travel is shown in Fig. 6.18 for extrusion of square section from round billet for 50% reduction both for lubricated

(m=0.38) and dry condition (m=0.75). It is observed that load increases gradually and later remains constant. The load is higher for dry condition compared to lubricated condition. The variation of extrusion load versus ram travel during extrusion of square section from round billet through curve dies for 70% and 90% reduction are also shown in similar manner in Fig. 6.19 and Fig. 6.20 respectively. The comparison of wet and dry extrusion pressure with respect to percent reduction for square section are shown in Fig. 6.21. It is observed that the extrusion pressure increases with increase in reduction and friction factor.

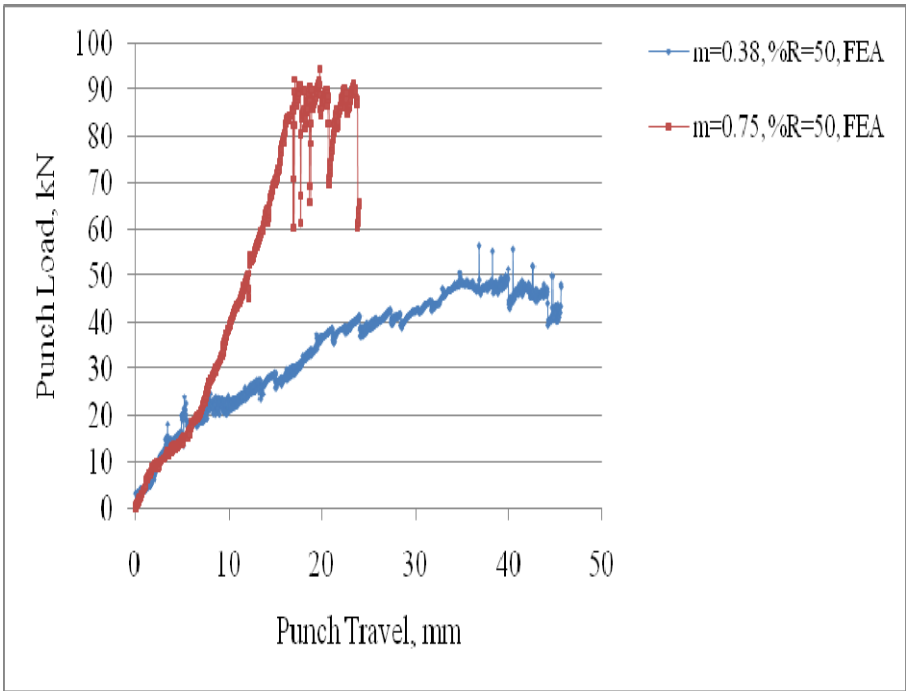

Fig. 6.18 Variation of punch load with respect to punch travel for extrusion of square section (50% reduction)

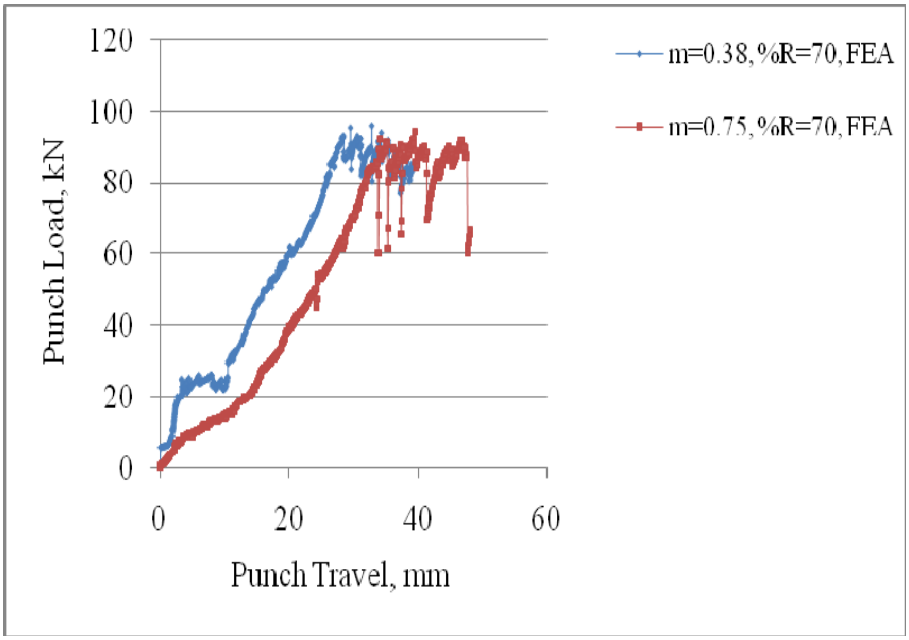

Fig. 6.19 Variation of punch load with respect to punch travel for extrusion of square section (70% reduction)

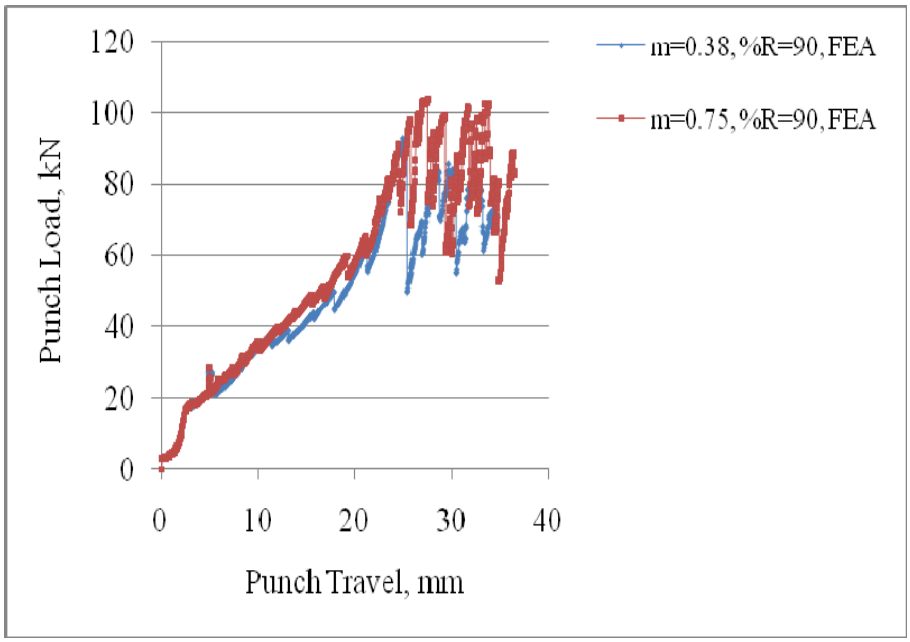

Fig. 6.20 Variation of punch load with respect to punch travel for extrusion of square section (90% reduction)

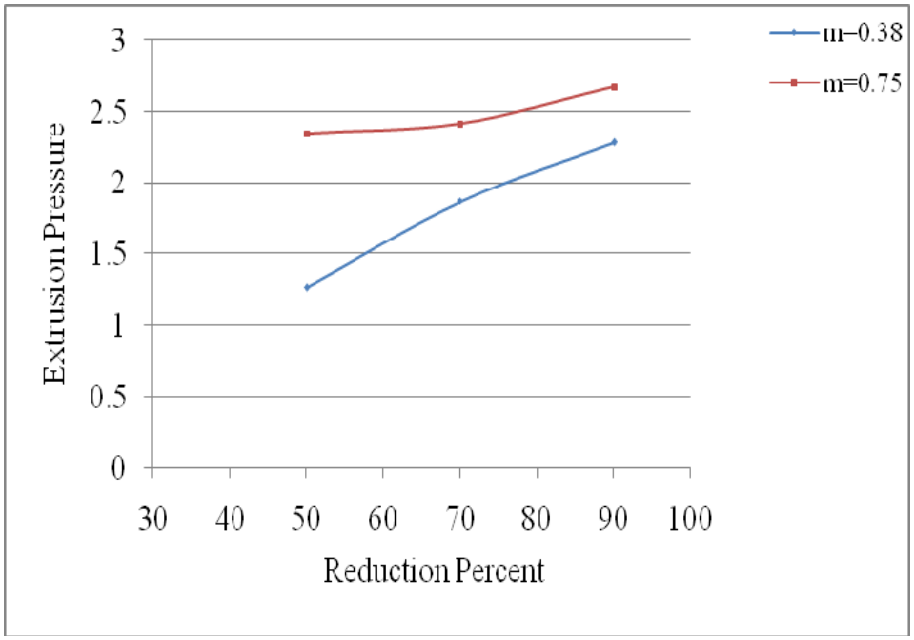

Fig. 6.21 Comparison of wet and dry extrusion pressure for extrusion of square section

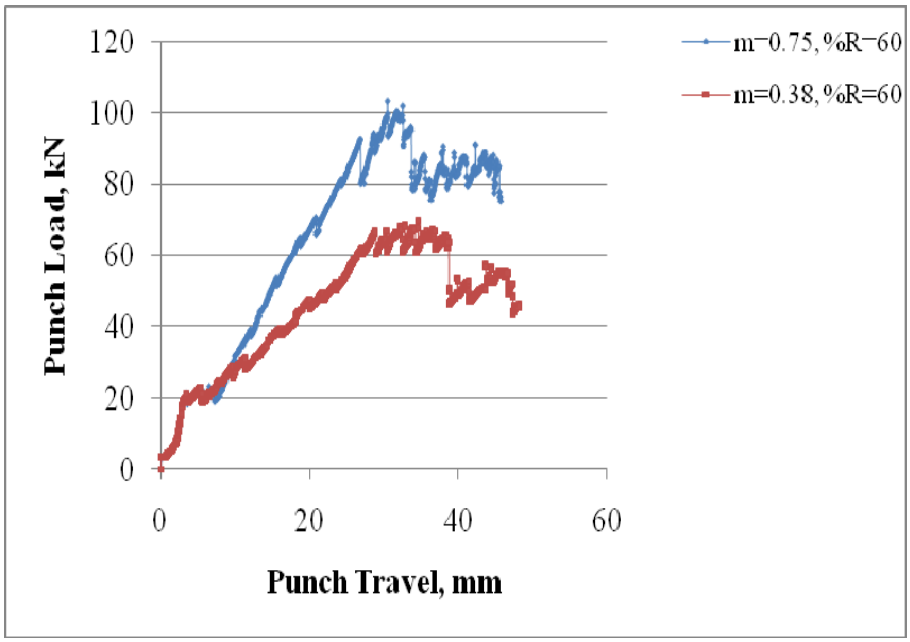

Fig.6.22 Variation of punch load with respect to punch travel for extrusion of triangular section (60% reduction)

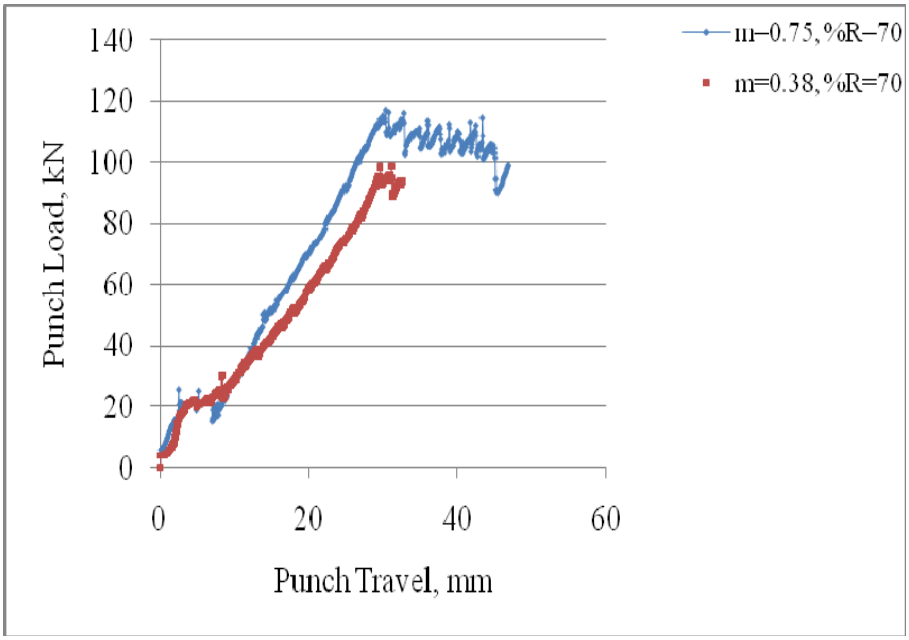

Fig. 6.23 Variation of punch load with respect to punch travel for extrusion of triangular section

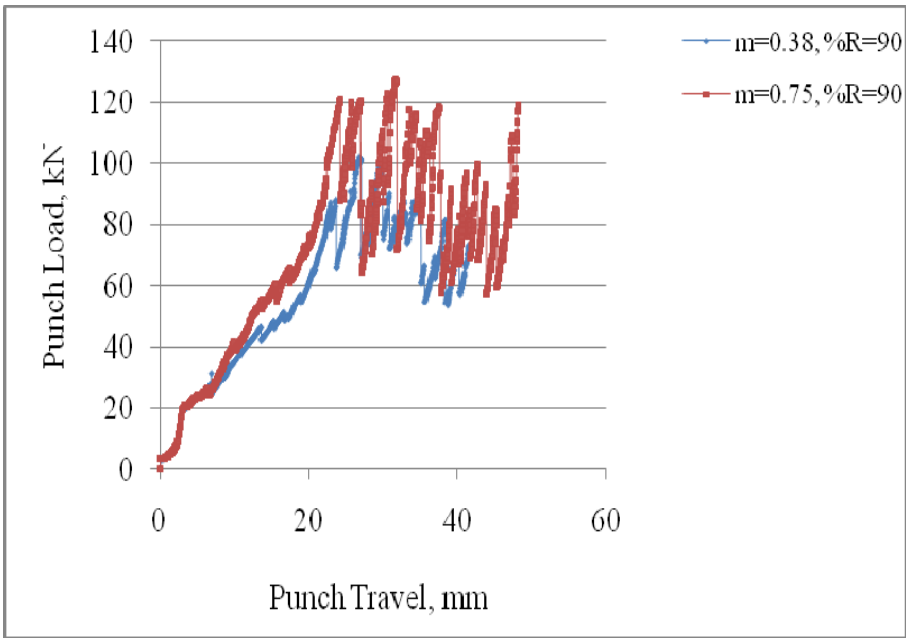

Fig. 6.24 Variation of punch load with respect to punch travel

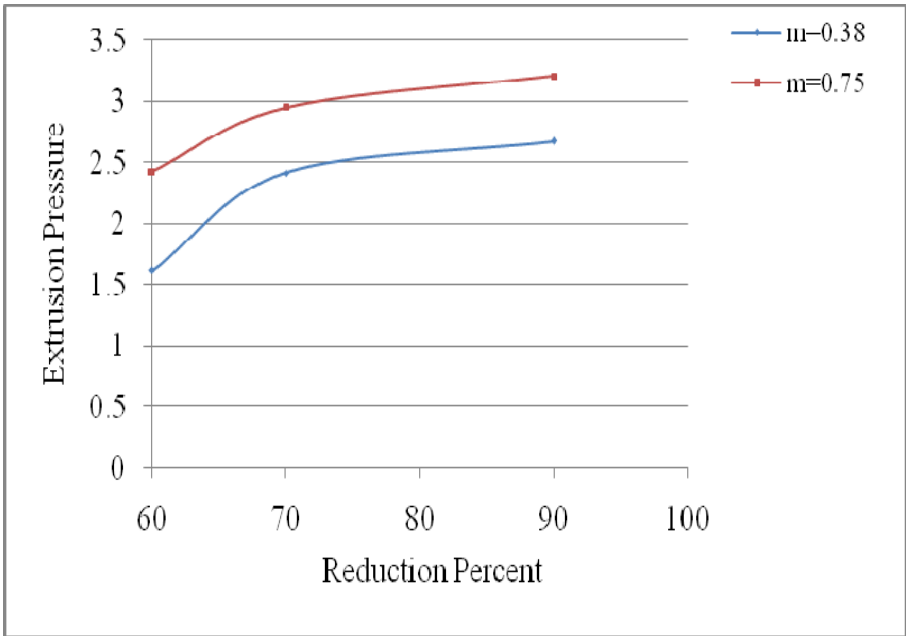

Fig. 6.25 Comparison of wet and dry extrusion pressure for extrusion of triangular sections

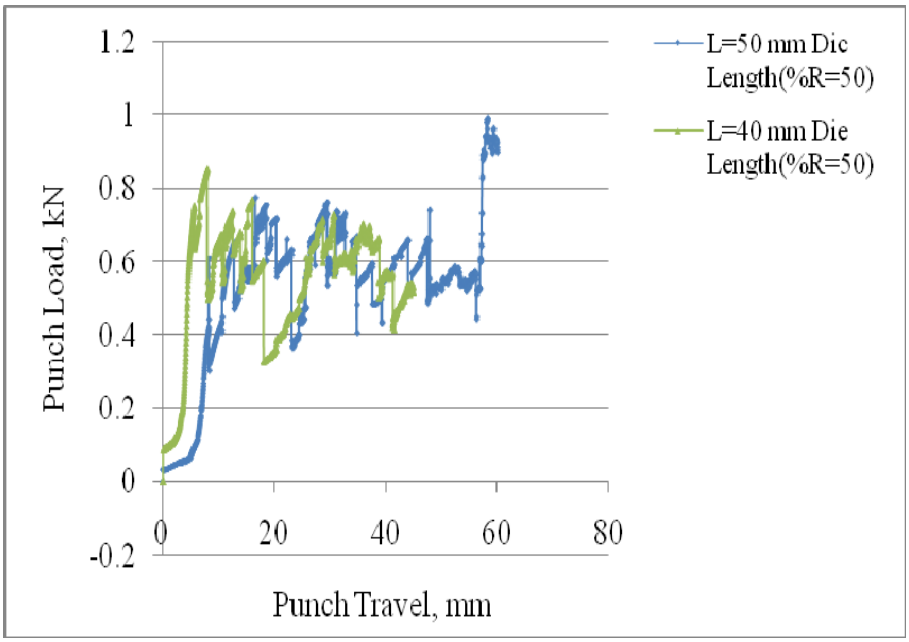

Fig. 6.26 Comparison of punch load with respect to punch travel for different die length of triangular section (50%)

The variation of extrusion load versus ram travel is shown in Fig. 6.22 for extrusion of triangular section from round billet through curve dies for reduction 60% in lubricated condition (m=0.38) and dry condition (m=0.75) at the die billet interface which qualitatively agrees with the results of extrusion of square section (Fig. 6.18). The similar variation of extrusion load versus ram travel for 70% and 90% reduction are shown in Fig. 6.23 and Fig. 6.24 for both dry and wet condition. It is indicated that the extrusion pressure increases with increase in reduction and friction factor. A comparison of extrusion pressure with respect to reduction is shown in Fig. 6.25 for extrusion of triangular section from round billet for dry and wet friction condition. It is observed that the extrusion pressure is higher for dry friction. The effect of change in die length for same reduction is also studied. Referring to Fig.6.26, it is observed that extrusion load increases when die length increases from 40 mm to 50 mm for 50% reduction.

6.5 Conclusion

(i) A die profile function have been developed for extrusion of triangular and square section from round billet using a mathematically contoured die profile. The procedure can also be used to develop other die profiles.

(ii) Solid CAD models of curved die profiles have been developed for extrusion of triangular and square section.

(iii) FEM modeling have been carried out by using DEFORM-3D software using tellurium lead as rigid plastic material for extrusion of triangular and square section from round billet.

(iv) The effective stress, the effective strain, the effective strain rate and the temperature distribution during deformation has been determined from FEM modeling.

(v) The extrusion pressure increases with increase in reduction, friction factor and die length.

Experimental Investigation

7.1 Introduction

In the slip-line or upper bound analysis, idealized assumptions are invariably made concerning the nature of deformation and material properties. Therefore, before applying the theoretical results to actual production situation, their suitability needs to be verified experimentally. A number of experimental studies on plane strain and axisymmetric extrusion using symmetric and asymmetric dies have been carried out in the past by different investigators. An exhaustive list of such work has been given by Johnson and Kudo [76].

Although a lot of studies have been carried out on plane strain and axisymmetric extrusion, no much work has been reported on extrusion of sections with re-entrant corners. Johnson [75] performed a series of tests on rectangular, triangular and I-section bars using circular billets of pure and tellurium lead. He also studied the effect of punch speed on extrusion load. Similar studies were carried out by Adeyemi and Chitkara [1] using square and round billets. However, none of these authors correlated their experimental investigation on extrusion of square, triangular, and elliptic sections from round bars using stream lined dies as reported by Yang et al. [195]. They have also compared their results with theoretical ones based on a generalized velocity field technique.

In the present investigation, some experimental studies are carried out with a view to comparing the experimental results with the theoretical ones obtained from proposed method of analysis. Experiments are performed on a Universal Testing Machine (UTM) for extrusion of triangular, rhomboidal, pentagonal and octagonal sections with different round to polygonal dies using round section billets of commercially available tellurium lead (Composition: Pb-75%, Ca-10% and SiO_2-15%). An extrusion test rig is designed and fabricated on thumb rule basis for the said purpose and all extrusions are carried out using round and square billets. The

following sections deal with brief description of the apparatus and the experimental procedure with results.

7.2 The Test Rig

The experimental set-up for the present investigation was shown in Fig.7.1. The apparatus mainly consists of four parts, namely, the container having a round extrusion chamber, the extruding punch, the die holder, and the supporting block for the die holder. The sectional view of experimental set-up is shown in Fig. 7.2. The photograph of the assembled set-up is shown in Fig. 7.3. Basically all parts are made up of low and medium carbon steel. The photographs of the individual parts including the container, die holder, punch and the die block are shown in Fig. 7.4.

The apparatus consists of four parts, namely, i) the container having a round extrusion chamber, ii) the extruding punch, iii) the die holder, and iv) the supporting block for die holder. The container (130mmΦ, 110 mm long) having the extrusion chamber (30mm Φ, 110mm long) is made from a round block (150mm long, 140mm Φ) of forged medium carbon steel. A 48mm Φ hole is made at the center surface of the block to accommodate the die which is kept inside the die holder of simple push fit type.. The die holder is made from medium carbon steel round block by shaping. During the extrusion process very high normal pressure is exerted on the chamber wall resulting in an increase in its cross-sectional area. In the present set up this is avoided by making the container a single block. The extrusion chamber and the die holder are fastened together rigidly by four allen fine bolts (M8 Φ).

The extrusion punch (30mm Φ x155mm) is made of EN31. A plate (160mm Φ, 20mm thick) is screwed at the top end. The top face of the round plate and the bottom face of the punch are made parallel. A supporting plate (130mm Φ, 20mm thick) is provided to upload both extrusion chamber and die holder. The photographs of the individual parts with wire frame modeling are shown in Figs. 7.5 -7.8 including detail dimensions in (Table-7.1)

Fig 7.1 The experimental set-up mounted on UTM for extrusion of polygonal section

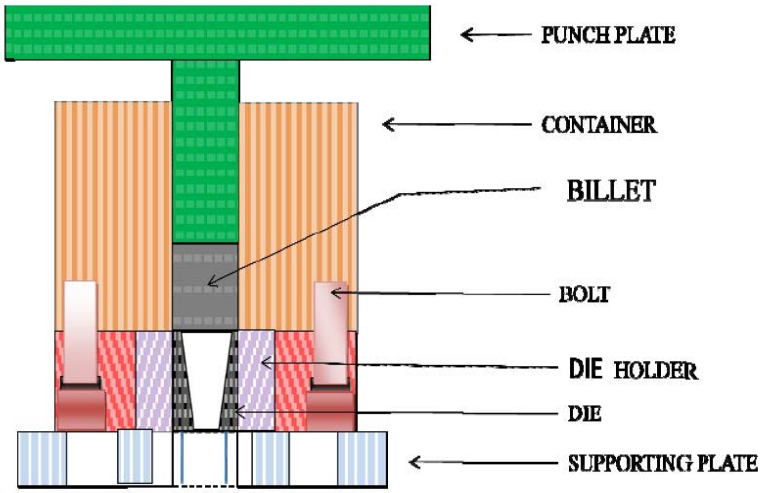

Fig. 7.2 Sectional view of the experimental set-up

Fig. 7.3 The assembly of the experimental set-up

Fig.7.4 Photograph showing all parts of the set-up

Table 7.1 Details of individual component of the experimental set-up

SI. NO.	Name of parts	Dimension of parts, mm		Dimension of original stocks, mm		Materials	Processes used
		Cross section	Length	Cross section	Length		
1	Container with extrusion chamber	130 ϕ	110	150 ϕ	140	Forged medium carbon steel	Turning, drilling and grinding
2	Punch	30 ϕ	155	35 ϕ	170	EN31	Grinding,Shaping & CNC milling
3	Punch plate	160 ϕ	20	180 ϕ	30	Medium carbon steel	Turning, milling & welding
4	Die holder with a recess	130 ϕ	40	150 ϕ	50	EN31	Turning, drilling and shaping
5	Supporting plate	130 ϕ	20	150 ϕ	30	Medium carbon steel	Turning, drilling & facing
6	Specimen	30 ϕ	45~65	35 ϕ	200	Lead	Casting, turning and facing
7	Dies with opening	30 ϕ	40	50 ϕ	200	EN31	Turning, facing and wire EDM
8	Bolts	Four numbers M8 Allen bolt	72	–	–	Medium carbon steel	As available in the market

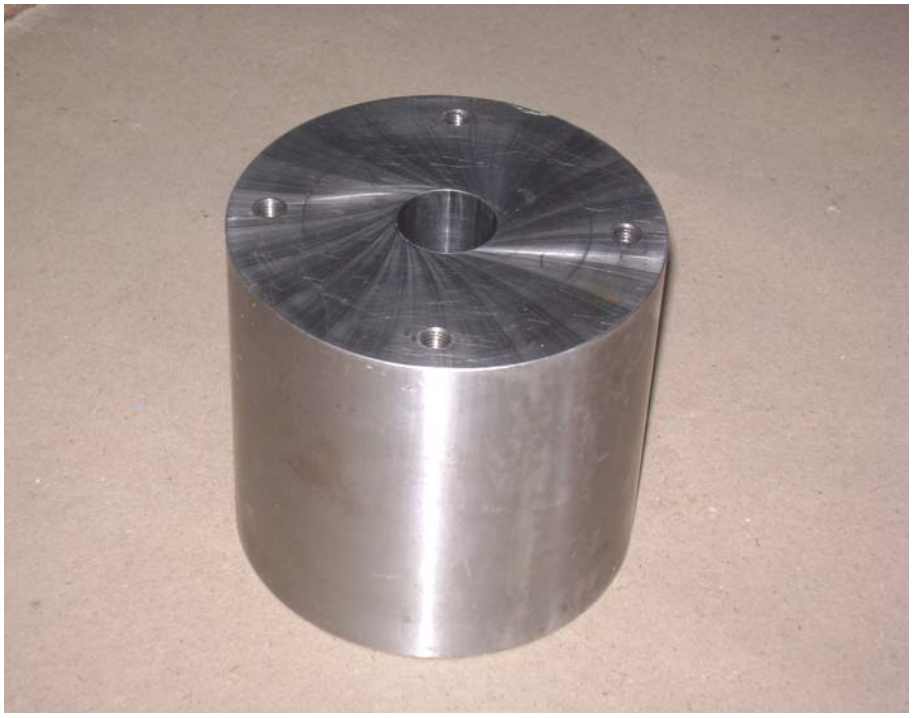

Fig.7.5 (a) Container with round extrusion chamber

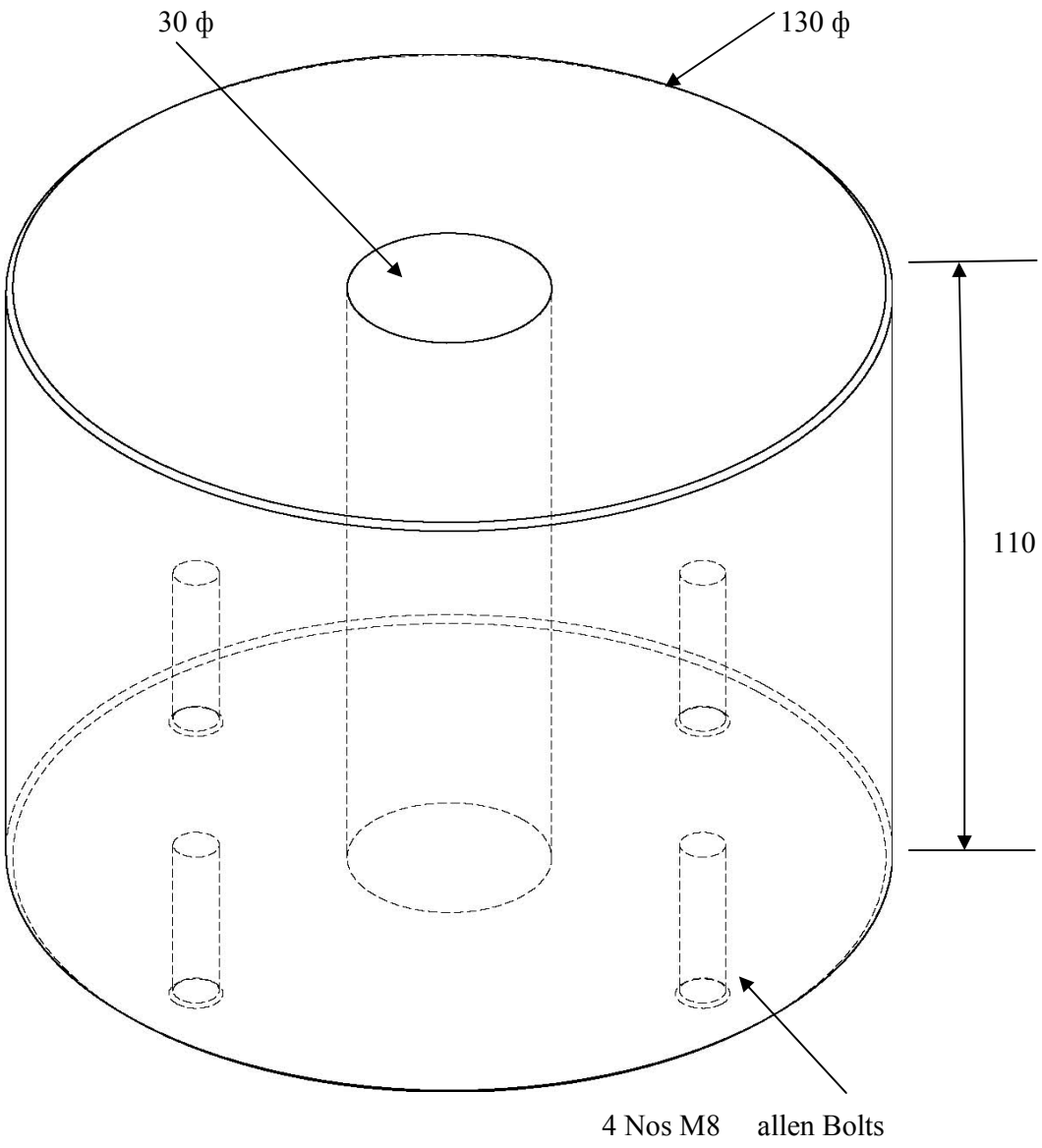

Fig.7.5 (b) Dimension of the Container with round extrusion chamber

Fig.7.6 (a) Die holder with casing along with a pair of split dies

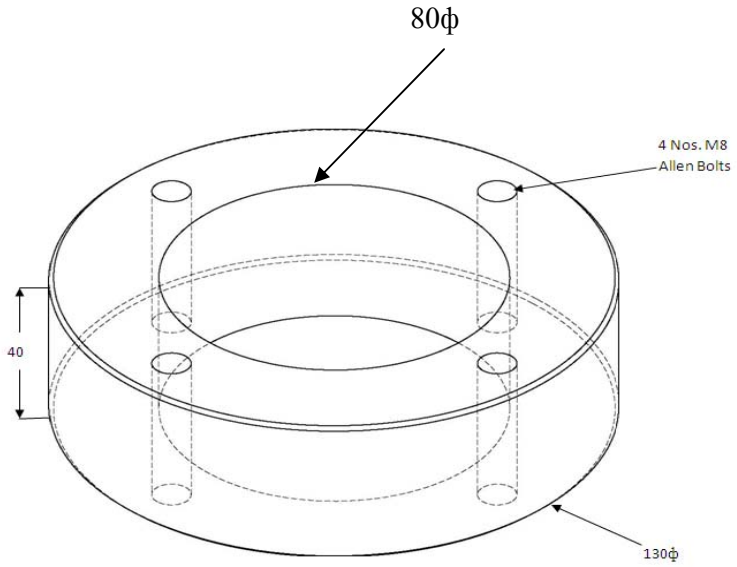

Fig.7.6 (b) Dimension of Die holder with casing

Fig.7.7 (a) Punch

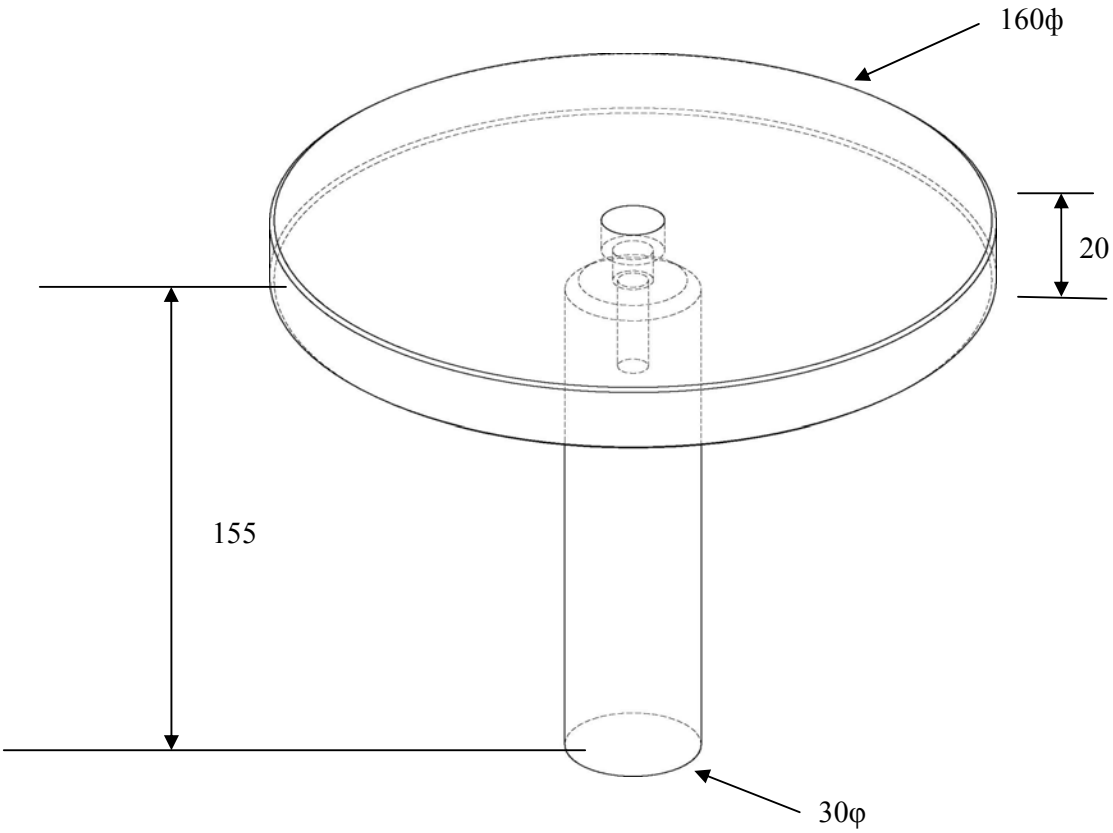

Fig.7.7 (b) Dimension of the Punch

Fig.7.8 (a) Top support plate with four allen bolts

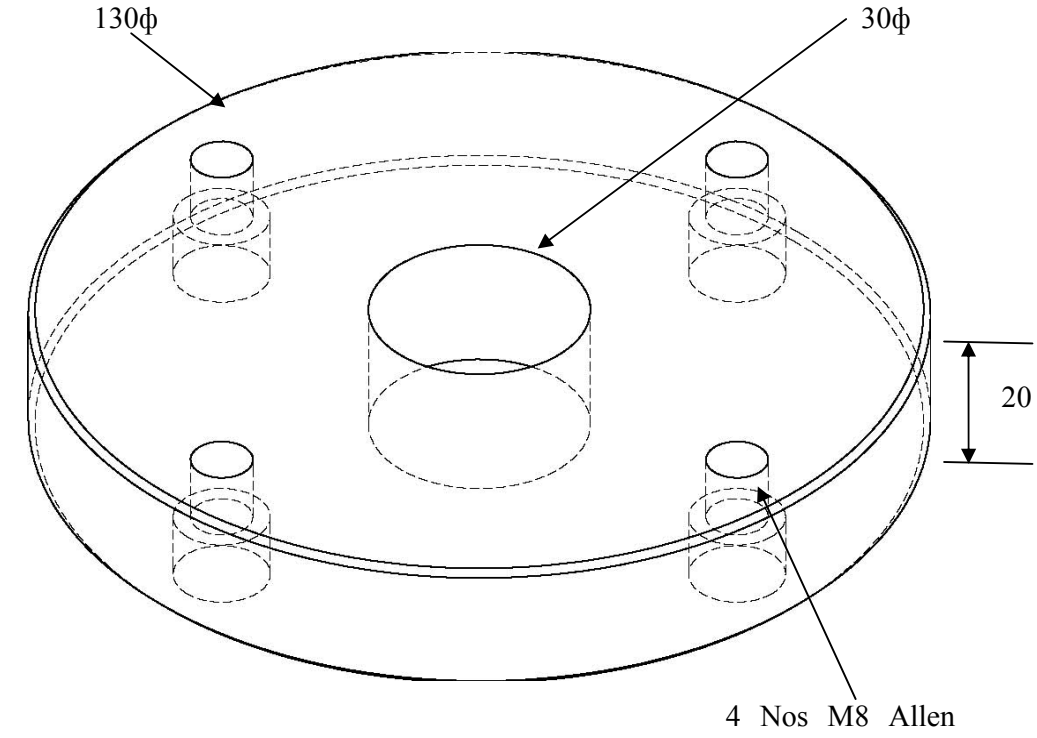

Fig.7.8 (b) Dimension of the Top support plate

7.3 Dies

The extrusion dies are made of two split halves for easy removal of the product after each extrusion cycle. These dies are manufactured using wire EDM from medium carbon steel (30mm Φ and 40 mm height). The orifices are located in such a way that the respective centers of gravity lie on the billet axis. Experiments are conducted with three sets of dies for triangular, rhomboidal, pentagonal and octagonal section dies. The split dies and the dimensions of the orifices for the above dies are presented in Fig 7.9 to Fig. 7.12 and Table 7.2.

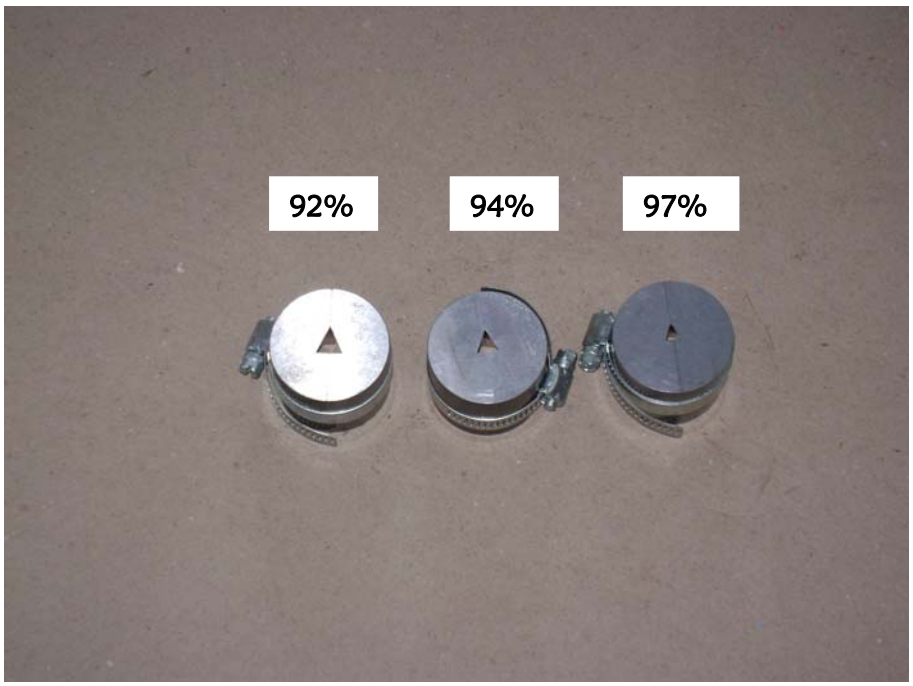

Fig.7.9 (a) Split dies used to extrude Triangular (Isosceles) section

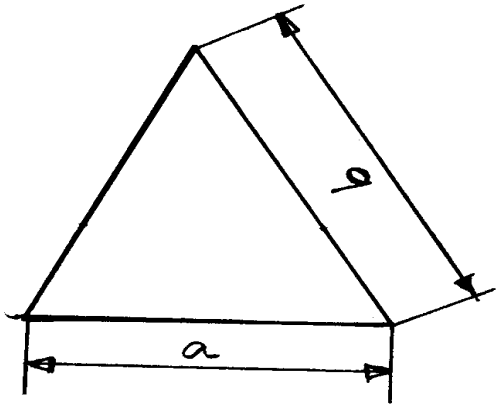

Fig.7.9 (b) Die orifice dimensions used to extrude Triangular section

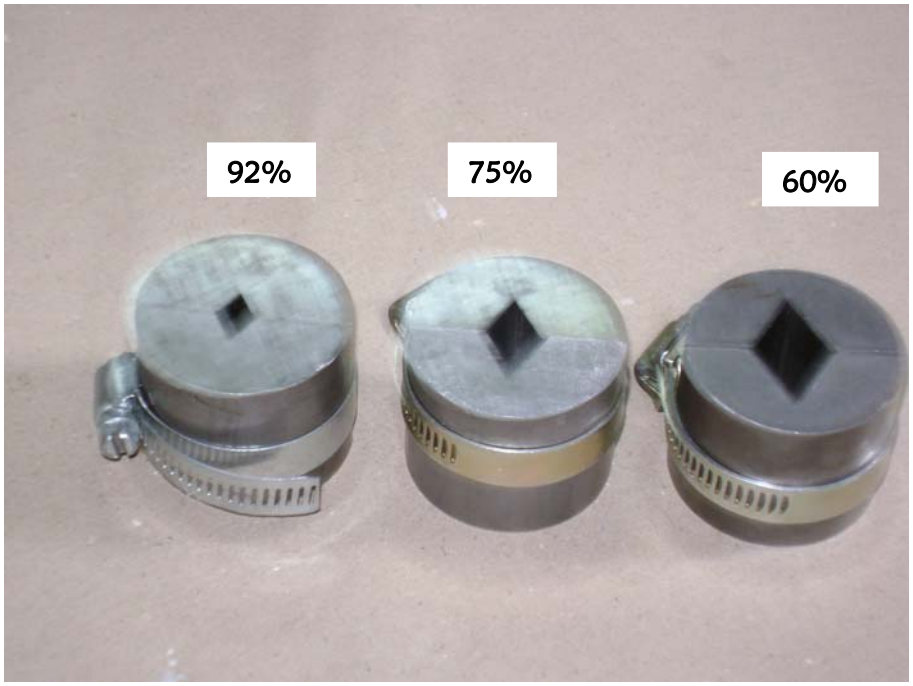

Fig.7.10 (a) Split dies used to extrude rhomboidal section

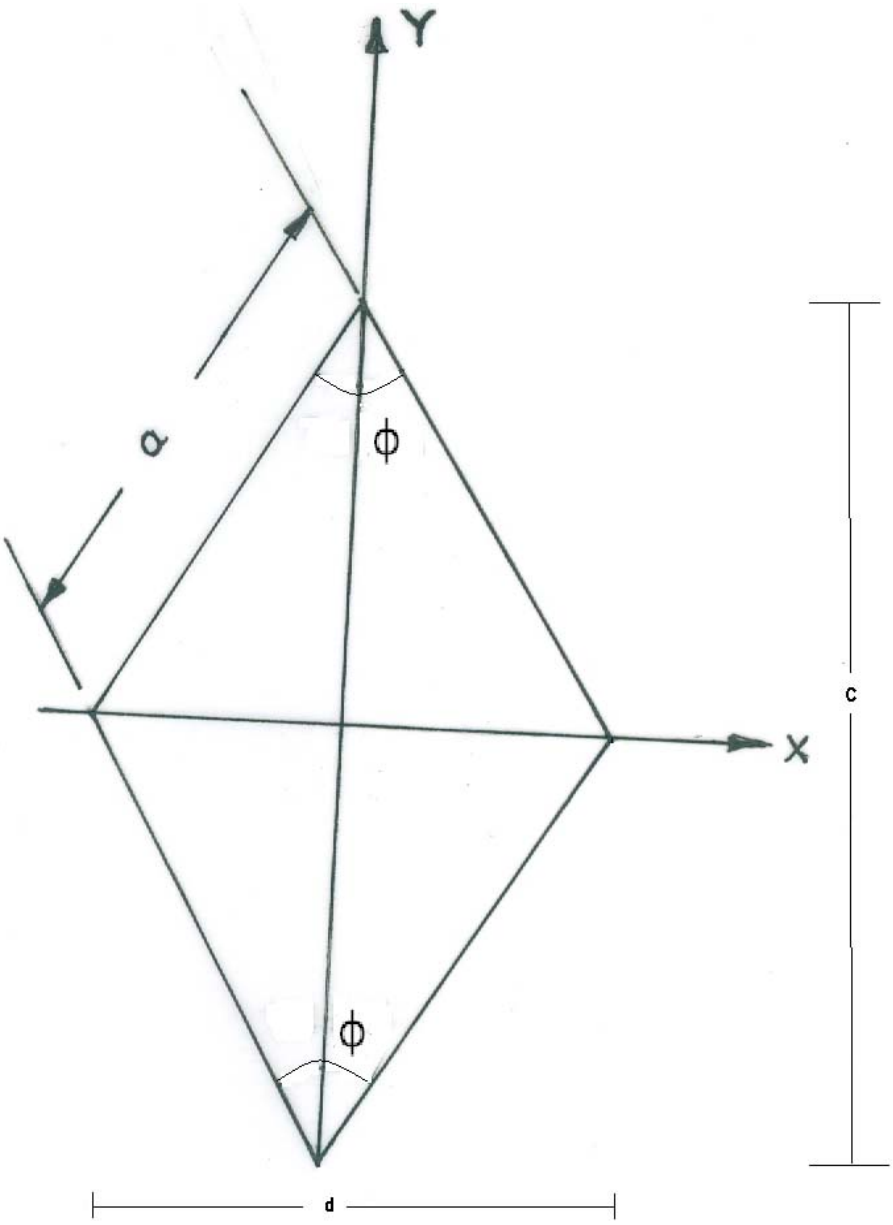

Fig.7.10 (b) Die orifice dimensions used to extrude rhomboidal section

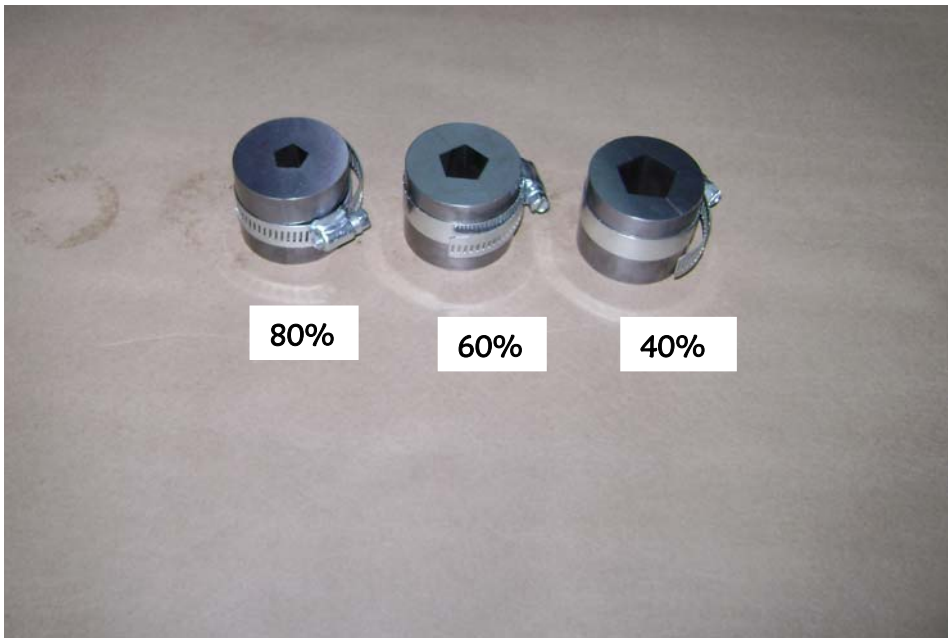

Fig.7.11 (a) Split dies used to extrude pentagonal section

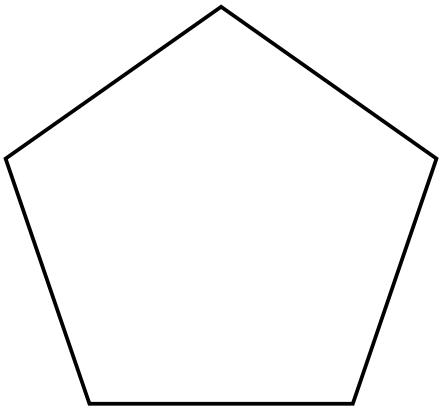

Fig.7.11 (b) Die Orifice dimensions used to extrude pentagonal section

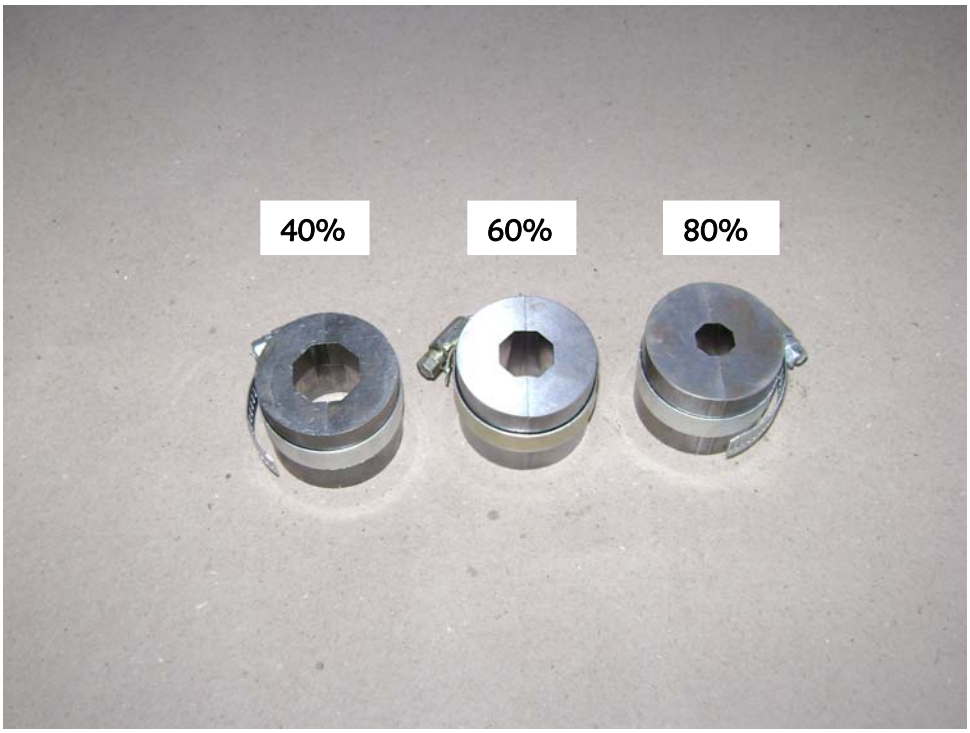

Fig.7.12 (a) Split dies used to extrude Octagonal section

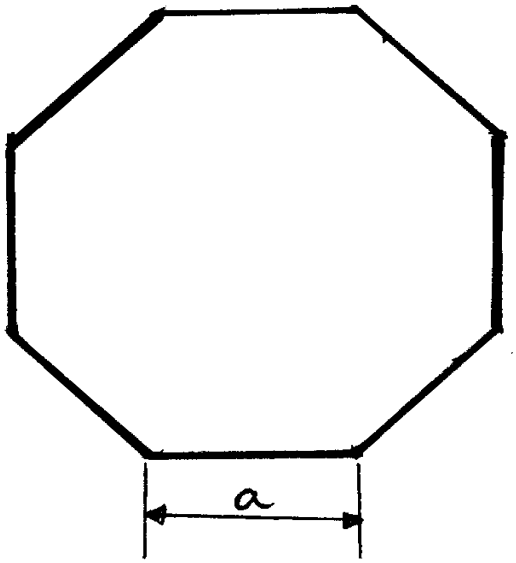

Fig.7.12 (b) Die orifice dimensions used to extrude Octagonal section

Table 7.2 Die dimensions

Section	% Reduction	Dimension in mm					Area, mm^2
		a	b	c	d	e	
TRIANGLE (Isoscales)	92	12.57	10.44	_	_	5.837	56.548
	94	10.27	8.53	_	_	4.768	42.411
	97	7.261	6.03	_	_	3.371	21.205
RHOMBUS	60	19.416	_	33.6298	16.8149	_	282.743
	75	15.349	_	26.5868	13.2934	_	176.714
	92	8.683	_	15.0397	7.5198	_	56.548
PENTAGON	40	15.7	_	_	_	13.35	424.115
	60	12.82	_	_	_	10.91	282.743
	80	9.06	_	_	_	7.71	141.371
OCTAGON	40	9.37	_	_	_	12.24	424.115
	60	7.65	_	_	_	9.99	282.743
	80	5.41	_	_	_	7.069	141.371

a=one side of the polygon; b=other side of the polygon; c=major axis of the polygon; d=minor axis of the polygon; e= distance of CG from any vertex of a polygon.

7.4 Specimens

All the experiments are conducted with commercially available tellurium lead (Composition: Pb-80%, Ca-10% and SiO_2-15%), shown in Fig. 7.13, as work material. round specimens of lead for the above purpose are prepared from commercially available block by open green sand mould casting. The specimens are then finished to size by turning using kerosene as cutting fluid. Specimens of three

different lengths were used during the tests. For reductions between forty and eighty percent, the specimen length was approximately 40 mm to 70 mm. These lengths were so chosen that the maximum length of the extruded product did not exceed the clearance between the die mouth and the upper crosshead of the universal testing machine, at the same time ensuring a steady state length of 20mm to 30mm for the extrusion pressure to be accurately determined. These lengths were decided after some initial trial runs using the round dies.

Fig.7.13 Lead specimen of different reductions

7.5 Experimental Procedure

Before starting the tests, the die sets, the die holder and the inside faces of the extrusion chamber were cleaned with kerosene and then carbon tetrachloride. The taper die block was then push-fitted into the die holder and the assembly was secured by screwing the four allen bolts with the container of the die set. The full assembly was then placed on the lower table of the universal testing machine as shown in Fig. 7.1. For carrying out an extrusion test, the die block was kept in dry condition and the specimen was placed inside the extrusion chamber. The punch was then inserted into

its position. After centering the apparatus on the machine lower table, the machine was started and the extrusion process was continued. The speed of the movement of the punch was adjusted to an optimum level to avoid the rate effect**.** Punch load was recorded at regular time interval of the punch travel by using personal computer. The application of load was continued until it started to rise again after reaching the steady state and the test was terminated. The die holder was then separated from the extrusion chamber and finally the die blocks with the extruded product were pushed out from the die holder. Experiments were conducted for three different reductions for all polygonal sections at dry as well as wet conditions. The photographs of the extruded products with specimens are shown in Fig.7.14-7.17.

Fig.7.14 Extruded triangular sections of different reduction

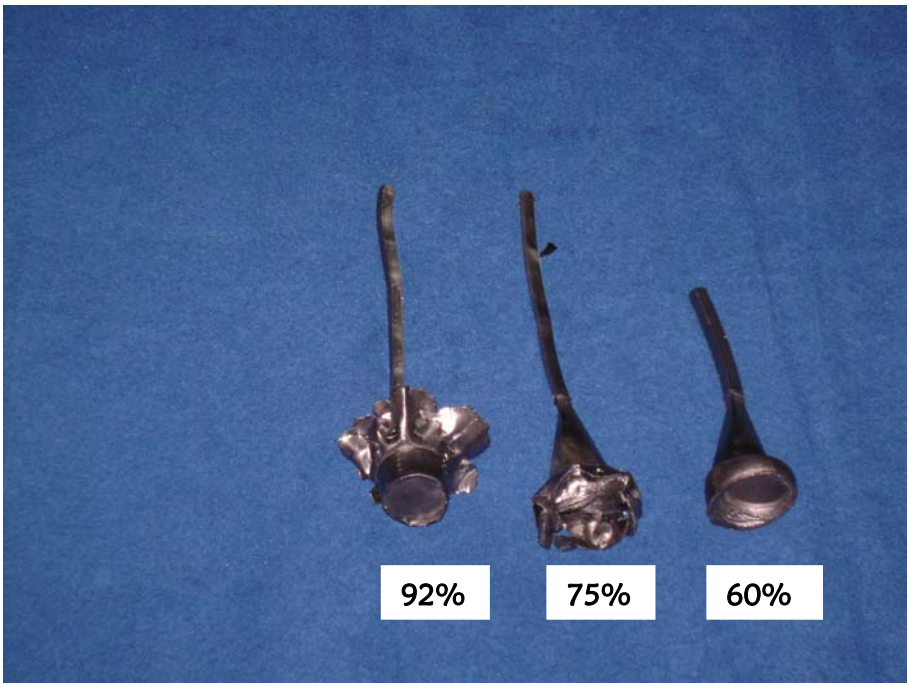

Fig.7.15 Extruded rhomboidal sections for different reduction

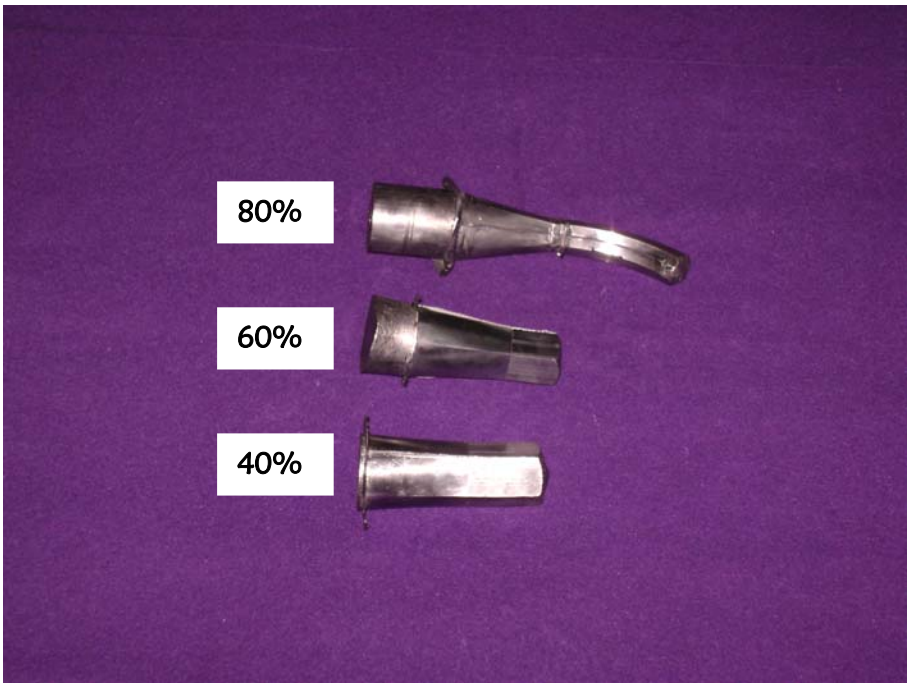

Fig.7.16 Extruded pentagonal sections for different reduction

Fig.7.17 Extruded octagonal section for different reduction

7.6 Determination of Stress-Strain characteristics of lead

In order to plot the stress-strain diagram, a cylindrical specimen of lead of 30 mm diameter and 45 mm length was machined from one of the casted specimens. After turning the specimen in boiling water for two hours, its ends were adequately lubricated with grease and it was tested in uniaxial compression on the Universal testing machine (UTM) using a sub-press (Fig. 7.18). The compression rate was the same as that used for the extrusion tests. The compressive load was recorded at every 0.05 mm of punch travel which was read from the visual display in the computer fitted on the machine. After compressing the specimen to about 15 mm, it was taken out from the sub-press, re-machined to cylindrical shape with the oil grooves again turned on both ends and tested in compression till the specimen was reduced to about 10 mm. At this point the test was stopped and the specimen was re-machined a second time. It was again tested till its height was reduced to about 4-6 mm. The stress-strain diagram of lead obtained in this manner is shown in Fig. 7.20. The curve has been extrapolated beyond a natural strain of about 0.5. To simulate a rigid-plastic material

the initial wavy portion of the diagram has been approximated by a smooth curve as shown by the dotted lines in the above figure.

To determine the uniaxial yield stress of the billet material for any given percentage reduction (PR), the corresponding strain imparted to the billet material during the extrusion process must be known to the priori. For the same reduction, the strain imparted to the billet during the extrusion process is always higher than that imparted to the billet during compression because of the redundant work done during the extrusion process. Following the principles laid by Johnson and Mellor [78], the above strain in the present case was calculated from the empirical relation,

$$\varepsilon = 0.8 + 1.5\, Ln\ \left(1/\left(1 - R\right)\right) \qquad (7.1)$$

where, R is the fractional reduction. The average stress of the extruded billet was then calculated by dividing the area under the stress-strain curve with the corresponding value of the abscissa. The magnitude of the strain calculated from the equation (7.1) and the magnitude of the average yield stress σ_0 for different reductions determined in the above manner are presented referring to Fig. 7.20 in Table 7.3.

Figure 7.18 The experimental equipment with test specimen for flow stress.

Figure 7.19 Uniform compression samples before and after deformation.

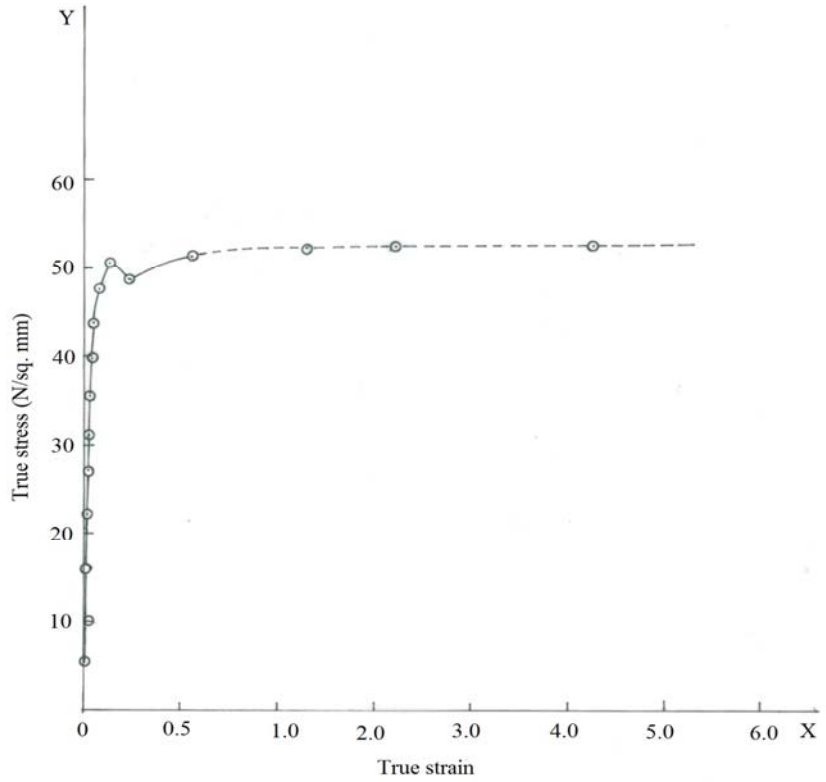

Fig. 7.20 Stress-Strain curve for lead

7.7 Measurement of Friction Factor

When a flat, ring shaped specimen is upset in the axial direction, the resulting shape change depends only on the amount of compression in the thickness direction and the frictional conditions at the die ring interfaces. If the interfacial friction were zero, the ring would deform in the same manner as a solid disk, with each element flowing outward radially from the center. In case of small but finite interfacial friction, the outside diameter is smaller than in the zero friction case. If the friction exceeds a critical value, frictional resistance to outward flow becomes so high that some of the ring material flows inward to the center. Measurements of the inside diameters of compressed rings provide a particularly sensitive means of studying interfacial friction, because the inside diameter increases if the friction is low and at higher friction the inside diameter decreases. The ring thickness is usually expressed

in relation to the inside and outside diameters. The experimental set-up for the ring compression test is shown in Fig.7.21.

The dimensions of the ring specimen in the ratio 6:3:2 (outer diameter: inner diameter: thickness) are made. Thus, by measuring the ratio of internal, external diameters after axial compression of a ring of standard dimensions, it is possible to obtain a measure of the friction. Fig 7.23 and Fig. 7.24 shows rings after compression in dry as well as wet conditions respectively.

Figure 7.21 Experimental equipment for ring compression test.

Fig. 7.22 Ring sample before compression

Figure 7.23 Resultant ring upset after various reductions in height in dry condition

Figure 7.24 Resultant ring upset after various reductions in height in wet condition

7.7.1 Experimental Procedure for ring compression test

A ring compression test was carried out at dry condition and with commercially available grease lubricated condition. The rings were compressed up to the 4 mm inner diameter, at each 0.5 mm of punch travel inner diameter and height was recorded. The friction factors were found to be 0.75 for dry condition and 0.38 for the lubricated condition by comparing our result with the theoretical calibration curve.

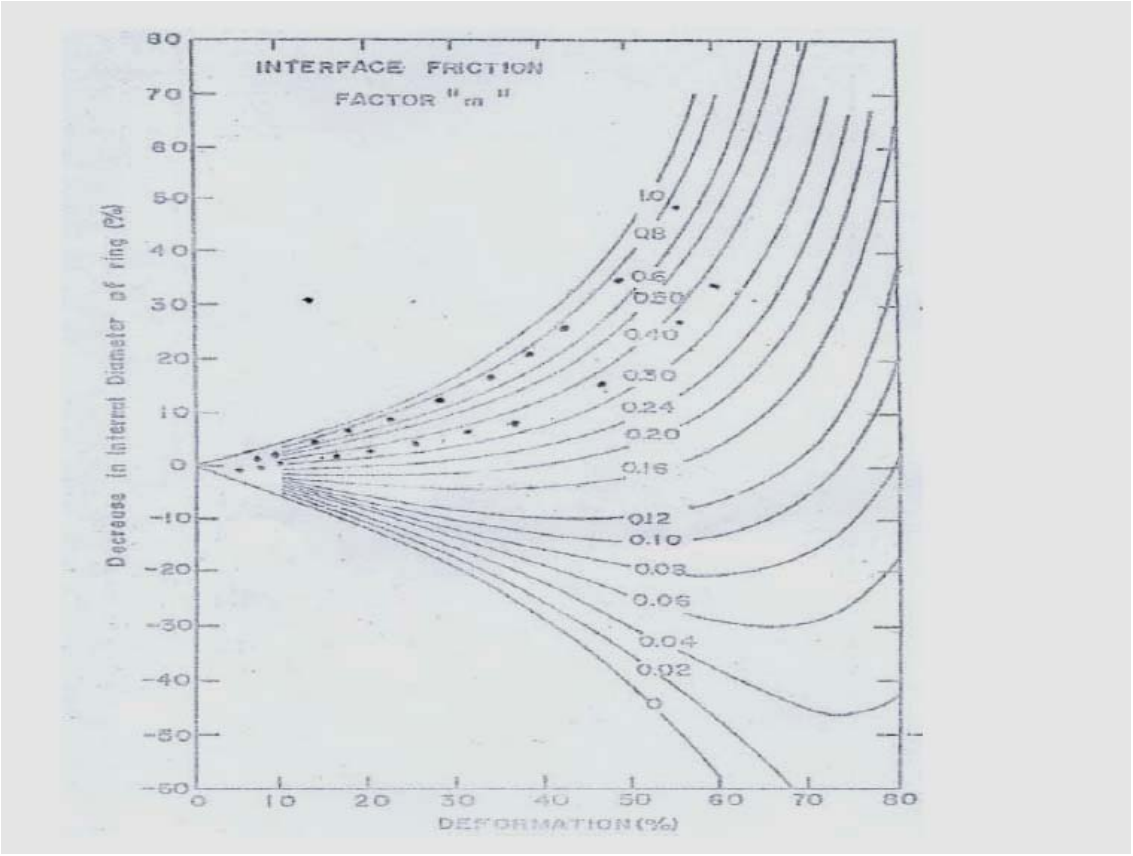

Fig 7.25 Theoretical calibration curve for standard ring 6:3:2 [8]

7.8 Results and discussion

The variation of punch load with punch travel for the rhomboidal, pentagonal, octagonal and triangular sections are shown in Fig.7.26 to Fig.7.29 respectively. Referring to any of the above diagrams, it is seen that it consists of three principal stages: namely; i) a coining stage in which the load gradually increases and reaches a peak value due to initial compression of the billet, ii) the second stage referring to steady state in which the load gradually drops from the peak value and remains fairly constant for a considerable time, and finally iii) an unsteady state where there is a drop in load followed by a steep rise. The drop in load in the third stage is because of a decrease in the frictional force between the billet and the extrusion chamber due to continuous decrease in billet length. However, the drop in load from the initial peak value is found to be marginal which may be due to adequate lubrication between the billet and the extrusion chamber.

The load corresponding to this point, considered as the extrusion load, is tabulated in table 7.3-7.6. This table also provides the value of the mean extrusion pressure P_{av}, the value of the uniaxial yield stress in compression σ_0 (as per section 7.6) and non-dimensional mean extrusion pressure P_{av}/σ_0. Theoretical values of P_{av}/σ_0 computed with the help of the proposed SERR technique, are presented in Table 7.3 to Table 7.6 for a comparison. The theoretical results are also compared with experiments in Fig. 7.30-7.34. It is seen that the agreement between the theoretical and experimental values is fairly good, and average percentage of variation is being limited to ten with maximum being fourteen.

The variation of mean extrusion pressure P_{av}/σ_0 (experimental) with ln(1/ (1-R)) is shown in Fig.7.35. The best fit line is found to obey the equation

$$\frac{P_{av}}{\sigma_0} = 0.666 + 2.133 \ln\left(\frac{1}{1-R}\right) \quad (7.2)$$

The above equation can be used to predict the extrusion pressure to a fairly accurate extent.

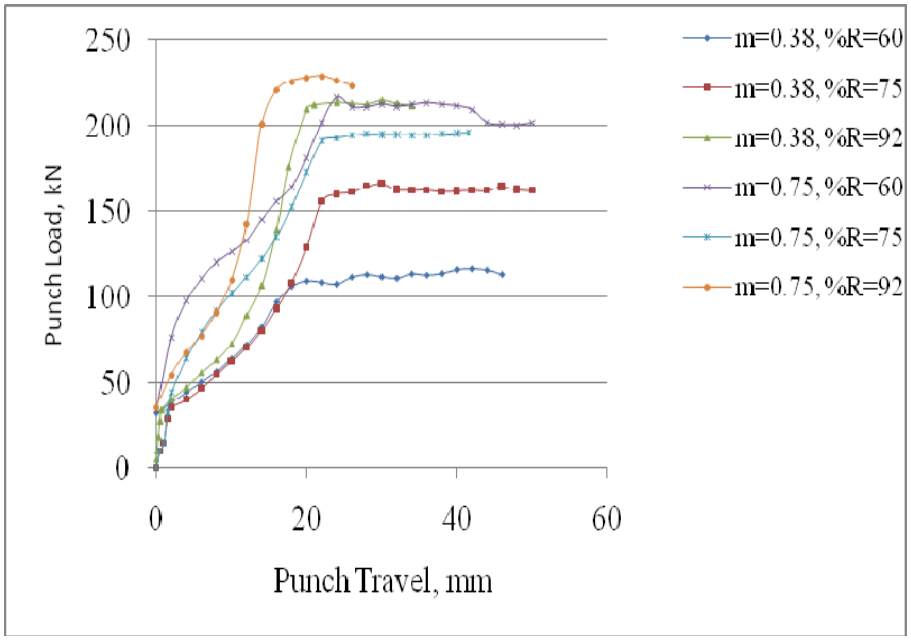

Fig.7.26 Variation of extrusion load versus ram travel for rhomboidal section

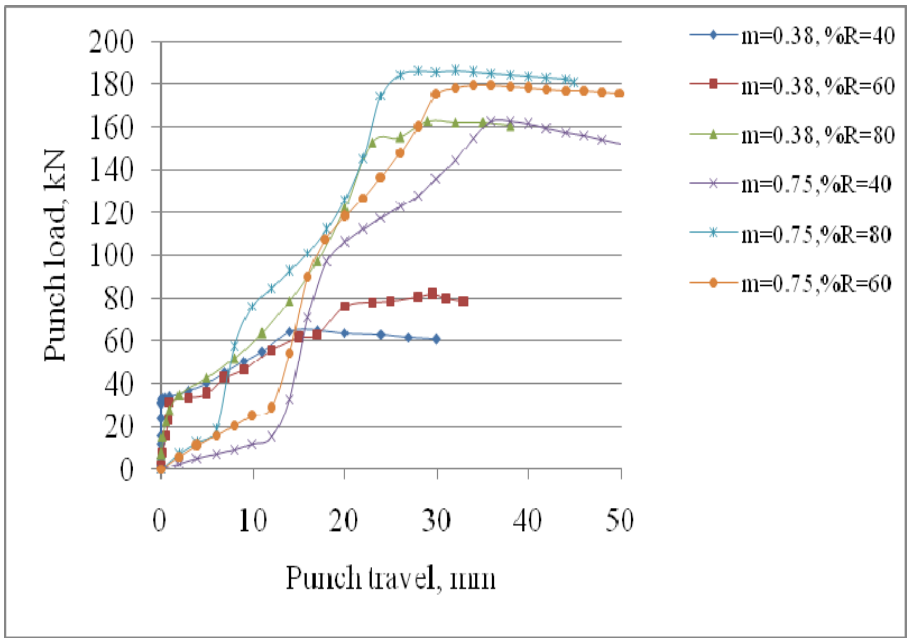

Fig. 7.27 Variation of extrusion load versus ram travel for pentagonal section

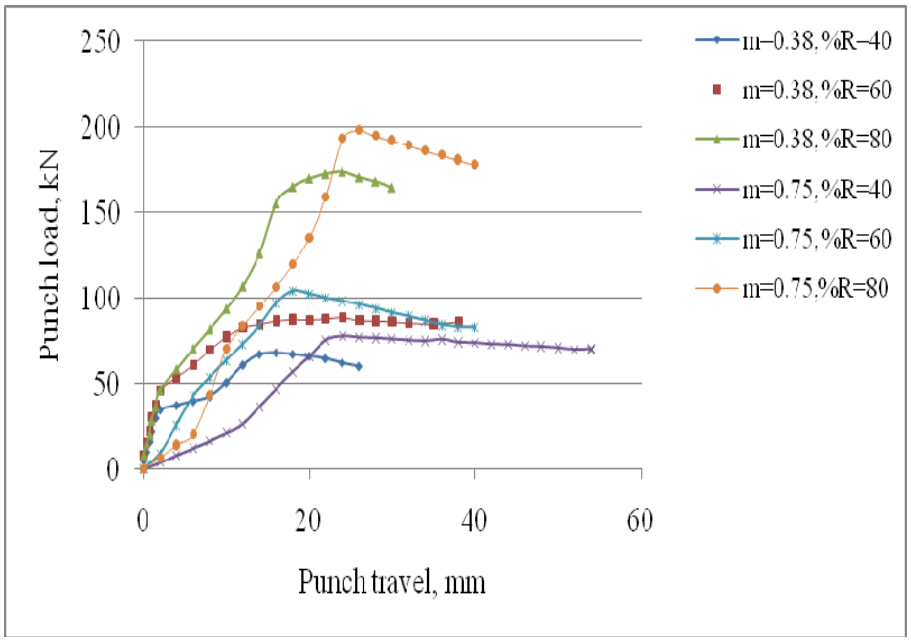

Fig. 7.28 Variation of extrusion load versus ram travel for Octagonal section

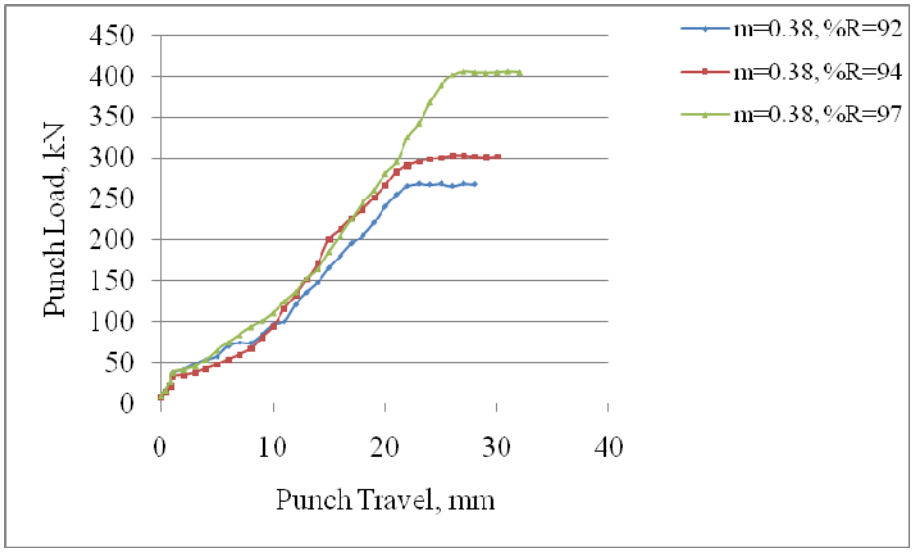

Fig. 7.29 Variation of extrusion load versus ram travel for isosceles Triangular section

Table 7.3 Comparison of experimental and computed results for rhomboidal

Section	Condition	Reduction (%)	ε (Eq. (26))	Punch Load(N)	Pav (N/mm2)	σ_0 (N/mm2)	Pav/ σ0		Error (%)
							Exp.	Comp.	
Rhombus	Wet (m=0.38)	60	2.1744	110,000	155.617	52.75	2.95008	3.6791	19.79
		75	2.8794	160,000	226.353	52.85	4.2829	5.524	1.2411
		92	4.588	215,000	304.162	52.95	5.7443	6.237	7.89
	Dry (m=0.75)	60	2.1744	210,000	297.088	52.75	5.632	6.976	19.26
		75	2.8794	215,000	304.162	52.85	5.7551	7.123	1.3679
		92	4.588	225,000	318.309	52.95	6.0115	7.123	15.6

section

Area of the round extrusion chamber of 30mm diameter = 706.86 sq. mm

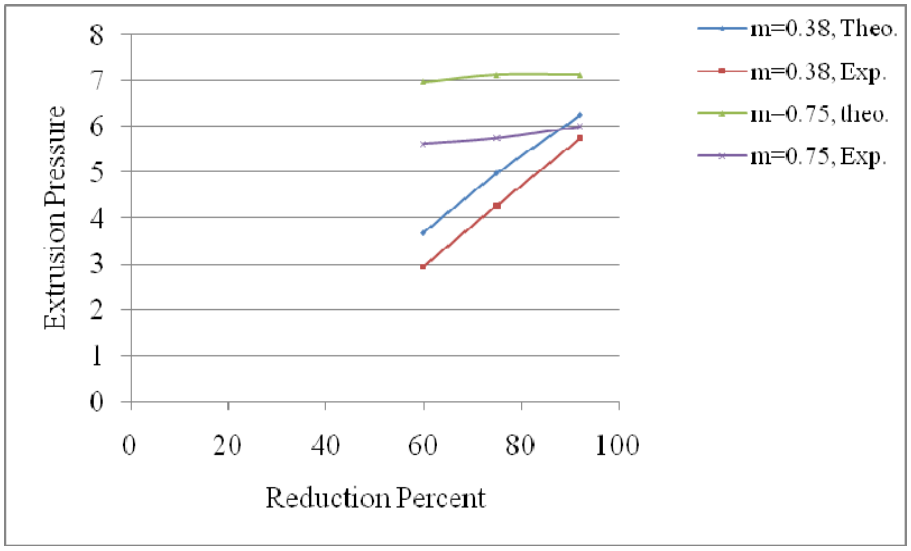

Fig. 7.30 Comparison of Theoretical and Experimental results of Rhomboidal Section

Table 7.4 Comparison of experimental and computed results for pentagonal section

Section	Condition	Reduction (%)	έ (Eq. (6.1))	Punch Load(N)	P_{av} (N/mm2)	σ_0 (N/mm2)	Pav/ σ0		Error (%)
							Exp.	Comp.	
Pentagon	Wet (m=0.38)	40	1.5662	62,000	87.7118	51.5	1.70314	1.9675	13.43
		60	2.17443	78,000	110.347	52.5	2.10184	2.5641	18.02
		80	3.21415	158,000	223.523	52.65	4.24545	4.6852	9.38
	Dry (m=0.75)	40	1.5662	158,000	223.523	51.5	4.34025	4.9123	11.645
		60	2.17443	175,000	247.573	52.5	4.71567	5.123	7.951
		80	3.21415	185,000	261.721	52.65	4.97095	5.431	8.471

Area of the round extrusion chamber of 30mm diameter = 706.86 sq. mm

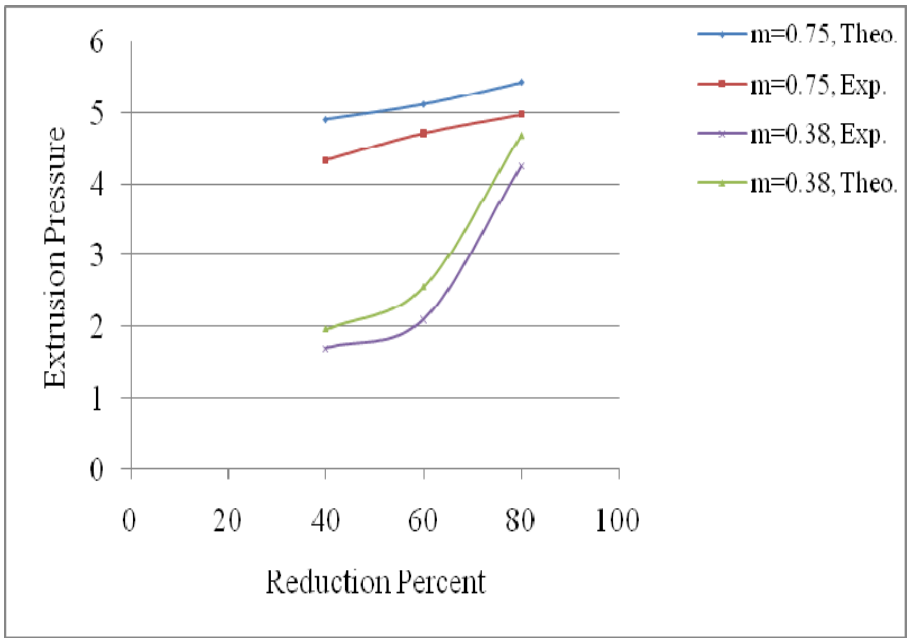

Fig. 7.31 Comparison of Theoretical and Experimental results of Pentagonal Section

Table 7.5 Comparison of experimental and computed results for octagonal section

Section	Condition	Reduction (%)	έ (Eq. (6.1))	Punch Load(N)	Pav (N/mm2)	σ0 (N/mm2)	Pav/ σ0		Error (%)
							Exp.	Comp.	
Octagon	Wet (m=0.38)	40	1.5662	65,000	91.955	51.5	1.7855	2.023	11.74
		60	2.17443	86,000	121.6648	52.5	2.3174	2.769	16.3
		80	3.21415	170,000	240.5	52.65	4.5679	5.125	10.87
	Dry (m=0.75)	40	1.5662	75,000	106.1	51.5	2.06019	2.567	19.74
		60	2.17443	95,000	134.397	52.5	2.5599	2.986	14.26
		80	3.21415	190,000	268.794	52.65	5.10529	6.235	18.11

Area of the round extrusion chamber of 30 mm diameter = 706.86 sq. mm

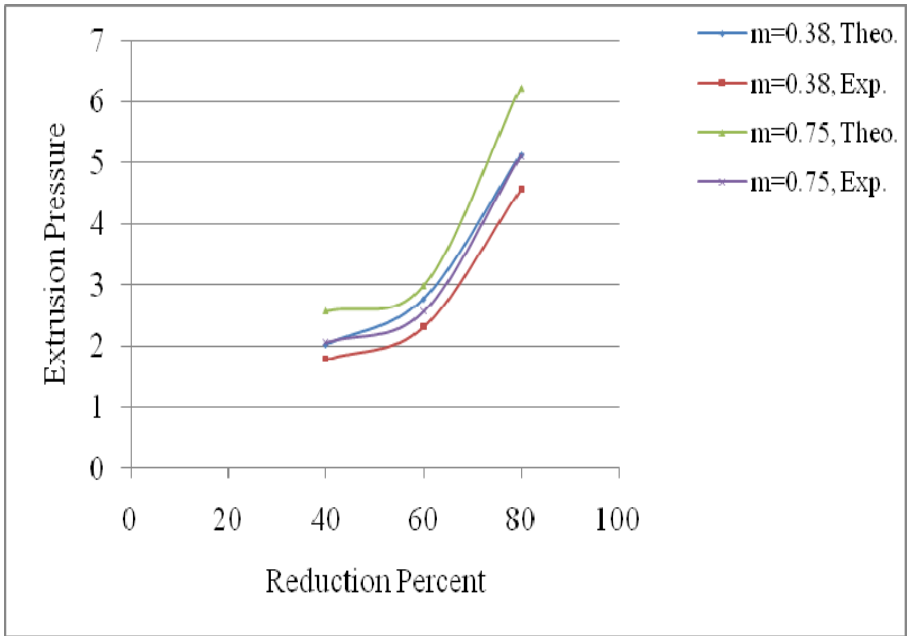

Fig. 7.32 Comparison of Theoretical and Experimental results of octagonal Section

Table-7.6 Comparison of experimental and computed results for isosceles triangular section

Section	Condition	Reduction (%)	ε (Eq. (26))	Punch Load(N)	Pav (N/mm2)	σ_0 (N/mm2)	Pav/ σ0		Error (%)
							Exp.	Comp.	
Isoscales Triangle	Wet (m=0.38)	92	4.588	269,000	380.55	52.75	7.214	8.9746	19.61
		94	5.019	301,000	425.83	52.95	8.0421	10.393	22.62
		97	6.05983	405,000	572.95	53	10.81	14.521	25.55

Area of the round extrusion chamber of 30 mm diameter = 706.86 sq. mm

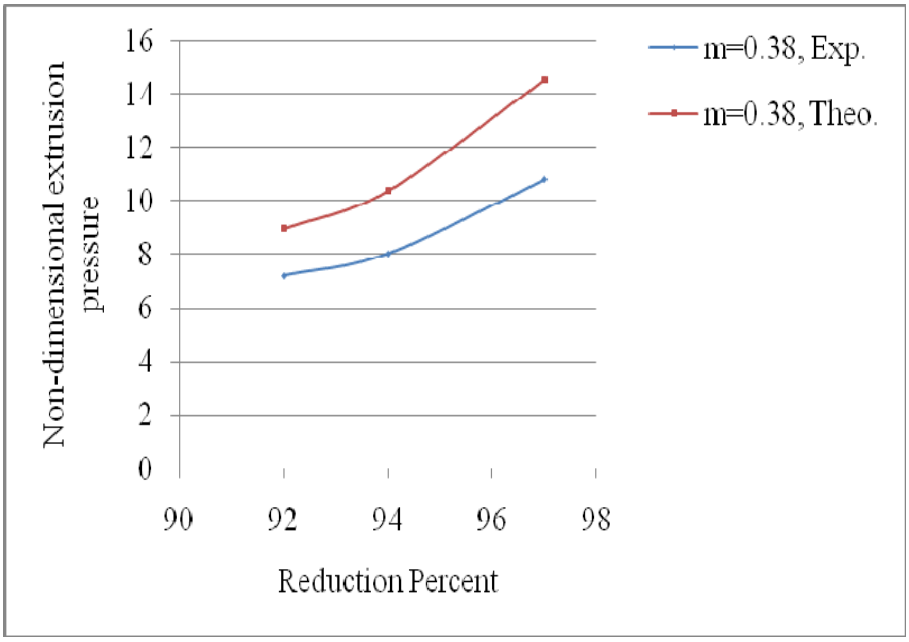

Fig. 7.33 Comparison of Theoretical and Experimental extrusion pressure s of isosceles triangular Section

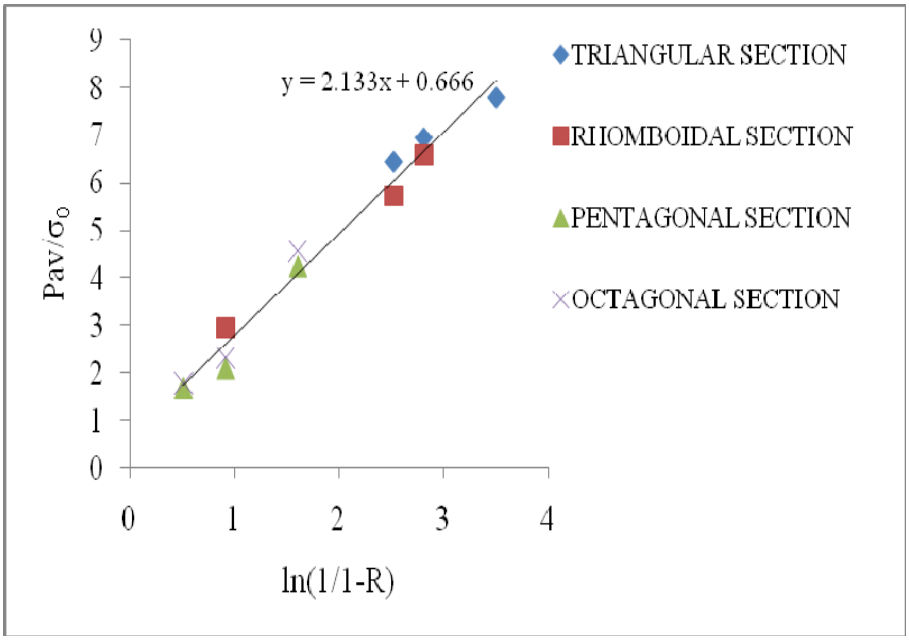

Fig. 7.34 Variation of P_{av}/σ_0 with Ln (1/1-R)

7.9 Experimental Verification of Extrusion of Square Section from Square Billet through Cosine, Polynomial and Bezier Shaped Curved Die

In this investigation, some experimental studies are carried out for comparison with theoretical analysis for extrusion of square section from square billet using universal testing machine and instron.

7.9.1 The Test Rig

An extrusion test rig is designed and fabricated on thumb rule basis for the said purpose and all extrusions are carried out using square billets. The following sections deal with brief description of the apparatus and the experimental procedure with results. The experimental set-up for the present investigation was shown in Fig.7.36. The apparatus mainly consists of four parts, namely, the container having a square extrusion chamber, the extruding punch, the die holder, and the supporting block for the die holder. Besides the main parts, the curve dies and the lead specimens are also the requirements for the experiment. Basically all parts are made up of low and medium carbon steel. The photographs of the container, die holder, punch and the

die block with polynomial shaped die profile along with detailed dimension are shown in Fig. 7.37.

The apparatus consists of four parts, namely, i) the container having a square extrusion chamber, ii) the extruding punch, iii) the die holder, and iv) the supporting block for die holder. The container (160mmΦ, 200 mm long) having the extrusion chamber (40 mm x 40mm x200mm) is made from a round block (220mm long, 180mm Φ) of forged medium carbon steel. This is accomplished first by drilling and then by slotting (with a tolerance of ± 0.05mm). A notch (15mm x 40mm) is made at the top surface of the block to accommodate the die which is kept inside the die holder. The die holder is made from medium carbon steel round block by turning and shaping. A recess (40mmx40mm) is provided in the die holder for good positioning of the dies which are of simple push fit type. During the extrusion process very high normal pressure is exerted on the chamber wall resulting in an increase in its cross-sectional area. In the present set up this is avoided by making the container a single block. The extrusion chamber and the die holder are fastened together rigidly by two hexagonal headed fine bolts (25mm Φ).

The extrusion punch (40mm x 40mm x230mm) is made of alloy steel. A plate (180mm Φ, 20mm thick) is welded at the top end. The top face of the square plate and the bottom face of the punch are made parallel. A supporting plate (180mm Φ, 25mm thick) is provided to upload both extrusion chamber and die holder. The photographs of the individual parts are shown in Figs. 7.38-7.40 including detail dimensions are in (Table 7.7)

Fig. 7.35 The experimental set-up mounted on INSTRON to extrude square section

Fig. 7.36 Container, Die holder, Punch and Die block

Table 7.7 Detail dimensions of individual component of the experimental set-up for similar geometry section

SI. NO.	Name of parts	Dimension of parts, mm		Dimension of original stocks, mm		Materials	Processes used
		Cross section	Length	Cross section	Length		
1	Container with square extrusion chamber	140 ϕ 40x40	200 200	160 ϕ	220	Forged medium carbon steel	Turning, drilling, slotting & facing
2	Punch	40x40	200	45x45	220	Alloy steel	Shaping & milling
3	Punch plate	160 ϕ	20	180 ϕ	30	Medium carbon steel	Turning, milling & welding
4	Die holder with a recess	140 ϕ	50	160 ϕ	60	Alloy steel	Turning, drilling & shaping
5	Supporting plate	140 ϕ	20	160 ϕ	30	Medium carbon steel	Turning, drilling & facing
6	Specimen	40x40	40~60	43x43	200	Lead	casting, milling & facing
7	Dies with opening	40x40	10~25	60x60	50	Alloy steel	CNC Milling and filing
8	Bolts	Two numbers 12mm bolt	110	–	–	Medium carbon steel	As available in the market

Fig.7.37 (a) Container with square extrusion chamber

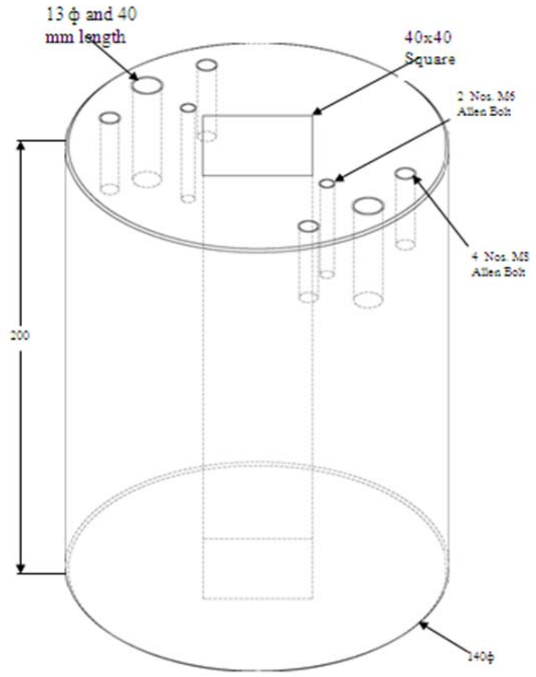

Fig.7.37 (b) Dimension of the Container with extrusion chamber

Fig. 7.38 (a) Die holder

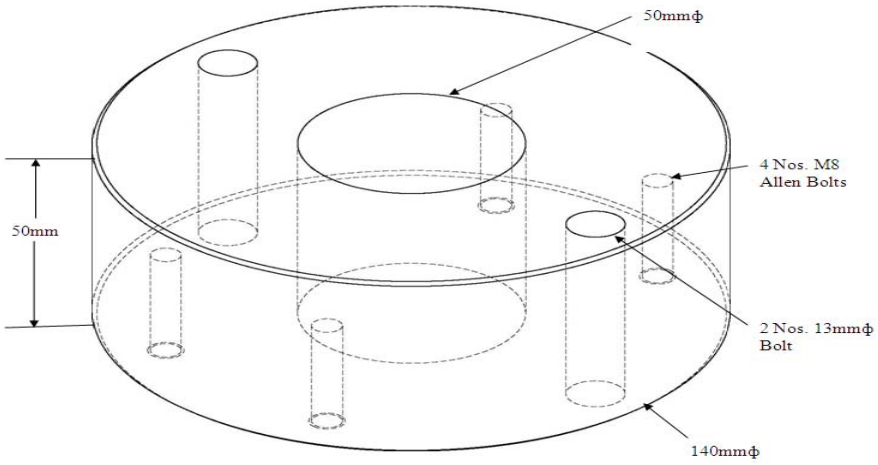

Fig. 7.38 (b) Dimension of Die holder

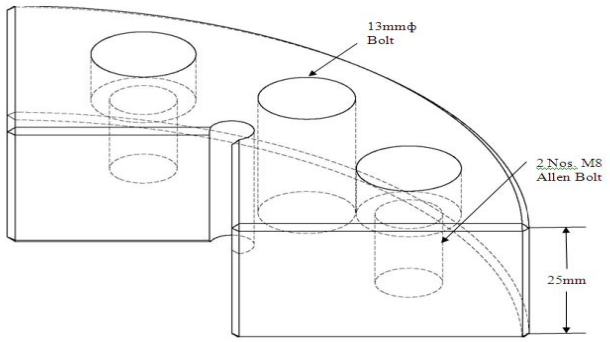

Fig.7.38 (c) Dimension of the projection of extrusion chamber

Fig. 7.39 (a) Punch

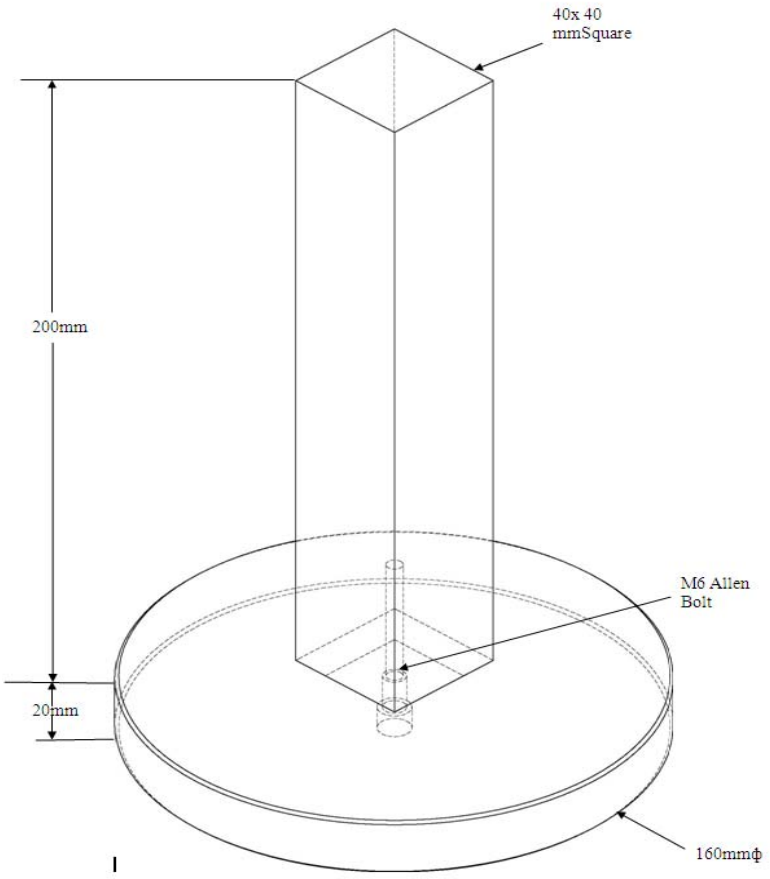

Fig. 7.39 (b) Dimension of the Punch

7.9.2 Dies

These dies are produced by CNC milling from die steel (flat, 20mm thick and 60mm width). The orifices are located in such a way that the respective centers of gravity lie on the billet axis. Experiments are conducted with three sets of dies for polynomial, Bezier and cosine shaped curved dies. The dimensions of the orifices and the photographs of these die sets are shown in Figs. 7.41-7.43.

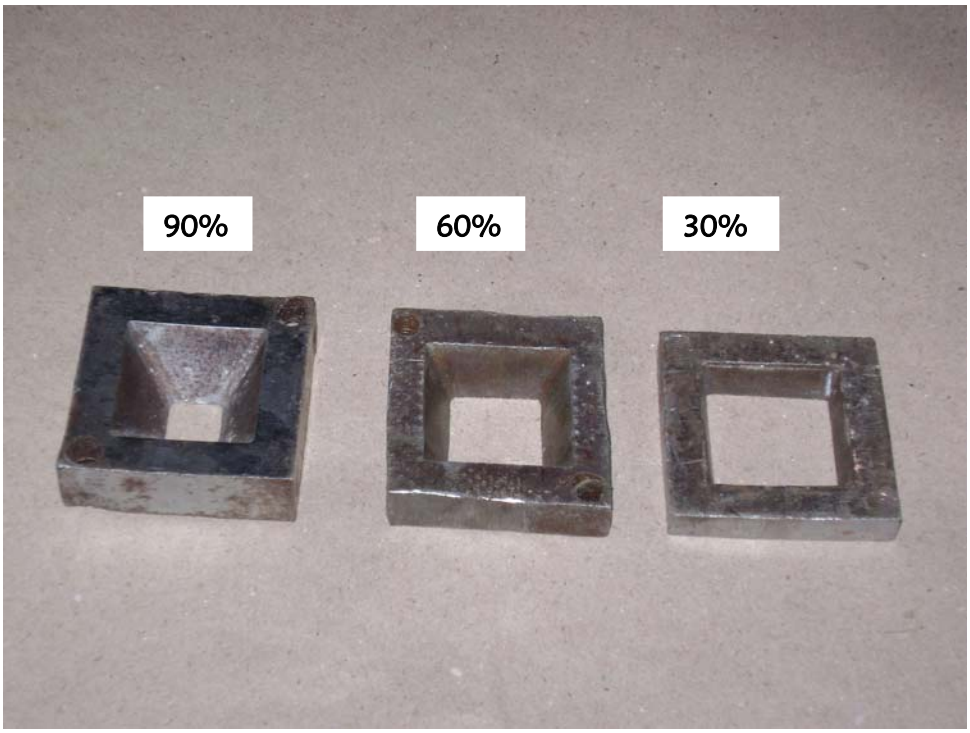

Fig. 7.40 (a) The extrusion dies of different reduction for polynomial die

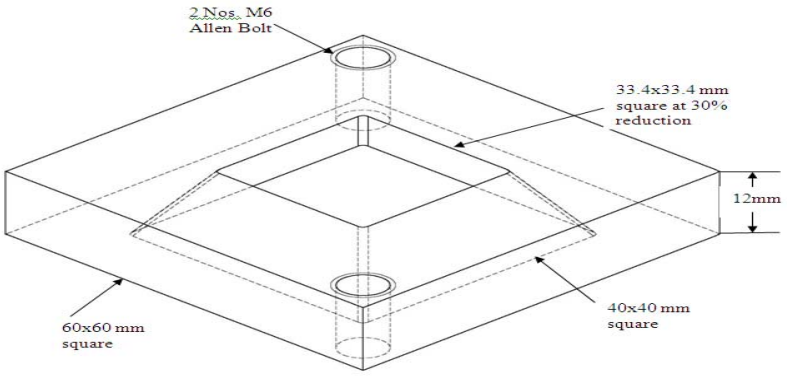

Fig. 7.40 (b) The dimension of extrusion die of 30% reduction of polynomial die.

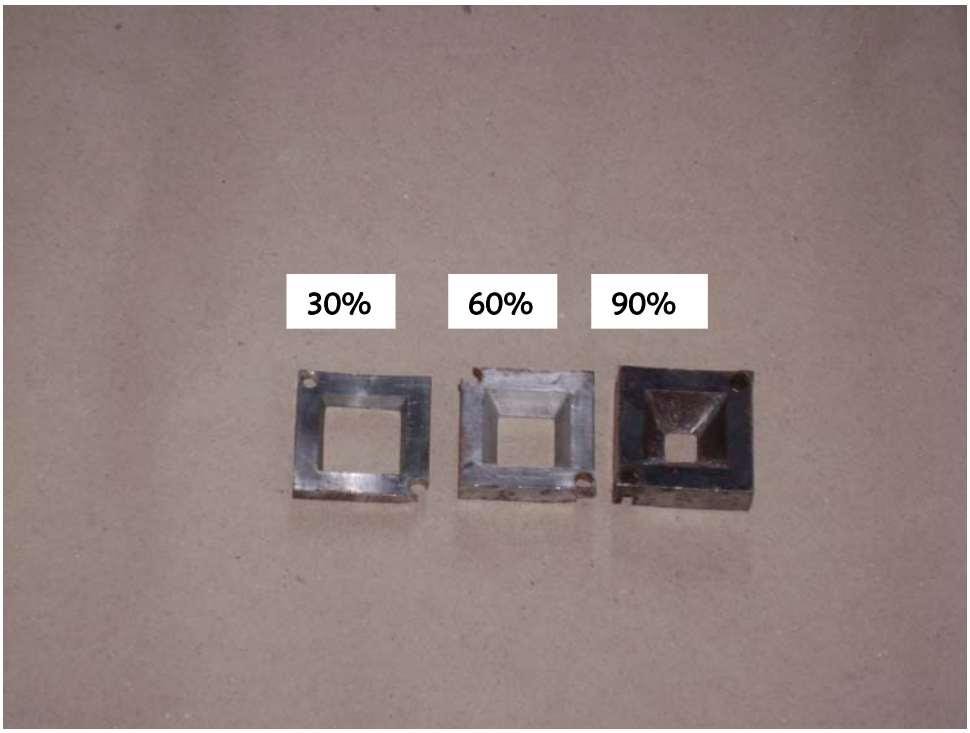

Fig. 7.41 (a) The extrusion dies of different reduction for Bezier die

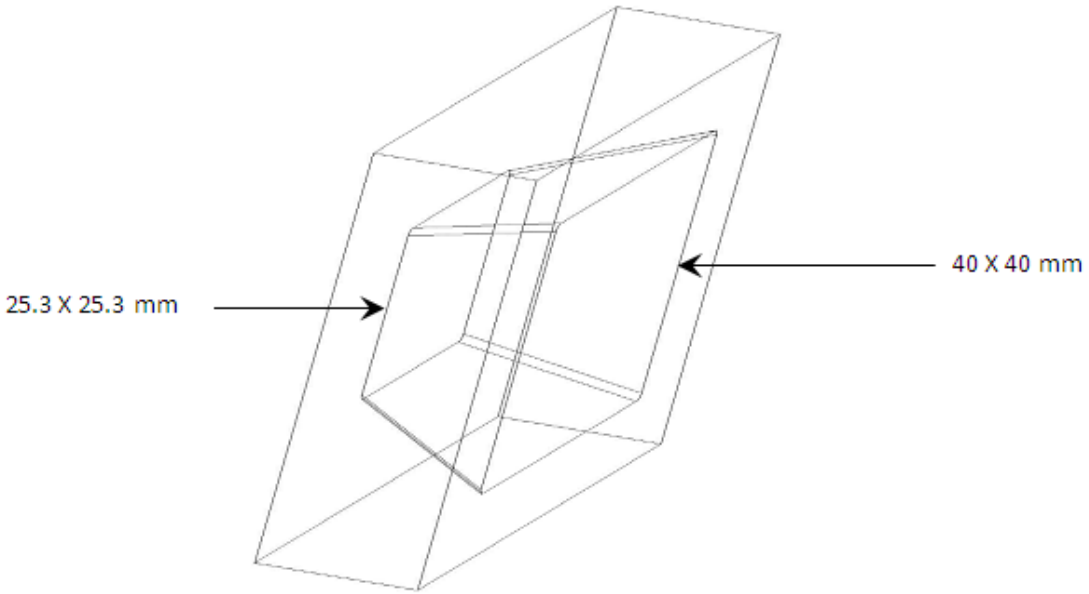

Fig. 7.41 (b) The extrusion die of 60% reduction for Bezier die

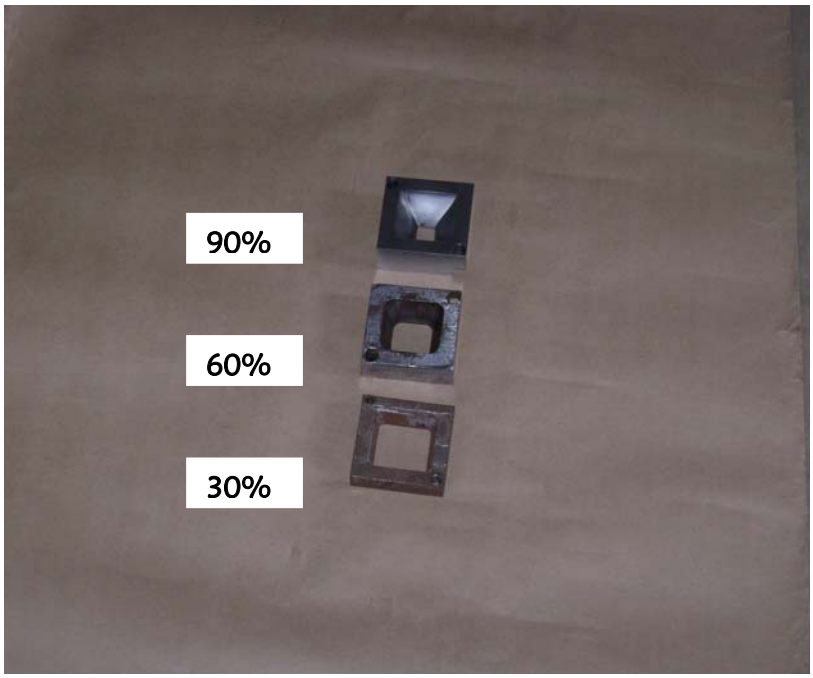

Fig. 7.42 (a) The extrusion die sof different reduction for cosine die

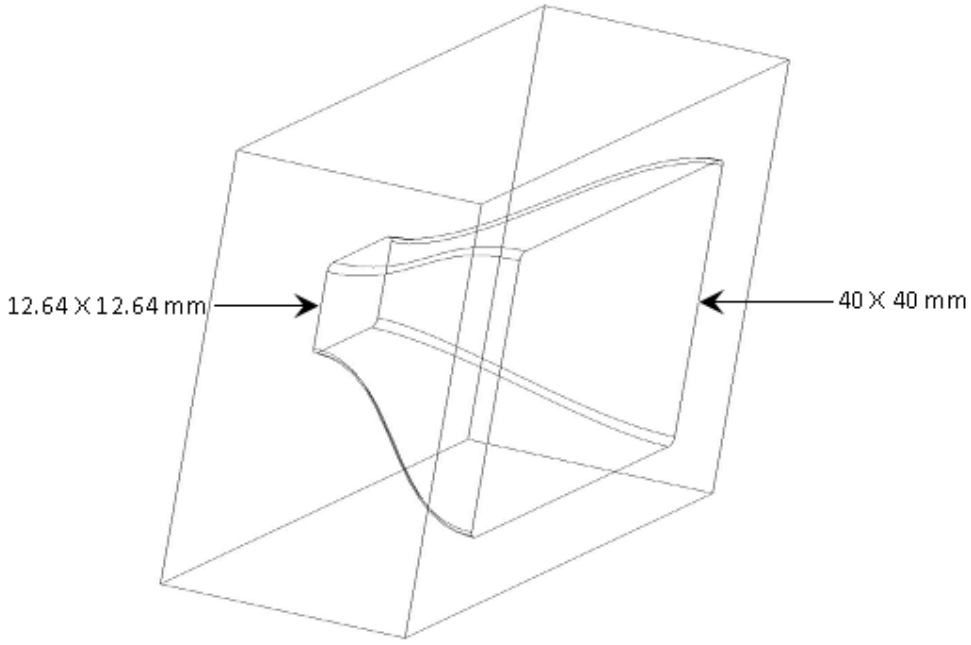

Fig. 7.42 (b) The dimension of extrusion die of 90% reduction of cosine die.

7.9.3 Specimens

All the experiments are conducted with commercially available tellurium lead (Composition: Pb-80%, Ca-10% and SiO_2-15%) as work material. Square specimens of lead for the above purpose are prepared from commercially available block by open green sand mould casting and milling using kerosene as cutting fluid.

Specimens of three different lengths were used during the tests which are shown in Fig. 7.44 for reductions between thirty and ninety percent, the specimen length was approximately 40 mm to 60 mm. These lengths were so chosen that the maximum length of the extruded product did not exceed the clearance between the die mouth and the upper crosshead of the universal testing machine. These lengths were decided after some initial trial runs using the square dies.

Fig. 7.43 Lead specimen of different reductions

7.9.4 Experimental Procedures

Before starting the tests, the die sets, the die holder and the inside faces of the extrusion chamber were cleaned with kerosene and then carbon tetrachloride. The mathematically contoured die block was then push-fitted into the die holder and the assembly was secured by screwing the two bolts with the container of the die set. The full assembly was then placed on the lower table of the universal testing machine / (Instron) as shown in Fig.7.36. For carrying out an extrusion test, the die block was kept in dry condition and the specimen was placed inside the extrusion chamber. The punch was then inserted into its position. After centering the apparatus on the machine lower table, the extrusion process continued. Punch load was recorded at regular time interval of the punch travel by using personal computer. The application of load was continued until it started to rise again after reaching the steady state and the test was terminated.

Experiments were conducted for three different reductions for wet and dry frictions. The photographs of the extruded products along with the respective dies are shown in Fig.7.45-7.47.

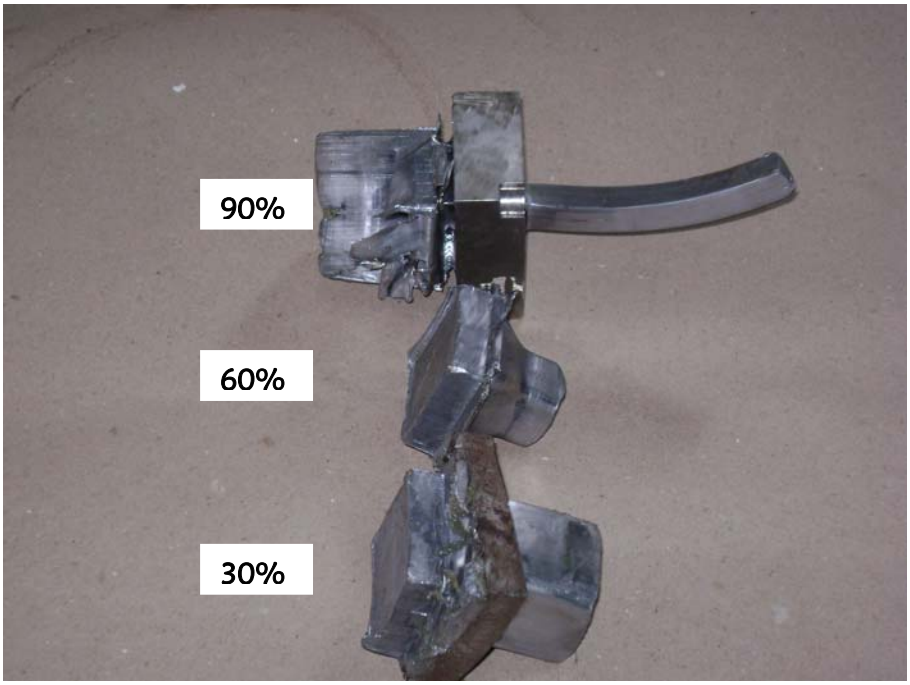

Fig. 7.44 Extruded products of cosine die of different reduction.

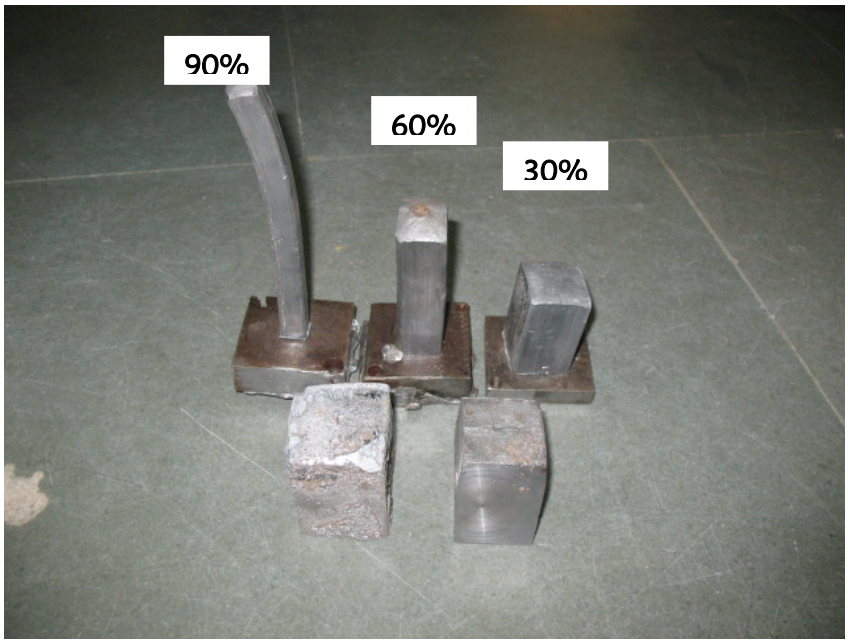

Fig. 7.45 Extruded products of polynomial die of different reduction.

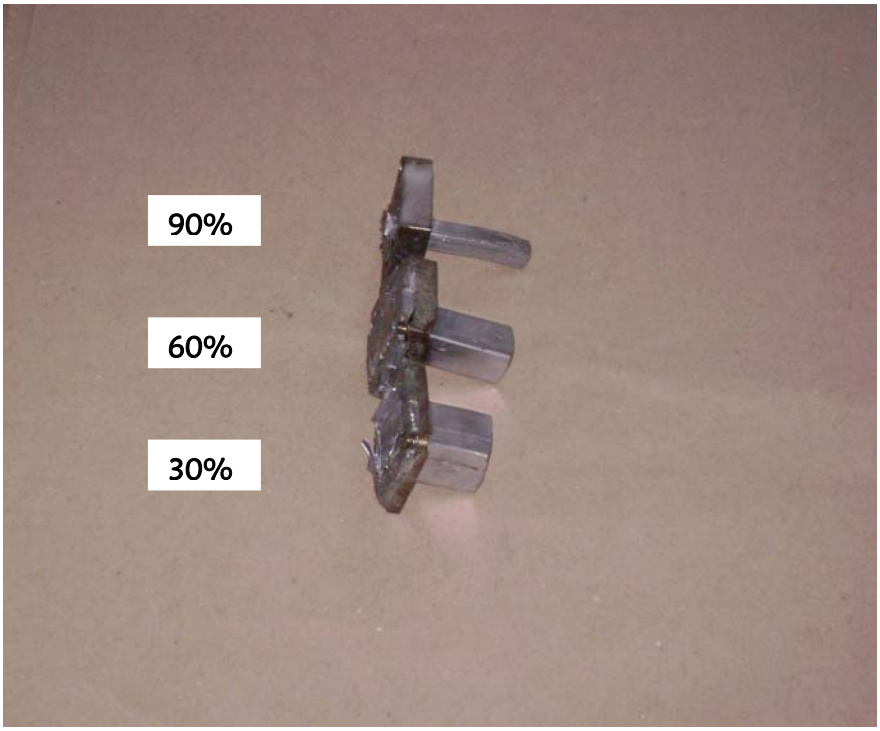

Fig. 7.46 Extruded products of Bezier die of different reduction.

7.9.5 Experimental Analysis (Steady state extrusion pressure)

The comparison of punch loads with punch travel for the cosine, polynomial and Bezier profile die with FEA simulation are shown in Fig. 7.48 to Fig. 7.52 respectively.

The travel of punch load versus punch travel is similar as described in section 7.8.

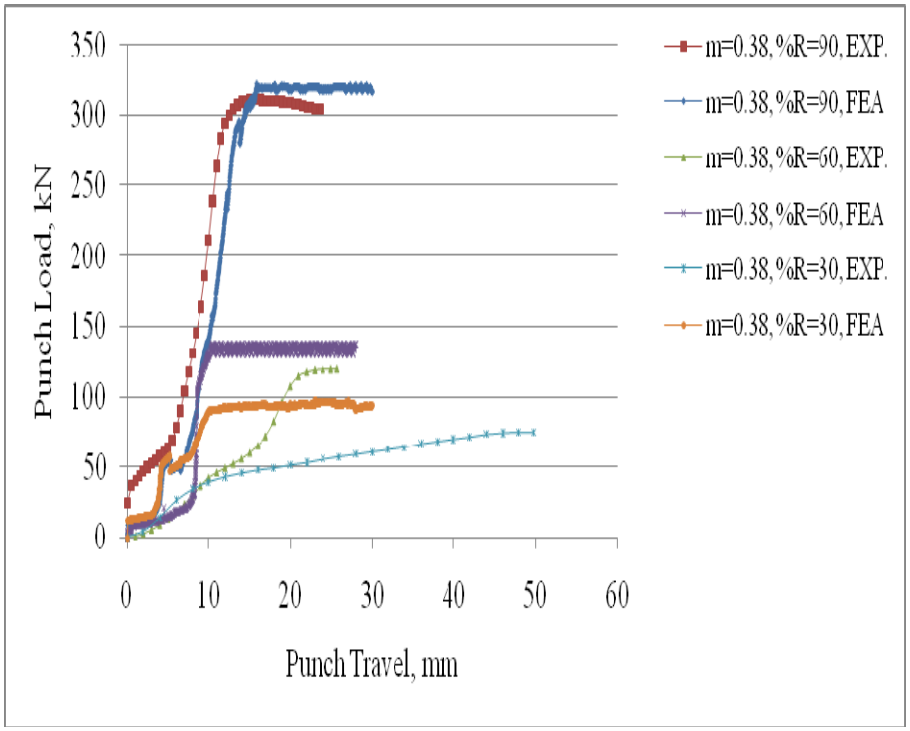

Fig. 7.47 Punch load vs. Punch travel for cosine profile in wet condition

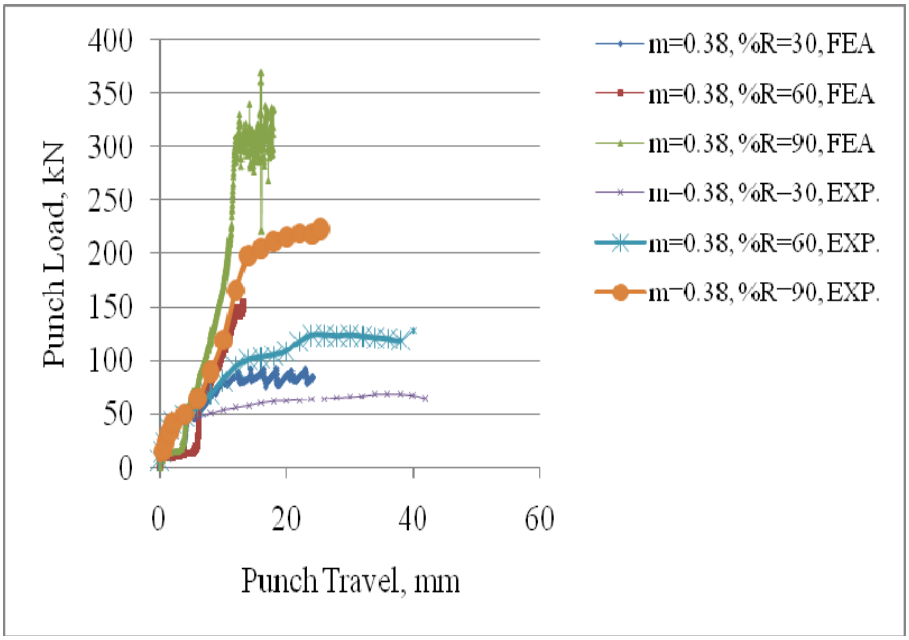

Fig. 7.48 Punch load vs. Punch travel for polynomial profile in wet condition

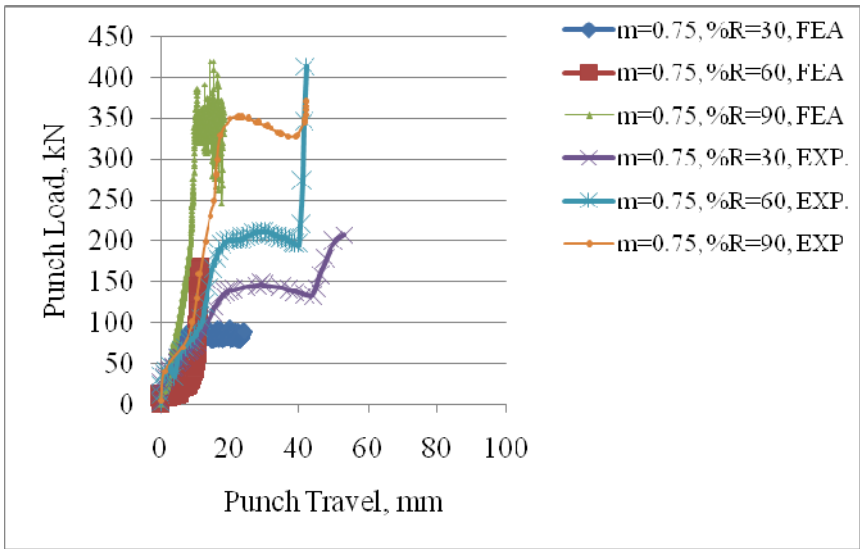

Fig. 7.49 Punch load vs. Punch travel for polynomial profile in dry condition

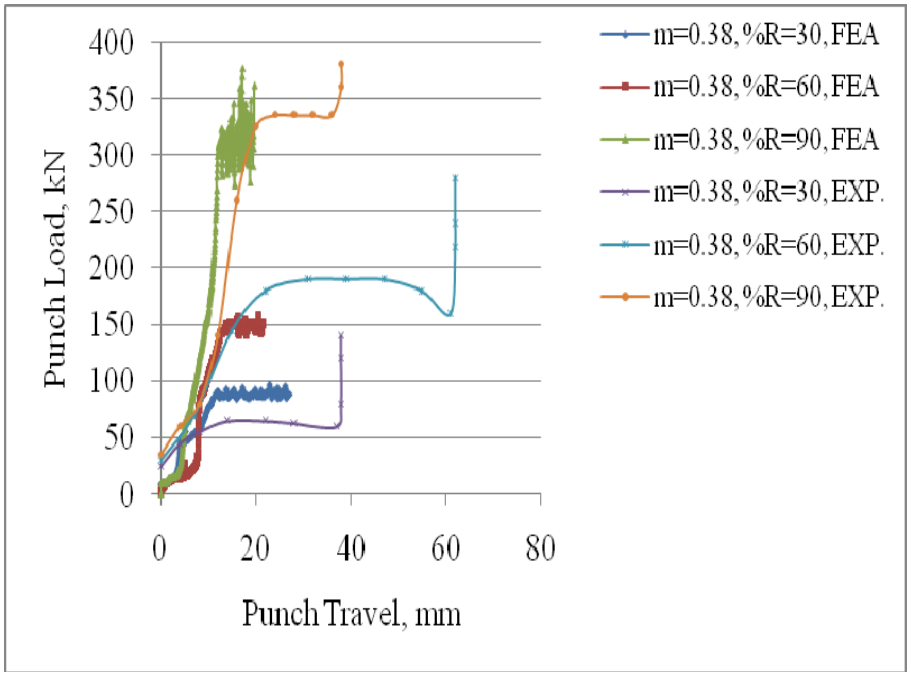

Fig. 7.50 Punch load vs. Punch travel for Bezier profile in wet condition

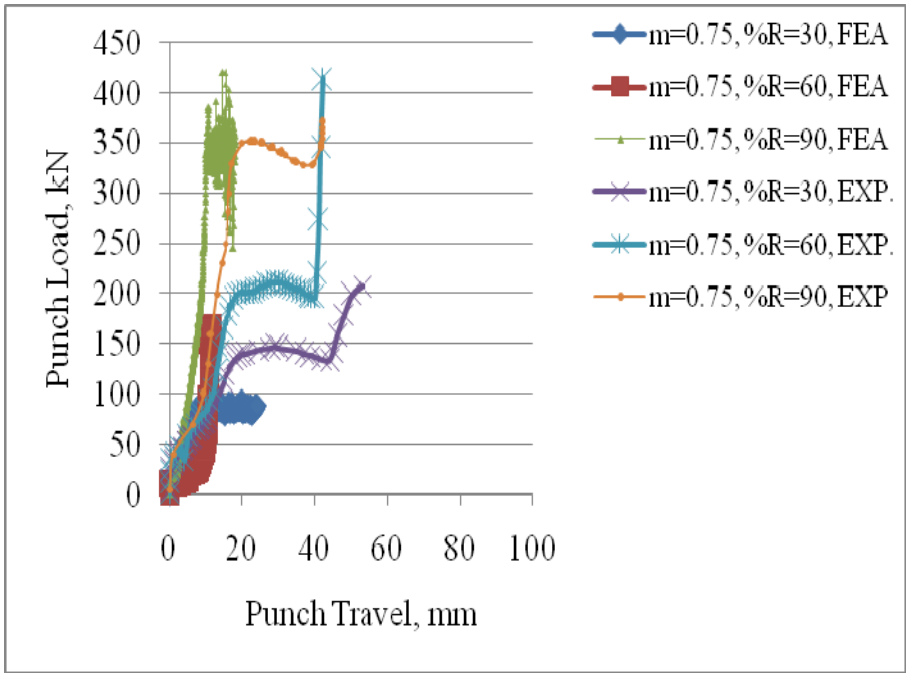

Fig. 7.51 Punch load vs. Punch travel for Bezier profile in dry condition

The wet friction condition at the die-billet interface corresponds to constant friction factor m=0.38, which was determined by ring compression test experimentally. The calculated non-dimensional extrusion pressure from FEM for cosine, polynomial and Bezier profile are compared with the experimental results as shown in Fig. 7.53 to Fig. 7.55 respectively and it is found that there is a good agreement among the results. The average flow stress as given in Table 7.8 is determined for different reductions in the similar manner referring to equation (7.1) as in section 7.6.

The computed results for different area reductions are also shown in Table 7.8 to Table7.10. It is evident that extrusion load increases with increase in reduction. Referring to Fig.7.53 to Fig.7.55, it is obvious that the non-dimensional extrusion pressure obtained from experimental investigation agrees with the theoretical modeling.

Table 7.8 Comparison of experimental and FEA extrusion pressure for Cosine die profile

Reduction (%)	Condition	ε (Eq.(7.1))	Punch Load (N)	Pav (N/mm^2)	σ0 (N/mm^2)	Pav/σ0		Error (%)
						Exp.	FEA	
30	Wet (m=0.38)	1.335	70,000	43.75	52.5	0.8333	0.9523	12.5
60		2.1744	125,000	78.125	52.75	1.4881	1.666	10.67
90		4.2538	310,000	193.75	52.85	3.6904	3.869	4.616

Area of the extrusion chamber = 1600 sq. mm

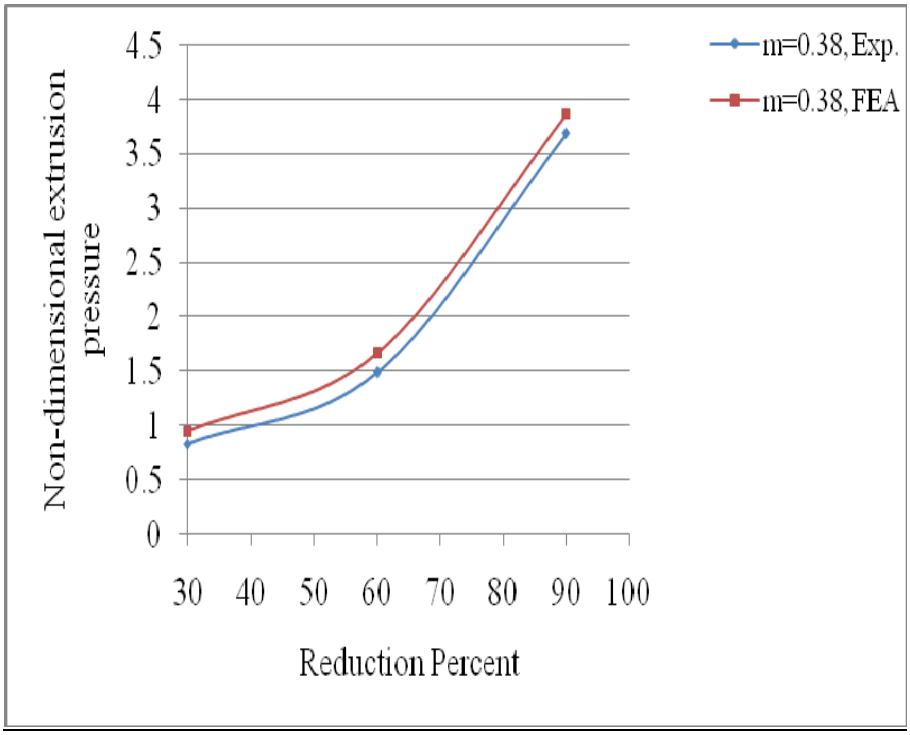

Fig. 7.52 Comparison of Theoretical and Experimental results for cosine profile.

Table 7.9 Comparison of experimental and computed extrusion pressure for Polynomial die profile

Section	Condition	Reduction (%)	ε (Eq. (7.1))	Punch Load(N)	P_{av} (N/mm^2)	σ_0 (N/mm^2)	P_{av}/σ_0		
							EXP.	FEA	COMP.
Polynomial	Wet (m=0.38)	30	1.335	75,000	46.87	52.5	0.8927	1.0119	0.918
		60	2.1744	160,000	100	52.75	1.89573	2.01421	1.867
		90	4.2538	330,000	206.25	52.85	3.90255	4.02081	4.039
Polynomial	Dry (m=0.75)	30	1.335	130,000	81.25	52.5	1.0476	1.13095	1.169
		60	2.1744	195,000	121.87	52.75	2.31033	2.36966	2.383
		90	4.2538	370,000	231.25	52.85	4.3756	4.55298	5.179

Area of the extrusion chamber = 16.00 sq. cm =1600 sq. mm

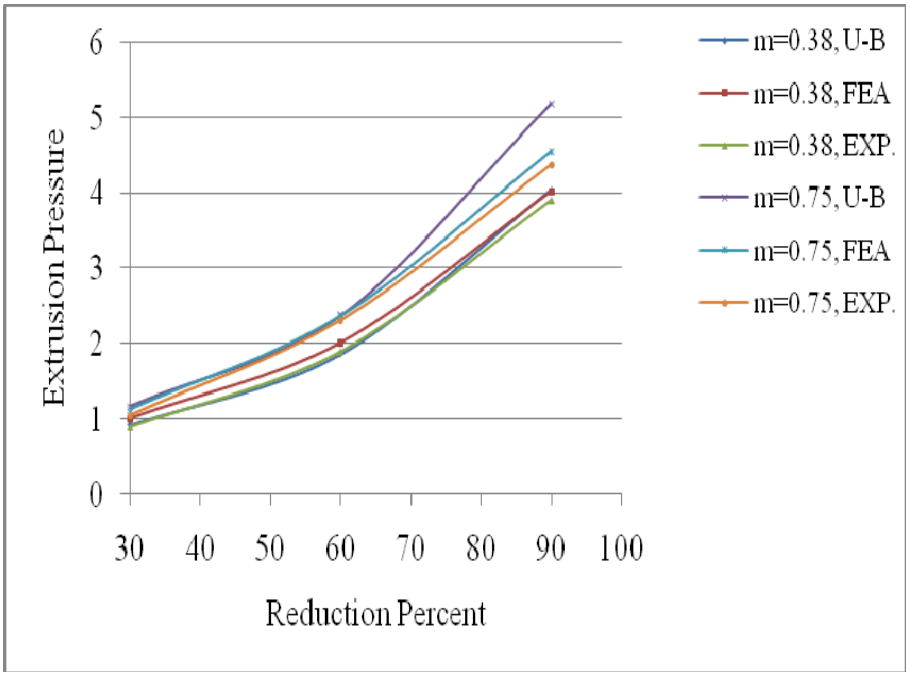

Fig. 7.53 Comparison of Theoretical and Experimental results for polynomial profile

Table 7.10 Comparison of experimental and computed extrusion pressure for Bezier die profile

Section	Condition	Reduction (%)	έ (Eq. (7.1))	Punch Load(N)	P_{av} (N/mm^2)	σ_0 (N/mm^2)	P_{av}/σ_0		
							EXP.	FEA	COMP.
Bezier	Wet (m=0.38)	30	1.335	75,000	46.87	52.5	0.8927	1.071428	0.918
		60	2.1744	160,000	100	52.75	1.89573	2.132701	1.867
		90	4.2538	330,000	206.25	52.85	3.90255	4.02081	4.039
Bezier	Dry (m=0.75)	30	1.335	130,000	81.25	52.5	1.0476	1.1848	1.169
		60	2.1744	195,000	121.87	52.75	2.31033	2.369668	2.383
		90	4.2538	370,000	231.25	52.85	4.3756	4.49385	5.179

Area of the extrusion chamber = 16.00 sq. cm =1600 sq. mm

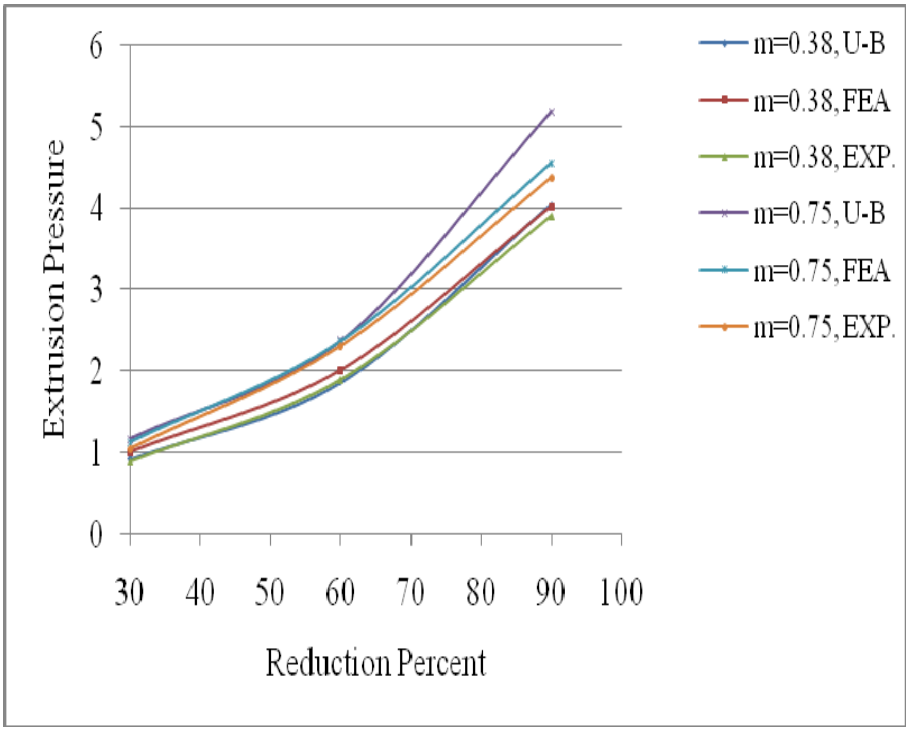

Fig. 7.54 Comparison of Theoretical and Experimental results for Bezier profile.

7.10 Experimental investigation of Extrusion of Triangular (Equilateral) and Square Sections from round Billet using linear and non-linear converging dies.

7.10.1 Experimental Investigation

The test rig with proper dimensions has been designed and manufactured as described earlier section 7.2 of this chapter as per section 7.9.2.

7.10.2 Dies

The extrusion dies of dissimilar geometry are made of two split halves for easy removal of the product after each extrusion cycle. These dies are produced by wire EDM machine from low carbon steel (40 mm height). The orifices are located in such a way that the respective centers of gravity lie on the billet axis. Experiments

are conducted with triangular and square dies, which are shown in Fig. 7.56 and Fig. 7.57 respectively.

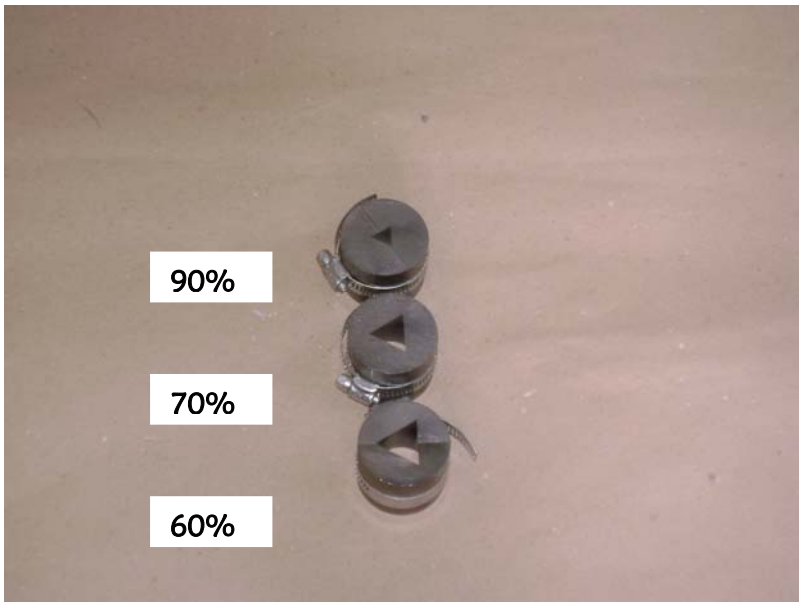

Fig. 7.55(a) Split curved dies used to extrude Triangular (equilateral) section of different reductions

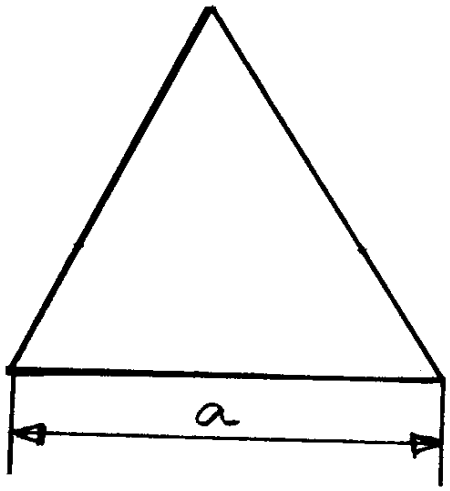

Fig. 7.55(b) The dimension of orifice of die used to extrude equilateral triangular section

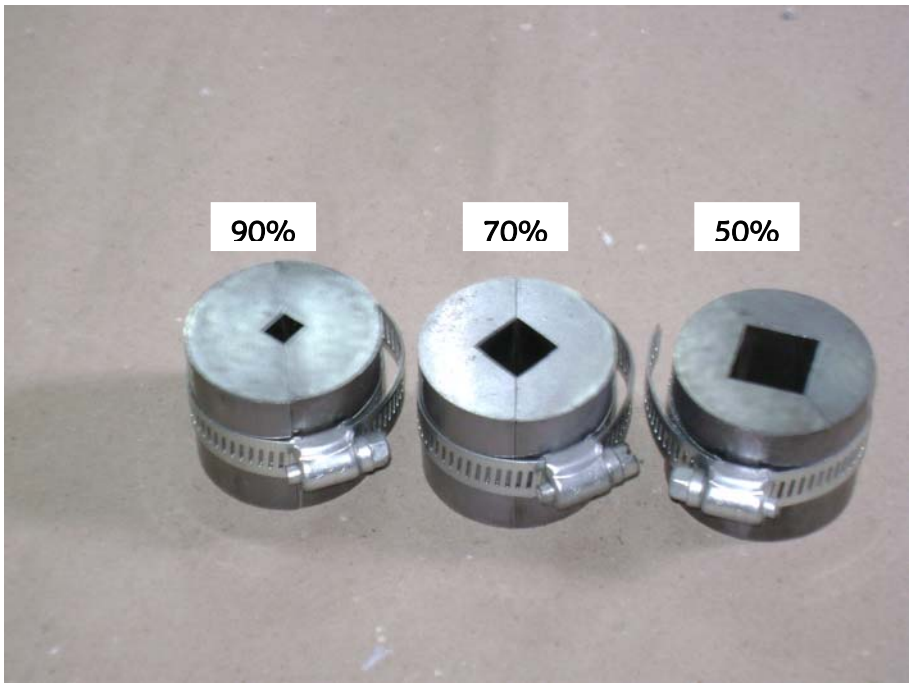

Fig. 7.56(a) Split curved dies used to extrude Square section of different reductions

a

Fig. 7.56(b) The dimension of the orifice of die used to extrude Square section

7.11 Experimental Procedure

7.11.1 Determination of extrusion pressure

The arrangement of the experimental set-up to find the non-dimensional extrusion pressure for triangular and square sections from round billets are described earlier in section 7.5 of this chapter. Experiments are conducted for extrusion of triangular and square sections from round billets in dry as well as wet conditions. The photographs of the extruded products for triangular and square sections are shown in Fig. 7.58 and Fig. 7.59 respectively for different reductions.

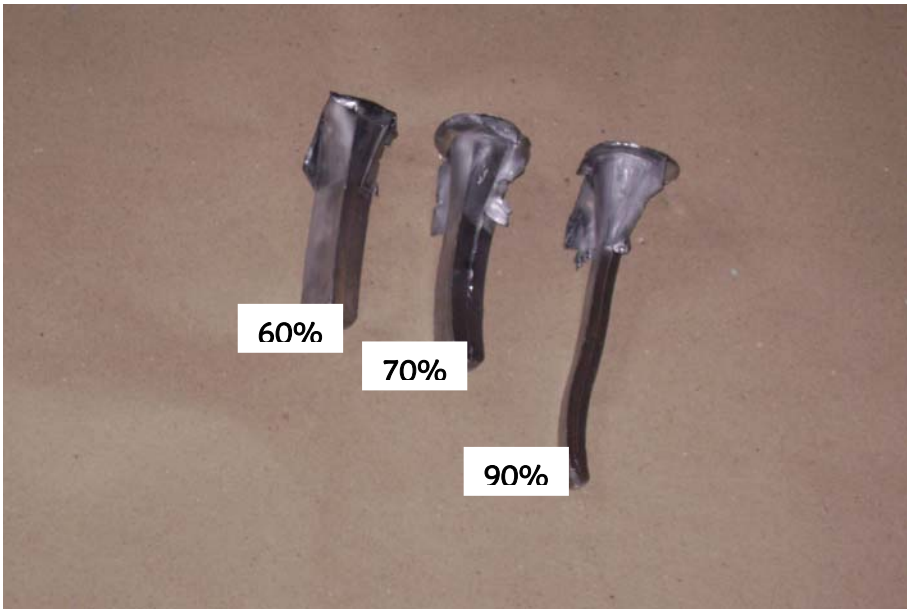

Fig. 7.57 Extruded Triangular sections of different reductions

Fig. 7.58 Extruded Square sections of different reductions

7.12 Results and discussion

7.12.1 Experimental Analysis (Steady state extrusion pressure)

The variation of punch loads with punch travel for the triangular (equilateral) and square sections are shown in Fig. 7.60 and Fig. 7.61 respectively.

The trend of punch load versus ram travel is similar as described earlier in the section 7.8. Also the comparison of punch load with punch travel between FEA and experiment for 70% reduction in wet as well as dry condition during extrusion of triangular section from round billet is shown in Fig. 7.62.

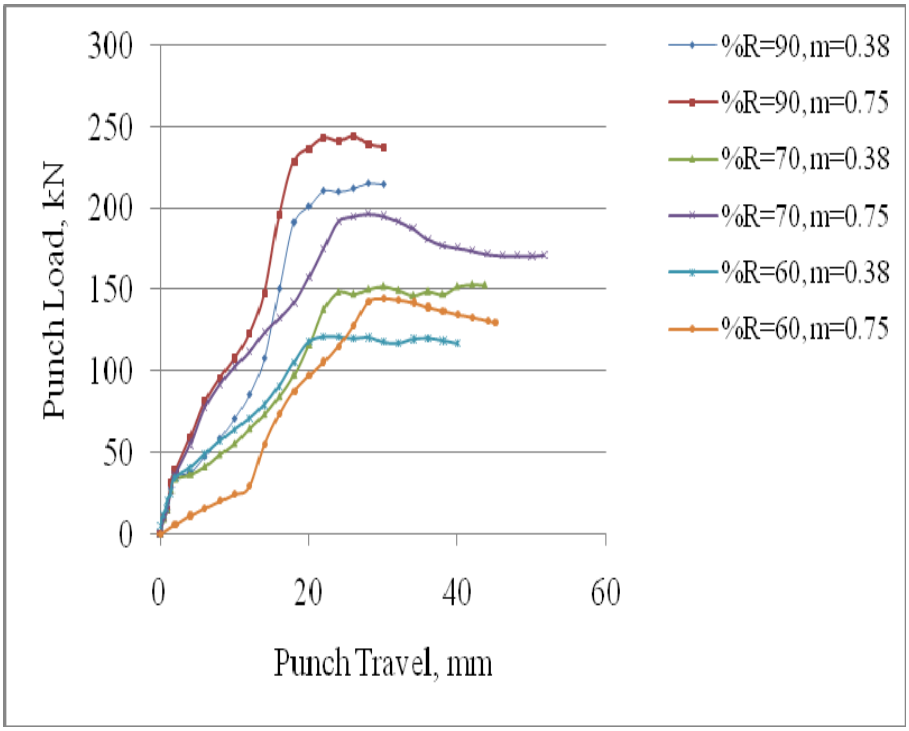

Fig. 7.59 Punch load vs. Punch travel for equilateral triangular section

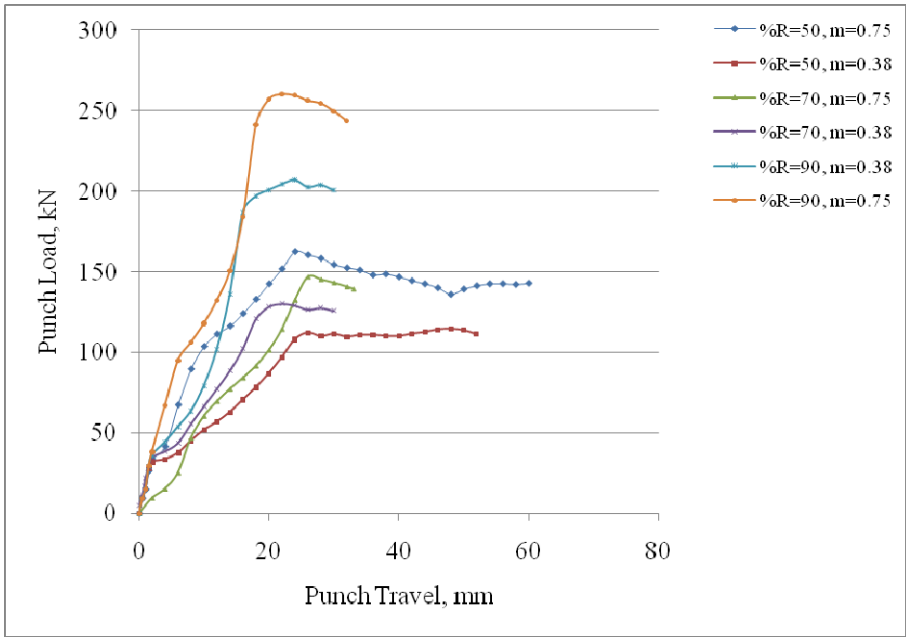

Fig. 7.60 Punch load vs. Punch travel for square section

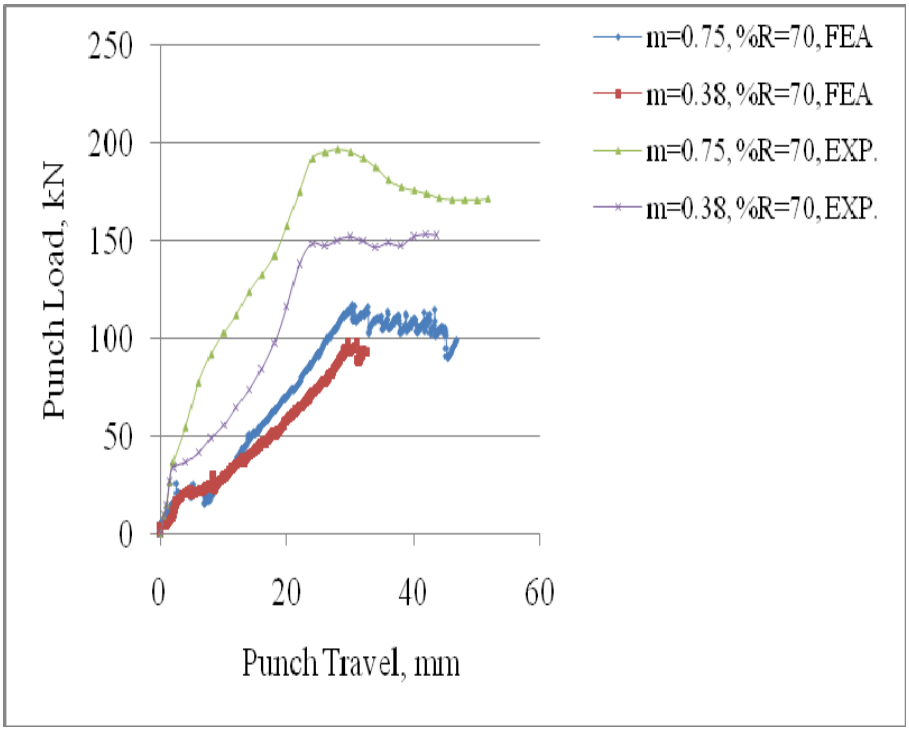

Fig. 7.61 Punch load vs. Punch travel for equilateral triangular section

A comparison is made for extrusion of triangular as well as square sections through curved and taper dies as shown in Fig. 7.63 to 7.64 respectively. The punch load or 60% reduction at dry friction (m=0.75) of taper die is compared with curved die and it is observed that the reduction in load in curved die is around 38%, where as it is around 10% in case of wet friction (m=0.38). The similar comparison is made for curved and taper dies for 70% reduction for dry and wet friction for extrusion of square section from round billet as shown in Fig. 7.64. In dry friction the decrease is around 10%, where as it is 15% for wet friction.

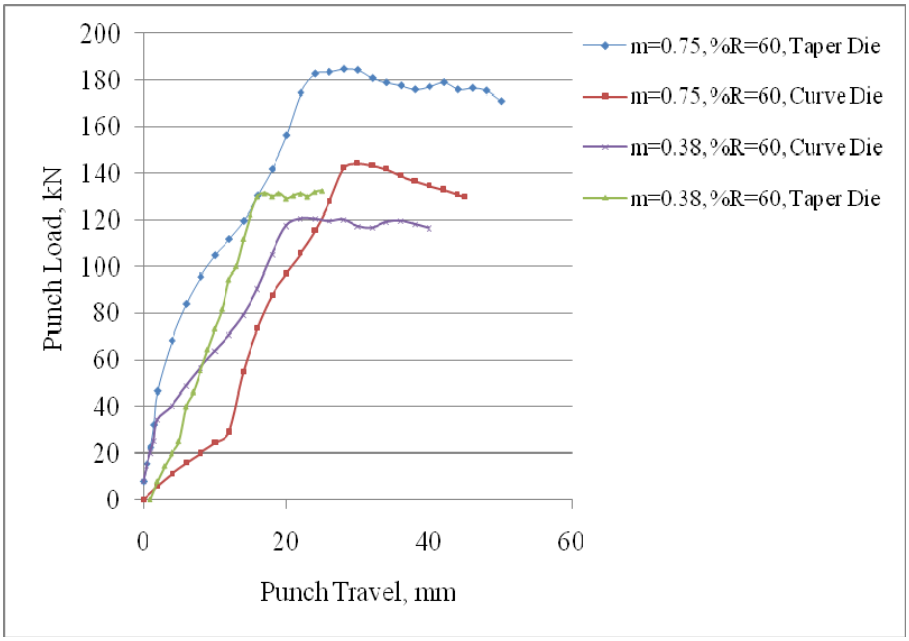

Fig. 7.62 Punch load vs. Punch travel for curve and taper die to extrude equilateral triangular section

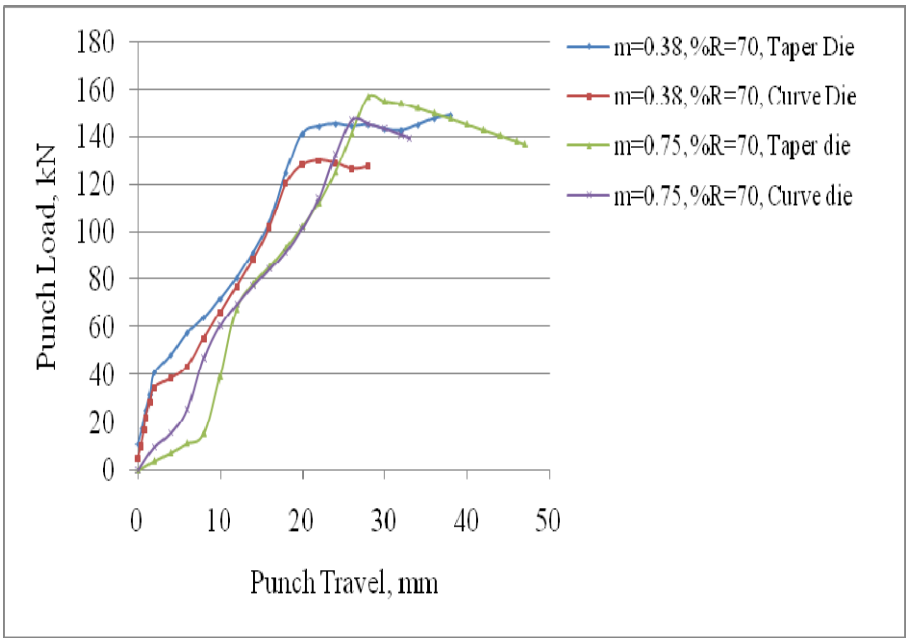

Fig. 7.63 Punch load vs. Punch travel for curve and taper die to extrude square section

7.13 The Microstructure Analysis by SEM

A sample test was carried out by examining the microstructure of the material in the process. The microstructures of the material before and after extrusion were studied using scanning electron microscope (SEM). The micro-structure of the material before deformation is shown in Fig. 7.65 and after deformation is shown in Fig. 7.66.

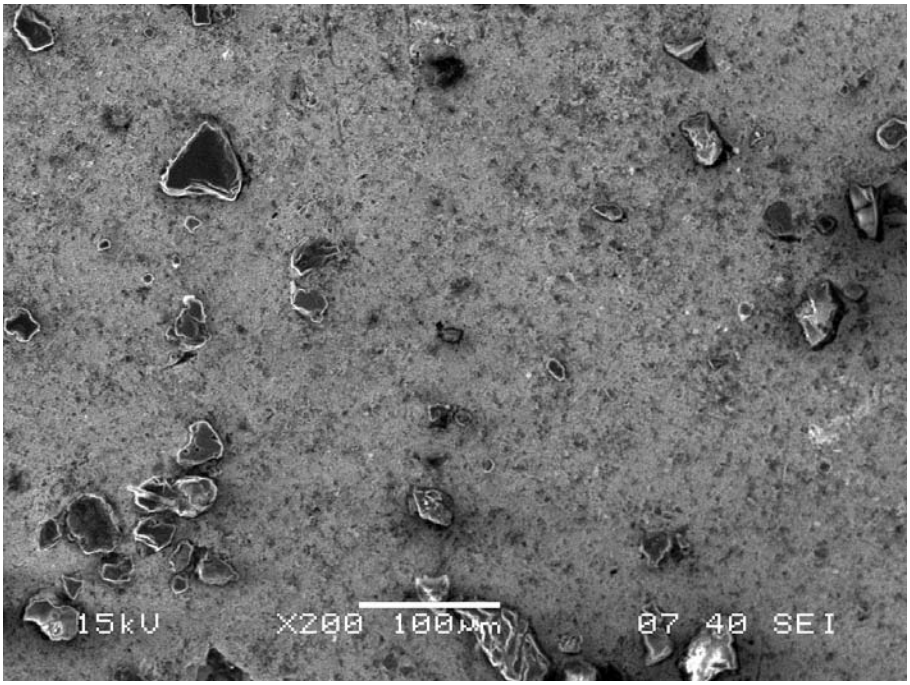

Fig. 7.64 The Display of microstructures before deformation by SEM

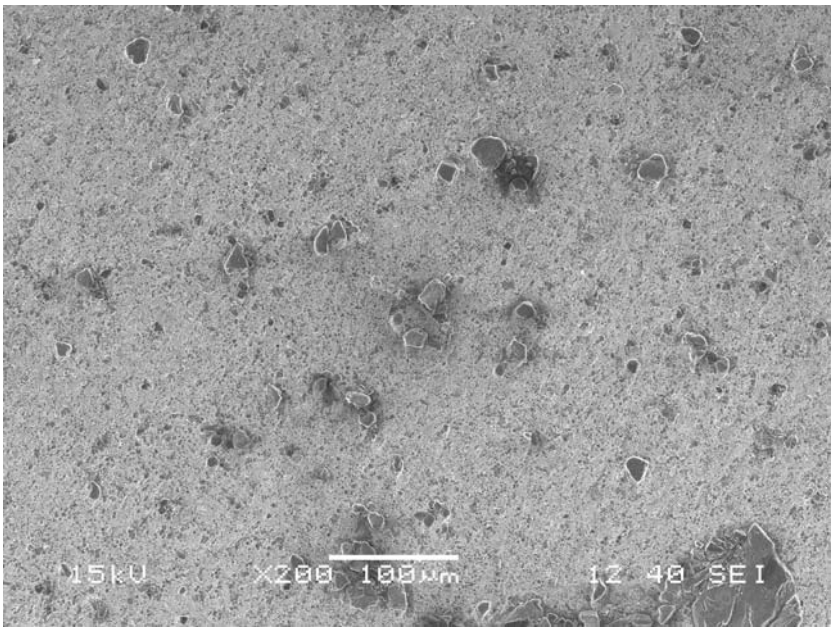

Fig. 7.65 The Display of microstructures after deformation by SEM

7.14 Conclusions

(i) Experimental set-ups have been fabricated for extrusion through converging dies with different die profiles for extrusion of different section from round and square billet.

(ii) The friction factor for die and billet material has been determined from ring compression test. It is 0.38 and 0.75 for wet as well as dry conditions respectively.

(iii) For any given reduction R, the pressure can be fairly calculated by using the equation

$$\frac{P_{av}}{\sigma_0} = 0.666 + 2.133 \ln\left(\frac{1}{1-R}\right)$$ for extrusion of

rhomboidal, pentagonal, octagonal and triangular section for converging dies.

(iv) A reduction in extrusion pressure is observed for extrusion of triangular and square section from round billet through curved die compared to taper die.

(v) The theory is partly validated with experiment.

Conclusions and Scope for Future Work

8.1 Conclusions

In the light of the present analysis, the following conclusions may be arrived at:-

(i) A class of upper bound solutions has been carried out for extrusion of triangular, octagonal, pentagonal and rhomboidal sections from round billet using linear converging dies. The SERR technique has been used based on discontinuous velocity field.

(ii) The optimum equivalent semi-cone angle is found to be 10^0 for general isosceles and 12^0 for right angled isosceles triangle section, where as it is 15^0 for equilateral triangular section for 40% reduction.

(iii) For any given reduction R, the experimental pressure can be fairly calculated by using the equation

$$\frac{P_{av}}{\sigma_0} = 0.666 + 2.133 \ln\left(\frac{1}{1-R}\right)$$ for extrusion of rhomboidal, pentagonal, octagonal and triangular for converging die.

(iv) The optimum equivalent semi-cone angle is 12^0 for extrusion of rhomboidal section, whereas the same is 15^0 for pentagonal and octagonal sections for 40% reduction.

(v) A class of upper bound solutions have also been carried out for extrusion of square sections form square billet through bezier and polynomial shaped non-linear converging dies. The dual stream function method based on continuous velocity field is used for analysis.

(vi) FEM modeling has been carried out for extrusion of square section from square billet using 3D DEFORM software through cosine, bezier and polynomial shaped die using rigid-plastic material model.

(vii) Mathematically contoured curved die profiles have been designed for extrusion of triangular and square sections from round billet. A parabolic function has been used for gradual convergence of circular shape to square and triangular shape.

(viii) FEM modeling has also been carried out for extrusion of square and triangular sections from round billet.

(ix) The extrusion pressure increases with increase in reduction and friction factor. It is observed that the effect of friction is more significant at high reductions.

(x) The bezier and polynomial die profiles are in general superior to cosine, circular, elliptic and hyperbolic die profiles. But in very low friction cosine die profile is found to be best.

(xi) The converging dies are superior in comparison to flat faced square die.

(xii) The theory is partly validated by experiment and it agrees fairly with the experiment.

8.2 Scope for future work

(i) Analysis using SERR technique for analytic geometry like cosine, parabolic, hyperbolic, and circular.

(ii) Analysis using SERR technique for non analytic geometry like polynomial and Bezier shaped die.

(iii) Analysis of extrusion of Triangular, Pentagonal, and Hexagonal section from square billet through curved die using SERR Technique.

(iv) FEM modeling of square section from square billet using curved dies

(v) FEM modeling of extrusion through linear converging die

REFERENCES

[1] Adeyemi, M. B. and Chitkara, N. R., Working pressure and deformation modes in forward extrusion of I and T shaped sections from square slugs, In: proceeding of 8th IMTDR Conference, London, 1977.

[2] Azad-Noorani, M., Jooybari-Bakhshi, M., Hosseinipour, S.J. and Gorji, A., Experimental and Numerical study of optimal die profile in cold forward rod extrusion of Al, International Journal of Materials Processing Technology, **164-165**, 2005, pp. 1572-1577.

[3] Altan, B. S., Purcek, G. and Miskioglu, I., An upper-bound analysis for equal channel angular extrusion, International Journal of Materials Processing Technology, **168**, 2005, pp. 137-146.

[4] Ajiboye, J. S. and Adeyemi, M. B., Upper bound analysis of die land length in cold extrusion, International Journal of Materials Processing Technology, **177**, 2006, pp. 608-611.

[5] Ajiboye, J. S. & Adeyemi, M. B., Upper-bound analysis for extrusion at various die land lengths and shaped profiles, International Journal of Mechanical Science, **49** (3), 2007, pp. 335-351.

[6] Abrinia, K. and Makaremi, M., A new three-dimensional solution for the extrusions of sections with larger dimensions than the initial billet, Int. J. of Materials Processing Technology, **205**, 2008, pp. 259-271.

[7] Assempour, A. and Hassannejasil, A., Minimization of the exit profile curvature in non- symmetric T-shaped sections in the extrusion process, International Journal of Materials and Design, **30**, 2009, pp. 1350-1355.

[8] Altan, T., Oh, Soo-lk and Gegel, H. L., Metal Forming Fundamentals and Applications, Copyright by the American Society For Metals, Carnes Publication Services, Inc, USA, pp. 85-86.

[9] Avitzur, B., Metal Forming: Processes and Analysis. McGraw-Hill, New York, 1968.

[10] Bacarach, B. I. and Samanta, S. K., Numerical method for computing plane plastic slip-line fields, ASME, Journal of Applied Mechanics, **45**, 1976, p. 97.

[11] Basily B. B. and Sansome D. H., Some theoretical considerations for the direct drawing of section rod from round bar, International Journal of Mechanical Science, **18**, 1976, pp. 201-208.

[12] Boer, C. B., Schneider, W. R. and Avitzur, B., An upper bound approach for the direct drawing of square section rod from round bar, Proceedings of the 20th International Machine and Tool Design Research Conference, Birmingham,1980, pp. 149–155.

[13] Bae, W. B. and Yang, D. Y., An U-B analysis of the backward extrusion of internally elliptic shaped tubes from round billets, International Journal of Materials Processing Technology, **30** (1), 1992, pp. 13-30.

[14] Bae W. B. and Yang, D. Y., An U-B analysis of the backward extrusion of tubes of complicated internal shapes from round billets, International Journal of Materials Processing Technology, **36** (2), 1993, pp. 157-173.

[15] Bae, W. B. and Yang, D. Y., An analysis of backward extrusion of internally circular-shaped tubes from arbitrarily-shaped billets by the U-B method, International Journal of Materials Processing Technology, **36** (2), 1993, pp. 175-185.

[16] Byon, S. M. and Hwang, S. M., Die shape optimal design in cold and hot extrusion, International Journal of Materials Processing Technology, **138**, 2003, pp. 316-324.

[17] Barisic, B. Cukor, G. and Math, M., Estimate of consumed energy at backward extrusion process by means of modeling approach, Int. J. of Materials Processing Technology, **153-154**, 2004, pp. 907-912.

[18] Bourke, L. S., Beyerlein, I. J., Alexander, D. J, and Clausen, B., FE Analysis of the plastic deformation zone and working load in equal channel angular extrusion, International Journal Material Science and Engineering. VA382, **25** (N.1-2), 2004, pp. 217-36.

[19] Bakhshi-Jooybari, M., Saboori, M., Noorani-Azad, M. and Hosseinipour, S. J., Combined upper bound and slab method, Finite element and experimental study of optical die profile in extrusion, International Journal of Materials and Design, **28,** 2007, pp. 1812-1818.

[20] Balasundar, I., Sudhakara Rao, M. and Raghu, T., Equal channel angular pressing die to extrude a variety of materials, International Journal of Materials and Design, **30**, 2009, pp. 1050-1059.

[21] Bhavikati, S. S., Finite Element Analysis, New age International (P) Limited Publishers, New Delhi.

[22] Chen, C. T. and Ling, F. F., Upper Bound solutions to axisymmetric extrusion problems, International Journal of Mechanical Science, **10** (11), 1968, pp. 863-879.

[23] Chang, K. T. and Choi, J. C., Upper bound solutions to symmetrical extrusion problems through curved dies, In: Proceedings of the 12th Midwestern Mechanical Conference, Bauingenieur, **6,** 1971, pp. 383-396.

[24] Chang, K. T. and Choi, J. C. Upper-Bound solutions to tube extrusion problems through curved dies. Transactions of the ASME, Journal of Engineering for Industry, **94**, 1972, SerB, N4, pp. 1108-1112.

[25] Chitkara, N. R. and Adeyemi, M. B., Working pressure and deformation modes in forward extrusion of I and T shaped sections from square sludges, in: Proceedings of the Eighth IMTDR Conference, London, 1977, pp. 39–46.

[26] Cho, N. S. and Yang, D. Y., Analysis of hydro film extrusion through optimized curved dies, International Journal of Mechanical Science, **24** (10), 1982, pp. 589-595.

[27] Cho, N. S. and Yang, D.Y, Hydrofilm Extrusion of tubes through optimized curved dies, Journal of Engineering for Industry transactions, ASME, **105** (N4), 1983, pp. 243-250

[28] Chitkara, N. R. and Celik, K. F., A generalized CAD/CAM solution to the three dimensional off-centric extrusion of shaped sections: Analysis, International Journal of Mechanical Science, **42** (2), 2000, pp. 273-294.

[29] Celik K. F. & Chitkara, N. R., Application of an Upper-bound method to off-centric extrusion of square sections, analysis and experiments, International Journal of Mechanical Science, **42** (2), 2000, pp. 321-345.

[30] Celik, K. F. and Chitkara, N. R., Off-Centric extrusion of circular rods through streamlined dies, CAD/CAM applications analysis and some experiments, International Journal of Mechanical Science, **42** (2), 2000, pp. 295-320.

[31] Clausen A. H., Tryland, T. and Remseth, S., An investigation and material properties and geometrical dimensions of Al extrusions, International Journal of Materials and Design, **22**, 2001, pp. 267-275.

[32] Chitkara, N. R. and Aleem, A., Extrusion of axi-symmetric bi-metallic tubes: some experiments using hollow billets and the application of a generalized slab method of analysis, International Journal of Mechanical Science**, 43**, 2001, pp. 2857-2882.

[33] Chitkara, N. R. and Aleem, A., Axi-symmetric tube extrusion/piercing using die-mandrel combinations: some experiments and a generalized U-B analysis, International Journal of Mechanical Science, **43,** 2001, pp. 1685-1709.

[34] Choi, J. C., Park, J. H. and Kim, B. M., Finite element analysis of the combined extrusion of semi-solid material and its experimental verification, International Journal of Materials Processing Technology, **105**, 2000, pp. 49-54.

[35] Caminaga, C., Neves, F. O., Gentile, F. C. and Button, S. T., Study of alternative lubricants to the cold extrusion of steel shafts, International Journal of Materials Processing Technology, **182**, 2007, pp. 432-439.

[36] Carnham, B., Luther, H. and Wilkes, J. O., Applied Numerical Methods, john Wiley and Sons Inc., 1969.

[37] Dodeja, L. C. and Johnson, W., On the multi-hole extrusion of sheet of equal thickness, Journal of Mechanics and Physics Solids, **5,** 1957, pp. 267-279.

[38] Dodeja, L. C. and Johnson, W., On the multi-hole extrusion of sheet of equal thickness. Journal of Mechanical Phys. Solids, **5**, 1957, pp. 267-279.

[39] Das, N. S. and Johnson, W., Slip-line fields of indirect type for end extrusion through partly rough square dies, International Journal of Mechanical Science, **30** (1), 1989, pp. 61-69.

[40] Darani, H. R. and Ketabchi, M., Simulation of L section extrusion using upper bound method, International Journal of Materials and Design, **25** (6), 2004, pp. 535-540.

[41] Das, N. S, and Maity, K. P., A class of slip line field solutions for extrusion through wedge shaped dies with slipping friction, International Journals of Materials and Design, **28** (2), 2007, pp. 380-386.

[42] DEFORM ™ 3D Version 6.1(sp2), User's Manual, Scientific Forming Technologies Corporation, 2545 Farmers Drive, Suite 200, Columbus, Ohio, 2008, 43235.

[43] Dieter, G. E., Mechanical Metallurgy, Tata McGraw-Hill Publishing Company Limited, New Delhi.

[44] EI-Behery, A. M., Lamble, J. H. and Johnson, W., Container wall pressure in the slow speed plane-strain direct extrusion of pure lead, In: Proceeding of 5th IMTDR Conference, Pergamon Press, 1964.

[45] Eivani, A. R., Taheri Karimi, A., An Upper Bound solution of ECAE process with outer curved corner, International Journal of Materials Processing Technology, **182**, 2007, pp. 555-563.

[46] Eivani, A. R. and Karimi Taheri, A., A new method for estimating strain in equal channel angular extrusion. International Journal of Materials Processing Technology, **183,** 2007, pp. 148-153.

[47] Eivani, A.R. and Taheri, A.K., A new method for estimating strain in equal channel angular extrusion, International Journal of Materials Processing Technology, **183**, 2007, pp. 148-153.

[48] Ebrahimi, R., Reihanian, M., Kanaani, M. and Moshksar, M. M., An Upper-bound analysis of the tube extrusion process, International Journal of Materials Processing Technology, **199**, 2008, pp. 214-220.

[49] E-solidworks, 2008

[50] Frisch, J. and Thomson, E. G., Stresses and strains in cold extruding 28-0 Aluminium, Transactions of the ASME, **77**, 1955, pp. 1343-1362.

[51] Frisch, J., and Mata-Pietric E., Metal flow through various mathematically contoured extrusion dies. In: Proceedings of the North America Metal-Working Research Conference, North America, **5,** 1977.

[52] Frisch, J. and Mata-Pietric, E., Experiments and the Upper Bound solution in Axisymmetric Extrusions, In: Proceedings of the 18th International Machined Tool Design Research Conference, London, Macmillan, 1978, p. 55.

[53] Forhoumand, A. and Ebrahimi, R., Analysis of forward-backword-radial extrusion process, International Journal of Materials and Design, **30**, 2009, pp. 2152-2157.

[54] Gatto, F. and Giarda, A., The characteristics of the three dimensional analysis of plastic deformation according to the SERR method, International Journal of Mechanical Science, **23** (3), 1981, pp. 129-148.

[55] Gunasekara, J. S., and Hoshino, S., Analysis of extrusion or drawing of polygonal sections through straightly converging dies, Journal of Engineering for Industry, Transactions ASME , **104**, 1982, pp. 38-44.

[56] Gunasekera, J. S. and Hoshino, S., Analysis of extrusion of polygonal sections through streamlined dies, Journal of Engineering for Industry, Transactions ASME, **107**(N3), 1985, pp. 229-233.

[57] Guo, Y-M., Yokochi, Y. and Suzuki, H., Analysis of hot forward-backward extrusion by the visco-plastic F.E. method, International Journal of Materials Processing Technology, **38** (1-2), 1993, pp. 103-114.

[58] Gouveia, B.P.P.A., Rodrigues, J.M.C and Martins, P.A.F., Steady-State F.E. analysis of cold forward extrusion, International Journal of Materials Processing Technology, **73,** 1998, pp. 281-288.

[59] Giuliano, G., Process design of the cold extrusion of a billet using FEM, International Journal of Materials and Design, **28** (2), 2007, pp. 726-729.

[60] Gordon, W. A., Van Tyne, C. J. and Moon, Y.H., Axisymmetric extrusion through adoptable dies- Part1: Flexible velocity fields and power terms, International Journal of Mechanical Science, **49** (1), 2007, pp. 86-95.

[61] Gordon, W.A., Van Tyne, C. J. and Moon, Y.H., Axisymmetric extrusion through adoptable dies- Part2: Comparison of velocity fields, International Journal of Mechanical Science, **49** (1), 2007, pp. 96-103.

[62] Gordon, W.A., Van Tyne, C. J. and Moon, Y.H., Axisymmetric extrusion through adoptable dies- Part3: Minimum pressure streamlined die shapes, International Journal of Mechanical Science, **49** (1), 2007, pp. 104-115.

[63] Gao, L. and Cheng, X., Microstructure and mechanical properties of Cu-10% Al-4% Fe alloy produced by equal channel angular extrusion, International Journal of Materials and Design, **29**, 2008, pp. 904-908.

[64] Hill, R., Mathematical Theory of Plasticity, Oxford University Press, London, 1950. [64]

[65] Halling, J. and Mitchell, L. A., An Upper-Bound solution for axisymmetric extrusion, International Journal of Mechanical Science, **7** (4), 1965, pp. 277-295.

[66] Hughes, K.E, Nair, K.D and Sellars, C.M., Temperature and Flow stress during the hot extrusion of steel Metals Technology, 1 (N4), 1974, pp. 161-169.

[67] Hwan. C. Li, plane strain extrusion by sequential limit analysis, International Journal of Mechanical Science, **39** (7), 1997, pp. 807-817.

[68] Heiburg, G., Brechet, Y., Jensrud, O. and Roven, H. J., Selection of Al alloys for extrusion profiles: Methodology and development of specialized software, International Journal of Materials and Design, 23, 2002, pp. 505-509.

[69] Hwang, B. C., Lee, H. I. and Bae, W. B., A UBET of the non-axisymmetric combined extrusion process, International Journal of Materials Processing Technology, **139**, 2003, pp. 547-552.

[70] Har, K. D., Choi, Y. and Yeo, H. T., A design method for cold backward extrusion using FE analysis, Journal of Finite elements in analysis and design, **40**, 2003, pp. 173-185.

[71] Huang, Guo-Ming, Wang, Jang-Ping, Lee, Hsien-Der and Chang, Cheng-Sung, Rigid-plastic boundaries approach to the analysis of arbitrary profile dies in axisymmetric extrusion, Journal of Materials Processing Technology, **209**, 2009, pp. 4351-4359.

[72] Hoshino, S. and Gunasekara, J. S., An upper bound solution for extrusion of square section from round bar through converging dies, proceedings of 21st International machine Tool Design and Research (IMTDR) conference, **21**, p. 97-105.

[73] Im, young-Taek, Kang, Seong-Hoon and Cheon, Jae-Seung, F E Investigation of friction condition in a backward extrusion of AL alloy, Journal of Manufacturing science and engineering, Transations of the ASME, **125**, 2003, pp. 378-383.

[74] Johnson, W., Experiments in plane strain extrusion, Journal of Mechanics and Physics Solids**, 4,** 1956, pp. 269-278.

[75] Johnson, W., Experiments in the cold extrusion of rods of non-circular sections, Journal of Mechanics and Physics Solids, **5,** 1957, pp. 267-281.

[76] Johnson, W. and Kudo, H., The Mechanics of Metal extrusion, Manchester University Press, Manchester, 1962.]

[77] Johnson, W., Sowerby, R. and Haddow, J. B.,Plane-strain Slip-line Fields. Theory and Bibliography, E. Arnold, London, 1970.

[78] Johnson, W. and Mellor, P. B., Engineering Plasticity, Van Nostrand Reinhold New York 1973, (chapter-6), pp. 110-113

[79] Joun, M.S. and Hwang, S.M., Pass schedule optimal design in multipass extrusion and drawing by Finite Element Method, International Journal of Machine Tools and Manufacture, **33** (5), 1993, pp. 713-724.

[80] Jooybari, Bakhshi. M., A Theoretical and Experimental study of friction in metal forming by the use of the forward extrusion process, International Journal of Materials Processing Technology, **125-126**, 2002, pp. 369-374.

[81] Jooybari- Bakhshi, M., Saboori, M., Hosseinipour, S.J., Shakeri, M. and Gorji, A., Experimental and Numerical study of optimum die profile in backward rod extrusion, International Journal of Materials Processing Technology, **177**, 2006, pp. 596-599.

[82] Jin, Shun Yi, Altenhof, William, Kapoor and Tanyo, An experimental investigation into the cutting deformation mode of AA 6061-T6 round extrusions, Journal of Thin-walled structures, **44**, 2006, pp. 773-786.

[83] Jufu, J., Ying, W., Zhiming, D., Jianjun, Q., Yi, S., and Shoujing, L., Enhancing room temperature mechanical properties of Mg-9Al-Zn alloy by multi-pass equal channel angular extrusion,, International Journal of Materials Processing Technology,**210,** 2010, pp. 751-758.

[84] Kudo, H., An Upper-Bound approach to plain strain forging and extrusion-III, International Journal of Mechanical Science, **1** (4), 1960, pp. 366-368.

[85] Kudo, H., Some analytical and experimental studies of axismetrical cold forging and extrusion, Part II, International journal of Mechanical Science**, 3**, 1961, pp. 125-138.

[86] Kobayashi, S. and Thomsen, G. E., Upper and Lower bound solution to axisymmetric compression and extrusion problems, International Journal of Mechanical Science, **7** (2), 1965, pp.127-143.

[87] Kuester, J. L. and Mize, J. H., Optimization Techniques with Fortran, Tata McGraw-Hill Publishing Company Limited, New Delhi, 1973. pp. 337-342.

[88] Kar, P. K., Das, N. S. and Subramanium, T. N., Upper Bound Analysis of Extrusion of square sections using square Dies, Journal of the Institution of Engineers (India), **66** (PE2), 1985, pp. 88-91.

[89] Knoerr, M., Lee, J. and Altan, T., Application of the 2D finite element method to simulation of various forming processes, International Journal of Materials Processing Technology, **33**(1-2), 1992, pp. 31-55.

[90] Kang, B.-Soo, Min-Kim, B. and Choi, J.C., Preform design in extrusion by the FEM and its experimental confirmation, International Journal of Materials Processing Technology, **41**(2), 1994, pp. 237-248.

[91] Kuzman, K., Pfeifer, E., Bay, N. and Hunding, J., Control of material flow in a combined backward and forward rod extrusion, International Journal of Materials Processing Technology, **60** (1-3), 1996, pp. 141-147.

[92] Kim, D. M., Cho, J. R., Bae, W. B. and Kim, Y.H., Upper-bound analysis of square-die forward extrusion, International Journal of Materials Processing Technology, **62** (1-3), 1996, pp.242-248.

[93] Kar P. K. and Das N. S., Upper Bound Analysis of extrusion of I-section bars from square/rectangular Billets through square dies, International Journal of Mechanical Science, **39** (8), 8, 1997, pp. 925-934.

[94] Kim, D. K., Cho, J. R., Bae, W. B., Kim, Y. H. and Bramley, A. N., An upper bound analysis of the square die extrusion of non-axisymmetric sections, International Journal of Materials Processing Technology, **71**, 1997, pp. 477-486.

[95] Kim, V. H., Bae W. B., Cho, J. R. and Park, J. W., An experimental study on the Non axis symmetric square-die extrusion using model material test, International Journal of Materials Processing Technology, **80**, 1998, pp. 653-656.

[96] Kumar, S., Shanker, K. and Lal, G. K., Analysis of cold extrusion of Non Re-entry product shapes, Journal of manufacturing science and Engineering, Transactions of the ASME, **124** (N1), 2002, pp. 71-78.

[97] Kang, C. G., Jung, Y. J. and Kwon, H. C., Finite element simulation of die design for hot extrusion process of Al/Cu clad composite and its experimental investigation, International Journal of Materials Processing Technology, **124**, 2002, pp. 49-56.

[98] Kang, S. H., Lee, J. H., Cheon, J. S. and Im, Y. T., The effect of strain hardening on frictional behavior in tip test, International Journal of Mechanical Science, **46** (6), 2004, pp. 855-869.

[99] Kumar, S. and Prasad, S. K., Feature based design of extrusion process using Upper-bound and Finite element techniques for extrudeable shapes, International Journal of Materials Processing Technology, **155-156**, 2004, pp. 1365-1372.

[100] Kumar, S. and Prasad, S. K.,A Finite Element Thermal Model for Axisymmetric Cold and Hot Extrusion using Upper Bound Technique, Journal of the Institution of Engineers (India), **85** (MC 2) , 2004, pp. 59-68.

[101] Kim, J. K. and Kim, W. J., Analysis of deformation behavior in 3D during equal channel angular extrusion, International Journal of Materials Processing Technology, **176**, 2006, pp. 260-267.

[102] Kumar, S. and Vijay, P., Die Design and experiments for shaped extrusion under cold and hot condition, International Journal of Materials Processing Technology, **190**, 2007, pp. 375-381.

[103] Ketabchi, M. and Seyedrezai, H., Energy analysis of L-section extrusion using two different streamlined dies, International Journal of Materials Processing Technology, **189,** 2007, pp. 242-246.

[104] Kar, P. K. and Sahoo, R. K., Application of the SERR technique to the analysis of extrusion of square sections from round billets, Journal of the Institution of Engineers (India), MC78, pp. 151-154.

[105] Kucukomeroglu, T., Effect of equal-channel angular extrusion on mechanical and wear properties of eutectic Al-12Si alloy, International Journals of Materials and Design, **31**, 2010, pp. 782-789.

[106] Krishnamoorthy, C. S., Finite Element Analysis,Tata McGraw-Hill Publishing Company Limited, New Delhi.

[107] Kobayashi Shiro, Ikoh-Soo and Altan Taylan, Metal Forming and the FEM, (Oxford series on advanced manufacturing).

[108] Kim, H., Sweeney, K., and Altan, T., Application of computer aided simulation to investigate metal flow in selected forging operations, International Journal of Materials Processing Technology, **46**(1-2), 1994, pp. 127-154.

[109] Lee, Rong-Shean and Shaw, Houy-chang, Analysis of tube extrusion using Upper-Bound Elemental Technique, Journal of the Chinese Society of Mech. Engineers, **7** (N6),1986, pp. 463-472

[110] Lee ,Yong-Shin and Hahm, Seung-Yeun, Mechanical properties changes in Drawing/Extrusion of hardening Viscoplastic materials with damage, International Journal of Mechanical Science, **39** (5), 1997, pp. 565-573.

[111] Lee ,Yong-Shin and Hahm, Seung-Yeun, Mechanical properties changes in Drawing/Extrusion of hardening Viscoplastic materials with damage, International Journal of Mechanical Science, **39** (5), 1997, pp. 565-573.

[112] Lee, S. K., Ko, D. C. and Kim, B. M., Optimal die profile design for uniform microstructure in hot extruded product, International Journal of Machine Tools and Manufacture, **40**, 2000, pp. 1457-1478.

[113] Lee, H. I., Hwang, B. C. and Bae, W. B., A UBET analysis of non-axisymmetric forward and backward extrusion, International Journal of Materials Processing Technology, **113**, 2001, pp. 103-108.

[114] Li, S., Bourke, M.A.M., Beyerlein, I. J. and Alexander, D. J., FEA of the plastic deformation zone and working load in equal channel angular extrusion, Journal of Material science and engineering**, 382**, 2004, pp. 217-236.

[115] Leung, Y.C., Chan, L.C., Tang, C.Y. and Lee, T.C., An effective process of strain measurement for severe and localized plastic deformation, International Journal of Machine Tools and Manufacture, **44**, 2004, pp. 669-676.

[116] Li, S. B. and Xie, J. X, Fabrication of thin walled 316L stainless steel seamless pipes by extrusion technology, Int. J. of Materials Processing Technology, 183, 2007, pp. 57-61.

[117] Maity, K. P, Analysis of Three-Dimensional Extrusion through Curved Dies, M. Tech Thesis, R.E.C. Rourkela, Sambalpur University, 1988.

[118] Maccarini, G., Glardini, C. and Bagini, A., Extrusion operations: Finite element modelling approach and experimental results, International Journal of Materials Processing Technology, **24,** 1990, pp. 395-402.

[119] Maity, K. P., Kar, P. K., and Das, N. S., A class of U-B solutions for the extrusion of square shapes from square billets through curved dies, International Journal of Materials Processing Technology, **62** (1-3), 1996, pp. 185-190.

[120] Mihelic, Ales. and Stok boris, Tool design optimization in extrusion processes, Computer and Structures, **68,** 1998, pp. 283-293 .

[121] Mamalis, A. G., Petrosyan, G. L., Manalakos, D. E. and Hambardzumyan, A. F., The effect of strain hardening in the extrusion of bimetallic tubes of porous internal layer, International Journal of Materials Processing Technology, **181**, 2007, pp. 241-245.

[122] Malpani, M. and Kumar, S., A feature based analysis of tubes extrusion, International Journal of Materials Processing Technology,**190**, 2007, pp. 363-374.

[123] Malayappan, S, Narayanasamy, R and K. Kalidasamurugavel, A study on barreling behaviour of Al billets during cold upsetting with an extrusion die constraint at one end, International Journal of Materials and Design, **28** (3),2007, pp. 954-961.

[124] Masoudpanah, S. M. and Mahmudi, R., The microstructure, tensile, and shear deformation behavior of an AZ31 magnesium alloy after extrusion and equal channel angular pressing, International Journals of Materials and Design, **31**, 2010, pp. 3512-3517.

[125] Nagpal. Vijay, Underwood and Ervin, E, Analysis of axisymmetric flow through curved dies using a generalized U-B approach, In: Proceeding of the North America Metalworking Research Conference, 2nd, 1974, Madison, WI, USA.

[126] Nagpal, V. and Altan, T., Analysis of the three-dimensional metal flow in extrusion of shapes with the use of dual stream function, Proceedings of the

Third North American Metal Research Conference, Pittsburgh, PA, 1975, pp. 26–40.

[127] Nagpal, V., on the solution of Three-Dimensional Metal-Forming Processes, Transactions of the ASME, Journal of Engineering for Industry, 1977, pp. 624-629.

[128] Narayanasamy, R., Metal Forming Technology, Ahuja Book Company Pvt. Ltd., 2000, New Delhi.

[129] Narayanasamy, R. and Ponalagusamy, R., Theory of Engineering Plasticity, Ahuja Book Company Pvt. Ltd., 2000, New Delhi.

[130] Narayanasamy, R., Textbook on Extrusion Technology, Ahuja Book Company Pvt. Ltd., 2000, New Delhi.

[131] Narayanasamy, R., Srinivasan, P. and Venkatesan, R., Computer aided design and manufacture of streamlined extrusion dies, International Journal of Materials Processing Technology, **138**, 2003, pp. 262-264.

[132] Narayanasamy, R., Ponalagusamy, R., Venkatesan, R., and Srinivasan, P., An Upper bound solution to extrusion of circular billet to circular shape through cosine dies, International Journal of Materials and Design, **27** (5), 2006, pp. 411-415.

[133] Narayanasamy, R., Baskaran, K., Arunachalam, S. and Krishna, D. M., An experimental investigation on barreling of aluminium alloy billets during extrusion-forging using different lubricants, International Journal of Materials and Design, **29**, 2008, pp. 2076-2088.

[134] Narayanasamy, R., Baskaran, K. and Muralikrishna, D., Some studies on stresses and strains of aluminium alloy during extrusion-forging at room temperature, International Journal of Materials and Design**, 29**, 2008, pp. 1623-1632.

[135] Peng D. S., An Upper Bound analysis of the geometric shape of the deformation zone in rod extrusion, International Journal of Materials Processing Technology, **21** (3),1990, pp. 303-311.

[136] Petzov, G. G., Jelezov, K. D. and Tzoneva, M. G., Model of the kinematic field in the axismmetrical high-temp extrusion of a bi-component (metal-

lubricant) system, nternational Journal of Materials Processing Technology,**21**, 1990, pp. 131-142.

[137] Ponalagusamy, R., Narayanasamy, R and Srinivasan, P., Design & Development of streamlined extrusion dies a Bezier curve approach, International Journal of Materials Processing Technology, **161**, 2005, pp. 375-380.

[138] Paydar, M. H., Reihanian, M., Ebrahim, R., Dean T. A. and Moshksar, M. M., An upper-bound approach for equal channel angular extrusion with circular cross section, International Journal of Materials Processing Technology,**198**, 2008, pp. 48-53.

[139] Ponalagusamy R, Narayanasamy R, Venkatesan R and Senthilkumar S, Computer aided metal flow investigation in streamlined extrusion dies, International Journal of Materials and Design, **29**, 2008, pp. 1228-1239.

[140] Paydar, M. H. , Reihanian, M. bagherpour, E. and Sharifzadeh, M., Equal channel angular pressing-forward extrusion (ECAP-FE) consolidation of AL particles, International Journal of Materials and Design ,**30**, 2009, pp. 429-432.

[141] Post, J., Vries, C. de, and Huetink, J., Validation tool for 2D multi-stage metal-forming processes on meta-stable stainless steels, Journal of Materials Processing Technology,**209**, 2009, pp. 5558-5572.

[142] Park, S. Y., Choi, W. J., Choi, H. S. and Kwon, H., Effects of surface pre-treatment and void content on GLARE laminate process characteristics, International Journal of Materials Processing Technology, **210,** 2010, pp. 1008-1016.

[143] Richmond O. and Devenpeek M. L., A die profile for maximum efficiency in strip drawing, ASME, In: Proceedings of the 4th U.S. Congress Applied Mechanics, 1962, p. 1053.

[144] Reinikainen, T., Andersson, K., Kivivuori, S. and Korhonen, A. S., Finite – element analysis of Copper extrusion process, International Journal of Materials Processing Technology, **34** (1-4), 1992, pp. 101-108.

[145] Reddy Venkata, N., Dixit P.M. and Lal, G.K., Die design for axisymmetric extrusion, International Journal of Materials Processing Technology, **55** (3-4), 1995, pp. 331-339.

[146] Reddy, Venkata. N., Sethuraman, R. and Lal, G.K., Upper-bound and FE analysis of axisymmetric hot extrusion, International Journal of Materials Processing Technology, **57** (1-2), 1996, pp.14-22.

[147] Reddy, N. V., Dixit, P.M. and Lal, G.K, Analysis of axisymmetric tube extrusion, International Journal of Machine Tools and Manufacture, **36** (2), 1996, pp. 1253-1267.

[148] Reddy, N. V., Dixit, P.M. and Lal, G.K., Die design for axisymmetric hot extrusion, International Journal of Machine Tools and Manufacture, **37**(2), 1997, pp. 1635-1650.

[149] Reihanian, M., Ebrahimi, R. and Moshksar, M. M., U-B analysis of equal channel angular extrusion using linear and rotational velocity fields, International Journal of Materials and Design, **30**, 2009, pp. 28-34.

[150] Rowe, G. W., Principles of Industrial Metal working processes, Edward Arnold (Publishers) Ltd., London.

[151] Shabaik, A. and Kobayashi, S., Computer application to the viscoplasticity method, Transactions of the ASME, Journal of Engineering for Industry, **89**, 1967, pp. 339-352.

[152] Shin, H. W., Kim, D. W. and Kim, N., A simplified three dimensional finite element analysis of the non-axisymmetric extrusion processes, International Journal of Materials Processing Technology,**38**, 1993, pp. 567-587.

[153] S. Storen, The theory of extrusion-Advances and challenges, International Journal of Mechanical Science, **35** (12), 1993, pp. 1007-1020.

[154] Sahoo, S. K., Kar, P. K., Singh, K. C. and Mohapatra, S. P., Upper Bound analysis of extrusion of hexagonal section bars from rectangular billets through the square dies, Journal of the Institution of Engineers (India), MC 77, 1996, pp. 164-168.

[155] Srinivasan, K. and Venugopal P., Adiabatic friction heating on the open die extrusion of solid and hollow bodies, International Journal of Materials Processing Technology, **70** (1-3), 1997, pp. 170-177.

[156] Sahoo, S. K., Kar, P. K. and Nayak, D., Upper Bound Solution Using SERR Technique for Extrusion of Square Section Bars from square Billets Through the Curved Die, Journal of the Institution of Engineers (India), **78**(MC3), 1997, pp. 155-160.

[157] Sahoo, S. K., Kar, P. K. and Singh, K. C., A 3D analysis using SERR Technique for Extrusion of triangular Section Bars from square/rectangular Billets through the square dies, Journal of the Institution of Engineers (India), PR **78** (1998), pp. 45-49.

[158] Sahoo, S. K., Kar, P. K. and Singh, K. C., Upper Bound analysis of the extrusion of a bar of channel section from square/rectangular billets through square dies, International Journal of Materials Processing Technology, **75**, 1998, pp. 75-80.

[159] Sahoo, S.K., Kar, P.K. and Singh, K.C., A numerical application of the U-Bound technique for round-to-hexagon extrusion through linearly converging dies, International Journal of Materials Processing Technology, **91**, 1999, pp.105-110.

[160] Sahoo, S. K. , Kar, P. K. and Singh, K. C., Direct Upper-Bound solution to Rectangular-to-Polygonal extrusion through square dies, Journal of Manufacturing Science and Engineering, ASME, **121**, 1999, pp. 195-201.

[161] Semiatin, S. L. and Delo, D. P., Equal channel angular extrusion of difficult-to- work alloys, International Journal of Materials and Design, **21**, 2000, pp. 311-322.

[162] Sahoo, S. K., Comparison of SERR analysis in extrusion with experiment, International Journal of Materials Processing Technology, **103**, 2000, pp. 293-303.

[163] Sahoo, S. K. and Kar, P. K., Round-to-hexagon drawing through straightly converging dies, an application of the SERR technique, International Journal of Mechanical Science, **42** (3), 2000, pp. 445-449.

[164] Sahoo, S. K. and Kar, P. K., Round –to-square Extrusion Through Taper Die: A Three –dimensional Analysis, Proceedings of the 19th AIMTDR Conference, New Delhi, India, 2000, pp. 217-222.

[165] Salimi, M., Strain distributions in plain strain deformation through wedge shaped dies, International Journal of Materials Processing Technology, **125-126**, 2002, pp. 317-322.

[166] Segal, V. M., Slip line solutions deformation mode and loading history during equal channel angular extrusion, Journal of Material science and engineering, **345**, 2003, pp. 36-46.

[167] Sahoo, S. K., an analysis of plastic flow through polygonal linearly converging dies: as applied to forward metal extrusion, International Journal of Materials Processing Technology, **132**, 2003, pp. 286-292.

[168] Sahoo, R. K., Kar, P. K. and Sahoo, S. K., 3D Upper-Bound modeling for round to triangle section extrusion using SERR technique, International Journal of Materials Processing Technology,**138**, 2003, pp. 499-504.

[169] Saboori, M., Jooybari- Bakhshi. M. Noorani-Azad, M. and Gorji, A. Experimental and Numerical study of energy consumption in forward and backward rod extrusion, International Journal of Materials Processing Technology, **177**, 2006, pp. 612-616.

[170] Son, I. H., Lee, J. H. and Im, Y. T., Finite element investigation of equal channel angular extrusion with back pressure, International Journal of Materials Processing Technology, **171**, 2006, pp. 480-487.

[171] Sheng, Z. Q., Taylor, R. and Strazzanti, M., FEM analysis and design bulb shield progressive draw die, International Journal of Materials Processing Technology, **189**, 2007, pp. 58-64.

[172] Segal, V. M., Equal channel angular extrusion of flat products, Journal of Material science and engineering, **476**, 2008, pp. 178-185.

[173] Serajzadeh, S. and Mahmoodkhani, Y., A combined U-B and F-E method for prediction of velocity and temperature fields during hot rolling process, International Journal of Mechanical Science, **50**, 2008, pp. 1423-1431.

[174] Sinha, M. K., Deb, S. and Dixit, U.S., Design of a multi-hole extrusion process, International Journal of Materials and Design, **30**, 2009, pp. 330-334.

[175] Sahoo, R. K., Samantaray, P. R. Sahoo, S. K., Sahoo, B. and Kar, P. K., Round –to –Channel section extrusion through linearly converging die: a

three-dimensional analysis, International Journal of Advanced Manufacturing Technology**, 41**, 2009, pp. 677-683.

[176] Segal, V. M., Mechanics of continuous equal-channel angular extrusion, International Journal of Materials Processing Technology, **210**, 2010, pp. 542-549.

[177] Song, M., He, Yue-hui, Effects of die-pressing pressure and extrusion on the microstructures and mechanical properties of SiC reinforced pure aluminum composites, International Journals of Materials and Design, **31**, 2010, pp. 985-989.

[178] Tomita, Y. and Sowerby, R., An approximate analysis for studying the plane strain deformation of strain rate sensitive materials, International Journal of Mechanical Science, **21** (8), 1979, pp. 505-516.

[179] Tjetta, S. and Heimlund, O., Finite-element simulations in cold-forging process design, International Journal of Materials Processing Technology, **36** (1), 1992, pp. 79-96. [179]

[180] Tryland, T., Hopperstad, Odd S. and Langseth, M., Design of experiments to identify material properties, International Journal of Materials and Design, **21**, 2000, pp. 477-492.[180]

[181] Ulysse, P, Optimal extrusion die design to achieve flow balance, International Journal of Machine Tools and Manufacture**, 39** (7), 1999, pp. 1047-1064.

[182] Ulysee, P., Extrusion die design for flow balance using FE and optimization methods, International Journal of Mechanical Science, **44** (2), 2002, pp. 319-341.

[183] Valberg, H., Metal flow in the direct axisymmetric extrusion of Aluminium, International Journal of Materials Processing Technology, **31** (1-2), 1992, pp. 39-55.

[184] Vickery, J. and Monaghan, J., An upper-bound analysis of a forging extrusion process," International Journal of Materials Processing Technology, **55** (2), 1995, pp.103-110.

[185] Watkins, M. T., Ashoroft, K. and McKenzie, J., Some aspects of the cold extrusion of metals, In: Proceeding of conference, Technical Engineering Manufacturing, Institution of Mechanical Engineers, London, 1958.

[186] Wifi, A. S., Shatla, M. N. and Hamid-Abdel, A., An optimum curved die profile for the hot forward rod extrusion process, International Journal of Materials Processing Technology, **73**, 1998, pp. 97-107.

[187] Williams, A. J., Croff, T. N. and Cross, M., Computational modeling of metal extrusion and forging processes, International Journal of Materials Processing Technology, **125-126**, 2002, pp. 573-582.

[188] Wang, D., Shi, T., Pan, J., Liao, G., Tang, Z., and Liu, L., Finite element simulation and experimental investigation of forming micro-gear with Zr-Cu-Ni-Al bulk metallic glass, International Journal of Materials Processing Technology,**210,** 2010, pp. 684-688. [188]

[189] Wifi, A. S., Abduljabbar, Z.S. and Sakar, M.T., A combined UBET/FEM investigation of metal flow and stress analysis of dies in extrusion process, International Journal of Materials Processing Technology, **24**, pp. 431-440.

[190] Xu, S., Zhao, G. and Ma, X., Finite element analysis and optimization of equal channel angular pressing for producing ultra fine grained materials. International Journal of Materials Processing Technology**, 184**, 2007, pp. 209-216.

[191] Xavier, C., Fortran 77 and Numerical Methods, New age international (P) limited, publishers, New Delhi.

[192] Yih, C. S, Stream Functions in Three-Dimensional Flow, La Haulle Blanche, **12**, 1957, p. 445.

[193] Yang, D.Y. and Lee, C. H., Analysis of three dimensional extrusion of sections through curved dies by conformal transformation, International Journal of Mechanical Science, **20** (9), 1978, pp. 541-552.

[194] Yamada, Y. and Hirakawa, H, Large deformation and Instability analysis in Metal Forming Process, ASME, Applied Mechanics Divisions, AMD, **28**, 1978, pp. 27-38.

[195] Yang, D.Y., Kum, M. U., and Lee, C. H., A new approach for generalized three dimensional extrusion of sections from round billets by conformal transformation, In: JUTAM Symposium on metal forming plasticity, Germany, 1979, pp 204-211.

[196] Yang, D. Y. and Lange K., Analysis of Hydrofilm extrusion of Three-dimensional shapes from round billets, International Journal of Mechanical Science, **26** (1), 1984, pp. 1-19.

[197] Yang, D.Y., Han, C. H. and Lee, B. C., The use of generalized deformation boundaries for the analysis of axisymmetric extrusion through curved dies, International Journal of Mechanical Science, **27** (10), 1985, pp. 653-663

[198] Yang, D. Y., Han, C. H. and Kim, M. U., A generalized method for analysis of three-dimensional extrusion of arbitrarily-shaped sections, International Journal of Mechanical Science, **28** (8), 1986, pp. 517-534.

[199] Yang, D.Y, New formulation of generalized velocity field for axisymmetric forward extrusion through arbitrarily curved dies, Journal of Engineering For Industry, Transactions ASME, **109** (N2), 1987, pp. 161-168.

[200] Yang, D.Y., Lee, C.M. and Yoon, J. H., Finite Element Analysis (FEA) of steady state three-dimensional extrusion of sections through curved dies, International Journal of Mechanical Science, **31**(2), 1989, pp. 145-156.

[201] Yang, D.Y., Kim, Y.G. and Lee C.M., An Upper-Bound solution for axisymmetric extrusion of composite rods through curved dies, International Journal of Machine Tools and Manufacture, **31**(4), 1991, pp. 565-575.

[202] Yang, Y. L. and Lee, S., Finite Element analysis of strain conditions after equal channel angular extrusion, International Journal of Materials Processing Technology, **140,** 2003, pp. 583-587.

[203] Yang, F., Saran, A. and Okazaki, K., Finite element simulation of equal channel angular extrusion, International Journal of Materials Processing Technology, **166,** 2005, pp. 71-78.

[204] Yang, H., Peng, Y., Ruan, X. and Liu, M., A Finite Element model for hydrodynamic lubrication of cold extrusion with frictional boundary condition. International Journal of Materials Processing Technology, **161**, 2005, pp. 440-444.

[205] Yoon, S. C., Quang, P. Hong, S. I., and Kim, H. S., Die design for homogeneous plastic deformation during equal channel angular pressing, International Journal of Materials Processing Technology, **187-188**, 2007, pp. 46-50.

[206] Zheng, P. F., Chan, L. C. and Lee, T. C., Numerical analysis of the sheet metal extrusion processes, Journal of Finite elements in analysis and design, **42**, 2005, pp. 189-207.

[207] Zeid, I., CAD/CAM Theory and Practice, Tata McGraw-Hill Publishing Company Limited, New Delhi.

Curriculum Vitae

AKSHAYA KUMAR ROUT

E-mail : akshayakumarrout@gmail.com

Present Address: MR. A. K. ROUT
S. S. Bhatnagar Hall of Residence, Room - B/112
NIT Campus, Rourkela-769008, Orissa
Ph (M) +91- 09437756207

Permanent Address: C/o Prof. P. C. Das
F-28, BJB Nagar
Bhubaneswar-751014, Orissa
Ph® 0674- 2434010

Personal Information

Date of birth : 23-01-1968

Nationality : INDIAN

Education

2010	Ph. D Dissertation Submitted
2004	M. Tech (Alternate Hydro Energy System), IIT-Roorkee (India)
1991	B. Tech (A.M.I.E) (Mechanical Engineering) The Institution of Engineers, Kolkata, India

Employment

Duration	Designation	Organization
1991-1993	Production Engineer	TNRM (P) Ltd. Chennai, India
1996-2000	Shift Engineer	SCHL (P) Ltd. Mehsana, Ahmadabad, N.G. , India
2000- 2006	Asst. Professor (Mech. Engg.)	C. V. Raman College of Engineering, Bhubaneswar, Orissa, India
2006-2010	Ph.D Research Scholar	National Institute of Technology, Rourkela, Orissa, India

RESEARCH PUBLICATIONS

International Journals Published

(1) K. P. Maity and **A. K. Rout,** *An Upper Bound solution to Three-Dimensional extrusion through a Bezier shaped curved die*, published in an *International Journal of Manufacturing Technology and Research*, **Vol. 5(1-2)**, **2009.**

(2) A. K. Rout and K. P. Maity, 3D upper-bound modeling for Round-to-Rhombus section extrusion: An application of the SERR technique, published in an *International Journal of Manufacturing Science and Technology*, **Vol. 3(1), 2009. pp. 111-122.**

(3) K. P. Maity, **A. K. Rout** and Kalu Majhi, "Computer-Aided Simulation of Metal Flow through Curved Die for Extrusion of Square Section from Square Billet", published in *the Journal Key Engineering Materials*, **Vol. 424, (2010), pp. 181-188**. (Trans Tech. Publications, Switzerland)

(4) K. P. Maity and **A. K. Rout**, "Three Dimensional Upper Bound Modeling for Extrusion of Round-To-Octagon Section Using Linearly Converging Die", published in *the Journal Key Engineering Materials*, **Vol. 424, (2010), pp. 189-196**. (Trans Tech. Publications, Switzerland)

(5) K. P. Maity and **A. K. Rout,** Analysis of Round-to-Pentagon extrusion through linearly converging dies using SERR Technique. published in the Journal of Modern Manufacturing Technology, **(JMMT), Vol.2 (N2), (2010)**

(6) A. K. Rout, K. P. Maity and S. K. Rath, "A Numerical Investigation of Extrusion through Bezier shaped curved Profile", published in *the Journal Key Engineering Materials* ***(*with the title Advances in Materials Processing IX)**, **Vol. 443, (2010), pp. 93-97,** (Trans Tech. Publications, Switzerland).

International Journals Communicated

(1) A. K. Rout and K. P. Maity**,** *Numerical and Experimental study on the three-dimensional extrusion of square section from square billet through a polynomial shaped curved die,* communicated to an Int. J. of Advanced Manufacturing Technology, (2007) **(Under FINAL Review)**

(2) K. P. Maity and **A. K. Rout,** A Numerical Application of SERR Technique for extrusion of Round-to-Triangle sections with unequal sides through linearly converging dies, communicated to an International Journal of Manufacturing Technology and Research, 2009.

(3) A. K. Rout, K. P. Maity and S. K. Sahoo, An analysis of plastic flow through polygonal section by linearly converging dies: as applied to forward metal extrusion. Communicated to an Int. Journal of Advanced Manufacturing Technology, (A-M-T**) (2010)**

(4) A. K. Rout, K. P. Maity, R. K. Ohdar and S. K. Rath**,** Comparison of **FEM** and Computational modeling with experiments of extrusion through Bezier shaped curved Die. Communicated to an International Journal of Modern Manufacturing Technology, **(JMMT).**

(5) A. K. Rout, K. P. Maity, S. K. Sahoo and R. K. Ohdar**, FEM** modeling for extrusion of square product from square billet through Cosine shaped Dies. **C**ommunicated to an International Journal of Manufacturing Technology and Research, 2010.

International Conference

(1) K. P. Maity and **A. K. Rout,** *An upper bound solution to extrusion of square section from square billet through polynomial shaped curved die,* published in the Proceedings of the **Eighth Asia-pacific International Conference on Materials Processing (8TH APCMP,2008)**, **hold at China, June 15-20, 2008, pp. 57-62. (Presented at China) OK**

(2) A. K. Rout and K. P. Maity, *Computer aided modelling of metal flow investigation of square billet to square shape through Bezier shaped curved dies,* published in the Proceedings of the International Symposium for Research Scholars on Metallurgy, Materials Science and Engineering, IIT Madras, Dec- 10-12, (2008). **OK**

(3) A. K. Rout and K. P. Maity, *Computer aided modelling of metal flow investigation of square billet to square shape through elliptical shaped dies,* published in the Proceedings of the VI International Conference on Mechanochemistry and Mechanical Alloying **(INCOME2008)**, hold at N.M.L, Jamshedpur, INDIA, Dec- 1-4, 2008. (Presented) **OK**

(4) A. K. Rout and K. P. Maity and S. K. Rath, A Numerical Investigation of Extrusion through Cosine Die Profile, *published* in the Proceedings of the 3rd International Conference on Advances in Mechanical Engineering (ICAME-2010), Sardar Vallabhbhai National Institute of Surat, Gujrat, January-4-6, 2010.

(5) A. K. Rout and K. P. Maity, Experimental Validation of SERR Analysis in Extrusion of Polygonal Section, published in the Proceedings of the International Conference on Frontiers in Mechanical Engineering (FIME 2010), National Institute of Technology, Surathkal, Karnataka, 20th -22nd May 2010.

National Conference

(1) Rout, A. K. and Sharma, M. P., *Rural Electrification by Solar Home Systems,* published in the Proceedings of the National Conference on Safety, Environment & Energy Management, N.I.T. Tiruchirapalli, Tamilnadu, India, 5th June-2004, pp.1-7.

(2) A. K. Rout and K. P. Maity, *Computer aided modeling of Metal flow investigation through cosine dies*, published in the Proceedings of the 1st National Symposium for Materials Research Scholars (MR-08), IIT Mumbai, May 17-18, (2008). (Presented)

(3) A. K. Rout and K. P. Maity**,** *Velocity, stress and strain analysis during metal flow investigation of square billet to square shape through cosine shaped dies,* published in National Conference on Mechanism Science and Technologies: from Theory to Application, NCMSTA'08 on Nov-13-14, 2008, at NIT, Hamirpur, H.P. OK

(4) A. K. Rout and K. P. Maity, *Numerical and Experimental study on the Three-Dimensional Extrusion of Square section from square billet through a Bezier shaped curved die*, published in the Proceedings of the 2nd National Symposium for Materials Research Scholars (MR-09), IIT Mumbai, May 8-9, (2009). **(ORAL) (Presented)**

(5) K. P. Maity and **A. K. Rout,** *Upper Bound Solution using SERR Technique for Extrusion of Square Section from Square billet through the Elliptical Die,* published in the Proceedings of the National Symposium for Materials Research Scholars (MR-09), IIT Mumbai, May 8-9, (2009). **(POSTER) (Presented)**

(6) A. K. Rout and K. P. Maity, Round-to-triangle section extrusion through linearly converging dies: A Three-dimensional analysis, published in the Proceedings of the National Conference of Advances in Mechanical Engineering (AME 2009), Vidya Vikas Institute of Engineering and Technology, Mysore, India, 5th October-2009.

(7) A. K. Rout and K. P. Maity, *Round-to-Hexagon section extrusion through linearly converging dies: A three-dimensional analysis*, published in the Proceedings of the Twenty-Fifth National Convention of Mechanical Engineers on the theme "Challenges for Manufacturing in the Next Decade", New Delhi, November 6-7, 2009.

(8) A. K. Rout and K. P. Maity, Round-to-Square Extrusion through straightly Converging Dies: An SERR technique application, published in the Proceedings of the National Conference on Recent Advances in Manufacturing Technology and Management (RAMTM-2010), Jadavpur University, Kolkata, Feb 19-20, 2010. **(Presented)**

(9) A. K. Rout and K. P. Maity, Modeling of Metal Flow investigation through curved dies, published in the Proceedings of the National Conference on Recent Advances in Fluid and Solid Mechanics (RAF&SM2010), National Institute of Technology, Rourkela, Feb 27-28, 2010. **(Presented)**

(10) A. K. Rout, K. P. Maity, R. K. Ohdar and R Kumar, FEM Modeling of Extrusion of Square billet to Square product through Cosine Dies. Published in the Proceedings of the 3rd National Workshop on Precision Forming (Modeling, Analysis and System Development), Birla Institute of Technology, Mesra, Ranchi, Jharkhand, 15th -16th February, 2010

(11) A. K. Rout, K. P. Maity, R. K. Ohdar and R Kumar, FEA Modeling of Extrusion of Polygonal Sections from Round Billet through Curved/Taper Dies, published in the Proceedings of the 3rd National Symposium for Materials Research Scholars (MR-10), IIT Mumbai, May 7-8, (2010).